COMBINATION RADIO-AND IMMUNE RECRUITMENT THERAPY

DEVELOPMENT OF A VERSATILE PLATFORM FOR COMBINATION TARGETED RADIONUCLIDE AND IMMUNE CELL RECRUITMENT THERAPIES USING BIO-ORTHOGONAL CHEMISTRY

By: STEPHANIE RATHMANN, M.Sc., B.Sc.

A Thesis Submitted to the School of Graduate Studies in Partial Fulfilment of the Requirements for the Degree Doctor of Philosophy

McMaster University DOCTOR OF PHILOSOPHY (2020) Hamilton, Ontario (Chemistry)

TITLE: Development of a Versatile Platform for Combination Targeted Radionuclide and Immune Cell Recruitment Therapies using Bio-orthogonal Chemistry

AUTHOR: Stephanie Rathmann, M.Sc., B.Sc. (McMaster University) SUPERVISOR: Professor J. F. Valliant Number of Pages: xxiv, 188

Abstract

This thesis describes a general platform for the synthesis of radiolabelled antibody recruiting small molecules (R-ARMs) for combination radio and immune recruitment therapies. The novel trifunctional ARM was synthesized and radiolabelled with beta (lutetium-177) and alpha (actinium-225) emitting radionuclides in high yield. Biodistribution of the lutetium-ARM revealed rapid renal clearance and minimal uptake in non-target tissues with all organs and tissues containing less than 0.3 %ID/g by 24 hours post-injection. Having determined the pharmacokinetic properties of the ligand, a biodistribution study was performed to determine the targeting potential of the platform. Through the use of a validated bone targeted bisphosphonate, uptake in the arm and leg bones was achieved. Flow cytometry studies successfully demonstrated ARM and antibody dependent immune cell recruitment. Based on the promising results of the ARM *in vitro* and *in vivo*, the next step was to perform therapy studies.

In order to validate the novel R-ARM, an intratumoral (i.t.) strategy was developed through the preparation of a TCO-bovine serum albumin (BSA) derivative. This new chemical entity was used in both an aggregated and non-aggregated form to retain the R-ARM in the tumour after i.t. administration. Biodistribution showed high retention of the aggregated and non-aggregated BSA out to 120 hours with 167 ± 94 and 81 ± 32 %ID/g respectively remaining in the tumour. An autoradiography study revealed the after i.t. administration the aggregated material was localized in specific regions within the tumour compared to the non-aggregated material which diffused throughout. The aggregated material was used in a single and multi-dosing radiotherapy study in which the latter induced a statistically significant survival advantage compared to the control. One additional multi-dosing study was performed with the non-

aggregated material which resulted in the largest survival advantage to date. Intratumoral administration of TCO-BSA linked to the trifunctional tetrazine showed promising radiotherapy results and future work on dose optimization with lutetium and actinium is required prior to the combination R-ARM therapy.

In parallel, the efficacy of the unlabelled ARM linked to TCO-BSA was interrogated in preclinical models. The compound was administered i.t. three times per week in a breast cancer tumour model, and response to therapy monitored. The immunized group showed no survival advantage compared to the control group comprised of naïve animals. Biodistribution studies were performed to determine if TCO-BSA was accessible to the bloodstream following i.t. administration in both the aggregated and non-aggregated forms. Saline, aggregated or non-aggregated TCO-BSA were administered i.t. followed by the R-ARM. The results showed very low uptake in the tumour for all three groups, with minimal change in distribution from that of the native R-ARM. This suggests that after i.t. administration, the TCO-BSA was not available to molecules in the bloodstream or the concentration was insufficient to promote *in vivo* coupling. Further work on this component of the platform is needed before further ARM studies are performed.

Acknowledgements

Over the many years I spent at McMaster I met countless talented, intelligent and motivated individuals who helped shape me as scientist as well as an individual. First and foremost, I would like to thank my supervisor, Professor John Valliant, who has been with me on this journey since the fourth year of my undergraduate degree. By providing an environment where everyone was encouraged to ask questions, and have high level discussions of experimental results, I was able to hone my research and problem-solving skills. In addition, experiencing John's passion and drive to bring radiopharmaceuticals to the clinic has been truly inspiring and motivating. I am very thankful for the many opportunities I have been provided over the years and would not be the scientist I am today without them.

I would also like to thank my committee members Dr. McNulty and Dr. Adronov for their insightful feedback over the years. I appreciate the time and effort that both of you have given throughout the years.

I would like to thank the Valliant group members that I have had the honour of working with over the years. I would like to thank Alyssa Vito for all of her help – from showing me the good kickboxing gyms around the neighbourhood, to the animal studies she performed for me in the final year of my degree. Her friendship is immensely valuable to me and I thank you for the time and effort that was required to produce scientifically sound data in a level-headed and efficient manner. To Natalie Mercanti, thank you for making NRB 227 such an oasis for the past three years and I very much appreciate your support in wrapping up the final studies for my project. Without the frequent discussion of foods, in particular desserts, I don't think I would have made it through the stressful times. I am thankful that I met George Baidoo – one person I can

always count on for a positive view or an uplifting quote. I appreciate the time you have taken to guide and inform me on the industrial side of science. Thank you to Afaf Genady for her contributions to the ARM project. To the rest of the Valliant Research Group, thank you for your help and support over the years.

Salma, thank you for all the time you take each day to answer questions and guide me through many of the ups and downs of chemistry research. Although Reza, Patricia and Denis left the group soon after I started, I have made lifelong friends and truly miss the days of chatting in the lab well into the evening hours. I would like to thank Andrea Armstrong for all of her help over the years, from hallway brainstorming sessions, to coordinating special dispensing dates to accommodate my studies. I am thankful to have met Zoya – the person who is solely responsible for keeping me well caffeinated for the majority of my degree. Thank you to my CPDC friends Steve, Renee, Rezwan and Scott for making the time to help with any questions, as well as have some laughs. To the members of health physics – Glenn, Duane, Mike and Derek, without your assistance I would not have been able to complete my countless labelling experiments over the years.

Last but not least I would like to thank my family for their unwavering support throughout my graduate endeavours. To Luke, thank you for supporting me through the day to day ups and downs of working in the lab. To Scott and Lindsay, thank you for always being good company and taking the time to lighten the mood. Finally, to my parents I appreciate all the love and encouragement you have provided me over the years. I would not have been able to complete this adventure or be the person I am today without you, for that I am extremely grateful.

Table of Contents

List of Figures

List of Tables

List of Schemes

Abbreviations

%ID/g = Percent Injected Dose per Gram

ABT = Antibody Binding Terminus

ACN = Acetonitrile

ACT = Adoptive T-Cell Therapy

ADCC = Antibody-Dependent Cellular Cytotoxicity

ADCP = Antibody Dependent Cellular-Phagocytosis

AF-488 = Alexa Fluor 488

AI = Auto Inhibition

AM = Assay Media

AP = Alkaline Phosphatase

ARM = Antibody-Recruiting Small Molecule

ATC = Adoptive T-cell Therapy

ATP = Adenosine Triphosphate

Boc = tert-butyloxycarbonyl

BSA = Bovine Serum Albumin

BZA = benzamide

CARs = Chimeric Antigen Receptors

CDC = Compliment Dependent Cytotoxicity

$CDCl_3$ = Deuterated Chloroform

CD_3OD = Deuterated Methanol

CHXA'' = N-[2-amino-3-(p-isothiocyanatophenyl)propyl]-trans-cyclohexane-1,2-diamine N,N',N'',N''',N''''-pentaacetic acid

CT = Computed Tomography

CTLA-4 = Cytotoxic T-Lymphocyte-Associated Protein

DAMP = Danger Associated Molecular Patterns

DCM = Dichloromethane

DIPEA = *N,N*-Diisopropylethylamine

DFO = Deferoxamine

DMF = Dimethylformamide

DMSO = Dimethyl Sulfoxide

DNA = Deoxyribonucleic Acid

DNP = Dinitrophenyl

DOTA = 1,4,7,10-tetraazacyclododecane-1,4,7,10-tetraaceticacid

EDC = 1-ethyl-3-(3-dimethylaminopropyl)carbodiimide

EDTA = Ethylenediaminetetraacetic acid

ELISA = Enzyme- Linked Immunosorbent Assay

EPR = Enhanced Permeability and Retention

ER = Estrogen Receptor

FA = Formic Acid

FACS = Fluorescence-Activated Cell Sorting

FBS = Fetal Bovine Serum

Fc = Fragment Crystallizable

FCA = Complete Freund's Adjuvant

FDA = Food and Drug Administration

FIA = Freund's Incomplete Adjuvant

FITC = Fluorescein

FMOC = 9-Fluorenylmethoxycarbonyl

FZD10 = Frizzled Homolog 10

GBM = Glioblastoma Multiforme

H&E = Hematoxylin and Eosin

HCC = Hepatocellular Carcinoma

HEPES = 4-(2-Hydroxyethyl)piperazine-1-ethanesulfonic acid, N-(2-Hydroxyethyl)piperazine-N′-(2-ethanesulfonic acid)

HER2 = Human Epidermal Growth Factor Receptor

HMGB1 = High Mobility Group Protein B1

HOMO = Highest Occupied Molecular Orbital

HPLC = High Performance Liquid Chromatography

HRMS = High Resolution Mass Spectrometry

HSA = Human Serum Albumin

IC_{50} = Half Maximal Inhibitory Concentration

IEDDA =Inverse Electron Demand Diels-Alder

IFN = Interferon

IGF-1R = Insulin-Like Growth Factor-1 Receptor

IgG = Immunoglobulin G

IgM = Immunoglobulin M

IHC = Immunohistochemistry

IL-2 = Interleukin-2

I.P. = Intraperitoneal

I.T. = Intratumoral

iTLC = Instant Thin Layer Chromatography

I.V. = Intravenous

K_0 = Average Intrinsic Association Constant

KLH = Keyhole Limpet Hemocyanin

LET = Linear Energy Transfer

LUMO = Lowest Unoccupied Molecular Orbital

MAA = Macroaggregated Albumin

MALDI = Matrix-Assisted Laser Desorption Ionization

MCRPC = Metastatic Castrate-Resistant Prostate Cancer

MDP = Methylene Diphosphonate

MeOH = Methanol

MFI = Mean Fluorescence Intensity

MRI = Magnetic Resonance Imaging

MS = Mass Spectrometry

NET = Neuroendocrine Tumour

NHL = non-Hodgkin's Lymphoma

NHS = N-Hydroxysuccinimide

NIS = Sodium-Iodide Symporter

NK-1 = Neurokinin Type-1 Receptor

NMR = Nuclear Magnetic Resonance

NSCLC = Non-Small-Cell Lung Cancer

OCT = Optimal Cutting Temperature

p-SCN = *p*-isothiocyanatobenzyl

PBS = Phosphate Buffered Saline

PD-1 = Programmed Cell Death Protein 1

PD-L1 = Programmed Death-Ligand 1

PEG = Poly(ethylene Glycol)

PET = Positron Emission Tomography

PNPP = para-Nitrophenylphosphate

PR = Progesterone Receptor

PRRT = Peptide Receptor Radionuclide Therapy

PSA = Prostate Serum Antigen

PSMA = Prostate Specific Membrane Antigen

PyBoP = (Benzotriazol-1-yloxy)tripyrrolidinophosphonium Hexafluorophosphate

R-ARM = Radiolabelled Antibody-Recruiting Small Molecule

RCP = Radiochemical Purity

RIT = Radioimmunotherapy

RPMI = Roswell Park Memorial Institute

RSA = Rat Serum Albumin

R_t = Retention Time

RT = Radiotherapy

S.C. = Subcutaneous

SD = Standard Deviation

SEC = Size Exclusion Chromatography

SEM = Standard Error of the Mean

SPARC = Secreted Protein Acidic and Rich in Cysteine

SPE = Solid Phase Extraction

SPECT = Single Photon Emission Computed Tomography

SEC = Size Exclusion Chromatography

TBT = Target Binding Terminus

TCO = *trans*-cyclooctene

TCO-BP = TCO-Functionalized Bisphosphonate

TEA = triethylamine

TFA = trifluoroacetic acid

TLC = Thin Layer Chromatography

TLR = Toll-Like Receptors

TNBC = Triple Negative Breast Cancer

TOF = Time of Flight

TRT = Targeted Radionuclide Therapy

uPAR = Urokinase-Type Plasminogen Activator Receptor

US = Ultrasound

USA = United States of America

Chapter 1 - Introduction

1.1 Targeted Radionuclide Therapy

There are three main types of radiation therapy currently used in the clinic: external beam, brachytherapy and targeted radionuclide therapy (TRT).[1] External beam is the most widely used, treating over 7 million patients each year through the use of a beam of high energy particles to irradiate the site of interest from outside of the body.[2] Brachytherapy is commonly used for the treatment of cervical, prostate, breast and skin cancers through the insertion of sealed radioactive "seeds" into a tumour for localized irradiation of the tissue.[3]

TRT is unique amongst the three in that it involves the systemic administration of a therapeutic medical isotope. Selective delivery can be achieved by conjugating the radioactive isotope to a vector such as a small molecule, protein or antibody which targets a specific site or receptor expressed on a cancer cell.[4, 5] This helps to direct the cytotoxic radionuclide to the cancerous tissue while minimizing uptake in healthy, non-target tissues. TRT is used in patients whose tumours have metastasized as the target can be expressed in both primary and secondary disease sites, which would be difficult to treat with either external beam or brachytherapy.[6-8] TRT agents are typically derived from medical isotopes that emit one of three types of radiation: alpha and beta particles and Auger electrons.[9] Each of these emissions can cause cytotoxic effects and have shown clinical utility as cancer therapies as either approved products or in clinical trials.[10-13]

1.2 Alpha Emitting Radiopharmaceuticals

Alpha emitting radionuclides, specifically radium-223, have been used since the early 1900s for treatment of ailments such as rheumatic disease and skin lesions.[14] Since then, the progress to the clinic has been limited with only one alpha emitter, Xofigo™, gaining FDA approval for the treatment of bone metastases associated with prostate cancer.[10] With respect to TRT, the properties of alpha emitters are attractive as they have high linear energy transfer (LET), a short path length (50-100 μm) in tissue, and cause cell death through direct double stranded DNA breaks leading to efficacy in both normoxic and hypoxic tumours.[15-17] Due to their short path length, alpha particles are of particular interest for micrometastases but can also be applied to larger tumours.[18]

Xofigo™ is a salt of radium ($RaCl_2$) which naturally localizes to regions of high calcium turnover and is therefore used to treat bone metastases. As a group II metal, there is no simple way to link radium to targeting molecules, so the emergence of targeted alpha therapies relies on other alpha emitting isotopes. While alpha radiotherapy holds promise, the initial development of targeted therapeutics was slow. This is due in part to issues accessing radionuclides with suitable half-lives for medical applications and the absence of the chemistry required to radiolabel targeting molecules.[19] In 1990, Simonson *et al.* used a bismuth-212 labelled antibody for radioimmunotherapy (RIT) of human adenocarcinoma tumours.[20] Mice were treated with four intraperitoneal (i.p.) doses of 3.3 or 6.7 MBq on consecutive days, which lead to an 85% reduction in tumour mass compared to the control. Despite the promising results published 30 years ago, bismuth-212 labelled radiopharmaceuticals are not prevalent in the clinic potentially due to the relatively short, 61 minute half-life of the metal and the two energetic gamma rays (2.6 MeV) emitted in the decay chain.[19, 21]

Another alpha emitting isotope that was used to prepare targeted alpha therapies using a variety of antibodies is the radiohalogen, astatine-211.[22-24] In 2018, Li *et al.* used a radiolabelled antibody conjugated with either astatine-211 or yttrium-90 to treat a synovial sarcoma flank tumour.[24] The radiolabelled antibody targeting frizzled homolog 10 (FZD10) was given as a single dose of 0.46, 0.93 or 1.9 MBq intravenously and the tumour volume and animal health monitored. The alpha therapy supressed the tumour growth rate as early as one day post-injection, which was not seen with the beta therapy. In addition, the alpha therapy resulted in a significant survival advantage compared to the control with no evidence of radiotoxicity but did suffer from significant de-astatination *in vivo*. Astatine-211 has shown success in small clinical trials using intracavitary administration for relapsed ovarian and recurrent brain cancers.[25, 26] Although these results are promising, obtaining high purity, clinical scale batches of astatine-211 proves challenging for larger scale studies.[19, 27, 28]

An alpha emitter that has gained significant interest in the past decade is actinium-225 due to the release of four alpha particles during its decay to a stable daughter (Figure 1-1).[19] The 10 day half-life of the isotope allows suitable time for production, radiolabelling and distribution of the radiopharmaceutical to clinical sites. Furthermore, it is also compatible with antibody-based targeting molecules which typically have longer circulation times.[29]

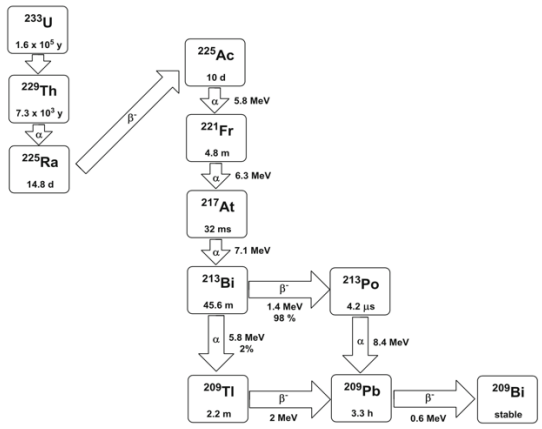

Figure 1-1. Decay scheme of actinium-225.[19] Reproduced with permission from Springer Nature.

As early as 2003, Borchardt *et al.* demonstrated the RIT capabilities of actinium-225 when conjugated to an anti-HER-2/*neu* antibody in a murine ovarian cancer model.[30] Mice administered three doses of [^{225}Ac]Ac-trastuzumab (4.1 kBq) every 7 days had a median survival time of 124 days compared to 33 days for the control group. More recently, Kelly *et al.* radiolabelled an albumin binding small molecule targeting prostate specific membrane antigen (PSMA), which is overexpressed on many prostate cancer tumours, with actinium-225 and evaluated the therapeutic efficacy in mice bearing LNCaP tumours.[31] It was shown that a single dose of 74 or 148 kBq had a significant anti-tumour response, however the tumour re-emerged in the lower dose group 42 days post-treatment. At 72 days post-treatment, 6/7 of the high dose animals were tumour free as confirmed by a PET/CT image, with starting tumour volumes as large as 624-808 mm^3.

In addition to preclinical work, there are a number of actinium-225 labelled small molecules and antibodies in active clinical trials. PSMA-617, a small molecule radiolabelled with actinium-225, has been investigated for the treatment of metastatic castrate-resistant prostate cancer (mCRPC) by targeting PSMA.[32] A pilot clinical study

run by Sathekge *et al.* involved using a de-escalation dose across three treatments from 8 MBq to 6 or 4 MBq, at which point prostate serum antigen (PSA) levels were measured, with a decrease representing response to the therapy.[32, 33] After two to three treatments, 82% of patients were able to achieve a greater than 90% decrease in serum PSA levels and in 11/17 patients all lesions had resolved.[32] In a separate clinical trial it was found that [^{225}Ac]Ac-PSMA-617 can be used to treat mCRPC that does not respond to the corresponding beta therapy, [^{177}Lu]Lu-PSMA-617. It was found that after two treatments with the beta therapy, PSA levels increased from 294 to 419 ng/mL despite sufficient tumour uptake.[34] The therapy was then switched to [^{225}Ac]Ac-PSMA-617 and the patient received three doses of 6.4 MBq every two months. After the three treatments the patient showed complete remission and a PSA level <0.1 ng/mL, however suffered severe xerostomia. This study, and data emerging from neuroendocrine tumour-targeting radiopharmaceuticals, suggests that patients who are refractory to beta therapy, with sufficient tracer uptake in the tumour, can be good candidates for the analogous alpha therapy.[34, 35]

In addition to small molecule targeted alpha therapies, a phase I clinical trial recently opened using an actinium-225 labelled antibody (FPI-1434) that targets insulin-like growth factor-1 receptor (IGF-1R) which is overexpressed on a variety of solid tumours.[12, 36] In preclinical human colon cancer models, treatment with low doses of [^{225}Ac]Ac-FPI-1434 (1.85 kBq) were shown to suppress tumour growth, whereas higher doses of 7.4 and 14.8 kBq resulted in tumour regression.[36] In addition to colon cancer, single doses of [^{225}Ac]Ac-FPI-1434 were efficacious in both human prostate and lung cancer xenografts demonstrating the versatility of this radioimmunoconjugate for the treatment of solid tumours.

Although the preclinical and clinical data are promising, there is concern moving to commercialization due to the limited availability and high cost of the isotope.[37] Actinium-225 is the decay product of thorium-229, which is isolated from weapons grade uranium-233. This provides a finite amount of approximately 1 Ci of actinium-225 per year which cannot meet the global demand for clinical use.[38] In order to increase the amount of isotope produced annually, proton irradiation of thorium-232 and radium-226 have been explored, resulting in high yields at lower costs. The biggest limitation of thorium bombardment is the co-production of long lived actinium-227, 21.8 year half-life, which cannot be chemically separated and poses disposal issues that could hinder clinical applications.[29, 39] The irradiation of radium-226 does not suffer from long lived impurities, however precautions must be taken as gaseous radon-222, a radioactive decay product with a 3.8 day half-life, is produced.[38, 40] As these accelerator techniques are refined and extraction from USA thorium-229 stocks continues, it is expected that actinium-225 will be readily available to meet clinical demands of these next generation radiopharmaceuticals.

1.3 Beta Emitting Radiopharmaceuticals

For many decades, beta emitting radiopharmaceuticals have been used clinically for the treatment of a variety of solid and liquid tumours.[41] One of the most well-known radiopharmaceuticals is sodium iodide for the treatment of thyroid cancer. Iodide is naturally taken up in the thyroid through the sodium-iodide symporter (NIS), as it is incorporated into many thyroid hormones.[42] [^{131}I]NaI is administered to the patient, where it then accumulates in the thyroid and emits high energy beta particles which destroy the thyroid cells. Unfortunately, the beta emissions are accompanied by high energy gamma rays which can be harmful to individuals interacting with the patient and

therefore the patient requires shielding or must be quarantined for a period of time to ensure the safety of the public.[43-45]

Yttrium-90, a pure beta emitter with a half-life of 64.1 hours, has been used clinically since the FDA approval of TheraSphere®, radiolabelled glass microspheres, in 1999.[11, 46] Used as a treatment for unresectable hepatocellular carcinoma (HCC), TheraSphere® studies have shown a one year survival rate of 62%. The survival rate is on par for treatment with chemoembolization, however the post-treatment side effects were mild for TheraSphere® relative to embolization.[47] The next yttrium-based therapeutic to gain FDA approval was a radiolabelled antibody, Zevalin®, for the treatment of non-Hodgkin's Lymphoma (NHL) in 2002.[48] Patients with complete or partial response after first line therapy received a single dose of Zevalin® (14.8 MBq/kg), which increased progression free survival from 13.3 months in the control to 36.5 months.[49] Yttrium-90 therapies have shown impressive results in the clinic, however there is a major limitation to the approach as there are no imageable emissions that can be used to assess the biodistribution of the therapeutic.[11] To circumvent this issue, prior to administration of a yttrium-90 based radiopharmaceutical, an analogous compound derived from an isotope that can be imaged such as technetium-99m or indium-111 is administered in order to estimate dosimetry.[50-52]

An alternative beta emitting isotope that has a 6.65 day half-life, and a gamma emission suitable for single-photon emission computed tomography (SPECT) imaging is lutetium-177. A recent push towards large scale production of no carrier added lutetium-177 has provided access to higher specific activity material, which can be very beneficial for radionuclide therapy.[53] In 2018, Lutathera®, a lutetium-177 based peptide receptor radionuclide therapy (PRRT) for the treatment of somatostatin receptor

positive neuroendocrine tumours (NETs), gained FDA approval.[53-56] The therapy utilizes no carrier added lutetium in order to produce a high specific activity radiopharmaceutical.[55] In addition to Lutathera®, an active phase II clinical trial for the treatment of mCRPC using a lutetium-177 labelled PSMA targeted small molecule is currently ongoing in North America based on promising results in European studies.[57, 58] Based on clinical efficacy data, nuclear properties and commercial availability, lutetium-177 is an attractive therapeutic radionuclide from which to build next generation targeted radiopharmaceuticals for the treatment of cancer.

1.4 Auger Emitting Radiopharmaceuticals

Although human studies of Auger emitting targeted radiopharmaceuticals have been reported for over 20 years, they are less prominent in the clinic than alpha and beta emitters.[59] Auger electrons have a high LET, however they have low energy and a short range in the body of nanometers to micrometers. The low range makes Auger electrons ideal for irradiating near the nucleus or cell membrane, where a significant amount of energy would be deposited in a small area with minimal damage to surrounding tissues or cells. Due to the short range of the cytotoxic radiation, auger emitters achieve the best results when linked to an internalizing vector.[60]

1.5 Interaction of Charged Particles with Biological Tissue

Charged particles can interact with biological tissues in a variety of ways, with the type and energy of the particle guiding the nature of the effect. Heavier particles, such as alpha particles, deposit a large amount of energy over short distances while following an almost linear path.[9] Due to their size, collisions with much lighter electrons do not disturb the path of alpha particles which continue to travel in a straight line inducing multiple ionization events. This is in contrast to beta particles, which are much

smaller and less energetic than alphas. Beta particles travel a non-linear path as collisions with orbital electrons in the surrounding tissues result in significant deflections from the initial trajectory.

As charged particles interact with the surrounding tissues, they can cause cell death through damage of the DNA present in the nucleus.[9] These ionization events are quite different between alpha and beta particles as the former rely on direct damage, whereas beta particles rely on indirect damage of DNA through the ionization of water. Direct ionization events happen through the alpha particle colliding with DNA, causing irreparable double stranded DNA breaks that are independent of hypoxia or cell cycle. This is contrasted by beta particles, which cause ionization of water and other organic molecules within the cell forming radicals such as hydroxyl, perhydroxyl and alkoxy radicals. These radicals are highly reactive and can cause irreversible damage to the DNA, such as single strand DNA damage, ultimately leading to impaired cell function and/or cell death.

1.6 Immunogenic Cell Death

A difficult task in designing effective cancer therapies is overcoming the natural or acquired immunosuppressant local environment that makes up many tumours.[61-63] Due to the downregulation of antigenic molecules, dendritic cell dysfunction and the presence of immunosuppressant cytokines in the tumour microenvironment, a patient's immune system may not be able to recognize and destroy cancer cells.[64, 65] The aim of many next generation cancer therapeutics is to "uncloak" the cancer cells, making them visible to the immune system for destruction.[65] This is a difficult task as not all cell death pathways stimulate a strong immune response and many immunotherapies can

struggle with long term effectiveness as tumours can up/down regulate certain cytokines rendering these therapies ineffective.[66, 67]

To overcome some of these issues, radiation therapy can be employed to induce cell death independently of cytokine regulation as it is an external stressor that does not act directly on the immune system.[68-71] When cancer cells are stressed by radiation they can present or release danger associated molecular patterns (DAMPs) such as ATP and HMBGB1.[67] The DAMPs act on receptors that are expressed on dendritic cells which leads to presentation of the tumour antigens to T-cells, eventually leading to tumour specific T-cells and anti-tumour immunity.[72] The so-called abscopal effect is rarely reported, but has been documented when a lesion outside of the irradiated field regresses.[73] The effect was first documented in 1953, and there were only 46 reported cases between 1969-2014.[73, 74] Unfortunately, the prevalence of these immunity events are limited, which might be due to the previously mentioned immunosuppressive tumour microenvironment.[75, 76]

1.7 Antibody Recruiting Small Molecule Therapies

In the last decade, advances in immunotherapy have had significant impact on the treatment of cancer and revolutionized the field of oncology.[77-81] Unfortunately, the leading therapies are only effective in specific types of cancer limiting the broad applicability of the treatment. In certain instances, particularly for solid tumours, they suffer from short term efficacy due to the development of tumour resistance, leading to disease relapse.[62]

An alternative form of immunotherapy, antibody-recruiting small molecules (ARMs), take advantage of endogenous antibodies to recruit immune cells to the site of disease leading to immune mediated destruction.[82-85] ARMs have two main components

(Figure 1-2): a target binding terminus (TBT), which interacts with the specific protein or receptor on the target cell, and an antibody binding terminus (ABT), which interacts with endogenous antibodies. The target cell, the ARM and the antibody make up a ternary complex which recruits effector cells and promotes immune mediated clearance (Figure 1-3). Having the ability to target specific tumour antigens and by leveraging the patient's own antibodies, this strategy is applicable to a wider variety of solid tumours than many traditional immunotherapies.

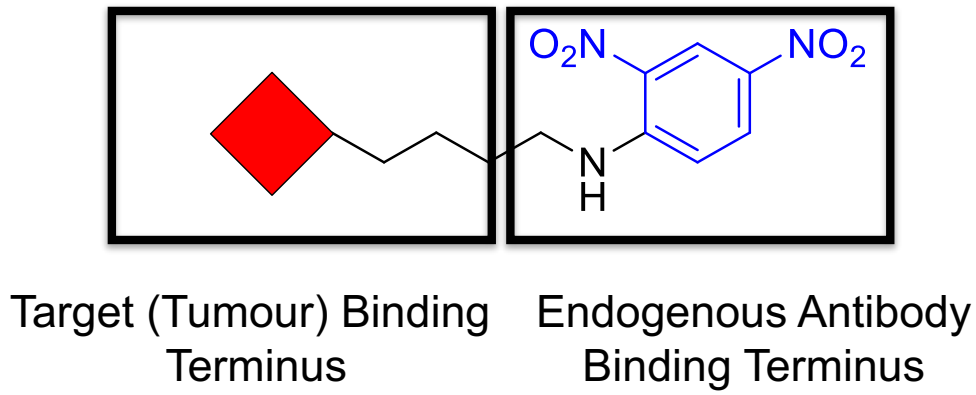

Figure 1-2. Schematic representation of an antibody recruiting small molecule that contains a targeting vector to bind a tumour and an antigen (a 2,4-dinitrophenyl group) for antibody recruitment.

There are two potential pathways for ARM stimulated clearance: complement dependent cytotoxicity (CDC) and antibody-dependent cellular cytotoxicity (ADCC).[86] CDC is part of the innate immunity pathway, and involves a complement protein, C1q, binding to the Fc region of the recruited antibody.[87] When the C1q binds more than one Fc region, the protein is activated through a conformational change which induces the production of a serine protease initiating the classical complement cascade. ADCC on the other hand involves the Fc region of the antibody binding to a Fc receptor on an immune cell leading to destruction of the target cell. This type of process is similar to that observed with therapeutic antibodies such as trastuzumab and rituximab.[88]

The initial approach to developing ARMs focused on a 2,4-dinitrophenyl (DNP) hapten as the ABT and a targeting vector for tumour associated proteins such as urokinase-type plasminogen activator receptor (uPAR), and PSMA.[82, 84, 89] Rullo *et al.* screened a variety of compounds containing a DNP antigen and a targeting vector for uPAR, a protein expressed on B16 melanoma tumours.[84] A two-colour flow cytometry antibody-dependent cellular phagocytosis (ADCP) assay showed dose-dependent phagocytosis with the lead construct, with maximum efficacy reported at 100 nM. A therapy study was performed in mice immunized to produce anti-DNP antibodies, bearing a melanoma tumour. Daily administration of the lead construct at doses of 20 or 100 mg/kg resulted in a median survival between 27 and 37 days compared to 17.5 days for the control mice. In 2011, Dubrovska *et al.* used a DNP-functionalized PSMA inhibitor to target human prostate cancer in a mouse with a fully humanized immune system.[82] Animals bearing a flank prostate cancer tumour were treated with 4 mg/kg of the ligand three times per week for two weeks. The treatment group had a 4.8-fold reduction in tumour growth rate compared to the control, and PSMA negative tumours showed no susceptibility towards the treatment. These results are promising and support the potential efficacy of ARMs, however no studies to our knowledge have been able to generate an anti-tumour response.

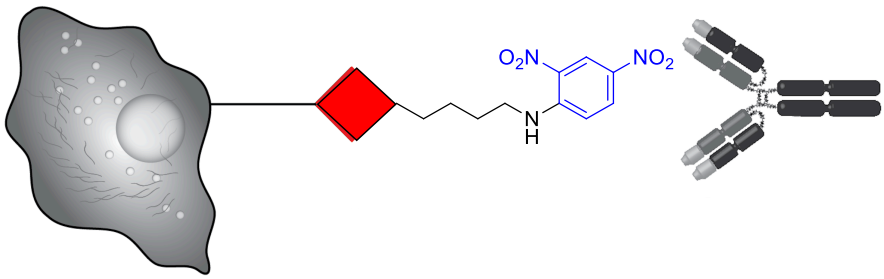

Figure 1-3. Schematic representation of a ternary complex consisting of a cancer cell, a DNP-based ARM (the red diamond is the TBT) and an antibody. Once the ternary complex forms, immune cells are recruited for ADCC of the cancer cell.

1.8 Combination Radiotherapy and Immunotherapy for Treatment of Cancer

Recently, it has been shown that combination radiotherapy and immunotherapy may be more efficacious than the corresponding monotherapies by working synergistically to overcome the immunosuppressant environment in tumours.[76, 90-93] Radiation therapy is known to induce immunogenic cell death, and when combined with immunotherapies a potent anti-tumour response can be generated.[90-93] One example that has shown success in phase II clinical trials, is the treatment of metastatic kidney cancer with stereotactic body radiation therapy in combination with interleukin-2 (IL-2).[94] IL-2 is a cytokine that functions by promoting and modulating T-cell activity and differentiation.[95] Irradiating up to 6 metastatic lesions in combination with IL-2 therapy was able to double the response rate with no significant increase in toxicity, compared to the IL-2 monotherapy.[94]

In addition, external beam radiation has been shown to sensitize previously unresponsive tumours to immune checkpoint inhibitors, such as anti-CTLA-4, while also sensitizing the distant, non-irradiated metastasis.[96] In a phase I clinical trial, 58 patients with metastatic or unresectable melanoma were treated with immune checkpoint blockade for CTLA-4 and PD-1, ipilimumab and nivolumab respectively, and 9 patients were treated with additional radiation therapy.[97] Improvement in response was noted in 33% of the patients receiving immunotherapy and RT, compared to 23% in the patients receiving only immunotherapy. Many of the reported clinical studies have been performed in small groups of patients that have exhausted other therapy

options. The results are encouraging, and larger clinical trials are active or recruiting in order to further evaluate combination radiotherapy and immunotherapy.

Although combining external beam radiation and immunotherapy has shown promise, only a small number of the lesions are irradiated. This poses a potential limitation as metastatic lesions can express unique tumour antigens, therefore the established T-cells may not be able to recognize metastases, which would persist.[98] Through changing the method of irradiation from external beam to TRT, it is more likely that metastases will be irradiated, which could improve systemic disease control and enhance long term immunity.

Despite the many examples of combination therapies using external beam radiation, there are few studies with TRT. One such preclinical example is immune checkpoint inhibitors (anti-PD-1, anti-PD-L1, and anti-CTLA-4 antibodies) in tandem with a beta emitting lutetium-177 radiopharmaceutical for treatment of melanoma. This study showed a survival advantage of 6-7 days for the group that received checkpoint and TRT and 1-5 days in the groups receiving checkpoint.[99] A 2018 preclinical study demonstrated the synergy of rituximab and a lutetium-labelled anti-CD37 antibody for treatment of NHL. It was found that mice treated with TRT and rituximab had a median survival of >222 days compared to 60 ± 9, 40 ± 11, and 31 ± 5 days for TRT, one or four doses of rituximab respectively.[100] The study was designed to show the strength of the combination therapy by using suboptimal doses of each of the monotherapies. In 2015, Ménager *et al.* used combination alpha RIT with adoptive T-cell therapy (ACT) in a preclinical multiple myeloma model.[101] On day 10 post tumour inoculation, bismuth-213 labelled rat anti-mouse CD138 was administered followed 24 hours later by ACT therapy. The combination of ACT and RIT significantly increased median

survival to 31 days compared to 28, 28, and 27 days for control, RIT or ACT monotherapies. This is relevant to the potential of combined TRT and immune stimulating therapies because the improved response is likely due to the radiation acting as an external stressor promoting tumour immunogenicity therefore increasing the recognition of the tumour by the T-cell therapy.

Based on the handful of examples of immunotherapy in combination with TRT and the plethora of data on combination external beam radiation studies, there is mechanistic rationale for the potential benefit of combining TRT and ARMs. The two components should work synergistically to cause direct tumour cell death while stimulating the immune system resulting in a systemic anti-tumour response and enhanced long term immunity to recurrence. Further, there is literature to support that immune cells, such as macrophages, can be activated when they are irradiated therefore it should be feasible to combine TRT and ARM therapy.[102-104] This can be achieved by administering an ARM with a TRT or combining both components into one molecule.

1.9 Radiolabelled Antibody Recruiting Small Molecules (R-ARMs)

There is evidence that suggests that optimal effectiveness of combination radiotherapy and immunotherapies is when both components are delivered simultaneously.[105, 106] This can be achieved by delivering both an ARM and a radiopharmaceutical to the tumour, but would require the development of two unique molecules with matched pharmacokinetic and mechanism of action profiles and complicates administration. Alternatively, it is possible to develop an ARM that carries a radionuclide; a radiolabelled antibody recruiting small molecule (R-ARM). A R-ARM platform offers the means to observe whether continuous cell targeted irradiation in the case with TRT, would better synergize with immune stimulation than external beam,

which delivers the full radiation dose over a shorter period of time. If the construct is designed correctly, it also allows for the comparison of how different types of radiation (e.g. Auger, alpha and beta) synergize with immune recruiting therapies.

R-ARMs are not well represented in the literature, with only one example to our knowledge. Genady and colleagues synthesized an iodinated-triazole, using the glutamate-urea-lysine inhibitor for PSMA and a 2,4-dinitrophenyl group for antibody recruitment.[107] The paper highlights the synergies between ARM therapy and TRT, such as the low concentrations (μM) required to initiate cell death and immune stimulation. They attempted to optimize linker length for both anti-DNP antibody recruitment and PSMA binding which proved to be difficult. The probe that had the lowest IC_{50} for PSMA was unable to recruit the antibody, and the probe that was best able to recruit the antibody had low uptake in the tumour. This article demonstrated a major issue surrounding ARMs, in that it was very difficult to generate a single molecule that would have high affinity for the target and the endogenous antibody while also having ideal pharmacokinetics. Further, these molecules must be designed in a way where the radioisotope is added in the final step which complicates the chemistry and requires unique molecules be created for each new tumour antigen being targeted. To alleviate these issues, research was initiated to develop a platform where the radiolabelled antibody recruiting portion of the molecule is kept constant, while incorporating a methodology for facile addition of a targeting vector through the use of bio-orthogonal chemistry.

1.10 References

1. https://www.cancer.gov/about-cancer/treatment/types/radiation-therapy#TRT (accessed November 11, 2019).

2. Jaffray, D. A.; Gospodarowicz, M. K., *Disease Control Priorities*. International Bank for Reconstruction and Development / The World Bank: Washington DC, 2015.
3. Frohlich, G.; Geszti, G.; Vizkeleti, J.; Agoston, P.; Polgar, C.*, et al.*, Dosimetric Comparison of Inverse Optimisation Methods Versus Forward Optimisation in Hdr Brachytherapy of Breast, Cervical and Prostate Cancer. *Strahlenther Onkol* **2019,** *195* (11), 991-1000.
4. Zalutsky, M. R.; Vaidyanathan, G., Astatine-211-Labeled Radiotherapeutics: An Emerging Approach to Targeted Alpha-Particle Radiotherapy. *Curr Pharm Des* **2000,** *6* (14), 1433-1455.
5. Brabander, T.; van der Zwan, W. A.; Teunissen, J. J. M.; Kam, B. L. R.; Feelders, R. A.*, et al.*, Long-Term Efficacy, Survival, and Safety of [(177)Lu-Dota(0),Tyr(3)]Octreotate in Patients with Gastroenteropancreatic and Bronchial Neuroendocrine Tumors. *Clin Cancer Res* **2017,** *23* (16), 4617-4624.
6. Baum, R. P.; Singh, A.; Schuchardt, C.; Kulkarni, H. R.; Klette, I.*, et al.*, (177)Lu-3bp-227 for Neurotensin Receptor 1-Targeted Therapy of Metastatic Pancreatic Adenocarcinoma: First Clinical Results. *J Nucl Med* **2018,** *59* (5), 809-814.
7. Cho, S. Y.; Gage, K. L.; Mease, R. C.; Senthamizhchelvan, S.; Holt, D. P.*, et al.*, Biodistribution, Tumor Detection, and Radiation Dosimetry of 18F-DCFBC, a Low-Molecular-Weight Inhibitor of Prostate-Specific Membrane Antigen, in Patients with Metastatic Prostate Cancer. *J Nucl Med* **2012,** *53* (12), 1883-1891.
8. Mortimer, J. E.; Bading, J. R.; Park, J. M.; Frankel, P. H.; Carroll, M. I.*, et al.*, Tumor Uptake of (64)Cu-DOTA-Trastuzumab in Patients with Metastatic Breast Cancer. *J Nucl Med* **2018,** *59* (1), 38-43.
9. Saha, G. B., Physics and Radiobiology of Nuclear Medicine. **2013**.
10. Makvandi, M.; Dupis, E.; Engle, J. W.; Nortier, F. M.; Fassbender, M. E.*, et al.*, Alpha-Emitters and Targeted Alpha Therapy in Oncology: From Basic Science to Clinical Investigations. *Target Oncol* **2018,** *13* (2), 189-203.
11. Reardon, K. A.; McIntosh, A. F.; Shilling, A. T.; Hagspiel, K. D.; Al-Osaimi, A.*, et al.*, Treatment of Primary Liver Tumors with Yttrium-90 Microspheres (Therasphere®) in High Risk Patients: Analysis of Survival and Toxicities. *Technol Cancer Res T* **2009,** *8* (1), 71-77.
12. Juergens, R. A.; Zukotynski, K. A.; Juneau, D.; Simms, R.; Forbes, J.*, et al.*, A Phase I Study of [225Ac]-FPI-1434 Radioimmunotherapy in Patients with IGF-1R Expressing Solid Tumors. Am Soc Clin Oncol: 2019.
13. Murray, R.; Giap, F.; Lin, R.; Kurtzhals, P.; Giap, H., Clinical Outcomes of Patients Treated with Accelerated Partial Breast Irradiation with High-Dose Rate Brachytherapy: Scripps Clinic Experience. *Transl Cancer Res* **2016,** *5* (1), 30-35.
14. Fisher, D. R., Alpha Particle Emitters in Medicine. In *Dosimetry of Administered Radionuclides*, Washington D.C., 1989.
15. Marcu, L.; Bezak, E.; Allen, B. J., Global Comparison of Targeted Alpha Vs Targeted Beta Therapy for Cancer: In Vitro, in Vivo and Clinical Trials. *Crit Rev Oncol Hematol* **2018,** *123*, 7-20.
16. Song, H.; Hobbs, R. F.; Vajravelu, R.; Huso, D. L.; Esaias, C.*, et al.*, Radioimmunotherapy of Breast Cancer Metastases with Alpha-Particle Emitter 225Ac: Comparing Efficacy with 213Bi and 90Y. *Cancer Res* **2009,** *69* (23), 8941-8948.

17. Pandit-Taskar, N., Targeted Radioimmunotherapy and Theranostics with Alpha Emitters. *J Med Imaging Radiat Sci* **2019**.
18. Scheinberg, D. A.; McDevit, M. R., Actinium-225 in Targeted Alpha-Particle Therapeutic Applications. *Curr Radiopharm* **2011,** *4* (4), 306-320.
19. Kim, Y. S.; Brechbiel, M. W., An Overview of Targeted Alpha Therapy. *Tumour Biol* **2012,** *33* (3), 573-590.
20. Simonson, R. B.; Ultee, M. E.; Hauler, J. A.; Alvarez, V. L., Radioimmunotherapy of Peritoneal Human Colon Cancer Xenografts with Site-Specifically Modified 212Bi-Labeled Antibody. *Cancer Res* **1990,** *50*, 985s-988s.
21. Couturier, O.; Supiot, S.; Degraef-Mougin, M.; Faivre-Chauvet, A.; Carlier, T.*, et al.*, Cancer Radioimmunotherapy with Alpha-Emitting Nuclides. *Eur J Nucl Med Mol Imaging* **2005,** *32* (5), 601-614.
22. Zalutsky, M. R.; Garg, P. K.; Friedman, H. S.; Bigner, D. D., Labeling Monoclonal Antibodies and F(Ab')2 Fragments with the Alpha-Particle-Emitting Nuclide Astatine-211: Preservation of Immunoreactivity and Invivo Localizing Capacity. *Proc Natl Acad Sci USA* **1989,** *86*, 7149-7153.
23. Cheng, J.; Ekberg, T.; Engstrom, M.; Nestor, M.; Jensen, H. J.*, et al.*, Radioimmunotherapy with Astatine-211 Using Chimeric Monoclonal Antibody U36 in Head and Neck Squamous Cell Carcinoma. *Laryngoscope* **2007,** *117* (6), 1013-1018.
24. Li, H. K.; Sugyo, A.; Tsuji, A. B.; Morokoshi, Y.; Minegishi, K.*, et al.*, Alpha-Particle Therapy for Synovial Sarcoma in the Mouse Using an Astatine-211-Labeled Antibody against Frizzled Homolog 10. *Cancer Sci* **2018,** *109* (7), 2302-2309.
25. Hallqvist, A.; Bergmark, K.; Back, T.; Andersson, H.; Dahm-Kahler, P.*, et al.*, Intraperitoneal Alpha-Emitting Radioimmunotherapy with (211)At in Relapsed Ovarian Cancer: Long-Term Follow-up with Individual Absorbed Dose Estimations. *J Nucl Med* **2019,** *60* (8), 1073-1079.
26. Zalutsky, M. R.; Reardon, D. A.; Akabani, G.; Coleman, R. E.; Friedman, A. H.*, et al.*, Clinical Experience with Alpha-Particle Emitting 211At: Treatment of Recurrent Brain Tumor Patients with 211At-Labeled Chimeric Antitenascin Monoclonal Antibody 81c6. *J Nucl Med* **2008,** *49* (1), 30-38.
27. Zalutsky, M. R.; Reardon, D. A.; Pozzi, O. R.; Vaidyanathan, G.; Bignerc, D. D., Targeted A-Particle Radiotherapy with 211At-Labeled Monoclonal Antibodies. *Nucl Med Biol* **2007,** *34* (7), 779-785.
28. Lucignani, G., Alpha-Particle Radioimmunotherapy with Astatine-211 and Bismuth-213. *Eur J Nucl Med Mol Imaging* **2008,** *35* (9), 1729-1733.
29. Weidner, J. W.; Mashnik, S. G.; John, K. D.; Ballard, B.; Birnbaum, E. R.*, et al.*, 225Ac and 223Ra Production Via 800 Mev Proton Irradiation of Natural Thorium Targets. *Appl Radiat Isot* **2012,** *70* (11), 2590-2595.
30. Borchardt, P. E.; Yuan, R. R.; Miederer, M.; McDevitt, M. R.; Scheinberg, D. A., Targeted Actinium-225 in Vivo Generators for Therapy of Ovarian Cancer. *Cancer Res* **2003,** *63*, 5084-5090.
31. Kelly, J. M.; Amor-Coarasa, A.; Ponnala, S.; Nikolopoulou, A.; Williams, C., Jr.*, et al.*, A Single Dose of (225)Ac-RPS-074 Induces a Complete Tumor Response in an Lncap Xenograft Model. *J Nucl Med* **2019,** *60* (5), 649-655.

32. Sathekge, M.; Bruchertseifer, F.; Knoesen, O.; Reyneke, F.; Lawal, I., *et al.*, (225)Ac-PSMA-617 in Chemotherapy-Naive Patients with Advanced Prostate Cancer: A Pilot Study. *Eur J Nucl Med Mol Imaging* **2019,** *46* (1), 129-138.
33. Swindle, P. W.; Kattan, M. W.; Scardino, P. T., Markers and Meaning of Primary Treatment Failure. *Urol Clin North Am* **2003,** *30* (2), 377-401.
34. Kratochwil, C.; Bruchertseifer, F.; Giesel, F. L.; Weis, M.; Verburg, F. A., *et al.*, 225Ac-PSMA-617 for PSMA-Targeted Alpha-Radiation Therapy of Metastatic Castration-Resistant Prostate Cancer. *J Nucl Med* **2016,** *57* (12), 1941-1944.
35. Feuerecker, B.; Knorr, K.; Beheshti, A.; Seidl, C.; D'Alessandria, C., *et al.*, Safety and Efficacy of Ac-225-PSMA-617 in Mcrpc after Failure of Lu-177-PSMA. *Nuklearmedizin* **2019,** *58* (02), L14.
36. Grinshtein, N.; Simms, R.; Hu, M.; Storozhuk, Y.; Moran, M., *et al.*, IGF-1R Targeted Alpha Therapeutic FPI-1434 Causes DNA Double-Stranded Breaks and Induces Regression in Preclinical Models of Human Cancer. *J Med Imag Radiat Sci* **2019,** *50* (1), S17-S18.
37. Apostolidis, C.; Molinet, R.; McGinley, J.; Abbas, K.; Mollenbeck, J., *et al.*, Cyclotron Production of Ac-225 for Targeted Alpha Therapy. *Appl Radiat Isot* **2005,** *62* (3), 383-387.
38. Morgenstern, A.; Apostolidis, C.; Bruchertseifer, F., Supply and Clinical Application of Actinium-225 and Bismuth-213. *Semin Nucl Med* **2020**.
39. Weidner, J. W.; Mashnik, S. G.; John, K. D.; Hemez, F.; Ballard, B., *et al.*, Proton-Induced Cross Sections Relevant to Production of 225Ac and 223Ra in Natural Thorium Targets Below 200 Mev. *Appl Radiat Isot* **2012,** *70* (11), 2602-2607.
40. Aliev, R. A.; Ermolaev, S. V.; Vasiliev, A. N.; Ostapenko, V. S.; Lapshina, E. V., *et al.*, Isolation of Medicine-Applicable Actinium-225 from Thorium Targets Irradiated by Medium-Energy Protons. *Solvent Extr Ion Exch* **2014,** *32* (5), 468-477.
41. Kojima, S.; Cuttler, J. M.; Shimura, N.; Koga, H.; Murata, A., *et al.*, Present and Future Prospects of Radiation Therapy Using Alpha-Emitting Nuclides. *Dose Response* **2018,** *16* (1), 1559325817747387.
42. Goncalves, C. F. L.; de Freitas, M. L.; Ferreira, A. C. F., Flavonoids, Thyroid Iodide Uptake and Thyroid Cancer-a Review. *Int J Mol Sci* **2017,** *18* (6), 1247-1252.
43. Johansen, K.; Woodhouse, N. J. Y.; Odugbesan, O., Comparison of 1073 Mbq and 3700 MBq Iodine-131in Postoperative Ablation of Residual Thyroid Tissue in Patients with Differentiated Thyroid Cancer. *J Nucl Med* **1991,** *32* (2), 252-254.
44. University of Michigan, Environment, Health and Saftey. Iodine-131 Radiological Safety Guide. 2018. https://ehs.umich.edu/wp-content/uploads/2016/04/Iodine-131.pdf (accessed November 12, 2019)
45. Nastos, K.; Cheung, V. T. F.; Toumpanakis, C.; Navalkissoor, S.; Quigley, A. M., *et al.*, Peptide Receptor Radionuclide Treatment and (131)I-MIBG in the Management of Patients with Metastatic/Progressive Phaeochromocytomas and Paragangliomas. *J Surg Oncol* **2017,** *115* (4), 425-434.
46. Watanabe, N.; Oriuchi, N.; Igarashi, H.; Higuchi, T.; Yukihiro, M., *et al.*, Preparation of Yttrium-90-Labeled Human Macroaggregated Albumin for Regional Radiotherapy. *Nucl Med Biol* **1997,** *24*, 465-469.
47. Geschwind, J. F.; Salem, R.; Carr, B. I.; Soulen, M. C.; Thurston, K. G., *et al.*, Yttrium-90 Microspheres for the Treatment of Hepatocellular Carcinoma. *Gastroenterology* **2004,** *127* (5 Suppl 1), S194-205.

48. Sanchez Ruiz, A. C.; de la Cruz-Merino, L.; Provencio Pulla, M., Role of Consolidation with Yttrium-90 Ibritumomab Tiuxetan in Patients with Advanced-Stage Follicular Lymphoma. *Ther Adv Hematol* **2014,** *5* (3), 78-90.
49. Morschhauser, F.; Radford, J.; Van Hoof, A.; Vitolo, U.; Soubeyran, P.*, et al.*, Phase Iii Trial of Consolidation Therapy with Yttrium-90-Ibritumomab Tiuxetan Compared with No Additional Therapy after First Remission in Advanced Follicular Lymphoma. *J Clin Oncol* **2008,** *26* (32), 5156-5164.
50. Conti, P. S.; White, C.; Pieslor, P.; Molina, A.; Aussie, J.*, et al.*, The Role of Imaging with 111In-Ibritumomab Tiuxetan in the Ibritumomab Tiuxetan (Zevalin) Regimen: Results from a Zevalin Imaging Registry. *J Nucl Med* **2005,** *46* (11), 1812-1818.
51. Salem, R.; Lewandowski, R. J.; Atassi, B.; Gordon, S. C.; Gates, V. L.*, et al.*, Treatment of Unresectable Hepatocellular Carcinoma with Use of 90Y Microspheres (Therasphere): Safety, Tumor Response, and Survival. *J Vasc Interv Radiol* **2005,** *16* (12), 1627-1639.
52. Murthy, R.; Nunez, R.; Szklaruk, J.; Erwin, W.; Madoff, D. C.*, et al.*, Yttrium-90 Microsphere Therapy for Hepatic Malignancy: Devices, Indications, Technical Considerations, and Potential Complications. *Radiographics* **2005,** *25*, S41-S55.
53. Ketring, A.; Ehrhardt, G.; Embree, M.; Bailey, K.; Tyler, T.*, et al.*, Production and Supply of High Specific Activity Radioisotopes for Radiotherapy Applications. *Alasbimn J* **2003,** *5* (19).
54. de Nijs, R.; Lagerburg, V.; Klausen, T. L.; Holm, S., Improving Quantitative Dosimetry in (177)Lu-DOTATATE SPECT by Energy Window-Based Scatter Corrections. *Nucl Med Commun* **2014,** *35* (5), 522-533.
55. Hennrich, U.; Kopka, K., Lutathera((R)): The First FDA- and EMA-Approved Radiopharmaceutical for Peptide Receptor Radionuclide Therapy. *Pharmaceuticals (Basel)* **2019,** *12* (3).
56. Uribe, C. F.; Esquinas, P. L.; Tanguay, J.; Gonzalez, M.; Gaudin, E.*, et al.*, Accuracy of (177)Lu Activity Quantification in SPECT Imaging: A Phantom Study. *EJNMMI Phys* **2017,** *4* (1), 2-22.
57. Hofman, M. S.; Violet, J.; Hicks, R. J.; Ferdinandus, J.; Thang, S. P.*, et al.*, [177 Lu]-PSMA-617 Radionuclide Treatment in Patients with Metastatic Castration-Resistant Prostate Cancer (LuPSMA Trial): A Single-Centre, Single-Arm, Phase 2 Study. *Lancet Oncol* **2018,** *19* (6), 825-833.
58. Calais, J.; Fendler, W.; Eiber, M.; Lassmann, M.; Dahlbom, M.*, et al.*, Resist-Pc Phase 2 Trial: 177Lu-PSMA-617 Radionuclide Therapy or Metastatic Castrate-Resistant Prostate Cancer. *J Urol* **2019,** *4S*, 1003-1004.
59. Ku, A.; Facca, V. J.; Cai, Z.; Reilly, R. M., Auger Electrons for Cancer Therapy - a Review. *EJNMMI Radiopharm Chem* **2019,** *4* (1), 2-36.
60. Kiess, A. P.; Minn, I.; Chen, Y.; Hobbs, R.; Sgouros, G.*, et al.*, Auger Radiopharmaceutical Therapy Targeting Prostate-Specific Membrane Antigen. *J Nucl Med* **2015,** *56* (9), 1401-1407.
61. Olcina, M. M.; Kim, R. K.; Melemenidis, S.; Graves, E. E.; Giaccia, A. J., The Tumour Microenvironment Links Complement System Dysregulation and Hypoxic Signalling. *Br J Radiol* **2018**, 20180069.
62. Restifo, N. P.; Smyth, M. J.; Snyder, A., Acquired Resistance to Immunotherapy and Future Challenges. *Nat Rev Cancer* **2016,** *16* (2), 121-126.

63. Gok Yavuz, B.; Gunaydin, G.; Gedik, M. E.; Kosemehmetoglu, K.; Karakoc, D.*, et al.*, Cancer Associated Fibroblasts Sculpt Tumour Microenvironment by Recruiting Monocytes and Inducing Immunosuppressive PD-1(+) Tams. *Sci Rep* **2019,** *9* (1), 3172-3187.
64. Rabinovich, G. A.; Gabrilovich, D.; Sotomayor, E. M., Immunosuppressive Strategies That Are Mediated by Tumor Cells. *Annu Rev Immunol* **2007,** *25*, 267-296.
65. Beatty, G. L.; Gladney, W. L., Immune Escape Mechanisms as a Guide for Cancer Immunotherapy. *Clin Cancer Res* **2015,** *21* (4), 687-692.
66. Krysko, D. V.; Denecker, G.; Festjens, N.; Gabriels, S.; Parthoens, E.*, et al.*, Macrophages Use Different Internalization Mechanisms to Clear Apoptotic and Necrotic Cells. *Cell Death Differ* **2006,** *13* (12), 2011-2022.
67. Krysko, D. V.; Garg, A. D.; Kaczmarek, A.; Krysko, O.; Agostinis, P.*, et al.*, Immunogenic Cell Death and DAMPS in Cancer Therapy. *Nat Rev Cancer* **2012,** *12* (12), 860-75.
68. Demaria, S.; Ng, B.; Devitt, M. L.; Babb, J. S.; Kawashima, N.*, et al.*, Ionizing Radiation Inhibition of Distant Untreated Tumors (Abscopal Effect) Is Immune Mediated. *Int J Radiat Oncol Biol Phys* **2004,** *58* (3), 862-870.
69. Demaria, S.; Formenti, S. C., Radiation as an Immunological Adjuvant: Current Evidence on Dose and Fractionation. *Front Oncol* **2012,** *2*, 1-7.
70. Pouget, J. P.; Georgakilas, A. G.; Ravanat, J. L., Targeted and Off-Target (Bystander and Abscopal) Effects of Radiation Therapy: Redox Mechanisms and Risk/Benefit Analysis. *Antioxid Redox Signal* **2018,** *29* (15), 1447-1487.
71. Walle, T.; Martinez Monge, R.; Cerwenka, A.; Ajona, D.; Melero, I.*, et al.*, Radiation Effects on Antitumor Immune Responses: Current Perspectives and Challenges. *Ther Adv Med Oncol* **2018,** *10*, 1758834017742575.
72. Kroemer, G.; Galluzzi, L.; Kepp, O.; Zitvogel, L., Immunogenic Cell Death in Cancer Therapy. *Annu Rev Immunol* **2013,** *31*, 51-72.
73. Abuodeh, Y.; Venkat, P.; Kim, S., Systematic Review of Case Reports on the Abscopal Effect. *Curr Probl Cancer* **2016,** *40* (1), 25-37.
74. Mole, R. H., Whole Body Irradiation — Radiobiology or Medicine? *Br J Radiol* **1953,** *26* (305), 234-241.
75. Ngwa, W.; Irabor, O. C.; Schoenfeld, J. D.; Hesser, J.; Demaria, S.*, et al.*, Using Immunotherapy to Boost the Abscopal Effect. *Nat Rev Cancer* **2018,** *18* (5), 313-322.
76. Vatner, R. E.; Cooper, B. T.; Vanpouille-Box, C.; Demaria, S.; Formenti, S. C., Combinations of Immunotherapy and Radiation in Cancer Therapy. *Front Oncol* **2014,** *4*, 1-15.
77. Aznar, M. A.; Tinari, N.; Rullan, A. J.; Sanchez-Paulete, A. R.; Rodriguez-Ruiz, M. E.*, et al.*, Intratumoral Delivery of Immunotherapy-Act Locally, Think Globally. *J Immunol* **2017,** *198* (1), 31-39.
78. Lee, T. H.; Cho, Y. H.; Lee, J. D.; Yang, W. I.; Shin, J. L.*, et al.*, Enhanced Antitumor Effect of Dendritic Cell Based Immunotherapy after Intratumoral Injection of Radionuclide Ho-166 against B16 Melanoma. *Immunol Lett* **2006,** *106* (1), 19-26.
79. Ziffels, B.; Pretto, F.; Neri, D., Intratumoral Administration of IL2- and TNF-Based Fusion Proteins Cures Cancer without Establishing Protective Immunity. *Immunotherapy* **2018,** *10* (3), 177-188.

80. Durgan, K.; Ali, M.; Warner, P.; Latchman, Y. E., Targeting Nkt Cells and PD-L1 Pathway Results in Augmented Anti-Tumor Responses in a Melanoma Model. *Cancer Immunol Immunother* **2011,** *60* (4), 547-558.
81. Nedrow, J. R.; Josefsson, A.; Park, S.; Ranka, S.; Roy, S.*, et al.*, Imaging of Programmed Cell Death Ligand 1: Impact of Protein Concentration on Distribution of Anti-PD-L1 Spect Agents in an Immunocompetent Murine Model of Melanoma. *J Nucl Med* **2017,** *58* (10), 1560-1566.
82. Dubrovska, A.; Kim, C.; Elliott, J.; Shen, W.; Kuo, T. H.*, et al.*, A Chemically Induced Vaccine Strategy for Prostate Cancer. *ACS Chem Biol* **2011,** *6* (11), 1223-1231.
83. Lu, Y.; Low, P. S., Folate Targeting of Haptens to Cancer Cell Surfaces Mediates Immunotherapy of Syngeneic Murine Tumors. *Cancer Immunol Immunother* **2002,** *51* (3), 153-162.
84. Rullo, A. F.; Fitzgerald, K. J.; Muthusamy, V.; Liu, M.; Yuan, C.*, et al.*, Re-Engineering the Immune Response to Metastatic Cancer: Antibody-Recruiting Small Molecules Targeting the Urokinase Receptor. *Angew. Chem. Int. Edit.* **2016,** *55* (11), 3706-3710.
85. Chirkin, E.; Muthusamy, V.; Mann, P.; Roemer, T.; Nantermet, P. G.*, et al.*, Neutralization of Pathogenic Fungi with Small-Molecule Immunotherapeutics. *Angew. Chem. Int. Edit.* **2017,** *56* (42), 13216-13220.
86. Sheridan, R. T.; Hudon, J.; Hank, J. A.; Sondel, P. M.; Kiessling, L. L., Rhamnose Glycoconjugates for the Recruitment of Endogenous Anti-Carbohydrate Antibodies to Tumor Cells. *ChemBioChem* **2014,** *15* (10), 1393-1398.
87. Murphy, K.; Weaver, C., *Janeway's Immunobiology, 9th Edition*. Garland Science/Taylor & Francis Group: New York, NY, 2017.
88. Iida, S.; Kuni-Kamochi, R.; Mori, K.; Misaka, H.; Inoue, M.*, et al.*, Two Mechanisms of the Enhanced Antibody-Dependent Cellular Cytotoxicity (ADCC) Efficacy of Non-Fucosylated Therapeutic Antibodies in Human Blood. *BMC Cancer* **2009,** *9* (58), 1-12.
89. Schrand, B.; Clark, E.; Levay, A.; Capote, A. R.; Martinez, O.*, et al.*, Hapten-Mediated Recruitment of Polyclonal Antibodies to Tumors Engenders Antitumor Immunity. *Nat Commun* **2018,** *9* (1), 1-10.
90. Ahmed, K. A.; Kim, S.; Arrington, J.; Naghavi, A. O.; Dilling, T. J.*, et al.*, Outcomes Targeting the PD-1/PD-L1 Axis in Conjunction with Stereotactic Radiation for Patients with Non-Small Cell Lung Cancer Brain Metastases. *J Neurooncol* **2017,** *133* (2), 331-338.
91. Chao, Y.; Xu, L.; Liang, C.; Feng, L.; Xu, J.*, et al.*, Combined Local Immunostimulatory Radioisotope Therapy and Systemic Immune Checkpoint Blockade Imparts Potent Antitumour Responses. *Nat. Biomed. Eng.* **2018,** *2* (8), 611-621.
92. Pike, L. R. G.; Bang, A.; Ott, P.; Balboni, T.; Taylor, A.*, et al.*, Radiation and PD-1 Inhibition: Favorable Outcomes after Brain-Directed Radiation. *Radiother Oncol* **2017,** *124* (1), 98-103.
93. Reynders, K.; Illidge, T.; Siva, S.; Chang, J. Y.; De Ruysscher, D., The Abscopal Effect of Local Radiotherapy: Using Immunotherapy to Make a Rare Event Clinically Relevant. *Cancer Treat Rev* **2015,** *41* (6), 503-510.
94. Hannan, R.; Ishihara, D.; Louder, K.; Ahn, C.; Margulis, V.*, et al.*, Phase Ii Trial of High-Dose Interleukin-2 (IL-2) and Stereotactic Radiation Therapy (SABR)

for Metastatic Clear Cell Renal Cell Carcinoma (Ccrcc): Interim Analysis. *J Clin Oncol* **2016,** *34* (2_suppl), 532-532.
95. Jiang, T.; Zhou, C.; Ren, S., Role of IL-2 in Cancer Immunotherapy. *Oncoimmunology* **2016,** *5* (6), e1163462.
96. Demaria, S.; Coleman, C. N.; Formenti, S. C., Radiotherapy: Changing the Game in Immunotherapy. *Trends Cancer* **2016,** *2* (6), 286-294.
97. Barker, C.; Postow, M.; Kronenberg, S.; Ma, J.; Yamada, Y.*, et al.*, Concurrent Radiation Therapy (Rt), Ipilimumab (Ipi) and/or Nivolumab (Nivo) on a Phase 1 Clinical Trial. *Int J Radiat Oncol* **2015,** *93* (3), S210-S211.
98. Cordon-Cardo, C.; Fuks, Z.; Drobnjak, M.; Moreno, C.; Eisenbach, L.*, et al.*, Expression of Hla-a,B,C Antigens on Primary and Metastatic Tumor Cell Populations of Human Carcinomas. *Cancer Res* **1991,** *51*, 6372-6380.
99. Choi, J.; Beaino, W.; Fecek, R. J.; Fabian, K. P. L.; Laymon, C. M.*, et al.*, Combined VLA-4-Targeted Radionuclide Therapy and Immunotherapy in a Mouse Model of Melanoma. *J Nucl Med* **2018,** *59* (12), 1843-1849.
100. Repetto-Llamazares, A. H. V.; Malenge, M. M.; O'Shea, A.; Eiriksdottir, B.; Stokke, T.*, et al.*, Combination of (177) Lu-Lilotomab with Rituximab Significantly Improves the Therapeutic Outcome in Preclinical Models of Non-Hodgkin's Lymphoma. *Eur J Haematol* **2018,** *101* (4), 522-531.
101. Menager, J.; Gorin, J. B.; Maurel, C.; Drujont, L.; Gouard, S.*, et al.*, Combining Alpha-Radioimmunotherapy and Adoptive T Cell Therapy to Potentiate Tumor Destruction. *PLoS One* **2015,** *10* (6), e0130249.
102. Coates, P. J.; Rundle, J. K.; Lorimore, S. A.; Wright, E. G., Indirect Macrophage Responses to Ionizing Radiation: Implications for Genotype-Dependent Bystander Signaling. *Cancer Res* **2008,** *68* (2), 450-456.
103. Conrad, S.; Ritter, S.; Fournier, C.; Nixdorff, K., Differential Effects of Irradiation with Carbon Ions and X-Rays on Macrophage Function. *J Radiat Res* **2009,** *50* (3), 223-231.
104. Leblond, M. M.; Pérès, E. A.; Moulin, D.; Anfray, C.; Divoux, D.*, et al.*, M2 Macrophages Are More Resistant Than M1 Macrophages Following Radiation Therapy in the Context of Glioblastoma. *Oncotarget* **2017,** *8* (42), 72597-72612.
105. Skrepnik, T.; Sundararajan, S.; Cui, H.; Stea, B., Improved Time to Disease Progression in the Brain in Patients with Melanoma Brain Metastases Treated with Concurrent Delivery of Radiosurgery and Ipilimumab. *Oncoimmunology* **2017,** *6* (3), e1283461.
106. Dovedi, S. J.; Adlard, A. L.; Lipowska-Bhalla, G.; McKenna, C.; Jones, S.*, et al.*, Acquired Resistance to Fractionated Radiotherapy Can Be Overcome by Concurrent PD-L1 Blockade. *Cancer Res* **2014,** *74* (19), 5458-5468.
107. Genady, A. R.; Janzen, N.; Banevicius, L.; El-Gamal, M.; El-Zaria, M. E.*, et al.*, Preparation and Evaluation of Radiolabeled Antibody Recruiting Small Molecules That Target Prostate-Specific Membrane Antigen for Combined Radiotherapy and Immunotherapy. *J Med Chem* **2016,** *59* (6), 2660-2673.

Chapter 2 – A Versatile Platform for the Development of Radiolabelled Antibody Recruiting Small Molecules

Disclaimer: Adapted with permission from Stephanie M. Rathmann, Afaf R. Genady, Nancy Janzen, Varun Anipindi, Shannon Czorny, Anthony F. Rullo, John F. Valliant. A Versatile Platform for the Development of Radiolabelled Antibody Recruiting Small Molecules.

2.1 Abstract

Building on clinical case reports of the abscopal effect, there has been considerable interest in the synergistic effects of radiation and immunotherapies for the treatment of cancer. Here, we describe the first radiolabelled antibody-recruiting small molecule that can chelate a variety of cytotoxic radionuclides as well as recruit endogenous antibodies. The platform consists of a dinitrophenyl hapten to recruit endogenous antibodies to elicit effector cell recruitment, a chelate capable of binding diagnostic and therapeutic radiometals, and a tetrazine for bio-orthogonal coupling with *trans*-cyclooctene modified targeting vectors. The dinitrophenyl-tetrazine ligand showed dose-dependent antibody recruitment and internalization by effector cells *in vitro* and delivery of the [^{177}Lu]Lu-complex to sites of calcium accretion *in vivo,* which was achieved using both active and pre-targeting strategies.

2.2 Introduction

Radiation therapy is the most widely used treatment for cancer with over 7 million procedures performed globally each year.[1] There is growing evidence that radiation can induce a beneficial immune response, notably increased effector $CD8^+$ T-cell function, which can lead to the regression of distant non-irradiated metastases.[2-8] The so-named abscopal effect has been observed in a small subset of patients where studies are

underway to better harness the therapeutic potential by combining external beam radiation with immunotherapies including anti-PD-1 and anti-CTLA-4 antibodies.[2, 3, 6, 9-12]

An alternative strategy to achieving a more robust immune response is to develop targeted radionuclide-based therapies that simultaneously engage the adaptive immune system.[13] The abscopal effect is thought to arise from radiation-induced transfer of tumour specific antigens to dendritic cells which in turn enables T-cells to seek out cancer cells at distant lesions.[3] The frequency of abscopal events could be enhanced by molecules that deliver radiation to tumours and mark cells for antibody-dependant cellular cytotoxicity (ADCC). Antibodies present on the surface of a tumour can bind to innate immune cells, such as monocytes or natural killer cells, through the Fc portion of the antibody. Once recruited to the tumour site, these innate immune cells are capable of destroying antibody-tagged cells as well as pick up tumour antigens from the radiation-damaged cells.

ADCC has been achieved through the use of antibody recruiting small molecules (ARMs) which recruit endogenous (or exogenous) hapten specific antibodies to tumour cells. Once the cell, ARM, and antibody form a ternary complex, the immune system is stimulated and the cell destroyed through plasma complement proteins and activation of effector cells (Figure 2-1).[14] The traditional approach to create ARMs involves conjugating a hapten, such as 2,4-dinitrophenyl (DNP), which has been shown to bind endogenous anti-DNP antibodies,[14-17] to a targeting molecule where notable examples include ARMs against Prostate Specific Membrane Antigen (PSMA) and Urokinase Plasminogen Activator Receptor (uPAR).[14, 16, 18] Rather than create unique ARMs for each target, the aim was to develop a general purpose platform and the first

radiolabelled-ARM (R-ARM) possessing a chelate to bind radiometals and a tetrazine to allow for the high yielding and bio-orthogonal inverse electron-demand Diels-Alder (IEDDA) ligation to a wide range of *trans*-cyclooctene (TCO)-derived targeting molecules. This platform offers the hitherto unknown opportunity to compare the efficacy of monotherapies (ADCC versus radionuclide therapy) administered alone or sequentially and to simultaneously combine these therapies using a single construct.

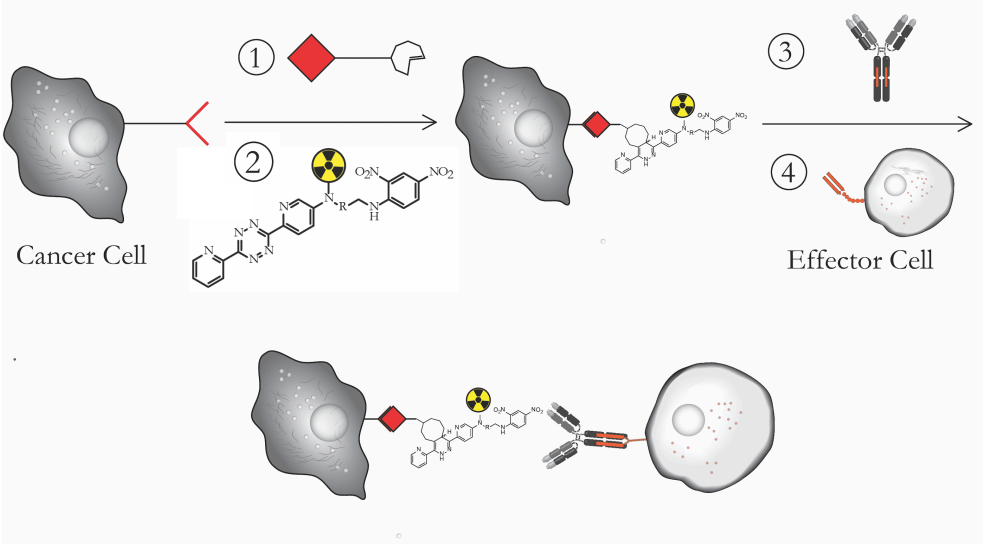

Figure 2-1. Schematic representation of a radiolabelled-antibody recruiting small molecule (R-ARM) platform engaged in immune cell recruitment. 1) Binding of a *trans*-cyclooctene functionalized targeting vector to a tumour cell 2) Coupling of a separately administered radiolabelled tetrazine derivative containing a dinitrophenyl hapten 3) Recruitment of anti-DNP antibodies which in turn 4) attracts effector cells leading to antibody dependent cellular cytotoxicity.

2.3 Results and Discussion

The design of the lead construct involves three key components; a dinitrophenyl (DNP) group for antibody recruiting, a 1,4,7,10-tetraazacyclododecane-1,4,7,10-tetraaceticacid (DOTA) chelate for radiolabelling with radiometals and a tetrazine, which acts as a site for functionalization with a TCO-targeting vector. The synthesis of the target, compound **7**, involved coupling 1-chloro-2,4-dinitrobenzene to a decaethylene glycol (PEG-10) linker. The linker size was selected based on literature

data on the minimum distance required between the cell binding and DNP termini to allow for antibody recruiting and formation of ternary complexes.[16] To link the DNP antigen and the tetrazine, our first strategy involved coupling the previously reported tetrazine, **1**[19], to Fmoc-Lys(Boc)-OH to produce **2a** in 85% yield (Scheme 2-1). Traditional deprotection of Fmoc with piperidine was not successful as piperidine caused decomposition of the tetrazine. However, the Fmoc-deprotection was done using diethylamine to produce **2b** in 35% yield. Attempts to conjugate **2b** with the DNP derivative **3**, prepared separately, or its NHS active ester, **4**, were not successful. As an alternative route to build the desired construct, we tried to couple Boc-Lys(Boc)-OH to **4** but the free amino group of the lysine was not reactive enough to form the desired adduct. Finally, the target compound was synthesized following the pathway shown in Scheme 2-2. The DNP derivative **4** was coupled to the free amino group of Boc-(L)-Lys-OH. Compound **5** was coupled to **1** using PyBOP where **6** was obtained in modest yield (44%). Deprotection of the Boc analogue with TFA was successful and the product readily coupled to the activated chelate (i.e. a DOTA-NHS-ester), to give compound **7**, which was isolated in 57% yield. The DOTA-like chelate was selected as it can be labelled with a range of different radiometals including lutetium-177, which is a beta and gamma emitter that is currently used to treat a variety of tumour types including prostate and neuroendocrine.[20, 21]

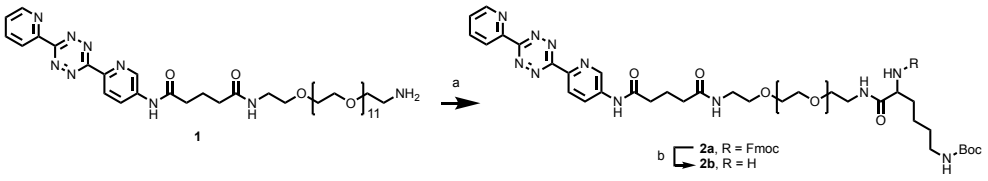

Scheme 2-1 . a) Fmoc-Lys(Boc)-OH, PyBOP, DIPEA, DMF, RT; b) DEA, RT. Fmoc = Fluorenylmethyloxycarbonyl, PyBOP = (benzotriazol-1-yloxy)tripyrrolidinophosphonium hexafluorophosphate, DIPEA = N,N-diisopropylethylamine, DMF = dimethylformamide, DEA = Diethylamine.

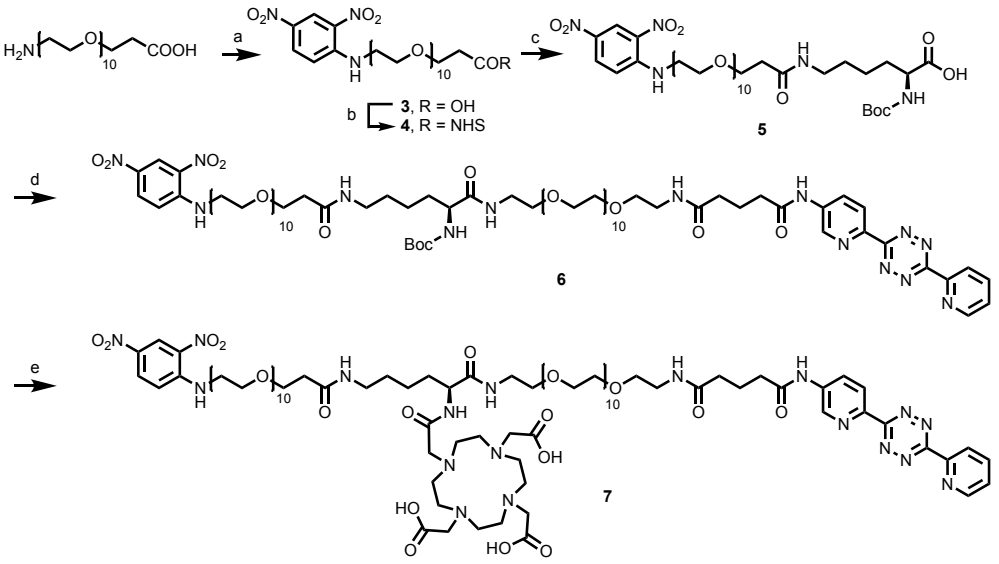

Scheme 2-2. a) 1-Chloro-2,4-dinitrobenzene, TEA, ethanol 80 °C; b) NHS, EDC, DCM; c) Boc-(L)-Lys-OH, DIPEA, DCM-ACN; d) **1**[19], PyBOP, DIPEA, DMF; e) i. TFA, DCM, ii. DOTA-NHS-ester, DMF. TEA = triethylamine, NHS = *N*-hydroxysuccinimide, EDC = 1-ethyl-3-(3-dimethylaminopropyl)carbodiimide, DCM = dichloromethane, Boc = *tert*-butyloxycarbonyl, DIPEA = *N,N*-diisopropylethylamine, ACN = acetonitrile, PyBOP = (benzotriazol-1-yloxy)tripyrrolidinophosphonium hexafluorophosphate, DMF = dimethylformamide, TFA = trifluoroacetic acid.

The next step was to screen **7** for its ability to bind anti-DNP antibodies, which is necessary to elicit an immune response *in vivo*. In addition, compound **9** (Figure 2-2) was screened to ensure that the DNP-antigen retains the ability to recruit anti-DNP antibodies after the IEDDA reaction of the tetrazine with a TCO-vector. Due to the radioactive nature of the target compound, preliminary screening studies were performed using **7** to prevent contamination of the instrumentation. The initial assay was a competitive colorimetric enzyme-linked immunosorbent assay (ELISA) with an alkaline phosphatase (AP) functionalized anti-DNP antibody (anti-DNP-AP).[22] Following an established procedure, DNP functionalized bovine serum albumin (BSA) was coated on an ELISA plate followed by the addition of anti-DNP-AP and compound **7** or **9** where dinitrophenol was used as a positive control. The results (Figure 2-2, A) show the average absorbance of 4 conditions; i) no ligand competitor, ii) 7.5 nmol **7**,

iii) 7.5 nmol **9**, iv) 7.5 nmol dinitrophenol. When the ELISA was performed with no ligand, a high absorbance of approximately 1.0 was seen which is due to the antibody interacting with the DNP-BSA on the plate. In both ii) and iii) the competitors (**7** and **9**) were able to interact with the antibody in solution, preventing it from binding to the DNP-BSA on the plate which resulted in a lower absorbance signal of approximately 0.1. The final condition was 7.5 nmol DNP, which acted as a positive control with a slightly higher absorbance value of 0.5 that indicated some antibody was still bound to the DNP-BSA on the plate. The difference in binding between ii), iii) and iv) is likely due to the aniline-type backbone of **7** and **9**, which has been reported to have a higher affinity for anti-DNP antibodies compared to phenols, where the average intrinsic association constant (K_0) values for 2,4-dinitroaniline and 2,4-dinitrophenol are 22 nM^{-1} and 2.7 nM^{-1} respectively.[23]

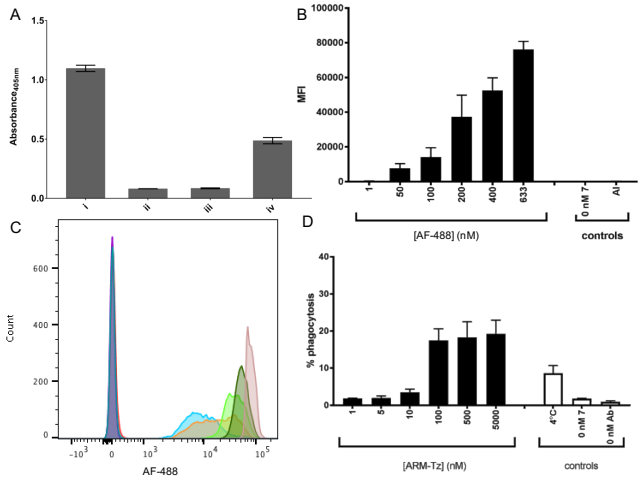

Figure 2-2. ELISA based antibody recruitment, flow cytometry-derived antibody recruitment and ligand mediated phagocytosis assay results. Data from: A) an ELISA assay measuring dose dependent recruitment of anti-DNP antibodies by **7**; absorbance at 405 nm: i) ligand free control (0 nmol **7**) ii) 7.5 nmol **7**, iii) 7.5 nmol **9**, iv) 7.5 nmol 2,4-dinitrophenol. B) Bar graph showing the dose-dependent antibody recruitment of AF-488 (anti-DNP Alexa-Fluor 488) with streptavidin beads pre-treated with **7** (AI = auto-inhibition). C) Flow cytometry derived histogram representing the dose-dependent antibody recruitment of AF-488 with streptavidin beads pre-treated with **7**. D) Bar graph

showing the extent of antibody-dependent cellular phagocytosis and dose-dependent internalization of beads modified with **7** by U937 monocytes (ARM-Tz = **7**).

The ability to form a ternary complex was assessed further by flow cytometry.[15] Streptavidin coated microspheres were treated with a commercially available TCO-derivative of biotin, which was subsequently combined with the DNP-functionalized tetrazine **7** and an anti-DNP antibody labelled with Alexa Fluor 488 (AF-488). Flow cytometry showed that as the amount of antibody was increased, the mean fluorescence intensity (MFI) of the microsphere population increased in a dose dependent manner, which is consistent with ternary complex formation (Figure 2-2, B). In the absence of **7**, the measured signal was comparable to background indicating there was no ternary complex formation and minimal non-specific binding of the antibody to the biotin-TCO modified beads. Consistent with the proposed mechanism, ternary complex formation could be suppressed through auto-inhibition (AI) via the addition of excess **7**.

The ability of **7** to not only promote anti-DNP recruitment but to also direct immune effector cell function was tested using an antibody dependent cellular-phagocytosis (ADCP) assay employing U937 monocytes. Antibody-dependent phagocytosis by the monocytes was assessed by flow cytometry where single live U937 cells and microspheres were gated and the Vybrant DiD, AF-488 double positive events were identified to calculate the phagocytosis efficiency. In order to determine the optimal bead to effector cell ratio, a preliminary experiment was performed testing three ratios 1:1, 1:4, and 1:8 ratio respectively. Prior to the addition of antibody or effector cells, the beads were incubated with an excess of both biotin-TCO and ARM to ensure the beads were fully saturated. The percent phagocytosis of the beads were 26%, 57% and 65% for 1:1, 1:4 and 1:8 ratio of beads to effector cells respectively. Two controls were performed with no antibody and no ARM, in the presence of 1:4 ratio of beads to

effector cells, resulting in a percent phagocytosis of 0.7 and 28% respectively where the latter is likely due to non-specific phagocytosis by the activated macrophages. Based on the results of this experiment, the remaining ADCP experiments were performed with a bead to effector cell ratio of 1:4 as the results were significantly different relative to the controls and a further increase in the number of effector cells did not result in a large increase in phagocytosis.

Fluorescent streptavidin microspheres were subsequently coated with TCO-biotin and incubated with varying concentrations of **7** (1-5000 nM), along with a human anti-DNP antibody and U937 monocytes at 37°C for 1 hour. The results (Figure 2-2, C, D) are consistent with a concentration-dependent increase in phagocytosis, which appears to plateau at approximately 100 nM of **7**, likely due to saturation of the available TCO-groups on the microspheres. As expected, phagocytosis was not observed in the absence of **7** or anti-DNP antibody, and was reduced by approximately 9% when experiments were performed at 4°C.

The use of a DOTA chelate provides the opportunity to label **7** with diagnostic and therapeutic radionuclides. The former can be used to assess the ability of candidate compounds to bind specific targets, assess pharmacokinetics using non-invasive imaging and quantitative tissue counting, while therapeutic isotopes can be used to deliver ionizing radiation as a second and complementary kill mechanism to ADCC. For these initial studies, radiolabelling was achieved by combining compound **7** (48 nmol) with [^{177}Lu]$LuCl_3$ in 0.2 M NH_4OAc at pH 5.5 and heating at 60°C for 5 min. The product, **8**, was purified by HPLC and C18 SPE, where the latter was used to remove TFA and salts. The SPE fraction containing the product was diluted with sterile isotonic saline ready for use in biological studies. Isolated radiochemical yields ranged

from 51-54% while the radiochemical purity of the isolated product was consistently 96-99% (Figure 2-3). The radiolabelled product was stable in solution overnight (19 h) and had a specific activity of 158-377 MBq mg^{-1}.

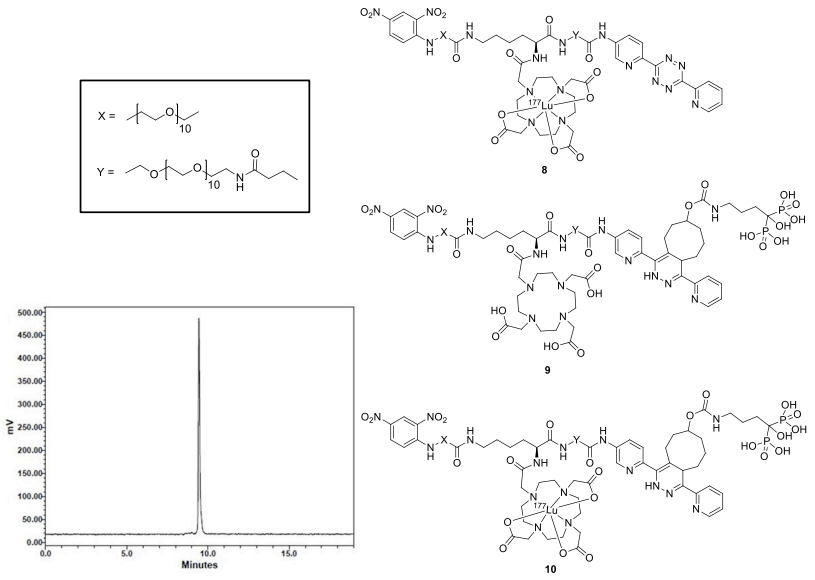

Figure 2-3. Structures of compounds **8**-**10** and the gamma HPLC radiochromatogram of compound **8** (see supporting information for additional details).

Before assessing the targeting capabilities of the platform, the distribution and pharmacokinetics of **8** alone were determined in normal mice as a basis of comparison. At 1, 4 and 24 hours post-injection, compound **8** showed predominately renal clearance, which is consistent with the measured Log P (-1.9). By one hour post-injection, the radioactivity had cleared most tissues with a small amount (3.14 ± 0.05 %ID g^{-1}) remaining in the kidneys which decreased further by 24 hours (1.38 ± 0.16 %ID g^{-1}). Based on the rapid renal clearance and minimal non-specific binding, the pharmacokinetics were nearly ideal for both active and pre-targeting strategies.

To demonstrate **8** can be targeted, a TCO-functionalized bisphosphonate (TCO-BP) was used as a proof of concept.[24] Bisphosphonates accumulate in areas of high bone turnover where radiolabelled derivatives, such as [^{99m}Tc]Tc-MDP are used for imaging bone metastases.[25, 26] Furthermore, calcium accretion is an attractive target to screen novel tetrazines because experiments can be done in normal mice using uptake in joints (shoulders and knees) as an indicator of effective targeting.[27] The first study employed an active targeting strategy that involved combining **8** and TCO-BP to form **10** before injection (Figure 2-3). The conjugate consistently showed around 9 and 15 %ID g^{-1} in the shoulder and knee respectively at 1, 4 and 24 hours post-injection (2-4, A). The bone uptake confirmed the ability of the bisphosphonate to direct the radiolabelled DNP derivative, as bone uptake was minimal in the biodistribution study of **8**. However, compound **10** did show significant accumulation in the lungs, notably 171.26 ± 15.04 %ID g^{-1} at 1 hr, which decreased to 128.27 ± 24.45 and 47.57 ± 3.93 %ID g^{-1} at 4 and 24 hours respectively. Other non-target uptake included the spleen and liver, having 14.91 ± 0.85 and 6.81 ± 0.23 %ID g^{-1} at 24 hours respectively suggesting the possible formation of a particulate that was not observed with the ligand alone.[28] Unfortunately attempts to filter the product prior to injection were not successful as nearly 100% of the activity for both **8** and **10** stuck to the filter.

In an attempt to address the unwanted uptake in the lungs and other non-target tissues, the pre-targeting capabilities of the TCO-tetrazine pair were exploited. Mice were injected with 20 mg kg^{-1} of TCO-BP, which was allowed to circulate for 1 hour, followed by **8**. Mice were sacrificed at 1, 4 and 24 hours and tissues and fluids counted (2-4, B). The results showed a substantial decrease in lung uptake compared to active targeting results, having only 1.65 ± 0.38 %ID g^{-1} in the lungs at 24 hours. Pre-targeting

also showed good uptake in the shoulder (6.95 ± 1.00 %ID g^{-1} at 24 hours) and the knee (9.99 ± 1.24 %ID g^{-1} at 24 hours) which were within 5 %ID g^{-1} of the values observed for active targeting. In order to validate the results that were seen in the biodistribution studies, a SPECT imaging study was performed using both active and pre-targeting strategies. The two SPECT/CT images (Figure 2-5) are set to the same threshold, and mice were injected with similar amounts of radioactivity and imaged after 24 hours. The images are consistent with the biodistribution studies in that the off-target uptake in the lungs using the active targeting strategy was reduced significantly through the use of the pre-targeting. This result emphasized the versatility of the R-ARM platform in that if active targeting results in off-target uptake that is detrimental to achieving a positive therapeutic window, a pre-targeting strategy, taking advantage of the bio-orthogonal click reaction, can be employed.

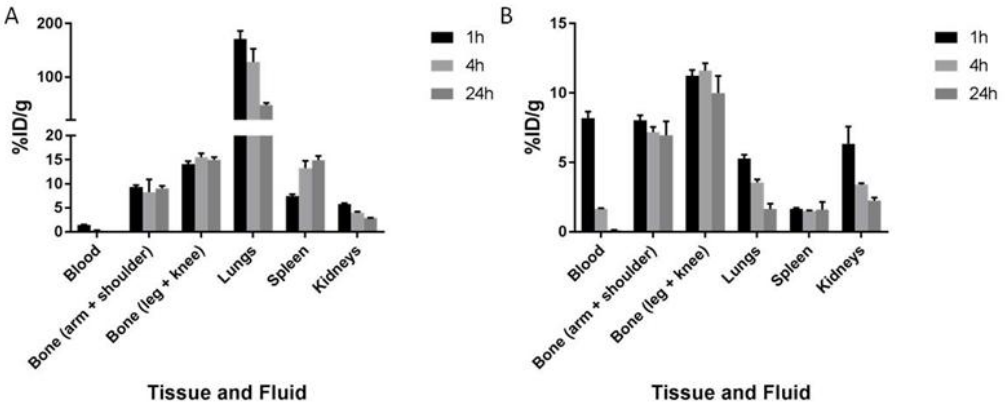

Figure 2-4. A) Biodistribution data for **10** administered to Balb/c mice (n = 3 at 1 and 24 hours, n = 2 at 4 hours). Data at the time points indicated are expressed as the mean percent injected dose per gram (%ID g^{-1}) ± SEM; B) Biodistribution data for a pre-targeting study where 20 mg kg^{-1} of TCO-BP was administered to Balb/c mice (n = 3 per time point) 1 h prior to **8**. Tissues were collected at 1, 4 and 24 h post administration of the labelled compound. Data are expressed as the mean percent injected dose per gram (%ID g^{-1}) ± SEM.

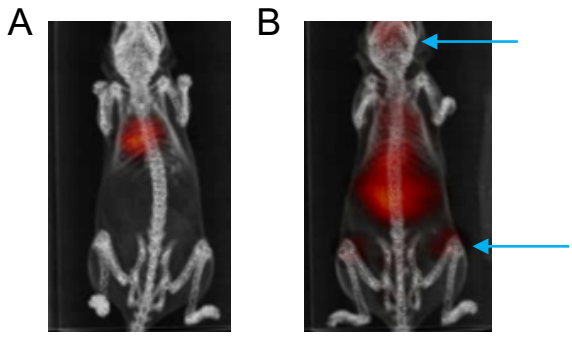

Figure 2-5. A) SPECT/CT image at 24 hours post-injection data for compound **10** administered to a Balb/c mouse. The image shows significant the lung uptake (red colour). B) SPECT/CT image at 24 hours post-injection for a pre-targeting study where 20 mg kg^{-1} of TCO-BP was administered to a Balb/c mouse 1 hour prior to compound **8**. The arrows indicate site of uptake in the skeleton (knees and skull). Images were set to the same intensity threshold.

2.4 Conclusion

A radiolabelled-antibody recruiting molecule that can be rapidly and selectively coupled to targeting vectors using bio-orthogonal chemistry was created. Compound **7** showed dose dependant antibody and human monocyte recruitment via antibody dependent cellular phagocytosis. High yielding radiolabelling with lutetium-177, a clinically relevant therapeutic radionuclide, was achieved and attractive pharmacokinetic properties observed in mice. The ability to use different targeting strategies with **8** was demonstrated and included both active and pre-targeting approaches with a TCO-bisphosphonate vector. The pre-targeting approach was able to significantly reduce the high lung uptake which was observed with active targeting. The versatility of the tetrazine was leveraged through reactions with both TCO-biotin and TCO-BP for *in vitro* and *in vivo* work respectively, demonstrating the wide potential of this platform. Due to the high lung uptake seen with active targeting and the rapid internalization of the TCO-BP, the presented bone target could not be used for therapy. The described work outlines how the platform could be used to explore targeting tumour

biomarkers through establishing a TCO-targeting vector with minimal internalization and ideal pharmacokinetics.

2.5 Experimental Section

2.5.1 Chemistry: Materials and Instrumentation

Chemicals and reagents for synthesis were purchased from Sigma-Aldrich, Conjuprobe, ChemPep and Macrocyclics and used without further purification. Flash chromatography on silica gel was performed using SiliCycle Silica. Biological reagents from multiple sources were used and are listed in the text below. Compound **5** was prepared following a literature procedure.[19] ^{1}H and ^{13}C NMR spectra were measured on a Bruker Avance AV-600 spectrometer (^{1}H = 600.13 MHz, ^{13}C = 150.90 MHz) where chemical shifts are expressed in ppm (δ units), and coupling constants are reported in Hz. HRMS data were obtained using a Waters Micromass Global Ultima Q-TOF in ESI mode. High-performance liquid chromatography (analytical and semi-preparative) were performed on a Waters 1525 Binary HPLC system connected to a Bioscan γ-detector and a 2998 photodiode array detector monitoring at 254 nm or a Waters 2545 binary gradient model, 2998 photodiode array equipped with a 2767 sample manager. For analytical runs, a Waters X-Bridge column (5 µm, 4.6 × 100 mm, C18) or a Waters Xselect (5 µm, 4.6 × 50 mm, CSH C18) were used, at a flow rate of 1.0 mL/min. For semi-preparative HPLC, a Waters X-Bridge column (5 µm, 10.0 × 100 mm, C18) was used, at a flow rate of 4.0 mL/min. The elution method for HPLC procedures were: Method A: Solvent A = 0.1% v/v trifluoroacetic acid (TFA) in water; Solvent B = 0.1% v/v TFA in acetonitrile: gradient elution, 95-26% A (0-14 min) and Method B: Solvent A = 0.1% v/v formic acid (FA) in water; Solvent B = 0.1% v/v FA in acetonitrile: gradient elution, 90-10% A (1-10 min). ^{177}Lu was produced by the McMaster Nuclear

Reactor (MNR, Hamilton, Ontario) using the ^{176}Lu (p,γ) reaction and was provided as a solution of [^{177}Lu]$LuCl_3$ in 0.01M HCl.

2.5.2 (9*H*-fluoren-9-yl)methyl *tert*-butyl (1,5,43-trioxo-1-((6-(6-(pyridin-2-yl)-1,2,4,5-tetrazin-3-yl)pyridin-3-yl)amino)-9,12,15,18,21,24,27,30,33,36,39-undecaoxa-6,42-diazaoctatetracontane-44,48-diyl)dicarbamate (2a)

N,N-Diisopropylethylamine (100 μL, 0.430 mmol) was added to a mixture of **1** (30 mg, 0.034 mmol), FMOC-Lys(Boc)-OH (16 mg, 0.034 mmol), and (benzotriazol-1-yloxy)tris(dimethylamino)phosphonium hexafluorophosphate (21 mg, 0.047 mmol) in DMF (2 mL). The reaction mixture was stirred at room temperature for 24 h. The solvent was evaporated under reduced pressure and the product purified by column chromatography on silica using a gradient of MeOH in DCM (0-10%) giving **2a** as a pink powder (38 mg, 85%). ^{1}H NMR ($CDCl_3$, 600 MHz): δ 9.80 (bs, 1H), 9.05 (b, 1H), 8.96 (d, *J* = 6Hz, 1H), 8.71 (t, 2H, *J* = 12 Hz, 2H), 8.62 (dd, *J* = 6, 3Hz, 1H), 8.01 (t, *J* = 12Hz, 1H), 7.71 (d, *J* = 6Hz, 3H), 7.60–7.54 (m, 3H), 7.36 (d, *J* = 6Hz, 2H), 7.34–7.24 (bs, 7H), 5.88-5.73 (m, 2H), 4.75 (bs, 1H), 4.36-4.31 (m, 2H), 4.16 (t, *J* = 6Hz, 2H), 3.60-3.54 (m, 32H), 3.43 (bs, 5H), 3.06 (bs, 2H), 2.55 (t, *J* = 6Hz, 2H), 2.38 (t, *J* = 6Hz, 2H), 2.07 (m, 2H), 1.80 (bs, 1H), 1.65 (m, 1H), 1.48-1.33 (m, 15 H) ppm. ^{13}C NMR (150 MHz, $CDCl_3$): δ 174.2, 172.8, 172.5, 162.3, 163.1, 160.1, 159.8, 156.3, 150.6, 149.8, 143.8, 143.2, 141.7, 141.3, 139.1, 138.0, 127.7, 127.2, 127.1, 126.8, 125.4, 125.1, 124.6, 120.0, 116.4, 114.5, 70.3, 70.2, 70.0, 70.0, 69.7, 66.9, 54.9, 47.1, 40.1, 39.5, 39.4, 36.0, 35.0, 32.4, 29.5, 28.4, 22.5, 21.4 ppm**.** HRMS (ESI, *m/z*): Calcd for $C_{67}H_{96}N_{11}O_{18}$ ($[M+H]^+$): 1342.6935, Found: 1342.6906.

2.5.3 *tert*-butyl (44-amino-1,5,43-trioxo-1-((6-(6-(pyridin-2-yl)-1,2,4,5-tetrazin-3-yl)pyridin-3-yl)amino)-9,12,15,18,21,24,27,30,33,36,39-undecaoxa-6,42-diazaoctatetracontan-48-yl)carbamate (2b)

Compound **2a** (0.030 g, 0.0224 mmol) was dissolved in DCM (2 mL). Diethylamine (200 μL) was diluted with DCM (1 mL) and added dropwise to the previous solution. The reaction mixture was stirred at RT for 2h. The resulting solution was concentrated under reduced pressure and the product was purified by column chromatography on silica using a gradient of MeOH in DCM (0-20%) to give **2b** as a pink oily solid (9 mg, 35%). MS (ESI, *m/z*): Calcd for $C_{52}H_{86}N_{11}O_{16}$ ($[M+H]^+$): 1120.4.

2.5.4 1-((2,4-dinitrophenyl)amino)-3,6,9,12,15,18,21,24,27,30-decaoxatritriacontan-33-oic acid (3)

To a solution of α-amine-ω-propionic acid decaethylene glycol (0.202 g, 0.381 mmol) in 3 mL of ethanol, was added 1-chloro-2,4-dinitrobenzene (0.084 g, 0.415 mmol) and triethylamine (0.105 mL, 0.755 mmol). The reaction was heated to reflux overnight with stirring. The reaction mixture was concentrated and the desired compound isolated by column chromatography (1-10% MeOH:DCM) to give compound **3** as a yellow oil (0.219 g , 83%). ^{1}H NMR ($CDCl_3$, 600 MHz) 9.11 (d, J = 2.6 Hz, 1H), 8.79 (bs, 1H), 8.25 (dd, J = 9.5, 2.5 Hz, 1H), 6.96 (d, J = 9.6 Hz, 1H), 3.82 (t, J = 5.3 Hz, 2H), 3.75 (t, J = 6.1 Hz, 2H), 3.68 (m, 4H), 3.62 (m, 38H), 2.58 (t, J = 5.9 Hz, 2H). ^{13}C NMR ($CDCl_3$, 150 MHz) 174.05, 148.46, 136.05, 130.51, 130.25, 124.29, 114.17, 70.77, 70.63, 70.60, 70.54, 70.52, 70.47, 70.28, 68.60, 66.62, 43.26, 35.03. HRMS (ESI): Calcd for $C_{29}H_{49}N_3O_{16}$ $[M-H]^-$ m/z 694.3040, found 694.3045.

2.5.5 2,5-dioxopyrrolidin-1-yl 1-((2,4-dinitrophenyl)amino)-3,6,9,12,15,18,21,24,27,30-decaoxatritriacontan-33-oate (4)

To a solution of **3** (0.219 g, 0.381 mmol) in 2.5 mL DCM was added EDC·HCl (0.102 g, 0.533 mmol) and NHS (0.0614 g, 0.533 mmol), and the solution stirred at room temperature overnight. The reaction mixture was concentrated and the desired compound isolated by column chromatography (5% MeOH:DCM) to isolate compound **4** as a yellow oil (0.209 g, 69%). ^{1}H NMR ($CDCl_3$, 600 MHz) 9.13 (d, J = 2.6 Hz, 1H), 8.79 (bs, 1H), 8.26 (dd, J = 9.5, 2.5 Hz, 1H), 6.96 (d, J = 9.6 Hz, 1H), 3.84 (m, 4H), 3.69 (m, 5H), 3.60 (m, 38H), 2.90 (t, J = 5.3 Hz, 2H), 2.83 (bs, 4H). ^{13}C NMR ($CDCl_3$, 150 MHz) 168.96, 166.73, 148.45, 136.10, 130.54, 130.27, 124.33, 114.11, 70.79, 70.72, 70.70, 70.64, 70.57, 68.62, 65.73, 43.29, 32.17, 25.59. HRMS (ESI): Calcd for $C_{33}H_{52}N_4O_{18}$ $[M+NH_4]^+$ m/z 810.3615, found 810.3624.

2.5.6 2,5-dioxopyrrolidin-1-yl 1-((2,4-dinitrophenyl)amino)-3,6,9,12,15,18,21,24,27,30-decaoxatritriacontan-33-oate 39-((tert-butoxycarbonyl)amino)-1-((2,4-dinitrophenyl)amino)-33-oxo-3,6,9,12,15,18,21,24,27,30-decaoxa-34-azatetracontan-40-oate (5)

To a solution of **4** (0.200 g, 0.252 mmol) was added Boc-Lys-OH (0.081 g, 0.328 mmol) in 2:1 v/v ACN/DCM (3 mL), and then DIPEA (0.131 mL, 0.757 mmol) and the mixture stirred at room temperature for 48 h. The resulting solution was concentrated under reduced pressure and the desired compound was isolated by column chromatography (0-15% MeOH:DCM 1%TEA) as a yellow oil (0.199 g, 85%). ^{1}H NMR ($CDCl_3$, 600 MHz): δ 9.13 (d, J = 2.6 Hz, 1H), 8.79 (bs, 1H), 8.26 (dd, J = 9.7, 2.6 Hz, 1H), 6.96 (d, J = 9.7 Hz, 1H), 6.79 (bs, 1H) 5.33 (m, 1H), 4.23 (m, 1H), 3.83-3.63 (m, 45H), 3.22 (q, J = 6.7 Hz, 2H), 2.46 (t, J = 5.6 Hz, 2H), 1.82 (m, 1H), 1.73 (m, 1H), 1.51 (m, 2H), 1.51-1.42 (m, 12H) ppm. ^{13}C NMR ($CDCl_3$, 150 MHz) 174.40, 172.29, 155.61, 148.45, 136.06, 130.1, 130.25, 124.28, 114.17, 79.65, 70.74, 70.64, 70.62, 70.48, 70.36, 70.24,

70.12, 68.61, 67.24, 53.65, 53.25, 43.27, 41.92, 38.96, 36.74, 32.00, 28.89, 28.38, 25.44, 22.24, 11.88. HRMS (ESI): Calcd for $C_{40}H_{69}N_5O_{19}$ $[M+Na]^+$ m/z 946.4484, found 946.4515.

2.5.7 *tert*-butyl (1-((2,4-dinitrophenyl)amino)-33,40,78,82-tetraoxo-82-((6-(6-(pyridin-2-yl)-1,2,4,5-tetrazin-3-yl)pyridin-3-yl)amino)-3,6,9,12,15,18,21,24,27,30,44,47,50,53,56,59,62,65,68,71,74-henicosaoxa-34,41,77-triazadooctacontan-39-yl)carbamate (6)

N,N-Diisopropylethylamine (0.150 mL, 0.646 mmol) was added to a stirring mixture of **5** (57.3 mg, 0.065 mmol), **1** (60.0 mg, 0.065 mmol), and (benzotriazol-1-yloxy)tris(dimethylamino)phosphonium hexafluorophosphate (40 mg, 0.090 mmol) in DMF (2 mL). After 24 h at RT, the reaction mixture was concentrated and the desired compound isolated by column chromatography (5-15% MeOH:DCM) giving **6** as an orange oil (51 mg, 44%). ^{1}H NMR ($CDCl_3$, 600 MHz): δ 9.86 (bs, 1H, NH), 9.12 (m, 2H, CH), 9.00 (d, *J* = 6 Hz, 1H, CH), 8.75 (m, 2H, CH), 8.65 (m, 1H, CH), 8.26 (dd, *J* = 8, 6 Hz, 1H, CH), 8.07 (m, 1H, NH), 7.63 (m, 1H, NH), 7.20 (bs, 1H, NH), 7.11 (bs, 1H, NH), 6.96 (d, *J* = 18 Hz, 1H, CH), 5.52 (bs, 1H, NH), 4.04 (bs, 1H, CH), 3.82 (t, *J* = 6 Hz, 2H, CH), 3.71-3.58 (m, 76H, CH), 3.52 (m, 2H, CH), 3.44 (m, 4H, CH), 3.22 (m, 2H, CH), 2.60 (t, *J* = 6 Hz, 2H, CH), 2.53 (m, 2H, CH), 2.41 (t, *J* = 6 Hz, 2H, CH), 2.08 (m, 2H, CH), 1.77 (m, 1H, CH), 1.62 (m, 1H, CH), 1.51 (m, 2H, CH), 1.42-1.35 (m, 11H, CH) ppm; ^{13}C NMR (150 MHz, $CDCl_3$): δ 174.4, 173.3, 172.9, 163.2, 163.0, 159.9, 159.6, 155.8, 150.5, 149.6, 148.4, 142.9, 141.4, 139.2, 138.3, 130.3, 127.5, 126.9, 125.5, 124.7, 124.3, 116.3, 114.4, 114.1, 70.7, 70.6, 70.4, 70.3, 70.2, 70.1, 70.0, 69.7, 69.6, 68.6, 67.0, 54.6,43.2, 39.5, 39.3, 39.1, 36.1, 36.0, 35.0, 32.0, 29.7, 28.7, 28.3, 22.6, 21.4 ppm; HRMS (ESI): Calcd for $C_{81}H_{132}N_{14}O_{31}$ $[M+2H]^{2+}$ m/z 899.4664, found 899.4665.

2.5.8 2,2',2''-(10-(4-(1-((2,4-dinitrophenyl)amino)-33-oxo-3,6,9,12,15,18,21,24,27,30-decaoxa-34-azaoctatriacontan-38-yl)-2,5,43,47-tetraoxo-47-((6-(6-(pyridin-2-yl)-1,2,4,5-tetrazin-3-yl)pyridin-3-yl)amino)-9,12,15,18,21,24,27,30,33,36,39-undecaoxa-3,6,42-triazaheptatetracontyl)-1,4,7,10-tetraazacyclododecane-1,4,7-triyl)triacetic acid (7)

Compound **6** (30.0 mg, 0.017 mmol) was stirred for 30 min at room temperature in a mixture of TFA (1 mL) and DCM (2 mL). After evaporation, the residue was dissolved in dry DCM (2 mL), NHS-DOTA (15.0 mg, 0.020 mmol) and triethylamine (0.040 mL, 0.27 mmol) were added and the mixture was stirred for 12 h. After evaporation, the residue was dissolved in water and purified by semi-preparative HPLC. After lyophilization, **7** (21 mg, 57%) was obtained as a waxy orange solid. ^{1}H NMR (CD_3OD, 600 MHz): δ 9.06 (d, *J* = 4 Hz, 1H, CH), 8.95 (d, *J* = 6, 1H, CH), 8.86 (d, *J* = 6 Hz, 1H, CH), 8.79 (d, *J* = 6 Hz, 1H, CH),8.74 (d, *J* = 6 Hz, 1H, CH), 8.44 (dd, *J* = 8, 6 Hz, 1H, CH), 8.23 (m, 2H, CH), 7.78 (t, *J* = 6 Hz, 1H, CH), 7.15 (d, *J* = 12 Hz, 1H, CH), 4.19 (bs, 2H, CH), 3.74 (t, *J* = 6 Hz, 3H, CH), 3.65-3.53 (m, 108H, CH), 3.49 (m, 6H, CH), 3.32 (m, 8H, CH), 3.24 (m, 4H, CH), 3.18 (m, 4H, CH), 2.48 (t, *J* = 6 Hz, 2H, CH), 2.36 (m, 2H, CH), 2.27 (t, *J* = 6 Hz, 2H, CH), 1.98 (m, 3H, CH), 1.87 (m, 1H, CH), 1.73 (m, 1H, CH), 1.61-1.44 (m, 3H, CH), 1.33-1.21 (m, 5H, CH) ppm; ^{13}C NMR (150 MHz, CD_3OD): δ 175.4 , 174.5, 174.0, 164.3, 164.2, 150.7, 150.3, 150.0, 142.3, 141.0, 140.7, 137.1, 131.2, 129.0, 128.8, 126.7, 126.1, 124.9, 116.4, 71.6, 71.5, 71.4, 71.3, 71.2, 70.6, 70.0, 68.3, 48.1, 44.1, 40.4, 40.3, 40.1, 37.7, 36.9, 36.1, 30.2, 27.3, 24.1, 22.6 ppm; HRMS (ESI): Calcd for $C_{92}H_{150}N_{18}O_{36}$ $[M+2H]^{2+}$ m/z 1042.5303, found 1042.5347.

2.5.9 Biology: Materials and Instrumentation

Antibodies and reagents were purchased from Sigma-Aldrich, Life Technologies, ThermoFisher, Bethyl Laboratories, Polysciences Inc, Acro Biosystems and Conjuprobe and used without further purification. ELISA absorbance measurements

were performed with a Tecan infinite M1000 plate reader. Flow Cytometry was performed using a BD LSRII™ flow cytometer (BD Biosciences, USA).

2.5.10 ELISA

A competition ELISA similar to that described by Huang *et al.* was conducted.[22] Briefly, 1 mg/mL DNP-BSA (Life Technologies, A23018) in sterile PBS (ThermoFisher, 10010023) was diluted 1/1000 with coating buffer (Bethyl Laboratories, E107) and transferred (100 µL) to a 96 well plate. Following a 1 h incubation at room temperature, the wells were washed three times with 200 µL of ELISA Wash buffer (Bethyl Laboratories, E106). ELISA blocking buffer (Bethyl Laboratories, E104) was then added to each well (200 µL) and left to incubate at room temperature for 0.5 h. The plate was washed three times with ELISA wash buffer (200 µL/well) before the addition of 100 µL of either 2,4-dinitrophenol (Sigma-Aldrich, D19850; range 0.3125 nmol – 40 nmol per well), **7** (7.5 nmol per well), **10** (7.5 nmol per well) in sample diluent (ELISA Blocking buffer + 0.05% Tween 20) or sample diluent alone followed by 100 µL of anti-DNP-AP (Sigma-Aldrich, A2831; 64 ng/mL). Following a 1 h incubation at room temperature, the plate was washed three times with ELISA wash Buffer (200 µL/well). To each well, 100 µL of PNPP substrate was added and the plate incubated in the dark at room temperature for 0.5 h. To quench the reaction, 50 µL of 2 M NaOH was added to each well and the absorbance subsequently measured at 405 nm on a plate reader.

2.5.11 Antibody Recruitment Assay

Streptavidin coated microspheres (Polysciences Inc, 1.05×10^8 microspheres/mL) were dispensed and centrifuged at 10000 × g for 5 min. The supernatant was removed and the microspheres resuspended in 500 µL of FACS buffer (0.5% BSA in PBS), and centrifuged. The supernatant was removed and the washing repeated two more times. The microspheres were then resuspended in FACS buffer at a concentration of 5×10^7 microspheres/mL and incubated with excess Biotin-TCO (Conjuprobe,1 µL of 21.9 mM solution in 1:1 DMSO:FACS buffer) for 30 min at 4°C. The microspheres were diluted to 500 µL with FACS buffer and washed as described above. The microspheres were then resuspended in 40 µL of FACS buffer, of which 4 µL was removed for a control. To the microspheres was added **7** (18 µL of 2.4 mM solution in FACS buffer) and the mixture incubated for 10 min at room temperature. The suspension was diluted to 500 µL with FACS buffer and washed as described above. The microspheres were resuspended in 360 µL of FACS buffer oh which 40 µL removed, centrifuged and resuspended in 38 µL of FACS buffer at which point 2 µL of 7 was added. The remaining 320 µL of microspheres was split into 19 µL aliquots and 1 µL of appropriate antibody stock (20× in FACS buffer) was added to each sample. The samples were incubated for 30 min at room temperature at which point the samples were diluted to 500 µL with FACS buffer and washed as described above. Each sample was resuspended in 300 µL of FACS buffer and read by flow cytometry. All experiments had three controls: (i) no ligand, **7** (ii) no antibody (iii) auto-inhibition sample with excess ligand **7**. The samples were run on a flow cytometer and the raw data was analyzed using FlowJo software (FlowJo, OR). Forward and side scatter parameters were used to identify singular beads and AF-488 fluorescence intensity was examined

using histogram plots. The median fluorescence intensity of AF-488 on the beads was tabulated, and data from samples in duplicate was represented as bar graph as mean ± SD in GraphPad Prism. Data is a representative of two independent experiments run in duplicate.

2.5.12 Effector cell culture

The human monocytic cell line U937 was obtained from ATCC and cultured in RPMI 1640 growth medium containing 2 mM glutamine (11875), 10% FBS (12483020), 2 mM L-glutamine (25030), 1 mM sodium pyruvate (11360), 10mM HEPES (15630), 1% Penicillin Streptomycin (15140) and 4.7% D-glucose (Sigma G8769). The cells were propagated as per supplier recommendations and maintained at 37°C, 5% CO_2. For experiments, cells were used at passage 6. When necessary, monocyte differentiation was achieved by adding 0.1 mg/mL IFN-γ (15 µL/10 mL of cells) to the culture media containing the required number of cells and incubating at 37°C, 5% CO_2 for 24 h. On the day of the assay, the cells were washed with PBS, and a small aliquot removed to count. The cells were resuspended in serum free RPMI at 1.0×10^6 cells/mL and 1 mL removed as a control. Vybrant DiD Cell-Labeling Solution (Thermofisher, V22887) was added to the cells to a final concentration of 1.9 µM and they were incubated at 37°C for 30 min. The cells were then pelleted and washed two times with serum free RPMI. The cells were washed with Assay Media (AM - 10% low IgG FBS in phenol free RPMI) and resuspended in AM at a concentration of 8.0×10^6 cells/mL for use in the assay.

2.5.13 Dual colour flow cytometry-based antibody dependent cellular phagocytosis assay

Streptavidin Fluoresbrite® microspheres (Polysciences Inc, 1.05 × 10^8 microspheres/mL) were dispensed, diluted to 500 µL with AM and centrifuged at 10000 × g for 5 min. The supernatant was removed and the microspheres resuspended in 500 µL of AM and the washing repeated two more times. The microspheres were then resuspended at a concentration of 5 × 10^7 microspheres/mL in AM and incubated with excess Biotin-TCO (1 µL of 21.9 mM solution in 1:1 DMSO:AM) for 30 min at 4°C. The microspheres were diluted to 500 µL with AM and washed as described above. The microspheres were then resuspended in 540 µL of AM, and dispensed into triplicate 19 µL aliquots for conditions 1-9 and an additional 19 µL for sample 10 (control). The samples were centrifuged at 10000 × g for 5 min and the supernatant removed. To each sample (excluding sample 9) was added 25 µL of human anti-DNP IgG1 (Acro Biosystems, 400 nM in AM), followed by 25 µL of the appropriate ligand (**7**) stock (excluding sample 8). To samples 8 and 9 were added 25 µL of AM in place of antibody or the test ligand. To each sample was added 4 × 10^5 U937 cells or AM where no cells were added. The samples were centrifuged at 200 × g for 2 min and then incubated at 37°C for 1 h, except sample 7 (100 nM **7**) which was incubated at 4°C for 1 h. The samples were diluted with 200 µL of AM and analyzed by flow cytometry. Data was analyzed by FlowJo software (FlowJo LLC, OR) and GraphPad Prism. Debris and dead cells were excluded, and forward and side scatter parameters were used to identify monocytes and singular microspheres, and represented on a bivariate plot of Vybrant DiD and AF488 (Flouresbrite). Non-phagocytosed beads were identified as single positive DiD^- $AF488^+$ events and phagocytosed beads were identified as double-positive Vybrant DiD^+ $AF488^+$ events. To assess phagocytosis efficiency, the

proportion of beads phagocytosed by U937 monocytes was normalized to the total population of beads in the samples (% phagocytosis = % phagocytosed beads / (% non-phagocytosed beads + % phagocytosed beads) × 100). Data is mean ± SD of triplicates of 3 independent experiments.

2.5.14 Radiochemistry General

Radioactive measurements were performed using a dose calibrator (Capintec, Remsey, NJ, USA) or a Perkin Elmer Wizard 1470 Automatic Gamma Counter. *Caution:* lutetium-177 is radioactive and should only be handled in an appropriately licensed and equipped laboratory.

2.5.15 Radiolabelling

To a solution of **7** (100 µg, 48 nmol) in 100 µL of 0.2M NH_4OAc (pH 5.5) was added [^{177}Lu]$LuCl_3$ (31-74 MBq). The reaction mixture was heated to 60°C for 5 min at which point the desired compound was isolated by HPLC. The peak that was collected was diluted with 6 mL of distilled water. The reaction mixture was loaded onto a Waters C18 Sep-pak cartridge that was pre-conditioned with 5 mL of acetonitrile followed by 5 mL of water. The cartridge was washed with 10 mL of distilled water followed by 400 µL of ethanol. The compound was eluted with 600 µL of ethanol and diluted with sterile saline for injection with radiochemical yields of 51-54% and radiochemical purity of >99% (HPLC Rt = 9.35 min, method A).

2.5.16 Preparation of 10

To a solution of TCO-BP (200 µg, 416 nmol) in 100 µL of normal saline was added **8** (13.7 MBq) in 2 mL normal saline 10% ethanol (v/v). The mixture was allowed to shake for 10 min prior to HPLC analysis. As would be expected for tetrazine reactions multiple isomers appeared (HPLC max peak Rt =8.71 min, method A).

2.5.17 Animal Studies General

All animal studies were approved by the Animal Research Ethics Board at McMaster University. Mice were maintained under clean conditions in an established animal facility with 12 hour light/dark cycles and given food and water ad libitum.

2.5.18 Biodistribution study of compound 8

Female, 5-6 week old, CD1 mice ordered from Charles River Laboratory (Kingston, NY) were injected with approximately 0.25 MBq of **8**. At 1 h, 4 h and 24 h post-injection (n = 3 per time point), mice were anesthetized with 3% isoflurane and euthanized by cervical dislocation. Blood, adipose, adrenals, bone, brain, gall bladder, heart, kidneys, large intestine and caecum (with contents), liver, lungs, pancreas, skeletal muscle, small intestine (with contents), spleen, stomach (with contents), thyroid/trachea, urine + bladder and tail were collected, weighed and counted in a gamma counter. Decay correction was used to normalize organ activity measurements to time of dose preparation for data calculations with respect to injected dose (i.e. %ID/g)

2.5.19 Biodistribution study of compound 10

Female, 6-8 week old, Balb/c mice were injected with approximately 0.55 MBq of **10**. At 1 h, 4 h and 24 h post-injection (n = 3 per time point for 1 h and 24 h, n = 2 for 4 h), mice were anesthetized with 3% isoflurane and euthanized by cervical dislocation. Blood, adipose, adrenals, bone (arm bones including shoulder and leg bones including knee joint), brain, gall bladder, heart, kidneys, large intestine and caecum (with contents), liver, lungs, pancreas, skeletal muscle, small intestine (with contents), spleen, stomach (with contents), thyroid/trachea, urine + bladder and tail were collected, weighed and counted in a gamma counter. Decay correction was used to normalize

organ activity measurements to time of dose preparation for data calculations with respect to injected dose (i.e. %ID/g).

2.5.20 Pre-targeting biodistribution study

Female 6-8 week old, Balb/c mice were injected with 20 mg/kg TCO-BP (5 mg/mL) formulated in 0.9% saline. After 1 h approximately 0.39 MBq of **8** was administered. At 1 h, 4 h and 24 h post-injection (n = 3 per time point), mice were anesthetized with 3% isoflurane and euthanized by cervical dislocation. Blood, adipose, adrenals, bone (arm bones including shoulder and leg bones including knee joint), brain, gall bladder, heart, kidneys, large intestine and caecum (with contents), liver, lungs, pancreas, skeletal muscle, small intestine (with contents), spleen, stomach (with contents), thyroid/trachea, urine + bladder and tail were collected, weighed and counted in a gamma counter. Decay correction was used to normalize organ activity measurements to time of dose preparation for data calculations with respect to injected dose (i.e. %ID/g).

2.5.21 SPECT/CT Imaging

Active targeting: Female, 6-8 week old, Balb/c mice were injected with approximately 27 MBq of **10**. Pre-targeting: Female 6-8 week old, Balb/c mice were injected with 20 mg/kg TCO-BP (5 mg/mL) formulated in 0.9% saline. After 1 h approximately 27 MBq of **8** was administered. SPECT/CT images were acquired at 1 and 24 hours post-injection and the acquisitions were 32 projections × 10 seconds (1 hr) and 32 projections × 20 seconds (24 hr).

2.5.22 Associated Content

The following supporting information is available in Appendix I:

^{1}H NMR and ^{13}C spectra of all target compounds; HRMS data for all target compounds; HPLC trace of compound **7**; full biodistribution tables; flow cytometry scatter plots (PDF)

2.5.23 Abbreviations

ADCC, antibody dependent cellular cytotoxicity; AI, Auto-Inhibition; ARM, antibody recruiting small molecule; DNP, dinitrophenyl; PSMA, prostate specific membrane antigen; uPAR, urokinase plasminogen activator receptor; R-ARM, radiolabelled antibody recruiting small molecule; TCO, *trans*-cyclooctene; DOTA, 1,4,7,10-tetraazacyclododecane-1,4,7,10-tetraaceticacid; PEG-10, decaethylene glycol; PyBoP, (benzotriazol-1-yloxy)tripyrrolidinophosphonium hexafluorophosphate; FMOC, 9-Fluorenylmethoxycarbonyl; NHS, N-Hydroxysuccinimide; Boc, tert-butyloxycarbonyl; TFA, trifluoroacetic acid; TEA, triethylamine; EDC, 1-ethyl-3-(3-dimethylaminopropyl)carbodiimide; DCM, dichloromethane; DIPEA, *N,N*-diisopropylethylamine; ACN, acetonitrile; DMF, dimethylformamide; AP, alkaline phosphatase; AF-488, Alexa Fluor 488; MFI, mean fluorescence intensity; ADCP, antibody dependent cellular-phagocytosis; SPE, solid phase extraction; TCO-BP, TCO-functionalized bisphosphonate; FACS, fluorescence-activated cell sorting; AM, assay media.

2.5.24 Acknowledgements

We would like to thank our funding sources Natural Sciences and Engineering Research Council (NSERC) of Canada, and the Canadian Cancer Society (Innovation grant 2015:703857). We would also like to thank Kevin Wyszatko for making the graphics for the abstract as well as Figure 2-1. We would also like to thank McMaster Nuclear Reactor (MNR) for supplying [^{177}Lu]$LuCl_3$ and Silvia Albu, Salma Al-Karmi, Ramesh

Patel and Dr. Fred Capretta for their guidance. Finally, we would like to thank Denis Snider and Saman Seyed for their help preparing the manuscript.

2.5.25 Author Information

* E-mail: valliant@mcmaster.ca

Author Contributions Stephanie Rathmann- investigation, writing the original draft, validation, formal analysis, data curation, validation (lead); Afaf Genady- investigation (supporting) data curation, writing the manuscript (supporting); Nancy Janzen- data curation, formal analysis, investigation (supporting); Varun Anipindi- data curation, formal analysis, investigation (supporting); Shannon Czorny- data curation, formal analysis (supporting); Anthony Rullo- data curation, formal analysis, investigation (supporting); John Valliant, PI responsible for running the program, funding acquisition, project administration, writing of original draft (lead).

2.6 References

1. Jaffray, D. A.; Gospodarowicz, M. K., *Disease Control Priorities*. International Bank for Reconstruction and Development / The World Bank: Washington DC, 2015.
2. Dewan, M. Z.; Galloway, A. E.; Kawashima, N.; Dewyngaert, J. K.; Babb, J. S.*, et al.*, Fractionated but Not Single-Dose Radiotherapy Induces an Immune-Mediated Abscopal Effect When Combined with Anti–CTLA-4 Antibody. *Clin. Cancer Res.* **2009,** *15* (17), 5379-5388.
3. Reynders, K.; Illidge, T.; Siva, S.; Chang, J. Y.; De Ruysscher, D., The Abscopal Effect of Local Radiotherapy: Using Immunotherapy to Make a Rare Event Clinically Relevant. *Cancer Treat. Rev.* **2015,** *41* (6), 503-510.
4. Demaria, S.; Ng, B.; Devitt, M. L.; Babb, J. S.; Kawashima, N.*, et al.*, Ionizing Radiation Inhibition of Distant Untreated Tumors (Abscopal Effect) Is Immune Mediated. *Int J Radiat Oncol Biol Phys* **2004,** *58* (3), 862-870.
5. Ngwa, W.; Irabor, O. C.; Schoenfeld, J. D.; Hesser, J.; Demaria, S.*, et al.*, Using Immunotherapy to Boost the Abscopal Effect. *Nat Rev Cancer* **2018,** *18* (5), 313-322.
6. Park, S. S.; Dong, H.; Liu, X.; Harrington, S. M.; Krco, C. J.*, et al.*, PD-1 Restrains Radiotherapy-Induced Abscopal Effect. *Cancer Immunol. Res.* **2015,** *3* (6), 610-619.

7. Pouget, J. P.; Georgakilas, A. G.; Ravanat, J. L., Targeted and Off-Target (Bystander and Abscopal) Effects of Radiation Therapy: Redox Mechanisms and Risk/Benefit Analysis. *Antioxid Redox Signal* **2018,** *29* (15), 1447-1487.
8. Rodriguez-Ruiz, M. E.; Vanpouille-Box, C.; Melero, I.; Formenti, S. C.; Demaria, S., Immunological Mechanisms Responsible for Radiation-Induced Abscopal Effect. *Trends Immunol* **2018,** *39* (8), 644-655.
9. Yasuda, K.; Nirei, T.; Tsuno, N. H.; Nagawa, H.; Kitayama, J., Intratumoral Injection of Interleukin-2 Augments the Local and Abscopal Effects of Radiotherapy in Murine Rectal Cancer. *Cancer Sci.* **2011,** *102* (7), 1257-1263.
10. Ahmed, K. A.; Kim, S.; Arrington, J.; Naghavi, A. O.; Dilling, T. J.*, et al.*, Outcomes Targeting the PD-1/PD-L1 Axis in Conjunction with Stereotactic Radiation for Patients with Non-Small Cell Lung Cancer Brain Metastases. *J. Neurooncol.* **2017,** *133* (2), 331-338.
11. Pike, L. R. G.; Bang, A.; Ott, P.; Balboni, T.; Taylor, A.*, et al.*, Radiation and Pd-1 Inhibition: Favorable Outcomes after Brain-Directed Radiation. *Radiother. Oncol.* **2017,** *124* (1), 98-103.
12. Chao, Y.; Xu, L.; Liang, C.; Feng, L.; Xu, J.*, et al.*, Combined Local Immunostimulatory Radioisotope Therapy and Systemic Immune Checkpoint Blockade Imparts Potent Antitumour Responses. *Nat. Biomed. Eng.* **2018,** *2* (8), 611-621.
13. Sutherland, R. M., Radiation-Enhanced Immune Response to Cancer: Workshop, Anaheim, Ca, April 17, 2005. *Int. J. Radiat. Oncol., Biol., Phys.* **2006,** *64* (1), 3-5.
14. McEnaney, P. J.; Parker, C. G.; Zhang, A. X.; Spiegel, D. A., Antibody-Recruiting Molecules: An Emerging Paradigm for Engaging Immune Function in Treating Human Disease. *ACS Chem. Biol.* **2012,** *7* (7), 1139-1151.
15. Chirkin, E.; Muthusamy, V.; Mann, P.; Roemer, T.; Nantermet, P. G.*, et al.*, Neutralization of Pathogenic Fungi with Small-Molecule Immunotherapeutics. *Angew. Chem. Int. Edit.* **2017,** *56* (42), 13216-13220.
16. Murelli, R. P.; Zhang, A. X.; Michel, J.; Jorgensen, W. L.; Spiegel, D. A., Chemical Control over Immune Recognition: A Class of Antibody-Recruiting Small Molecules That Target Prostate Cancer. *J. Am. Chem. Soc.* **2009,** *131* (47), 17090-17092.
17. Dubrovska, A.; Kim, C.; Elliott, J.; Shen, W.; Kuo, T. H.*, et al.*, A Chemically Induced Vaccine Strategy for Prostate Cancer. *ACS Chem. Biol.* **2011,** *6* (11), 1223-1231.
18. Rullo, A. F.; Fitzgerald, K. J.; Muthusamy, V.; Liu, M.; Yuan, C.*, et al.*, Re-Engineering the Immune Response to Metastatic Cancer: Antibody-Recruiting Small Molecules Targeting the Urokinase Receptor. *Angew. Chem. Int. Edit.* **2016,** *55* (11), 3706-3710.
19. Rossin, R.; Verkerk, P. R.; van den Bosch, S. M.; Vulders, R. C.; Verel, I.*, et al.*, In Vivo Chemistry for Pretargeted Tumor Imaging in Live Mice. *Angew. Chem. Int. Edit.* **2010,** *49* (19), 3375-3378.
20. Brabander, T.; van der Zwan, W. A.; Teunissen, J. J. M.; Kam, B. L. R.; Feelders, R. A.*, et al.*, Long-Term Efficacy, Survival, and Safety of [(177)Lu-DOTA(0),Tyr(3)]Octreotate in Patients with Gastroenteropancreatic and Bronchial Neuroendocrine Tumors. *Clin. Cancer Res.* **2017,** *23* (16), 4617-4624.

21. Rahbar, K.; Ahmadzadehfar, H.; Kratochwil, C.; Haberkorn, U.; Schäfers, M.*, et al.*, German Multicenter Study Investigating 177Lu-PSMA-617 Radioligand Therapy in Advanced Prostate Cancer Patients. *J. Nucl. Med.* **2017,** *58* (1), 85-90.
22. Huang, Z.; Olsen, N. A.; You, W.; Haugland, R. P., A Sensitive Competitive Elisa for 2, 4-Dinitrophenol Using 3, 6-Fluorescein Diphosphate as a Fluorogenic Substrate. *J Immunol Methods* **1992,** *149* (2), 261-266.
23. Eisen, H. N.; Siskind, G. W., Variations in Affinities of Antibodies During the Immune Response. *Biochemistry* **1964,** *3* (7), 996-1008.
24. Yazdani, A.; Bilton, H.; Vito, A.; Genady, A. R.; Rathmann, S. M.*, et al.*, A Bone-Seeking Trans-Cyclooctene for Pretargeting and Bioorthogonal Chemistry: A Proof of Concept Study Using (99m)Tc- and (177)Lu-Labeled Tetrazines. *J. Med. Chem.* **2016,** *59* (20), 9381-9389.
25. Ogawa, K.; Mukai, T.; Inoue, Y.; Ono, M.; Saji, H., Development of a Novel 99mTc-Chelate–Conjugated Bisphosphonate with High Affinity for Bone as a Bone Scintigraphic Agent. *J Nucl Med* **2006,** *47* (12), 2042-2047.
26. Rogers, M. J.; Gordon, S.; Benford, H. L.; Coxon, F. P.; Luckman, S. P.*, et al.*, Cellular and Molecular Mechanisms of Action of Bisphosphonates. *Cancer* **2000,** *88* (12), 2961-2978.
27. Russell, R.; Graham, G., Bisphosphonates: Mode of Action and Pharmacology. *Pediatrics* **2007,** *119* (Suppliment 2), S150-S162.
28. Vallabhajosula, S.; Killeen, R. P.; Osborne, J. R., Altered Biodistribution of Radiopharmaceuticals: Role of Radiochemical/Pharmaceutical Purity, Physiological, and Pharmacologic Factors. *Semin. Nucl. Med.* **2010,** *40* (4), 220-241.

Chapter 3 – Preparation and Testing of TCO-Derived Biomolecules for Targeting R-ARMs

3.1 Overview

A novel R-ARM construct was developed in Chapter 2 and initial targeting studies were performed using a TCO-bisphosphonate derivative. With this approach, the R-ARM (**8**) successfully accumulated in areas of high calcium turnover in bone through both active and pre-targeting strategies. In addition, the core ARM construct (**7**) showed anti-DNP antibody recruitment *in vitro*. Although TCO-BP was useful in these initial studies, it has limitations with respect to testing in animals as bone tumours are typically created by implanting cancer cells orthotopically. Monitoring the animals' response therefore becomes challenging as the bone must be imaged instead of the more standard and convenient approach of measuring tumour size using calipers. Furthermore, orthotopic bone tumours are generally more difficult to extract and analyze *ex vivo* compared to tumours located in the hind flank.

The most common approach used to target tetrazine derivatives to tumours *in vivo* are TCO-derived antibodies. However, due to the immunocompetent nature of the animals required for ARM therapies, an antibody targeting vector would bind the murine form of an antigen which ultimately complicates use in humans. In addition, for the antibody recruiting therapy strategy to be successful the antigen must be available on the surface of the cell and not rapidly internalized so that the appended R-ARM can be recognized by the immune system. With these requirements, there are a limited number of targeting molecules that can be used to

test R-ARMs. Consequently, the focus of this chapter was to prepare and evaluate new TCO-derivatives that could achieve high tumour binding, minimal internalization and low off-target binding to ultimately be able to test the R-ARM therapy approach.

3.2 Materials and Methods

3.2.1 General materials and instruments

Chemicals and reagents for synthesis were purchased from Sigma-Aldrich, and Conjuprobe and used without further purification. Biological reagents from multiple sources were used and are listed below. Compound **7** was prepared according to the method described in chapter 2. MALDI data were obtained using a Bruker Ultraflextreme spectrometer. High-performance liquid chromatography (analytical) was performed on a Waters 1525 Binary HPLC system connected to a Bioscan γ-detector and a 2998 photodiode array detector monitoring at 254 nm and 280 nm or a Waters 2545 binary gradient model, 2998 photodiode array equipped with a 2767 sample manager. For analytical runs, a Waters X-Bridge column (5 µm, 4.6 × 100 mm, C18) or a Phenomenix Yarra (3 µm, 7.8 × 300 mm, SEC-3000) were used, at a flow rate of 1.0 mL/min. The elution method for HPLC procedures were: Method A: Solvent A = 0.1% v/v trifluoroacetic acid (TFA) in water; Solvent B = 0.1% v/v TFA in acetonitrile: gradient elution, 95-26% A (0-14 min) and Method B: Solvent A = 50 mM $NaPO_4$ pH 6.8 + 300 mM NaCl isocratic elution. [^{177}Lu]Lu was produced by the McMaster Nuclear Reactor (MNR, Hamilton, Ontario) using the $^{176}Lu(n,\gamma)^{177}Lu$ reaction and was provided as a solution of [^{177}Lu]$LuCl_3$ in 0.01 M HCl.

3.2.2 Radiochemistry

*Radiolabelling Protocol (**8**).* To a solution of **7** (100 µg, 48.0 nmol) in 100 µL of 0.1 M NaOAc (pH 5.5) was added [^{177}Lu]$LuCl_3$ (31-74 MBq). The reaction mixture was heated to 60°C for 5 min at which point a radio-TLC (cellulose/silica plate) was run in 50 mM EDTA solution. The radiochemical yield of the reaction was determined to be >99% with >99% radiochemical purity. Compound **8** was used without further purification.

3.2.3 Synthesis of TCO-functionalised Bovine Serum Albumin (11)

To a solution of bovine serum albumin (0.200 g, 3.0 µmol) in water (2.0 mL) was added *trans*-4-cycloocten-yl 2,5-dioxo-1-pyrrolidinyl ester carbonic acid (9.3 mg, 61.0 µmol) dissolved in DMSO (200 µL). The reaction mixture was left to shake at 4 °C for 12 h at which point the mixture was purified by dialysis against MilliQ water for 12 h. The product was lyophilized and isolated as a white solid. It was determined by MALDI-TOF MS that there was an average of 2.7 TCO groups per BSA molecule.

3.2.4 Synthesis of TCO-BSA aggregates (12)

A solution of **11** (2.0 mg/mL) in saline (pH 5.5) was heated to 80 °C for 10 minutes, at which point the mixture was centrifuged at 5 × g for 5 minutes. The supernatant was removed and the aggregates (**12**) resuspended in sterile saline (2.0 mg/mL) for injection.

3.2.5 Synthesis of BSA aggregates (13)

A solution of BSA (20.0 mg/mL) in saline (pH 5.5) was heated to 80 °C for 10 minutes at which point the mixture was centrifuged at 5 × g for 5 minutes. The

supernatant was removed and the aggregates resuspended in sterile saline (2.0 mg/mL) for injection.

3.2.6 Synthesis of [^{177}Lu]Lu-DNP-DOTA-Tz-TCO-BSA aggregates (14)

To a solution of **12** (2.0 mg/mL) in saline was added **8** (100 µg, 48.0 nmol) and the mixture heated to 37 °C for 1 hour. The mixture was then centrifuged at 5 × g for 5 minutes, the supernatant removed by pipette and the aggregates resuspended in sterile saline (2.0 mg/mL). The centrifugation procedure was completed a second time at which point the aggregates were resuspended in sterile saline (2.0 mg/mL) for injection. The conjugation efficiency of the reaction was 36 ± 10% (n=4).

3.2.7 Synthesis of [^{177}Lu]Lu-DNP-DOTA-Tz-TCO-BSA (15)

To a solution of **11** (2.0 mg/mL) in saline was added **8** (100 µg, 48.0 nmol) and the mixture allowed to react at room temperature for 10 minutes. The reaction was added to a 50 kDa spin filter and centrifuged at 4000 rpm for 10 minutes, which had been previously activated with 1.00 mL of saline. The supernatant was washed twice with 1 mL of sterile saline and centrifuged as stated above, followed by resuspension in sterile saline for injection. The conjugation efficiency of the reaction was 46 ± 5% (n=3).

3.2.8 Synthesis of DNP-DOTA-Tz-TCO-BSA aggregates (16)

To a solution of **12** (2.0 mg/mL) was added **7** (100 µg, 48.0 nmol) and the mixture heated to 37 °C for 1 hour. The mixture was then centrifuged at 5 × g for 5 minutes, the supernatant removed by pipette and the aggregates resuspended in sterile saline (2.0 mg/mL). The centrifugation procedure was completed a second time after which the aggregates were resuspended in sterile saline (2.0 mg/mL).

3.2.9 Synthesis of DNP-DOTA-Tz-TCO-BSA (17)

To a solution of **11** (2.0 mg/mL) was added **7** (100 µg, 48.0 nmol) and the mixture left at room temperature for 10 minutes. The reaction was added to a 50 kDa spin filter and centrifuged at 4000 rpm for 10 minutes, which had been previously activated with 1.00 mL of saline. The supernatant was washed twice with 1 mL of sterile saline and centrifuged as stated above, followed by resuspension in sterile saline for injection.

3.2.10 ELISA

A competitive ELISA similar to that described by Huang *et al.* was conducted.[1] Briefly, 1.00 mg/mL DNP-BSA (Life Technologies, A23018) in sterile PBS (ThermoFisher, 10010023) was diluted a thousand fold with coating buffer (Bethyl Laboratories, E107) and transferred (0.1 mL) to a 96 well plate. Following a 1 hour incubation at room temperature, the wells were washed three times with 0.2 mL of ELISA Wash buffer (Bethyl Laboratories, E106). ELISA blocking buffer (Bethyl Laboratories, E104) was then added to each well (0.2 mL) and left to incubate at room temperature for 0.5 h. The plate was washed three times with ELISA wash buffer (0.2 mL/well) before the addition of 0.1 mL of either 2,4-dinitrophenol (Sigma-Aldrich, D19850; range 0.312 nmol – 40.000 nmol per well), **12** or **16** (0.160-0.640 nmol per well) in sample diluent (ELISA blocking buffer + 0.05% TWEEN 20) or sample diluent (Bethyl Laboratories, E104 0.05% TWEEN 10) alone followed by 0.1 mL of anti-DNP-AP (Sigma-Aldrich, A2831; 64.0 ng/mL). Following a 1 h incubation at room temperature, the plate was washed three times with ELISA wash buffer (0.2 mL/well). To each well, 0.1 mL of PNPP substrate was added and the plate incubated in the dark at room temperature for 0.5 h. To

quench the reaction, 50.0 µL of 2 M NaOH was added to each well and the absorbance subsequently measured at 405 nm on a plate reader.

3.2.11 Biodistribution Studies General

All animal studies were approved by the Animal Research Ethics Board at McMaster University. Mice were maintained under clean conditions in an established animal facility with 12 hour light/dark cycles and given food and water ad libitum.

3.2.12 143B Osteosarcoma Model

Female, 6-7 week old NCr Nu/nu mice ordered from Charles River Laboratory (Kingston, NY) were inoculated with 2×10^6 143B osteosarcoma cancer cells in the right flank. After 10 days the animals were administered 0.41 – 0.70 MBq of [^{99m}Tc]Tc-MDP or [^{99m}Tc]Tc-TCO-BP. At 1 h post-injection (n = 3 per time point), mice were anesthetized with 3% isoflurane and euthanized by cervical dislocation. Blood, adipose, adrenals, bone, brain, gall bladder, heart, kidneys, large intestine and caecum (with contents), liver, lungs, pancreas, skeletal muscle, small intestine (with contents), spleen, stomach (with contents), thyroid/trachea, urine + bladder, tumour and tail were collected, weighed and counted in a gamma counter. Decay correction was used to normalize organ activity measurements to time of dose preparation for data calculations with respect to injected dose (i.e. %ID/g).

3.2.13 B16F1 Melanoma Model

Female, 7-8 week old C57BL/6 mice ordered from Charles River Laboratory (Kingston, NY) were inoculated with 4×10^5 B16F1 melanoma cancer cells in the right flank. After 10 days the mice were administered TCO-BZA (20.0 mg/kg)

followed 1, 4 or 21 h later by **8** (0.41 – 0.44 MBq). At 1 h post-injection of **8** (*n* = *2,* 3, 2 at each time point respectively), mice were anesthetized with 3% isoflurane and euthanized by cervical dislocation. Blood, adipose, adrenals, bone, brain, gall bladder, heart, kidneys, large intestine and caecum (with contents), liver, lungs, eyes, skeletal muscle, small intestine (with contents), spleen, stomach (with contents), thyroid/trachea, urine + bladder, tumour and tail were collected, weighed and counted in a gamma counter. Decay correction was used to normalize organ activity measurements to time of dose preparation for data calculations with respect to injected dose (i.e. %ID/g).

3.2.14 4T1 Breast Cancer Model

Female, 5-6 week old Balb/c mice ordered from Charles River Laboratory (Kingston, NY) were inoculated with 1×10^6 4T1 breast cancer cells in the right flank. After 7 days the mice were injected i.t. or i.v. with 0.07-0.33 MBq of **8**, **14** or **15**. At 24 h post-injection (*n* = 3 per time point), mice were anesthetized with 3% isoflurane and euthanized by cervical dislocation. Blood, adipose, adrenals, bone, brain, gall bladder, heart, kidneys, large intestine and caecum (with contents), liver, lungs, pancreas, skeletal muscle, small intestine (with contents), spleen, stomach (with contents), thyroid/trachea, urine + bladder, tumour and tail were collected, weighed and counted in a gamma counter. Decay correction was used to normalize organ activity measurements to time of dose preparation for data calculations with respect to injected dose (i.e. %ID/g).

3.3 Results and Discussion

3.3.1 Evaluating TCO-Targeting Vectors

3.3.1.1 Targeting Osteosarcoma

In order to leverage the success reported in the previous chapter with TCO-BP, a flank osteosarcoma model was pursued. Tumours generated by subcutaneous injection of 143B osteosarcoma cells have been shown to contain bone and therefore can be targeted with bisphosphonates.[2] For example, alendronate-functionalized nanoparticles have been shown to accumulate in 143B osteosarcoma flank tumours via this mechanism.[3] The nanoparticles were coated with poly(acrylic acid) that was functionalized with alendronate. The nanoparticles were injected i.v. through the tail vein, and the whole-body distribution monitored by fluorescence imaging. The images reveal uptake as early as 5 minutes post-injection, which continued to increase to approximately 30% of the recovered fluorescence at 8 days post-injection. This model therefore may provide the opportunity of using TCO-BP to target compound **8** and test the therapeutic response to R-ARMs. Consequently, two radiolabelled bisphosphonates were evaluated in the 143B osteosarcoma model to determine if the uptake in the tumour would be sufficient for R-ARM therapy.

To evaluate the model, the commercially available gold standard for bisphosphonate bone imaging, [^{99m}Tc]Tc-methylene diphosphonate (MDP), was assessed along with [^{99m}Tc]Tc-TCO-BP.[4] The compounds were injected i.v. into Balb/c mice bearing 143B flank tumours, and the distribution evaluated 1 hour post-injection. It was apparent that both compounds cleared predominantly through the

renal pathway with urine and bladder concentrations of 199 ± 113 and 619 ± 320 %ID/g for [^{99m}Tc]Tc-MDP and [^{99m}Tc]Tc-TCO-BP respectively. [^{99m}Tc]Tc-MDP and [^{99m}Tc]Tc-TCO-BP showed high uptake in the bone of 11.9 ± 0.9 and 15.3 ± 2.2 %ID/g respectively, however the uptake in the tumour was quite low at 1.0 ± 0.1 for both compounds. Although it was reported in the literature that the highest uptake of the alendronate-coated nanoparticles was after 8 days, the amount of activity left in the blood for [^{99m}Tc]Tc-MDP and [^{99m}Tc]Tc-TCO-BP were 0.67 ± 0.03 and 0.97 ± 0.20 %ID/g respectively after one hour. This suggests that the uptake in the tumour would not increase significantly over time as the majority of the tracer had already cleared. The bone microenvironment consists of nutrients such as calcium and other minerals, which are absent in the flank of an animal.[2] Due to these differing microenvironments, it can be expected that bone tumours grown in each of these regions would have different characteristics. As a result, bisphosphonates may not be a suitable targeting vector for flank tumours due to the lower amounts of calcium accretion when compared to that in an orthotopic model. Due to the low level of activity in the tumour, this model and bisphosphonates were deemed to be unsuitable for testing R-ARMs and other strategies were pursued in order to increase tumour uptake.

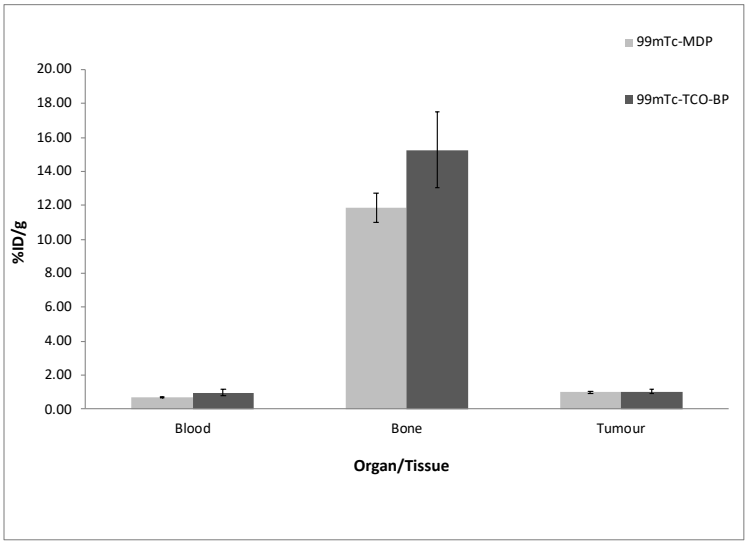

Figure 3-1. Biodistribution data for [^{99m}Tc]Tc-MDP and [^{99m}Tc]Tc-TCO-BP administered to Balb/c nude mice bearing a 143B osteosarcoma flank tumour 10 days post tumour inoculation (n=3). Data at the time points indicated are expressed as the mean percent injected dose per gram (%ID/g) ± SEM 1 hour post-injection.

3.3.1.2 Targeting Melanoma

Malignant melanoma is an aggressive form of skin cancer that is associated with high rates of metastasis and low survival rate at late stages.[5, 6] Many melanoma tumours overexpress melanin; a group of pigment proteins that are synthesized in melanocyte cells.[7] The pigments contain multiple carboxylic and phenolic functional groups which possess a negative charge at physiological pH. The presence of these groups presents an opportunity to target the cancers through an electrostatic interaction with positively charged vectors.[8] The most explored melanin-targeted radiopharmaceutical derivatives in the literature are N,N-dialkyl benzamides, which use a tertiary amine for binding melanin, and an aromatic substituent as a site for labelling with radiohalogens (Figure 3-2).[5, 7] The first benzamide construct to advance to the clinic was N-(2-diethylaminoethyl)- 4-iodobenzamide labelled with iodine-123 ([^{123}I]I-BZA) for SPECT imaging of

malignant melanoma.[5] In a phase II study, 110 patients with a history of melanoma were imaged with conventional imaging techniques such as CT or US in order to identify any lesions. Patients were then administered [^{123}I]I-BZA and imaged after 20-24 hours; the number of lesions identified by the SPECT images were compared to the conventional images and it was determined that the diagnostic sensitivity, accuracy and specificity of [^{123}I]I-BZA was 81%, 87% and 100% respectively. More recently, the BZA core was modified with a 1,3-benzodioxole group leading to an increased uptake of the iodine-123 labelled form in melanoma tumours, which was followed by radiolabelling with iodine-131 for therapy.[9]

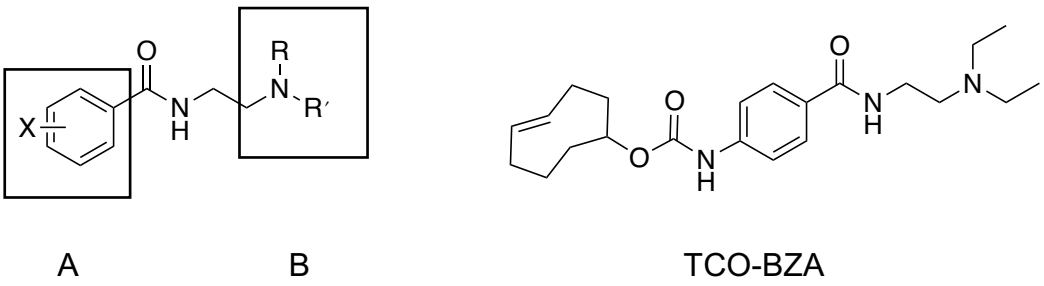

Figure 3-2. Left – Schematic representation of a benzamide with an aromatic group (A) that can be radiolabelled with a radiohalogen, and a tertiary amine targeting vector (B) in which R and R′ are typically alkyl chains. Right- Structure of TCO-BZA which was reported previously.[10]

Based on the success and simplicity of the BZA core, a TCO-BZA derivative was synthesized through a one-step coupling reaction between a TCO-carbonate ester and procainamide as previously reported (Figure 3-2).[10] TCO-BZA was injected i.v. into mice bearing a B16F1 melanoma flank tumour and after 1, 4 and 21 hours compound **8** was administered. All mice were sacrificed 1 hour post-injection of **8**, and the activity in different tissues and fluids determined. There were two target tissues in this study, the tumour and the eyes as both are high expressors

of melanin and uptake in these tissues would suggest the probe is "on mechanism".[9, 11] The uptake in the tumour and eyes were 2.22 ± 0.23 and 0.30 ± 0.02 %ID/g respectively for the 1 hour pre-targeting study which decreased to 0.99 ± 0.09 and 0.11 ± 0.03 %ID/g respectively by 21 hours. Although the early uptake at one hour seemed promising at first, the blood concentration of 3.06 ± 0.15 %ID/g was higher than the tumour which draws into question whether the activity in the tumour was simply due to residual blood. The blood concentration was significantly higher than that observed from compound **8** alone, 0.64 ± 0.10 %ID/g, suggesting that the *in vivo* click reaction occurred in the blood. In order to determine if the uptake in the tumour was specific, or from residual blood in the tissue, the study could have been repeated with a longer time point after the administration of **8** to allow the activity to clear, which could potentially increase the tumour to blood ratio. However, the uptake in the tumour was not sufficiently promising to warrant further investigation since improvement would require modification to the TCO-BZA core to increase accumulation in the target tissue. Due to the significant amount of time likely required to synthesize, characterize and test new TCO-BZA derivatives, this strategy was abandoned.

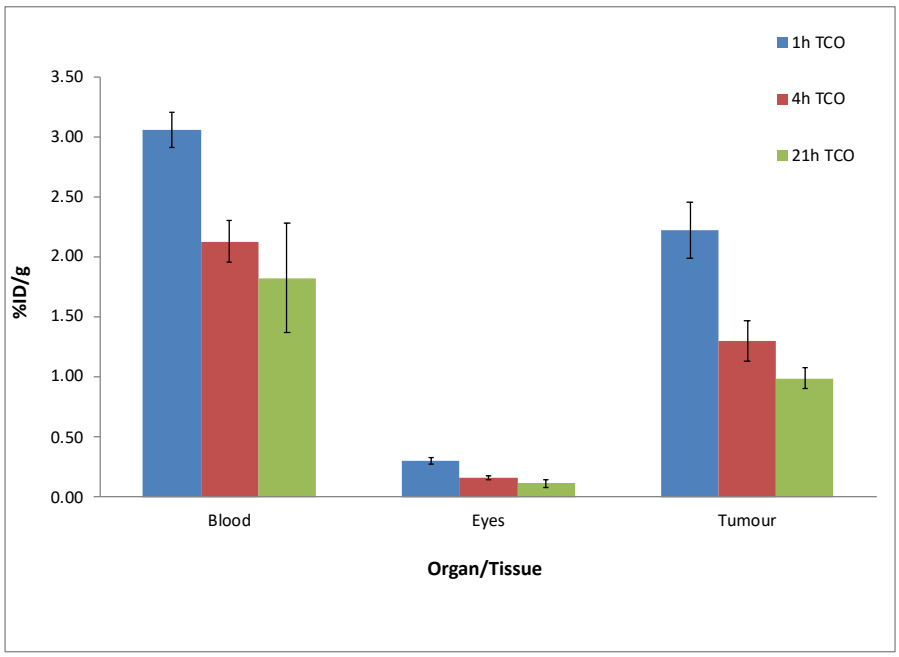

Figure 3-3. Biodistribution data for a pre-targeting study with TCO-BZA administered to C57BL/6 mice bearing B16F1 flank tumours 10 days post inoculation (n=2 at 1 and 21 hours, n=3 at 4 hours) followed by administration of 8. All animals were sacrificed 1 hour post 8 administration. Data at the time points indicated are expressed as the mean percent injected dose per gram (%ID g^{-1}) ± SEM.

3.3.2 Development of an Albumin-Based R-ARM

3.3.2.1 Intratumoral Delivery

Targeting TCO-derivatives via i.v. injection of small molecules proved to be challenging and resulted in low target uptake. This is likely due to the influence of the TCO group on pharmacokinetics and target binding and also the washout or short residency time on the surface of the target cells. The focus of this research was not to develop novel targeting strategies but rather to compare the efficacy of R-ARMs versus radiotherapy and ARM therapy alone. As a result, an alternative strategy based on intratumoral (i.t.) injections was pursued. If the combination proves to be more effective than the monotherapies, research can revert to finding the optimal TCO-targeting vectors.

In recent years, direct delivery of therapeutics into solid tumours has gained popularity as a less invasive alternative to surgical resection.[12, 13] Intratumoral injections help to overcome the typical challenges of systemic therapeutics such as achieving high tumour uptake, toxicity, and limited tumour penetration, where the latter is due in part to interstitial pressures.[14] In rare cases, i.t. administration of therapeutics has been shown to result in regression at distant non-treated sites, which is thought to be due to immune activation.[13, 15-17] One of the issues that can arise from i.t. administration is the rapid clearance of the agent from the tumour, which can be mitigated through conjugation of the therapeutic to a nanoparticle or micelle.[18] Although these strategies have shown promising results *in vivo*, they can require complex chemical syntheses and suffer from stability issues as well as toxicity from the scaffold itself.[19, 20]

3.3.2.2 Human Serum Albumin Conjugates

Human serum albumin (HSA) is the most abundant blood protein, constituting approximately 50% of all blood proteins.[21] HSA and its derivatives have been used in the clinic for several years for both diagnostic and therapeutic purposes.[22, 23] There are cases in which a poorly soluble drug such as paclitaxel, a chemotherapeutic, has been bound to HSA in order to reduce the toxicity and increase solubility.[24] With respect to radiopharmaceuticals, albumin has been used clinically to image the cardiac blood pool through the direct labelling of the protein with technetium-99m.[21, 25] In addition, macroaggregated technetium labelled-albumin ([^{99m}Tc]Tc-MAA) is used in patients for dosimetry prior to liver embolization therapy, as well as identification of non-palpable lesions and sentinel

node localization in breast cancer patients.[26-28] In the case of occult breast lesions, [^{99m}Tc]Tc-MAA is injected i.t. prior to surgical excision to enable radiation-guided localization of tumour masses.[26, 27] In a study of 959 patients administered [^{99m}Tc]Tc-MAA i.t., 99.6% of breast lesions were identified and removed surgically with negative margins in 91.6% of the cases.[26] The study used HSA aggregates with a particle size range of 10-150 μm, labelled with 10-15 MBq of technetium-99m, injected into the center of the lesion.

Building on the success of i.t. delivery of radiolabelled albumin, a TCO-derivative was prepared as a platform to localize R-ARMs via i.t. administration. Herein we describe the development and evaluation of a new bovine serum albumin (BSA) derivative that can be used to deliver compound **8** i.t. through the application of a *trans*-cyclooctene (TCO) tetrazine ligation reaction.

3.3.2.3 TCO-BSA Aggregate Synthesis

TCO-BSA was synthesized through treatment of BSA with a TCO-carbonate ester, which reacts with the (epsilon) amine group on lysines.[29] The reaction mixture was purified through dialysis tubing in order to separate the large molecules, BSA (functionalized and unfunctionalized) from the unreacted small molecule, TCO-carbonate ester, and low molecular weight impurities. The product (**11**) was analyzed by MALDI mass spectrometry and when compared to BSA, it was found to have an average of 2.7 TCO groups per BSA molecule.

Based on the aggregate size range of 10-150 μm documented in the literature,[26] attempts to aggregate **11** to a similar size was done by varying temperature, pH and concentration. Particles in this size range are thought to cause

vascular blockage when administered i.t. thereby resulting in high tumoral retention.[22] The optimal aggregation conditions were found to be a 2.0 mg/mL solution of **11** in saline at pH 5.6, heated to 80 °C for 10 minutes. The aggregates (**12**) were visualized by light microscopy on a hemocytometer, and the size distribution quantified with Nikon NIS elements software. The average size of the aggregates was determined to be 16.6 ± 15.6 µm which was consistent with a SEM image (Figure 3-4) showing the globular shape of a single aggregate with an approximate size of 30 µm.

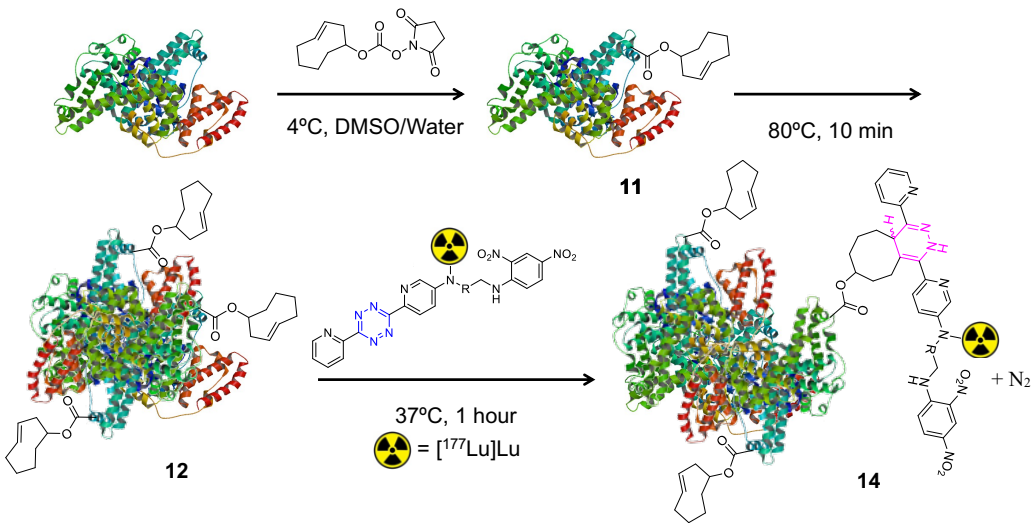

Scheme 3-1. Schematic representation of the synthesis and radiolabelling of TCO-BSA aggregates (**14**).

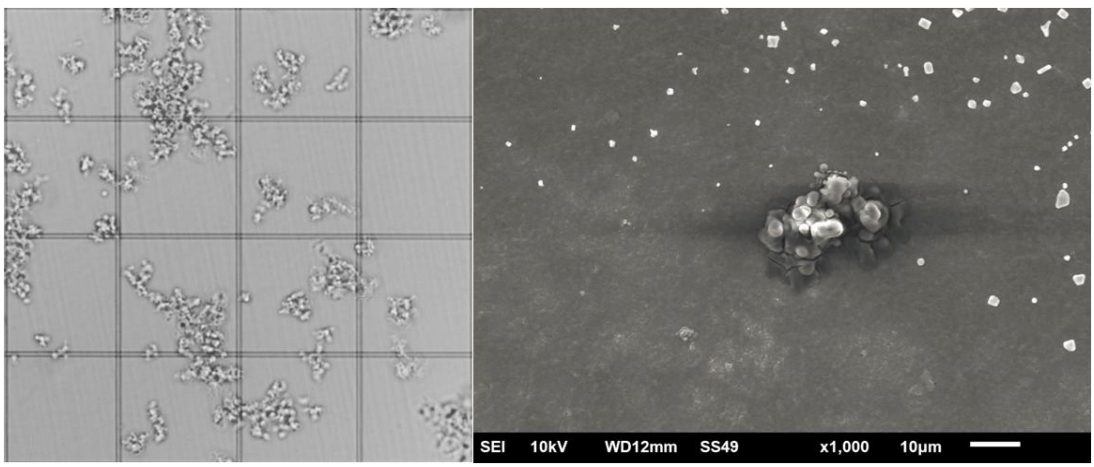

Figure 3-4. Left – A light microscope image of the TCO-BSA aggregates (12), where each square is 50 × 50 μm; Right – SEM image of a single aggregate measuring approximately 30 μm (note that in the background there are salt crystals formed during evaporation of the saline solution containing the product).

3.3.2.4 Probing the Reactivity of the TCO-BSA aggregates (12)

Once the aggregates, **12**, were prepared and characterized, the next step was to explore the reactivity of the TCO groups post-aggregation as the double bond may have isomerized to the *cis*-form due to the reaction temperature.[30, 31] TCO-BSA aggregates were incubated with **8** at room temperature and 37 °C for 10, 30 and 60 minutes. The reaction mixtures were then centrifuged for 5 minutes to separate the aggregates from the supernatant, which contained unreacted **8**. The amount of activity in the pellets were counted, and the results shown in Table 3-1. The data indicated that the reaction between **8** and **12** was complete after 10 minutes at room temperature where increasing the time or temperature of the reaction did not result in more product. To check the specificity of the reaction, a control reaction was performed where **8** was incubated with BSA aggregates (**13**) containing no TCO groups, for 1 hour at 37 °C. The mixture was centrifuged where only 9% of the activity remained in the pellet compared to 28% for the TCO-aggregates. The final specificity test was performed by incubating lutetium-177 with **12** where only 4% of the activity remained in the pellet after 1 hour at 37 °C. The data collectively suggests that the specific reaction between TCO and tetrazine did occur as significantly more activity remained in the pellet when both TCO and tetrazine groups were present. The modest radiochemical yield of 28% is likely due to some of the TCO groups being buried within the protein or potentially isomerized or

reduced, which would impact the coupling reaction. Nevertheless, the procedure developed here provided sufficient material to proceed to *in vivo* studies.

Table 3-1. Data comparing the reaction yield of **8** with **12** at room temperature and at 37°C for 10, 30 and 60 minutes. Each reaction was completed 2 times.

Reaction Time (min)	Room Temperature	37 ºC
10	33 ± 2%	35 ± 3%
30	28 ± 1%	31 ± 0.1%
60	33 ± 2%	28 ± 2%

3.3.2.5 ELISA

As mentioned in Chapter 2, in order for the combination R-ARM therapy to be efficacious, the construct must be able to recruit anti-DNP antibodies for ADCC.[32-34] One potential concern was that the aggregation process could have rendered the DNP groups inaccessible. To this end, the same ELISA protocol employed in Chapter 2 was used to evaluate the antibody recruiting capabilities of the unlabelled aggregate, **16**. The results are shown in Figure 3-5 where a high absorbance value represents the antibody interacting with the antigen coated on the plate, and a low absorbance represents the antibody binding to the synthesized compounds. At each of the tested concentrations (0.19 – 0.64 nmol), it was apparent that the TCO-BSA aggregates (**12**) did not have a strong interaction with the antibody, as the signal on the plate was high. The DNP-functionalized aggregates (**16**) in contrast, showed a large decrease in signal which is representative of an interaction with the anti-DNP antibody. The ELISA results are consistent with DNP groups on BSA binding the anti-DNP antibodies suggesting compound **16** is a viable scaffold that can be used for ARM therapy.

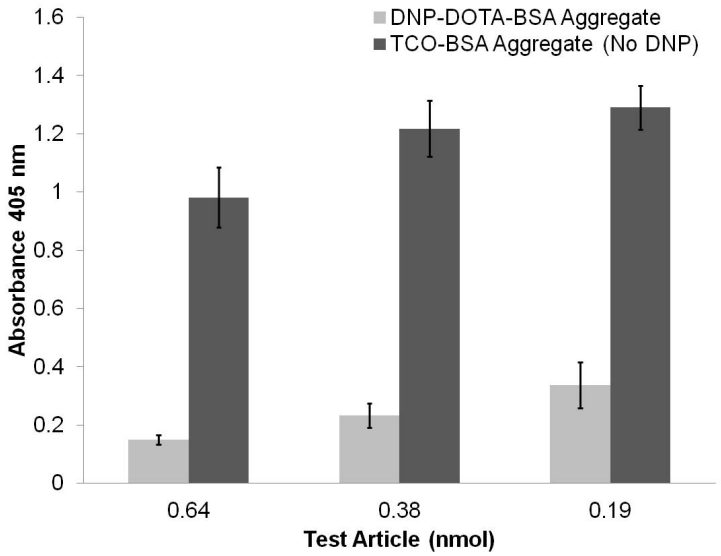

Figure 3-5. An ELISA measuring dose dependent recruitment of anti-DNP antibodies; absorbance at 405 nm: light grey **16**, dark grey **12** at three concentrations (0.64, 0.38, 0.19 nmol per well).

3.3.2.6 Biodistribution Study of TCO-BSA

In addition to aggregates, there is literature to support that i.t. and i.v. injection of non-aggregated albumin drug conjugates can result in high retention and accumulation in a tumour. Matsumura *et al.* showed that an i.t. injection of an Evans blue dye-albumin complex was highly retained in a murine sarcoma tumour while clearing rapidly from non-tumour tissue.[35] The amount of dye remaining in the tumour and skin was quantified spectrophotometrically *ex vivo* at 620 nm, which showed the complex cleared normal skin by one hour post-injection while being retained in the tumour until at least 72 hours post-injection. In addition, the Evans blue-albumin complex was administered i.v. and showed accumulation in the tumour over time, which peaked at 48 hours with minimal washout by 72 hours post-injection. It is thought that i.v. administered albumin-drug conjugates may accumulate in tumour tissue via secreted protein acidic and rich in cysteine (SPARC) which is overexpressed in some cancers.[36-38] In one example it was found

that in the presence of albumin, a chemotherapeutic complex had greater than two-fold increase in internalization in SPARC positive cells relative to the same drug in the absence of albumin.[37] Based on this literature, radiolabelled non-aggregated TCO-BSA was administered both i.t. and i.v. for assessing tumour retention or uptake, and the data compared to the aggregated material.

TCO-BSA (**11**) was treated with the radiolabelled tetrazine **8** at room temperature for 10 minutes. Purification was performed using a 50 kDa spin filter to separate unreacted **8** from TCO-BSA and the radiolabelled albumin. SEC HPLC was used to confirm successful conjugation, which was evident through the shift in retention time from 7.2 minutes (**8**) to 4.6 minutes (**15**). In addition, it was shown that when **8** was incubated with BSA (no TCO), 0% of the activity remained in the supernatant after the spin filtering protocol compared to 46% in the presence of **11**.

3.3.2.7 Intratumoral Administration

To evaluate the retention of the non-aggregated (**15**) and aggregated (**14**) albumin-conjugates, biodistribution studies were performed in a murine syngeneic 4T1 breast cancer tumour model. The model was selected because it is well characterized in the literature and can potentially be used to test R-ARMs if sufficient uptake and retention is observed. Compounds **8**, **14** or **15** were administered i.t. and the distribution evaluated after 24 hours. At 24 hours post-injection, the aggregates (**14**) showed the highest tumour retention (Figure 3-6) albeit with high variability (950 ± 771 %ID/g), followed by non-aggregates (**15**) (55.8 ± 17.6 %ID/g), with the radiolabelled tetrazine (**8**) showing the lowest retention (10.5 ± 4.3 %ID/g). The high degree of variability for the aggregates may

be attributed to the heterogeneous nature of the solution. If a dose contained more smaller aggregates, the retention in the tumour is likely to be lower than with larger aggregates as they are likely to clear more rapidly. Low uptake in non-target tissues was seen for both **14** and **15** with the highest activity in the renal clearance organs, the kidneys (10.2 ± 3.7 and 3.35 ± 0.85 %ID/g) and bladder (7.29 ± 2.73 and 3.22 ± 2.10 %ID/g) respectively. The non-aggregated material (**15**) had higher amounts in non-target tissues at 24 hours which is likely due to the compound leaking out of the tumour. This observation is consistent with the amount of activity in the blood which was 2.12 ± 0.61 %ID/g versus 0.16 ± 0.05 for the aggregates at the same time point.

Given the high retention of **14** and **15** in the tumour at 24 hours post-injection, biodistribution studies adding 72 and 120 hour time points were performed. Compound **14** showed high retention in the tumour of 167 ± 94 and 81.4 ± 31.9 %ID/g at 72 and 120 hours respectively. Compound **15** also demonstrated high retention in the tumour notably 95.7 ± 16.7 and 61.6 ± 31.3 %ID/g at 72 and 120 hours respectively, which is less than that seen with the aggregated material. Compound **15** had less than 2 %ID/g in the bone at 120 hours, with some uptake in the liver and kidneys of 6.72 ± 1.81 and 5.08 ± 1.83 %ID/g respectively. Compound **14** showed an increase in liver uptake from 0.33 ± 0.17 to 4.08 ± 0.56 %ID/g at 24 and 72 hours post-injection respectively, followed by a decrease to 1.83 ± 0.76 %ID/g at 120 hours. This could be representative of smaller aggregates escaping the tumour, and being taken up by the Kupffer cells in the liver and metabolized.[39] This would cause release of the radioisotope, lutetium-177, which is known to

localize to bone.[40] This hypothesis is consistent with the increase in bone uptake of 0.63 ± 0.39, 11.4 ± 6.3 and 19.7 ± 10.7 %ID/g at 24, 72 and 120 hours respectively.

3.3.2.8 Intravenous Administration

To evaluate the uptake of radiolabelled albumin after i.v. administration in a murine syngeneic 4T1 breast cancer model, a biodistribution study was performed with compound **15**. The animals were sacrificed after 24 and 72 hours, and the organs and tissues counted. The uptake in the blood, (Figure 3-6), was 4.68 ± 0.14 %ID/g at 24 hours post-injection which decreased to 0.29 ± 0.09 %ID/g by 72 hours. At 72 hours post-injection, the liver had the highest amount of activity with 6.93 ± 1.35 %ID/g, followed closely by the tumour with 5.12 ± 0.89 %ID/g. Other clearance organs such as the kidneys and bladder had 3.33 ± 0.43 and 2.93 ± 0.60 %ID/g respectively. These results are similar to the distribution of ^{111}In-BSA which has been reported previously in the literature. Interestingly, the extent of conjugation is known to have a large impact on the distribution of albumin.[41, 42] One study documented that as the number of drug molecules conjugated to rat serum albumin (RSA) increased from 1-20, tumour uptake decreased from 25% to 2% while liver uptake increased from 6% to 60% at 24 hours post-injection.[41] Based on this information, should it be necessary in the future, the conjugation ratio of TCO groups to BSA could be decreased in order to increase tumour concentrations of **15**, and decrease uptake in the liver. Notwithstanding, compounds **14** and **15** administered i.t. had high tumour retention and lower non-target uptake compared to i.v. administration. Based on these results, therapy studies were pursued with these constructs which is described in Chapter 4.

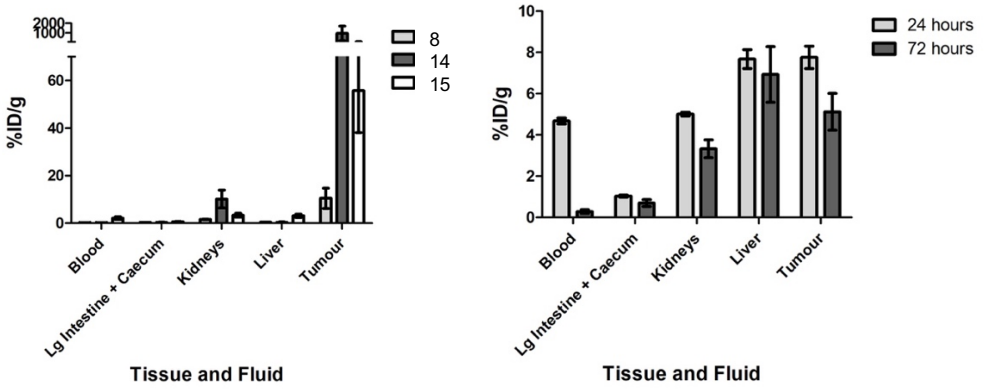

Figure 3-6. Left – 24 hour biodistribution results of **8**, **14** and **15** i.t. administration in Balb/c mice bearing 4T1 breast cancer tumours (n=3 per compound); Right – 24 and 72 hour biodistribution results of 15 after intravenous administration in Balb/c mice bearing 4T1 breast cancer tumours (n=3). Data at the time points indicated are expressed as the mean percent injected dose per gram (%ID g^{-1}) ± SEM.

3.4 Conclusion

In order to evaluate the R-ARM platform developed in Chapter 2, a suitable targeting vector was required. Small molecule vectors targeting osteosarcoma and melanoma were tested in an attempt to find a model with high tumour uptake and low non-target binding. Unfortunately, these approaches resulted in insufficient uptake and retention in the tumour. Using a previously unknown TCO-derivative of albumin, it is possible to deliver the R-ARM directly into a tumour with high retention out to 120 hours. It was determined that both aggregated and non-aggregated materials were suitable for testing R-ARMs with respect to the tumour uptake and retention. Initial studies into the therapeutic efficacy of each component of the proposed R-ARM, notably radiation from the isotope and the antibody recruiting associated with the ARM, were pursued in order to determine the

thresholds required for curative dosing prior to combination R-ARM therapy studies.

3.5 References

1. Huang, Z.; Olsen, N. A.; You, W.; Haugland, R. P., A Sensitive Competitive Elisa for 2, 4-Dinitrophenol Using 3, 6-Fluorescein Diphosphate as a Fluorogenic Substrate. *J Immunol Methods* **1992,** *149* (2), 261-266.
2. Jacques, C.; Renema, N.; Lezot, F.; Ory, B.; Walkley, C. R.*, et al.*, Small Animal Models for the Study of Bone Sarcoma Pathogenesis:Characteristics, Therapeutic Interests and Limitations. *J Bone Oncol* **2018,** *12*, 7-13.
3. Morton, S. W.; Shah, N. J.; Quadir, M. A.; Deng, Z. J.; Poon, Z.*, et al.*, Osteotropic Therapy Via Targeted Layer-by-Layer Nanoparticles. *Adv Healthc Mater* **2014,** *3* (6), 867-875.
4. Yazdani, A.; Bilton, H.; Vito, A.; Genady, A. R.; Rathmann, S. M.*, et al.*, A Bone-Seeking Trans-Cyclooctene for Pretargeting and Bioorthogonal Chemistry: A Proof of Concept Study Using (99m)Tc- and (177)Lu-Labeled Tetrazines. *J Med Chem* **2016,** *59* (20), 9381-9389.
5. Michelot, J. M.; Moreau, M. F. C.; Veyre, A. J.; Bonafous, J. F.; Bacin, F. J.*, et al.*, Phase Ii Scintigraphic Clinical Trial of Malignant Melanoma and Metastases with Iodine- 123-N-(2-Diethylaminoethyl 4-Iodobenzamide). *J Nucl Med* **1993,** *34* (8), 1260-1266.
6. Lauden, L.; Siewiera, J.; Boukouaci, W.; Ramgolam, K.; Mourah, S.*, et al.*, TGF-Beta-Induced (TGFBI) Protein in Melanoma: A Signature of High Metastatic Potential. *J Invest Dermatol* **2014,** *134* (6), 1675-1685.
7. Chang, C. C.; Chang, C. H.; Lo, Y. H.; Lin, M. H.; Shen, C. C.*, et al.*, Preparation and Characterization of a Novel Al(18)F-NOTA-BZA Conjugate for Melanin-Targeted Imaging of Malignant Melanoma. *Bioorg Med Chem Lett* **2016,** *26* (16), 4133-4139.
8. Borel, M.; Lafarge, D.; Moreau, M. F.; Bayle, M.; Audin, L.*, et al.*, High Resolution Magic Angle Spinning NMR Spectroscopy Used to Investigate the Ability of Drugs to Bind to Synthetic Melanin. *Pigment Cell Res* **2005,** *18* (1), 49-54.
9. Mier, W.; Kratochwil, C.; Hassel, J. C.; Giesel, F. L.; Beijer, B.*, et al.*, Radiopharmaceutical Therapy of Patients with Metastasized Melanoma with the Melanin-Binding Benzamide 131I-Ba52. *J Nucl Med* **2014,** *55* (1), 9-14.
10. Rathmann, S. Functional Group Influence on Uptake and Tumour to Non-Target Ratios for Iodinated Melanoma Imaging and Therapy Agents. McMaster University, 2014.
11. Denoyer, D.; Greguric, I.; Roselt, P.; Neels, O. C.; Aide, N.*, et al.*, High-Contrast PET of Melanoma Using (18)F-MEL050, a Selective Probe for Melanin with Predominantly Renal Clearance. *J Nucl Med* **2010,** *51* (3), 441-447.
12. Al-Ghananeem, A. M.; Malkawi, A. H.; Muammer, Y. M.; Balko, J. M.; Black, E. P.*, et al.*, Intratumoral Delivery of Paclitaxel in Solid Tumor from

Biodegradable Hyaluronan Nanoparticle Formulations. *AAPS PharmSciTech* **2009,** *10* (2), 410-417.
13. Aznar, M. A.; Tinari, N.; Rullan, A. J.; Sanchez-Paulete, A. R.; Rodriguez-Ruiz, M. E.*, et al.*, Intratumoral Delivery of Immunotherapy-Act Locally, Think Globally. *J Immunol* **2017,** *198* (1), 31-39.
14. Holback, H.; Yeo, Y., Intratumoral Drug Delivery with Nanoparticulate Carriers. *Pharm Res* **2011,** *28* (8), 1819-1830.
15. Castano, A. P.; Mroz, P.; Hamblin, M. R., Photodynamic Therapy and Anti-Tumour Immunity. *Nat Rev Cancer* **2006,** *6* (7), 535-545.
16. Zamarin, D.; Holmgaard, R. B.; Ricca, J.; Plitt, T.; Palese, P.*, et al.*, Intratumoral Modulation of the Inducible Co-Stimulator Icos by Recombinant Oncolytic Virus Promotes Systemic Anti-Tumour Immunity. *Nat Commun* **2017,** *8*, 1-14.
17. Bakker, R. C.; Lam, M.; van Nimwegen, S. A.; Rosenberg, A.; van Es, R. J. J.*, et al.*, Intratumoral Treatment with Radioactive Beta-Emitting Microparticles: A Systematic Review. *J Radiat Oncol* **2017,** *6* (4), 323-341.
18. Zubillaga, M. B.; Boccio, J. R.; Nicolini, J. O.; Ughetti, R.; Lanari, E.*, et al.*, Pirocarbotrat™ a New Radiopharmaceutical for the Treatment of Solid Tumors--Comparative Studies in N-Nitrosomethylurea-Induced Rat Mammary Tumors. *Nucl Med Biol* **1997,** *24*, 559-564.
19. Nel, A.; Xia, T.; Madler, L.; Li, N., Toxic Potential of Materials at the Nanolevel. *Science* **2006,** *311* (5761), 622-627.
20. Hoshino, A.; Manabe, N.; Fujioka, K.; Suzuki, K.; Yasuhara, M.*, et al.*, Use of Fluorescent Quantum Dot Bioconjugates for Cellular Imaging of Immune Cells, Cell Organelle Labeling, and Nanomedicine: Surface Modification Regulates Biological Function, Including Cytotoxicity. *J Artif Organs* **2007,** *10* (3), 149-157.
21. Lodhi, N. A.; Park, J. Y.; Kim, K.; Kim, Y. J.; Shin, J. H.*, et al.*, Development of (99m)Tc-Labeled Human Serum Albumin with Prolonged Circulation by Chelate-Then-Click Approach: A Potential Blood Pool Imaging Agent. *Mol Pharm* **2019,** *16* (4), 1586-1595.
22. Order, S. E.; Siegel, J. A.; Lustig, R. A.; Principato, R.; Zeiger, S.*, et al.*, A New Method for Delivering Radioactive Cytotoxic Agents in Solid Cancers. *IJROBP* **1994,** *30* (3), 715-720.
23. Taguchi, K.; Chuang, V. T.; Maruyama, T.; Otagiri, M., Pharmaceutical Aspects of the Recombinant Human Serum Albumin Dimer: Structural Characteristics, Biological Properties, and Medical Applications. *J Pharm Sci* **2012,** *101* (9), 3033-3046.
24. Narvekar, M.; Xue, H. Y.; Eoh, J. Y.; Wong, H. L., Nanocarrier for Poorly Water-Soluble Anticancer Drugs-Barriers of Translation and Solutions. *AAPS PharmSciTech* **2014,** *15* (4), 822-833.
25. Thrall, J. H.; Freitas, J. E.; Swanson, D.; Rogers, W. L.; Clare, J. M.*, et al.*, Clinical Comparison of Cardiac Blood Pool Visualization with Technetium-99m Red Blood Cells Labelled in Vivo and with Technetium-99m Human Serum Albumin. *J Nucl Med* **1978,** *19*, 796-803.

26. Monti, S.; Galimberti, V.; Trifiro, G.; De Cicco, C.; Peradze, N.*, et al.*, Occult Breast Lesion Localization Plus Sentinel Node Biopsy (Snoll): Experience with 959 Patients at the European Institute of Oncology. *Ann Surg Oncol* **2007,** *14* (10), 2928-2931.
27. Thind, C. R.; Tan, S.; Desmond, S.; Harris, O.; Ramesh, H. S.*, et al.*, Snoll. Sentinel Node and Occult (Impalpable) Lesion Localization in Breast Cancer. *Clin Radiol* **2011,** *66* (9), 833-839.
28. Ahmadzadehfar, H.; Sabet, A.; Biermann, K.; Muckle, M.; Brockmann, H.*, et al.*, The Significance of 99mTc-Maa SPECT/CT Liver Perfusion Imaging in Treatment Planning for 90Y-Microsphere Selective Internal Radiation Treatment. *J Nucl Med* **2010,** *51* (8), 1206-1212.
29. Dasari, R.; La Clair, J. J.; Kornienko, A., Irreversible Protein Labeling by Paal-Knorr Conjugation. *ChemBioChem* **2017,** *18* (18), 1792-1796.
30. Cope, A. C.; Pawson, B. A., Molecular Asymmetry of Olefins. Iv. Kinetics of Racemization of (+ or -)-Trans-Cyclooctene. *J Am Chem Soc* **1965,** *87* (16), 3649-3651.
31. Andrews, U. H.; Baldwin, J. E.; Grayston, M. W., On the Thermal Isomerization of Trans -Cyclooctene to Cis -Cyclooctene. *J Org Chem* **1982,** *47* (2), 287-292.
32. Chirkin, E.; Muthusamy, V.; Mann, P.; Roemer, T.; Nantermet, P. G.*, et al.*, Neutralization of Pathogenic Fungi with Small-Molecule Immunotherapeutics. *Angew. Chem. Int. Edit.* **2017,** *56* (42), 13216-13220.
33. Murelli, R. P.; Zhang, A. X.; Michel, J.; Jorgensen, W. L.; Spiegel, D. A., Chemical Control over Immune Recognition: A Class of Antibody-Recruiting Small Molecules That Target Prostate Cancer. *J Am Chem Soc* **2009,** *131* (47), 17090-17092.
34. Rullo, A. F.; Fitzgerald, K. J.; Muthusamy, V.; Liu, M.; Yuan, C.*, et al.*, Re-Engineering the Immune Response to Metastatic Cancer: Antibody-Recruiting Small Molecules Targeting the Urokinase Receptor. *Angew. Chem. Int. Edit.* **2016,** *55* (11), 3706-3710.
35. Matsumura, Y.; Maeda, H., A New Concept for Macromolecular Therapeutics in Cancer Chemotherapy: Mechanism of Tumoritropic Accumulation of Proteins and the Antitumor Agent Smancs. *Cancer Res* **1986,** *46*, 6387-6392.
36. Desai, N.; Trieu, V.; Damascelli, B.; Soon-Shiong, P., SPARC Expression Correlates with Tumor Response to Albumin-Bound Paclitaxel in Head and Neck Cancer Patients. *Transl Oncol* **2009,** *2* (2), 59-64.
37. Hoang, B.; Ernsting, M. J.; Roy, A.; Murakami, M.; Undzys, E.*, et al.*, Docetaxel-Carboxymethylcellulose Nanoparticles Target Cells Via a SPARC and Albumin Dependent Mechanism. *Biomaterials* **2015,** *59*, 66-76.
38. Miele, E.; Spinelli, G. P.; Miele, E.; Tomao, F.; Tomao1, S., Albumin-Bound Formulation of Paclitaxel (Abraxane® Abi-007) in the Treatment of Breast Cancer. *Int J Nanomed* **2009,** *4*, 99-105.
39. Finbloom, D. S.; Abeles, D.; Rifai, A.; Plotz, P. H., The Specificity of Uptake of Model Immune Complexes and Other Protein Aggregates by the Murine Reticuloendothelial System. *J Immunol* **1980,** *125* (3), 1060-1065.

40. Gleisner, K. S.; Brolin, G.; Sundlov, A.; Mjekiqi, E.; Ostlund, K.*, et al.*, Long-Term Retention of 177Lu/177mLu-DOTATATE in Patients Investigated by Gamma-Spectrometry and Gamma-Camera Imaging. *J Nucl Med* **2015,** *56* (7), 976-984.
41. Stehle, G.; Sinn, H.; Wunder, A.; Schrenk, H.; Schutt, S.*, et al.*, The Loading Rate Determines Tumor Targeting Properties of Methotrexate-Albumin Conjugates in Rats *Anti-Cancer Drugs* **1997,** *8*, 677-685.
42. Takakura, Y.; Fujita, T.; Hashida, M.; Sezaki, H., Disposition Characteristics of Macomolecules in Tumor-Bearing Mice. *Pharm Res* **1990,** *7* (4), 339-346.

Chapter 4 – Preparation of Actinium-225 and Lutetium-177 Labelled Bovine Serum Albumin using Bio-orthogonal Chemistry and Preliminary Evaluation Following Intratumoral Administration

4.1 Introduction

Traditionally, targeted radionuclide therapies (TRTs) are administered i.v. and accumulate at the site of interest through either a unique property of the molecule (e.g. affinity for hydroxyapatite and calcium turnover) or through the use of a targeting vector that directs the drug to the tumour.[1-6] One of the major challenges with this approach is on-target uptake in non-target tissues and non-specific binding, which results in the irradiation of healthy tissue potentially leading to unwanted side-effects. An alternative approach which was first used clinically as early as 1901, is direct infusion of a radiopharmaceutical into a tumour.[7] One such product which is used clinically, is yttrium-90 glass microspheres for the treatment of hepatocellular carcinoma (HCC) that was approved by the FDA in 1999.[8] HCC is a common form of liver cancer that is typically inoperable and has a one year survival rate of 20-24%.[9] In order to treat the inoperable mass, yttrium-90 labelled microspheres are infused directly into the tumour matrix or the hepatic artery. This procedure has been reported to increase the one-year survival rate to 54.5% in patients with stage II disease compared to 21 and 15% with the traditional treatments.[10]

Another form of cancer where i.t. administration is important is glioblastoma multiforme (GBM). GBM is an aggressive brain tumour that has a median overall survival of 10-15 months with standard treatments.[11] A recent

publication reported the direct infusion of a radiolabelled ligand targeting the neurokinin type-1 receptor (NK-1), into GBM tumours.[12] The ligand was labelled with both alpha and beta emitting radionuclides in order to determine the most efficacious option. It was found with the beta emitter, yttrium-90, there was improved patient survival but unfortunately there was also damage to healthy brain tissue due to the long-range beta emissions.[12, 13] This was rectified through the use of an alpha emitter, bismuth-213, which showed similar efficacy and reduced side effects due to the short path length of the emitted alpha particles.

A recent advancement in alpha therapy involves the implantation of a solid wire that releases alpha emitting radionuclides into a tumour. This is similar to brachytherapy where multiple seeds are implanted throughout a tumour mass, however brachytherapy seeds are typically composed of gamma or beta emitters. In the case of the alpha wire, the recoil energy from the decay of radium-224 releases the daughter isotopes from the wire at which point, unlike in the case of conventional brachytherapy where all isotopes are contained within the device, they migrate 2-3 mm into the surrounding tissue.[14] The wire has been used clinically in small numbers with the largest study treating 28 patients bearing squamous cell carcinomas of the skin and head and neck.[15] The wires were inserted directly in the lesions for 15-30 days at which point they were removed and the patient was evaluated for tumour response at 30-45 days post-implantation. A complete response (100% reduction in tumour dimensions) was seen in 78.6% of cases and a partial response (30-100% reduction in tumour dimensions) in 21.4% of the treated lesions. There were minimal toxicity related events, with the major documented

side-effect being pain at the implantation site. Currently, larger studies are underway to confirm these findings, and trials of patients with oral, skin and breast cancer are ongoing.[15, 16]

In general, direct infusion of radiopharmaceuticals is used for primary tumours that cannot be resected surgically, and is thought to not be useful for metastatic lesions.[9, 12, 17, 18] However, due to the immunogenic cell death that is seen with radiotherapy, it may be possible to generate a potent anti-tumour response in metastatic disease through treatment of a single lesion.[19-22] That being said, existing radiolabelled products for i.t. injection are not specifically designed to promote an immune response. Further, for existing compounds like MAA, the type of isotope cannot be easily varied making it challenging to assess the optimal type of radiation to promote the abscopal effect.

The TCO-bovine serum albumin (TCO-BSA) platform described in Chapter 3 offers a simple way to deliver different isotopes into preclinical tumours via i.t. administration. The platform easily lends itself to labelling with both alpha and beta emitting radionuclides to evaluate systemic anti-tumour response to different types of radiation.[23, 24] The approach has the added advantage that it allows the radiation dose delivered to the tumour to be readily varied which would be challenging with targeted radiopharmaceuticals that can suffer from systemic toxicity when attempting to deliver higher doses. As a result, prior to evaluating the combination R-ARM therapy *in vivo*, the most efficacious dosing regimen using different isotopes must be determined.

4.2 Materials and Methods

4.2.1 General Materials and Instruments

Chemicals and reagents for synthesis were purchased from Sigma-Aldrich and used without further purification. SABST80 buffer was made as follows: 500 mL water, 4.1 g NaOAc, 500 mL water, 4.1 g NaOAc, 1.7 g NaCl, 5 mL 1% tween 80 solution, 50 µL, 8 M HCl pH 6.5. ^{177}Lu[Lu] was produced by the McMaster Nuclear Reactor (MNR, Hamilton, Ontario) using the ^{176}Lu (p,γ) reaction and was provided as a solution of [^{177}Lu]$LuCl_3$ in 0.01 M HCl. [^{225}Ac]Ac was supplied by the U.S. Department of Energy Isotope Program in the Office of Science for Nuclear Physics as a dried powder ([^{225}Ac]Ac$(NO_3)_3$). Radio-TLC was performed using a Bioscan AR-2000 imaging scanner on iTLC-SG glass microfiber chromatography paper (SGI0001, Agilent Technologies) plates using 0.1 M EDTA as the eluent. For each TLC performed, plates were spotted with approximately 2 µL (~3.7 kBq) and run for 5 minutes.

4.2.2 Radiochemistry

To a solution of **7** (100 µg, 48 nmol) in 100 µL of SABST80 buffer (pH 6.5) was added [^{225}Ac]Ac$(NO_3)_3$ (0.43-0.44 MBq). The reaction was heated to 60°C for 5 min at which point the reaction mixture was spotted on an iTLC plate and developed. Once the plate reached secular equilibrium (12 h) the iTLC was analyzed and the radiochemical yield of **18** was determined to be >99% (n=3). The mixture was then added to a solution of **12** (2.0 mg, 30 nmol) in 1 mL of saline and heated to 37°C for 1 hour. The mixture was then centrifuged at 5 × g for 5 min, the supernatant removed and the aggregates resuspended in sterile saline (2.0 mg/mL). The centrifugation procedure was completed a second time at which point the

aggregates were resuspended in sterile saline (2.0 mg/mL). After the formulated aggregates reached secular equilibrium (12 h) the radiochemical yield of **19** was measured and found to be 50-72% (n=3).

4.2.3 Animal Studies General

All animal studies were approved by the Animal Research Ethics Board at McMaster University. Mice were maintained under clean conditions in an established animal facility with 12 hour light/dark cycles and given food and water ad libitum.

4.2.4 Actinium Therapy Study

Female, 6-8 week old Balb/c mice ordered from Charles River Laboratory (Kingston, NY) were inoculated with 2×10^6 4T1 cells in the flank. Once the tumours were palpable ~ 100 mm^3, the mice were split into 4 groups (n=5), and administered 50 µm of **16** (control), low dose (0.74 kBq), medium dose (3.5 kBq) or high dose (7.0 kBq) of **19**. Mice were followed for survival and tumours measured every 2-3 days. Mice were sacrificed when they reached endpoint (tumour volume=10% of body weight).

4.2.5 Multi-dosing Study of Lutetium Aggregates

Female, 6-8 week old, C57BL/6 mice ordered from Charles River Laboratory (Kingston, NY) were inoculated with 5×10^6 E0771 cells in the left flank. Once palpable tumours arose (~100 mm^3) mice were treated with 2 doses of **14** (0.19 – 0.74 MBq, 100 µg) one week apart. The four groups consisted of a control (**16**), low dose (0.19 MBq), medium dose (0.37 MBq) and high dose (0.74

MBq) of **14**. Mice were followed for survival and tumours measured every 2-3 days. Mice were sacrificed when they reached endpoint (tumour volume=1000 mm^3).

4.2.6 Single Dose Study of Lutetium Aggregates

Female, 6-8 week old, C57BL/6 mice ordered from Charles River Laboratory (Kingston, NY) were tumour inoculated with 5×10^6 E0771 cells in the left flank. Once palpable tumours arose (~100 mm^3) mice were treated with a single dose of **14** (1.1 – 3.3 MBq, 100 μg) intratumorally. The four groups (n=5) consisted of a control (**16**), low dose (1.1 MBq), medium dose (2.2 MBq) and high dose (3.3 MBq) of **14**. Mice were followed for survival and tumours measured every 2-3 days. Mice were sacrificed when they reached endpoint (tumour volume = 1000 mm^3).

4.2.7 Autoradiography

C57BL/6 mice bearing an E0771 flank tumour were administered a single dose of **14** or **15** (0.15 – 0.33 MBq, 100 μg) i.t. on day 12 of growth when the tumours were palpable (~100 mm^3). The mice were sacrificed after 24, 72 or 120 hours (n=3) at which point the tumours were harvested, placed on a cryomold and submerged in optimal cutting temperature (OCT) compound. The cryomold was then wrapped in plastic wrap, and flash frozen in liquid nitrogen for 15 seconds. The tumours were sent for analysis where they were sliced and placed on a phosphor screen for 10 days.

4.2.8 Multi-dosing Study of Lutetium Labeled TCO-BSA (Non-Aggregate)

Female, 6-8 week old, C57BL/6 mice ordered from Charles River Laboratory (Kingston, NY) were inoculated with 5×10^6 E0771 cells in the left flank. Once palpable tumours arose (~100 mm^3) mice were treated with 2 doses of

15 (0.74 – 4.8 MBq, 100 μg) five days apart. The five groups (n=5) consisted of a saline group, control (**17**), low dose (0.74 MBq), medium dose (2.6 MBq) and high dose (4.8 MBq) of **15**. Mice were followed for survival and tumours measured every 2-3 days. Mice were sacrificed when they reached endpoint (tumour volume = 1000 mm^3).

4.3 Results and Discussion

4.3.1 Radiolabelling

From the work described in Chapter 3, a method for labelling the TCO-BSA derivatives with a beta emitter was already developed. For alpha emitters, a method for labelling with actinium-225 was needed. Actinium-225 was selected due to its long half-life, emission of multiple alpha particles and recent promise in clinical trials.[25] Typical conditions for labelling DOTA-derivatives with actinium-225 are similar to that of lutetium-177, however the detection methods differ. Due to the low penetration depth of alpha particles, they cannot be detected by the same instrumentation commonly used for lutetium-177 radiochemical analysis. Typically, gas-filled detectors are used in analytical instruments such as dose calibrators, HPLC detectors and radio-TLC scanners. The gas in the detectors is ionized by incoming radiation, and the change in electric potential caused by the ionization events is measured by two electrodes.[26] Since the alpha particles are not able to penetrate deep enough to cause ionization events in these detectors, the methods are not useful in the direct characterization of radiopharmaceuticals labelled with alpha emitters.[27] In the case of actinium-225, there are two gamma emissions in the decay chain, one from the daughter francium-221 and the other from bismuth-213.[28] The gamma emissions allow actinium-225 to be detected

"indirectly" and analyzed after reaching secular equilibrium. This occurs when the number of short-lived daughter isotopes decaying per unit time becomes equal to the number that are forming.[29] In the case of actinium-225 reactions, secular equilibrium is reached after 4-5 hours at which point the gamma emissions from the daughters can be analyzed by radio-TLC and measured using a dose calibrator.[30, 31] As a result, all analytical measurements were taken at least 4 hours post-isolation.

Compound **7** was incubated with [^{225}Ac]Ac(NO_3)$_3$ at 60 °C for 5 minutes at which point the reaction was loaded onto an activated Sep-Pak C18 light cartridge and washed with EDTA solution to remove any unreacted radiometals. The radiolabelled product (**18**) was then eluted from the SPE cartridge using ethanol. A radio-TLC study was performed to analyze the purity of the isolated compound. The plate was run in a 0.1 M EDTA solution, with the unreacted metal travelling to the solvent front (R_f=1.0) and the radiolabelled product remaining on the baseline (R_f=0.0). The isolated radiochemical yield of **18** was 68 ± 1% with radiochemical purity of >98%.

The radiolabelled ligand was added to a solution of **12** (2.0 mg/mL) for one hour at 37 °C followed by centrifugation to isolate the radiolabelled aggregates from the unreacted ligand, actinium and low molecular weight impurities. After reaching secular equilibrium, the radiochemical yield of the reaction was measured using a dose calibrator, with only 2% of the activity remaining in the pellet. This result was much lower than expected, consequently the reaction was repeated with a new batch of **18** and the same result was observed. It was apparent from the radio-

TLC analysis of the ligand that the chelation reaction was successful, with greater than 98% radiochemical purity (Figure 4-1). The cause of the low yield was potentially due to an issue with the TCO-tetrazine reaction which was further investigated.

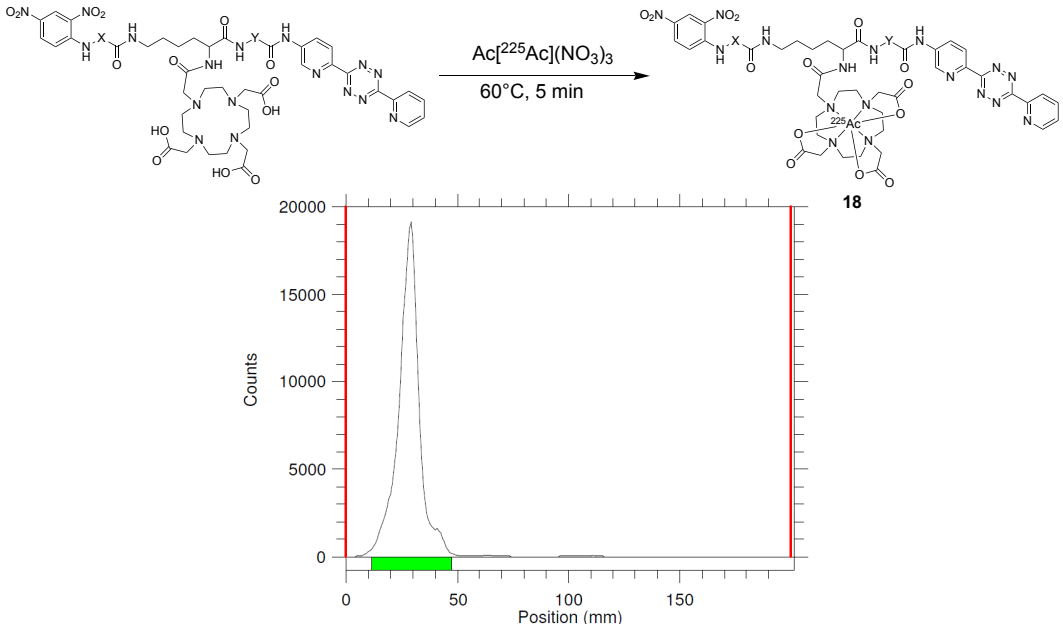

Figure 4-1. Radiolabelling scheme and radio-TLC data following the preparation of **18**, where the eluent was 0.1 M EDTA (iTLC-SA stationary phase). The peak at the baseline represents the radiolabelled ligand where had there been "free" radiometal a peak would be evident at the solvent front.

The coupling reaction between the lutetium-177 tetrazine ligand (**8**) and TCO-BSA aggregates (**12**) was demonstrated in Chapter 3 in a mixture of saline and 0.1 M NaOAc buffer. The IEDDA reaction is documented to be rapid in protic solvents due to both hydrophobic effects and the ability of the solvent to hydrogen bond with the tetrazine which lowers the HOMO-LUMO gap.[32, 33] Previously, **8** had been successfully coupled to a small molecule TCO-targeting vector in a solution of 10% ethanol in saline. Based on this information, it was surprising that after one hour at 37 °C in a mixture of ethanol and saline only 2% of the tetrazine

had reacted. We hypothesized that the reaction of **18** with TCO-BSA might have been impacted by the presence of ethanol which could impact the structure of the protein, reducing the accessibility of the TCO groups. The ethanol was required to remove **8** from the SPE during purification. Three options were thus considered: 1) evaporate the ethanol prior to the click reaction, 2) use a different purification method or 3) use compound **8** without SPE purification which would eliminate the need to use ethanol. As the evaporation process could lead to decomposition of the radiolabelled product, and the traditional method of purification, HPLC, is not a simple option for an actinium complex, and it would still require solvent evaporation, option 3 was pursued. The use of compound **18** without SPE purification was deemed reasonable given that the radiolabelling yield was >98%. When the coupling reaction between **18** and **12** was performed in a mixture of saline and SABST80 buffer with no ethanol, the reaction yield increased from 2% to 70% producing sufficient material to move on to therapy studies.

4.3.2 Alpha Therapy

Prior to performing a full therapy study, the actinium-labelled aggregates (**19**) were evaluated for their tolerability in a 4T1 mouse model. As there is limited literature available for the ideal dose range for i.t. administration of actinium-225 in mice, the first study served as a preliminary test of radiotoxicity. The typical dose range for an actinium radiopharmaceutical administered i.v. in a mouse is 1.85-15 kBq.[34, 35] It has been reported that mice treated with 13 kBq of an actinium-225 labelled antibody i.v. had an average of 50-60% lower body weight than control animals, with the maximum tolerated dose considered to be 14.8 kBq.[34, 36, 37] Since

our strategy involves the direct injection of the radiopharmaceutical into the tumour, we used slightly lower doses of 0.74-7.4 kBq as the activity is highly retained in the tumour, based on the data presented in Chapter 3 for compound **14**, with minimal loss to the surrounding tissue. Once the tumours were palpable, ~ 100 mm^3, the mice were split into 4 groups (n=5), and administered control (**16**), low dose (0.74 kBq), medium dose (3.5 kBq) or high dose (7.4 kBq) of **19** intratumorally. The doses were calculated by multiplying the volume of the injected dose by the concentration of the stock solution containing **19**. This was done, as opposed to simply direct counting of the syringe, as the secular equilibrium of the stock solution was disrupted by preparing doses, therefore the syringes could not be read in the dose calibrator until secular equilibrium was once again reached. Mice were followed for overall health and their tumours were measured every 2-3 days. On day 7, the animals were sacrificed, and the tumours were harvested for IHC.

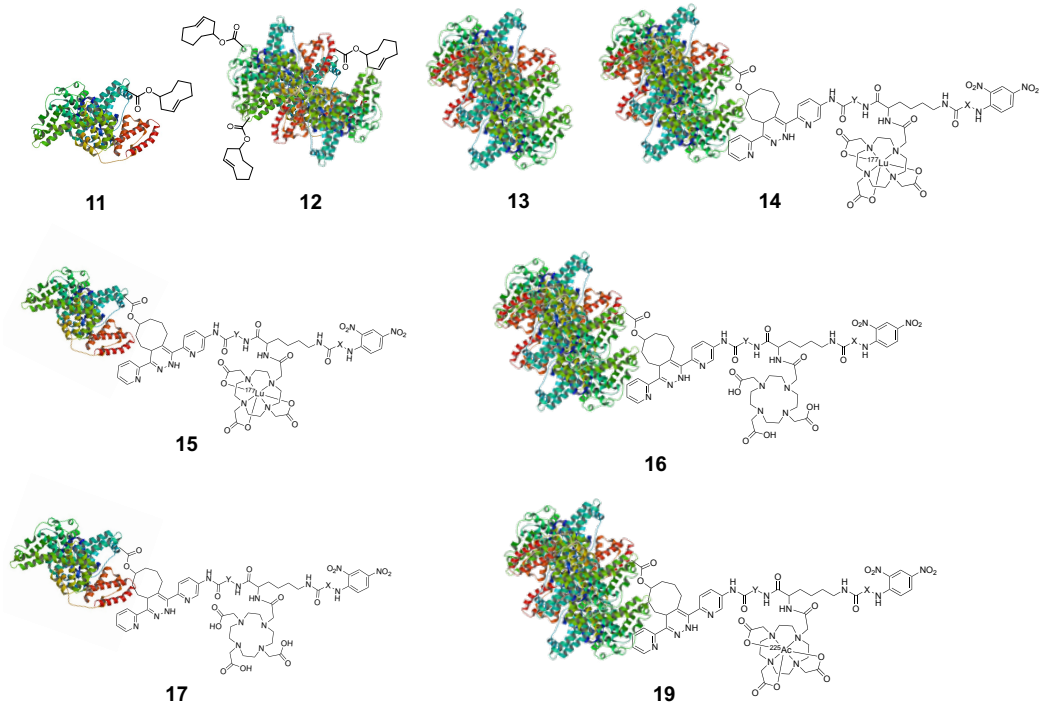

Figure 4-2. Structures of compounds **11-17** and **19**

Throughout the course of the treatment, the mice were monitored for signs of distress as well as changes in body weight for any evidence of radiotoxicity from the therapy. The relative body weight of the animals is shown in Figure 4-3, with all of the mice except two gaining or maintaining their body weight over the seven day period with no documented signs of distress. Two of the mice in the high dose group lost 5% of their relative body weight between days 5-7 but did not demonstrate any additional behaviour that would suggest a radiotoxicity related side effect. Despite the radiotoxicity that can be seen with high doses of [^{225}Ac]Ac-radiopharmaceuticals administered i.v., the results suggest that the i.t. treatments were well tolerated. The size of the tumours were also monitored over the seven day period and there was no apparent difference in tumour growth rate between the control and the treatment groups (Figure 4-4). This prompted us to look at the

pathology of these tumours post-treatment to determine if there was damage to the cells that was not reflected in the volume measurements.

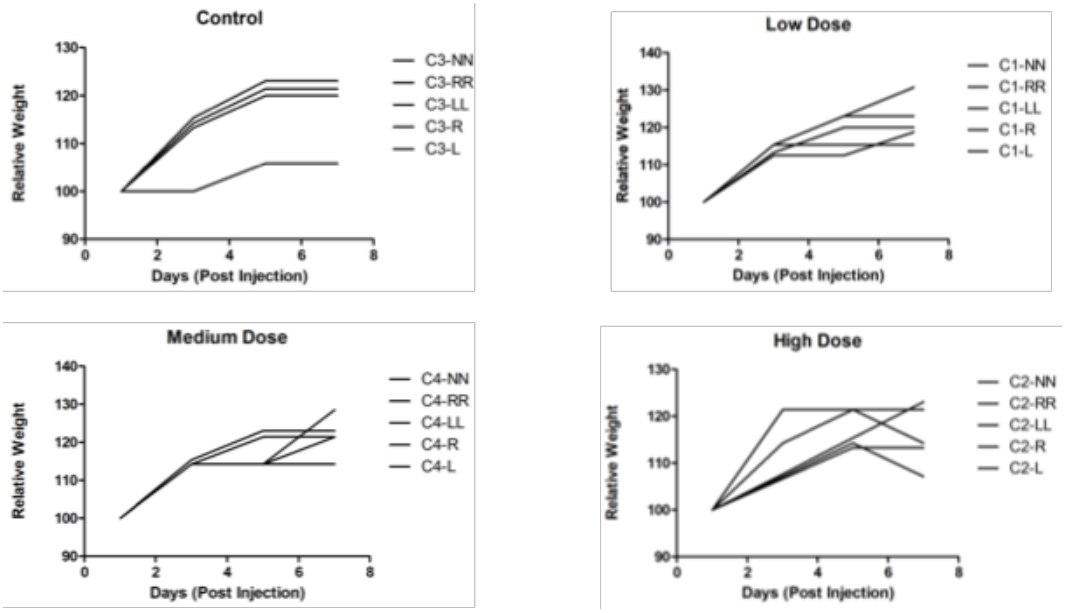

Figure 4-3. Relative body weight of the animals in the four dose groups of the actinium-225 therapy study (Balb/c mice with 4T1 breast cancer tumours, n=5 per group). The majority of animals maintained or gained weight over the 7 day period with two animals in the high dose group losing 5% of their relative weight between day 5 and 7. Legends represent the cage number and ear notch location for each of the animals.

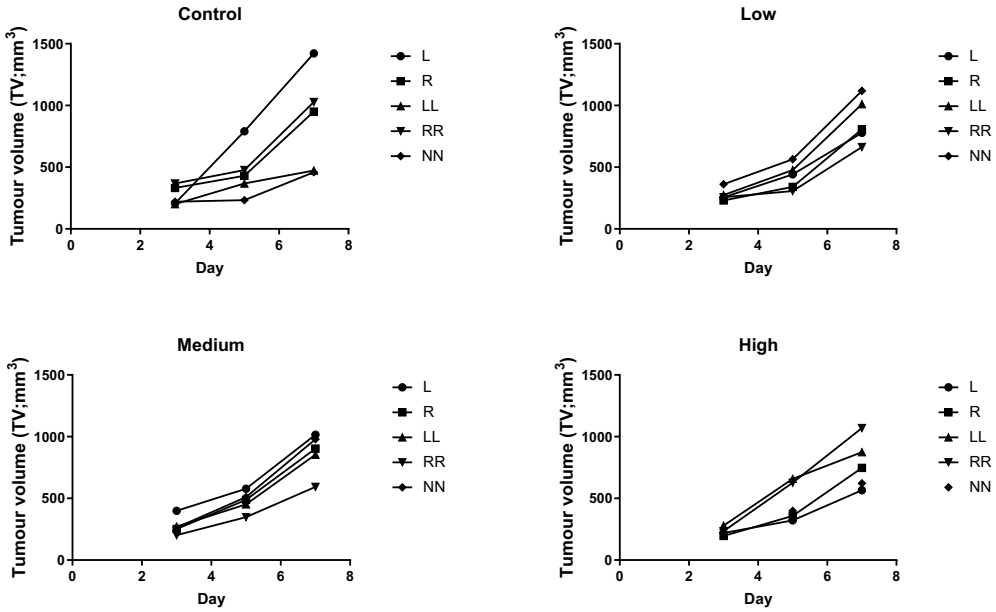

Figure 4-4. Tumour volume measurements of the alpha therapy study (Balb/c mice with 4T1 breast cancer tumours, n=5 per group, compound **19**). Legends represent the ear notch location for each of the animals.

4.3.3 Immunohistochemistry

Tumours were harvested and stained with H&E in order to visualize any morphological changes to the tumour cells that can be attributed to the radiopharmaceutical injection. The tumour slides were inspected and damage to tumour cells was observed in the medium and high dose groups in the form of increased necrosis compared to the control group (Figure 4-5). Since the tumour cells showed a response to the therapy which was not reflected in the tumour volume measurements, we believe that the rapid growth kinetics of the 4T1 breast cancer tumour did not provide enough time to demonstrate a response to the alpha therapy.[38]

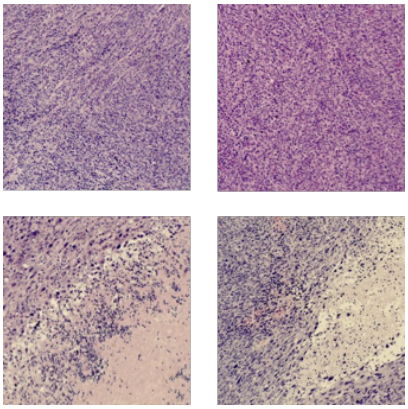

Figure 4-5. H&E staining of tumour slices from the tolerability study of **19**; top left – control, top right – low dose, bottom left – medium dose, bottom right – high dose (5× magnification). Purple/blue spots are the cell nuclei, pink areas are the cytoplasm and the off-white areas are areas of necrosis.[39]

4.3.4 Optimization of the Animal Model

It has been documented in the literature that it can take upwards of 10 days for a tumour to respond to some actinium therapies, which supports the hypothesis that the 4T1 model is likely not suitable for our purposes.[40] As the therapeutic was

administered i.t., it is not possible to simply inject the compound earlier in the tumour growth cycle as there must be a palpable tumour in which to administer the injection. The 4T1 model could be optimized in order to produce a slower growth rate and an increased duration between palpable size and endpoint, however in the interest of time we opted to change the model.[41]

4.3.5 Testing the E0771 Flank Tumour Model

The E0771 cell line was pursued for therapy as it, along with the 4T1 model, fall in the category of murine triple negative breast cancers (TNBCs).[42] TNBC is the most aggressive form of breast cancer, associated with the worst patient outcomes.[42, 43] This is in part due to the lack of expression of estrogen receptors (ER), progesterone receptors (PR), and human epidermal growth factor receptor 2 (HER2) which are typically used as therapeutic targets. That being said, due to the challenging task of identifying molecular targets for TNBC therapy, this model lends itself to i.t. administration of therapeutics and has slower growth kinetics than the 4T1 model. In addition, to better optimize the TCO-BSA therapy, we opted to do the initial studies with the beta emitter lutetium-177. This is due to the ability to directly detect the radiolabelled compounds and more easily validate the protocol, which can then be translated to actinium-225 studies.

The lutetium-labelled aggregates were synthesized as previously mentioned and formulated in 0.9% saline. C57BL/6 mice bearing an E0771 flank tumour were administered **14** (0.19-0.74 MBq, 100 μg). Unfortunately, when the aggregate doses were administered, the majority of the activity was retained in the syringe. Since the doses were significantly lower than anticipated a second dose was administered

in an attempt to improve efficacy. Based on literature data for multi-dosing lutetium therapies, the second dose was administered 7 days after the first.[44-46] Mice were followed for survival and tumours measured every 2-3 days. Mice were sacrificed when they reached endpoint (tumour volume=1000 mm^3).

The Kaplan Meier plot (Figure 4-6) shows that treatment with the highest dose slowed tumour progression and while not curative, it did confer a statistically significant ($P < 0.1$) survival advantage compared to the control group. These results were promising and further investigation into dose optimization and addressing the issue of sticking to the syringe were completed.

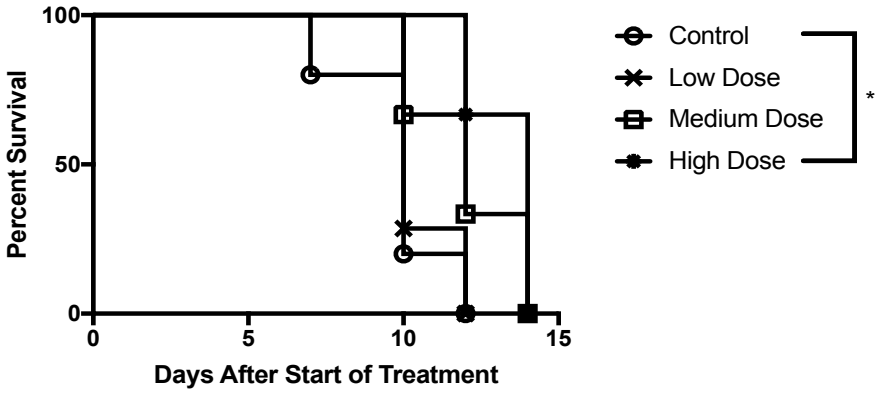

Figure 4-6. Kaplan-Meier plot of the therapy study. Compound **14** was administered i.t. in a range of doses from low (~0.19 MBq × 2) to high (~0.74 MBq × 2) showing a statistically significant survival advantage in the high dose group.

Prior to use in animal studies, the extent to which a radiolabelled compound adheres to surfaces, including syringes for injection, are often measured. A typical procedure involves measuring the amount of activity in the syringe using a dose calibrator, followed by expulsion of the liquid into a vial. The radioactivity in the vial and the syringe are then counted and the amount of radioactivity recorded. This test helps to determine the amount of activity that remains in the syringe post-injection, which can be used to determine accurate doses for animal studies. This

test was completed for the aggregates where it was found that 65-80% of the calculated dose was expelled from the syringe. This was not in agreement with the therapy study where 2-14% of the activity was expelled and the rest remained in the syringe. It was then determined that when left for extended periods of time without constant agitation, the radiolabelled aggregates stick to the syringe. All subsequent studies performed with the aggregates involved drawing the activity into the syringe, measuring the activity, which was followed by prompt administration.

After determining the reason for the activity remaining in the syringe, a single dose study was performed as was intended for the previous study. Lutetium-labelled aggregates were synthesized as before and formulated in 0.9% saline. C57BL/6 mice bearing an E0771 flank tumour were administered a single dose of **14** (1.1-3.3 MBq, 100 µg) intratumorally. The mice were followed for survival and tumours measured every 2-3 days. Mice were sacrificed when they reached endpoint (tumour volume=1000 mm^3).

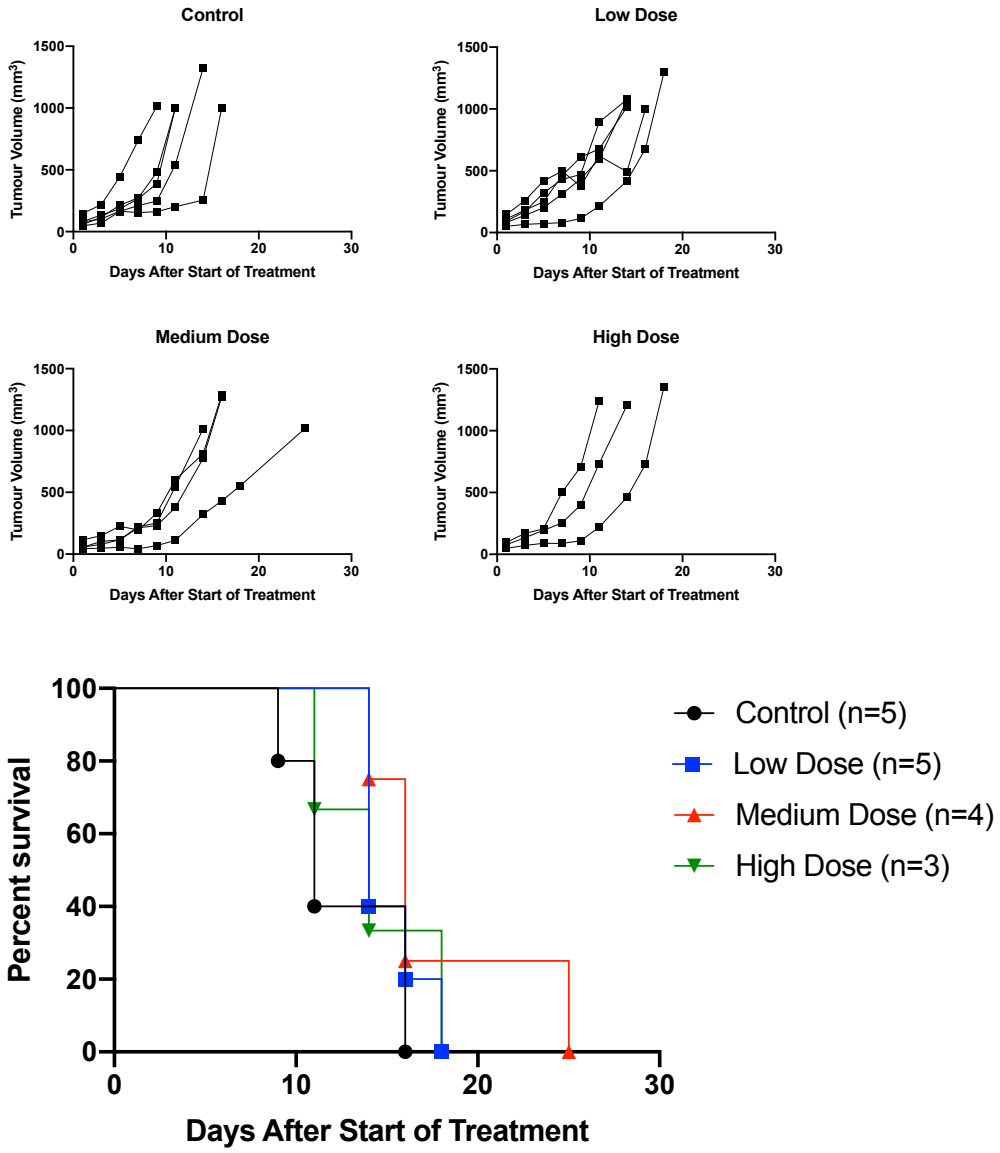

Figure 4-7. Top- Tumour volume graphs for each dose group over time; bottom - Kaplan-Meier plot of the therapy study. Compound **14** was injected in a range of doses from 1.1-3.3 MBq. No statistically significant survival advantage was seen in the treatment groups compared to the control.

The results of the therapy study are shown in Figure 4-7. Unfortunately, there did not seem to be a correlation between survival and increased dose. There is evidence in the literature that i.t. injection of lutetium-labelled nanoparticles can reduce the growth rate of the tumour relative to the control.[47-50] When analyzing the

experimental protocols of the nanoparticle studies, the compounds showed similar tumoral retention to the aggregates, and the employed dose range was similar at 2-8 MBq. A single injection with as low as 2 MBq resulted in a significant decrease in tumour mass after 7 days, but it is interesting to note that these articles do not include an *in vivo* dose optimization study.[49] The reported studies were not done in the E0771 tumour model, and since tumours have different levels of radiosensitivity the results cannot be directly correlated with our studies, but used more as a general guide.

Moving forward, increasing the amount of activity given in a single dose might result in a better response as the maximum tolerated dose was not reached, however the literature and the preliminary results with compound **14** suggests that a multi-dosing approach could be more efficacious. A notable study compared a single dose of 18.5 MBq of lutetium therapy to 4 doses of 4.63 MBq one week apart.[45] The study showed the median time to endpoint for the single dose and fractionated dose were 32 and 49 days respectively, with the single dose group developing metastasis that were not seen in the fractionated group.

4.3.6 Autoradiography

In addition to dose optimization, an important factor to consider is the spatial distribution of the radiolabelled aggregates within the tumour. As they are a microparticle, it is possible that once injected they become anchored to the injection site and are not able to migrate within the tumour, leaving only a small portion of the tumour directly exposed to ionizing radiation. Although a direct encounter with cytotoxic radiation is not required for cell death due to the bystander effect,[21, 51, 52]

a more even distribution of the radiopharmaceutical throughout the tumour is optimal particularly in the case of R-ARM therapies.[53] In order to validate the distribution within the tumour storage-phosphor autoradiography was performed. C57BL/6 mice bearing an E0771 flank tumour were administered a single dose of **14** or **15** (0.15-0.33 MBq, 100 μg) i.t. on day 12 of growth when the tumours were palpable (~100 mm^3). The mice were sacrificed after 24, 72 or 120 hours at which point the tumours were harvested and flash frozen in liquid nitrogen. The tumours were sent for analysis where they were sliced and placed on a storage phosphor screen for a 10 day exposure.

The spatial distribution of the radioactivity in the tumour slices were analyzed at different time points, and the results depicted in Figure 4-8. Each image represents an individual tumour at 72 or 120 hours post-injection with the darkest spots representing the highest amount of activity. The outer edges of the tumours are not defined in the images as only the distribution of the radioactivity on the screen is represented using this technique. It can be seen in the images associated with **14** that the activity is generally concentrated in a single area, or a few small areas. The activity does not appear to get more dispersed over time as both the 72 and 120 hour images have similar distribution patterns. This drastically differs from the pattern observed for **15**, which appears more evenly dispersed throughout the tumour at both 72 and 120 hours post-injection.

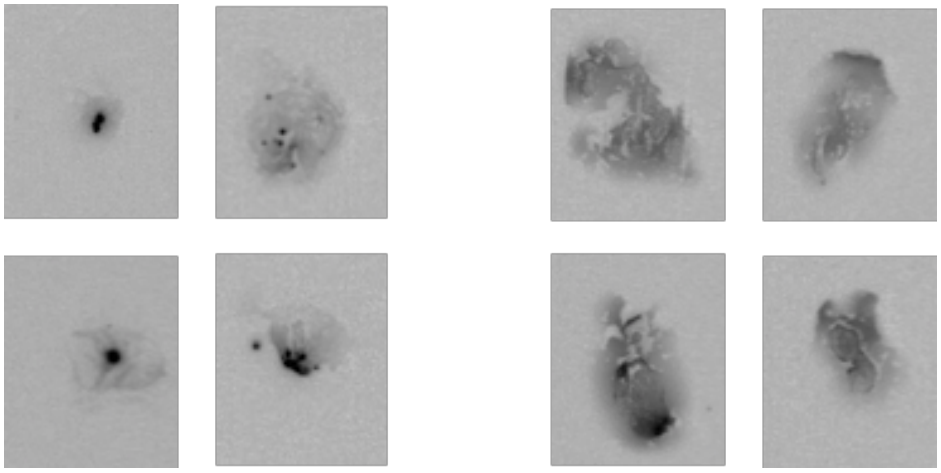

Figure 4-8. Autoradiography images of **14** (left) and **15** (right) at 72 (top) and 120 (bottom) hours post i.t. injection.

Based on the autoradiography results it appears that moving forward with **15** could provide a better result due to the more uniform distribution within the tumour. To this end C57BL/6 mice bearing an E0771 flank tumour were administered 2 doses of **15** (0.74-4.8 MBq, 100 μg) 5 days apart. Mice were followed for survival and tumours measured every 2-3 days. Mice were sacrificed when they reached endpoint (tumour volume=1000 mm^3).

It is clear from this study that there were signs of efficacy in both the high and medium dose groups that slowed tumour growth compared to the control (Figure 4-9). There was a statistically significant survival advantage ($P < 0.05$) for the high dose group compared to both the saline and **17** groups. A saline group was included in this study to analyze the impact of compound **17** on the tumour growth kinetics. Since the mice have an immune system and the tumours were being dosed with 100 μg of BSA with each injection, there was the potential that the scaffold possessed anti-tumour properties. It does not appear that the unlabelled compound had any impact on the tumour growth kinetics or the survival time when compared

to the saline control. This data suggests that the therapeutic efficacy that is seen in the high dose group is a result of the radionuclide and not the scaffold. Throughout the study, animals were monitored for signs of toxicity and all three dose groups handled the therapy well, with no apparent adverse effects. Overall, the results of this study are promising and future work towards further optimizing a corresponding multi-dosing study should be pursued.

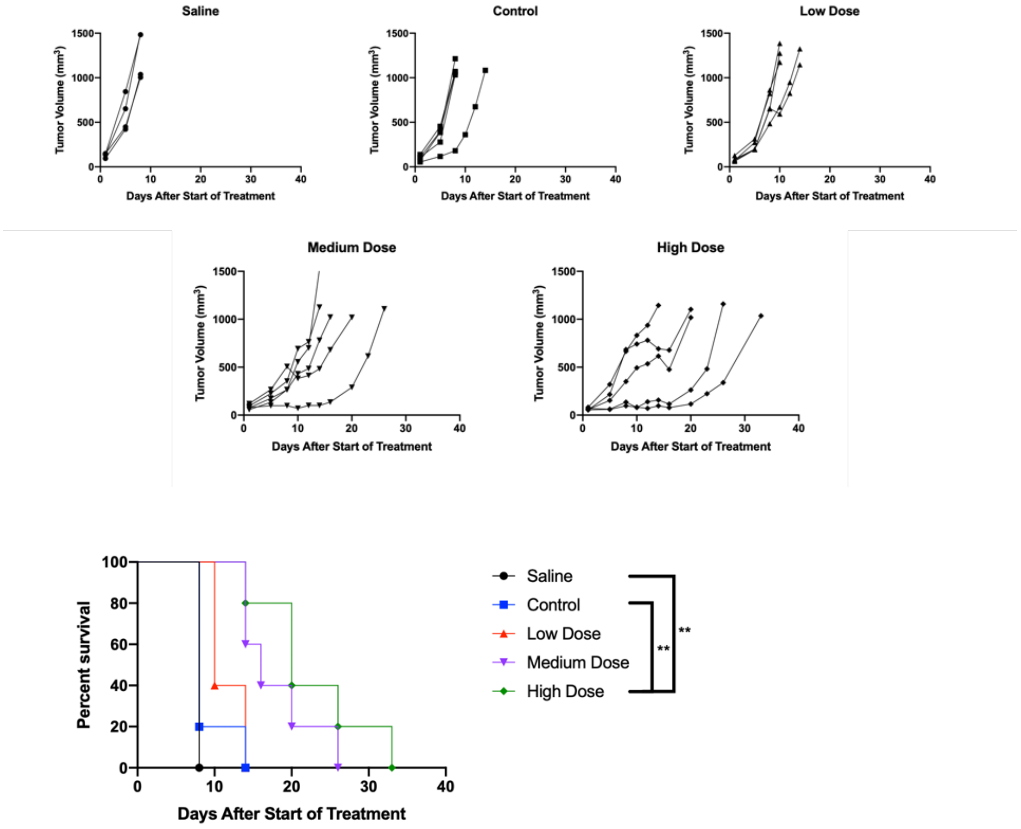

Figure 4-9. Top- Tumour volume versus time graphs for each dose group; Bottom - Kaplan-Meier plot for the therapy study. Compound **15** was injected in a range of doses from 0.74 – 4.8 MBq with a second injection 5 days later. A statistically significant survival advantage was seen in the high dose group compared to the control ($P<0.05$).

It is difficult to draw direct comparisons between the studies using **14** and **15** due to the differences in dosing regimen. Nevertheless, some key learnings

emerged from these studies. The autoradiography results demonstrated that the radiolabelled aggregates were more localized to the site of injection when compared to the non-aggregates. However, the biodistribution data suggested that the aggregates are better retained in the tumour with 81.5 ± 31.9 %ID/g at 120 hours compared to 61.6 ± 31.3 %ID/g for the non-aggregates, although the values are not statistically different. The data from the biodistribution and autoradiography studies seem to support the use of non-aggregated BSA, therefore future studies focusing on optimization of the frequency and amount of activity administered in addition to studies with the alpha emitter actinium-225 are warranted.

4.4 Conclusion

A novel actinium-225 tetrazine was radiolabelled, coupled to TCO-BSA aggregates and evaluated for tolerability in a murine breast cancer model. The mice showed no signs of distress over the 7 day period after i.t. injection of doses up to 7.4 kBq. A multi-dosing lutetium-177 BSA aggregate therapy study was also performed and showed a statistically significant survival advantage in the high dose group compared to the control. In an attempt to improve these results, a single dose study was performed at higher activity levels, however it showed no therapeutic efficacy when compared to the control. Through autoradiography it was determined that the spatial distribution of the radiolabelled aggregates was not ideal as the majority of the activity remained in one area of the tumour. In contrast, radiolabelled non-aggregated TCO-BSA showed a more homogenous distribution in the tumour. Based on these results, two doses of lutetium-labelled non-aggregated BSA were given 5 days apart and resulted in the most efficacious results

to date with statistically significant survival advantage ($P<0.05$) compared to the control. Overall, a TCO-BSA platform has been developed as a way to functionalize BSA with tetrazine derived molecules for i.t. delivery of cytotoxic radionuclides. In the future this approach can be combined with therapies that increase the immune cell presence at the tumour site such as ARM therapies in order to increase efficacy and build anti-tumour immunity.

4.5 References

1. Demirci, E.; Kabasakal, L.; Toklu, T.; Ocak, M.; Sahin, O. E.*, et al.*, 177Lu-DOTATATE Therapy in Patients with Neuroendocrine Tumours Including High-Grade (Who G3) Neuroendocrine Tumours: Response to Treatment and Long-Term Survival Update. *Nucl Med Commun* **2018,** *39* (8), 789-796.
2. Gleisner, K. S.; Brolin, G.; Sundlov, A.; Mjekiqi, E.; Ostlund, K.*, et al.*, Long-Term Retention of 177Lu/177mLu-Dotatate in Patients Investigated by Gamma-Spectrometry and Gamma-Camera Imaging. *J Nucl Med* **2015,** *56* (7), 976-984.
3. Hofman, M. S.; Violet, J.; Hicks, R. J.; Ferdinandus, J.; Thang, S. P.*, et al.*, [177 Lu]-PSMA-617 Radionuclide Treatment in Patients with Metastatic Castration-Resistant Prostate Cancer (LuPSMA Trial): A Single-Centre, Single-Arm, Phase 2 Study. *Lancet Oncol* **2018,** *19* (6), 825-833.
4. van der Zwan, W. A.; Brabander, T.; Kam, B. L. R.; Teunissen, J. J. M.; Feelders, R. A.*, et al.*, Salvage Peptide Receptor Radionuclide Therapy with [(177)Lu-DOTA,Tyr(3)]Octreotate in Patients with Bronchial and Gastroenteropancreatic Neuroendocrine Tumours. *Eur J Nucl Med Mol I* **2018**, 704-717.
5. Wustemann, T.; Bauder-Wust, U.; Schafer, M.; Eder, M.; Benesova, M.*, et al.*, Design of Internalizing PSMA-Specific Glu-Ureido-Based Radiotherapeuticals. *Theranostics* **2016,** *6* (8), 1085-1095.
6. Raedler, L. A., Xofigo (Radium Ra 223 Dichloride): The First Alpha Particle–Emitting Radioactive Agent for the Treatment of Castration-Resistant Prostate Cancer with Symptomatic Bone Metastases. *AHDB* **2014,** *7*, 195-199.
7. Lederman, M., The Early History of Radiotherapy: 1895:1939. *Int. J. Radiat. Oncol., Biol., Phys.* **1981,** *7*, 639-648.
8. Reardon, K. A.; McIntosh, A. F.; Shilling, A. T.; Hagspiel, K. D.; Al-Osaimi, A.*, et al.*, Treatment of Primary Liver Tumors with Yttrium-90 Microspheres (Therasphere®) in High Risk Patients: Analysis of Survival and Toxicities. *Technol Cancer Res T* **2009,** *8* (1), 71-77.
9. Lin, W.-Y.; Tsai, S.-C.; Hsieh, J.-F.; Wang, S.-J., Effects of 90Y-Microspheres on Liver Tumors: Comparison of Intratumoral Injection Method and Intra-Arterial Injection Method. *J Nucl Med* **2000,** *41* (11), 1892-1897.

10. Salem, R.; Lewandowski, R. J.; Atassi, B.; Gordon, S. C.; Gates, V. L., *et al.*, Treatment of Unresectable Hepatocellular Carcinoma with Use of 90Y Microspheres (Therasphere): Safety, Tumor Response, and Survival. *J Vasc Interv Radiol* **2005,** *16* (12), 1627-1639.
11. Cordier, D.; Krolicki, L.; Morgenstern, A.; Merlo, A., Targeted Radiolabeled Compounds in Glioma Therapy. *Semin Nucl Med* **2016,** *46* (3), 243-249.
12. Majkowska-Pilip, A.; Rius, M.; Bruchertseifer, F.; Apostolidis, C.; Weis, M., *et al.*, In Vitro Evaluation of (225) Ac-DOTA-Substance P for Targeted Alpha Therapy of Glioblastoma Multiforme. *Chem Biol Drug Des* **2018,** *92* (1), 1344-1356.
13. Krolicki, L.; Bruchertseifer, F.; Kunikowska, J.; Koziara, H.; Krolicki, B., *et al.*, Safety and Efficacy of Targeted Alpha Therapy with (213)Bi-DOTA-Substance P in Recurrent Glioblastoma. *Eur J Nucl Med Mol I* **2019,** *46* (3), 614-622.
14. Cooks, T.; Schmidt, M.; Bittan, H.; Lazarov, E.; Arazi, L., *et al.*, Local Control of Lung Derived Tumors by Diffusing Alpha-Emitting Atoms Released from Intratumoral Wires Loaded with Radium-224. *Int J Radiat Oncol Biol Phys* **2009,** *74* (3), 966-973.
15. Popovtzer, A.; Rosenfeld, E.; Mizrachi, A.; Bellia, S. R.; Ben-Hur, R., *et al.*, Initial Safety and Tumor Control Results from a "First-in-Human" Multicenter Prospective Trial Evaluating a Novel Alpha-Emitting Radionuclide for the Treatment of Locally Advanced Recurrent Squamous Cell Carcinomas of the Skin and Head and Neck. *Int J Radiat Oncol Biol Phys* **2020,** *106* (3), 571-578.
16. Alphatau Clinical Trials. https://www.alphatau.com/alpha-dart-clinical-trials.
17. Kim, J. K.; Han, K. H.; Lee, J. T.; Paik, Y. H.; Ahn, S. H., *et al.*, Long-Term Clinical Outcome of Phase IIb Clinical Trial of Percutaneous Injection with Holmium-166/Chitosan Complex (Milican) for the Treatment of Small Hepatocellular Carcinoma. *Clin Cancer Res* **2006,** *12* (2), 543-548.
18. Morgenstern, A.; Bruchertseifer, F., Development of Targeted Alpha Therapy from Bench to Bedside. *J Med Imag Radiat Sci* **2019,** *50* (4), S18-S20.
19. Demaria, S.; Ng, B.; Devitt, M. L.; Babb, J. S.; Kawashima, N., *et al.*, Ionizing Radiation Inhibition of Distant Untreated Tumors (Abscopal Effect) Is Immune Mediated. *Int J Radiat Oncol Biol Phys* **2004,** *58* (3), 862-870.
20. Dewan, M. Z.; Galloway, A. E.; Kawashima, N.; Dewyngaert, J. K.; Babb, J. S., *et al.*, Fractionated but Not Single-Dose Radiotherapy Induces an Immune-Mediated Abscopal Effect When Combined with Anti–CTLA-4 Antibody. *Clin Cancer Res* **2009,** *15* (17), 5379-5388.
21. Pouget, J. P.; Georgakilas, A. G.; Ravanat, J. L., Targeted and Off-Target (Bystander and Abscopal) Effects of Radiation Therapy: Redox Mechanisms and Risk/Benefit Analysis. *Antioxid Redox Signal* **2018,** *29* (15), 1447-1487.
22. Rodriguez-Ruiz, M. E.; Vanpouille-Box, C.; Melero, I.; Formenti, S. C.; Demaria, S., Immunological Mechanisms Responsible for Radiation-Induced Abscopal Effect. *Trends Immunol* **2018,** *39* (8), 644-655.

23. Confino, H.; Hochman, I.; Efrati, M.; Schmidt, M.; Umansky, V.*, et al.*, Tumor Ablation by Intratumoral Ra-224-Loaded Wires Induces Anti-Tumor Immunity against Experimental Metastatic Tumors. *Cancer Immunol Immunother* **2015,** *64* (2), 191-199.
24. Yokouchi, H.; Yamazaki, K.; Chamoto, K.; Kikuchi, E.; Shinagawa, N.*, et al.*, Anti-Ox40 Monoclonal Antibody Therapy in Combination with Radiotherapy Results in Therapeutic Antitumor Immunity to Murine Lung Cancer. *Cancer Sci* **2008,** *99* (2), 361-367.
25. Sathekge, M.; Bruchertseifer, F.; Knoesen, O.; Reyneke, F.; Lawal, I.*, et al.*, (225)Ac-PSMA-617 in Chemotherapy-Naive Patients with Advanced Prostate Cancer: A Pilot Study. *Eur J Nucl Med Mol Imaging* **2019,** *46* (1), 129-138.
26. Saha, G. B., Physics and Radiobiology of Nuclear Medicine. **2013**.
27. McDowell, W., *Liquid Scintillation Alpha Spectrometry*. CRC Press: 2018.
28. Scheinberg, D. A.; McDevit, M. R., Actinium-225 in Targeted Alpha-Particle Therapeutic Applications. *Curr Radiopharm* **2011,** *4* (4), 306-320.
29. Prince, J. R., Comments on Equilibrium, Transient Equilibrium, and Secular Equilibrium in Serial Radioactive Decay. *J Nucl Med* **1979,** *20*, 162-164.
30. McDevitt, M. R.; Ma, D.; Lai, L. T.; Simon, J.; Borchardt, P.*, et al.*, Tumor Therapy with Targeted Atomic Nanogenerators. *Science* **2001,** *294* (5546), 1537-1540.
31. McDevitt, M. R.; Finn, R. D.; Sgouros, G.; Ma, D.; Scheinberg, D. A., An 225Ac/213Bi Generator System for Therapeutic Clinical Applications: Construction and Operation. *Appl Radiat Isot* **1999,** *50*, 895-904.
32. Oliveira, B. L.; Guo, Z.; Bernardes, G. J. L., Inverse Electron Demand Diels-Alder Reactions in Chemical Biology. *Chem Soc Rev* **2017,** *46* (16), 4895-4950.
33. Blackman, M. L.; Royzen, M.; Fox, J. M., Tetrazine Ligation: Fast Bioconjugation Based on Inverse-Electron-Demand Diels-Alder Reactivity. *J Am Chem Soc* **2008,** *130* (41), 13518-13519.
34. Essler, M.; Gartner, F. C.; Neff, F.; Blechert, B.; Senekowitsch-Schmidtke, R.*, et al.*, Therapeutic Efficacy and Toxicity of 225Ac-Labelled Vs. 213Bi-Labelled Tumour-Homing Peptides in a Preclinical Mouse Model of Peritoneal Carcinomatosis. *Eur J Nucl Med Mol I* **2012,** *39* (4), 602-612.
35. Josefsson, A.; Nedrow, J. R.; Park, S.; Ranka, S.; Sgouros, G., Combining A-Particle Radiopharmaceutical Therapy Using Actinium-225 and Immunotherapy with Anti-PD-L1 Antibodies in a Murine Immunocompetent Metastatic Breast Cancer Model. 2016; pp 3052-3052.
36. Jaggi, J. S.; Seshan, S. V.; McDevitt, M. R.; LaPerle, K.; Sgouros, G.*, et al.*, Renal Tubulointerstitial Changes after Internal Irradiation with Alpha-Particle-Emitting Actinium Daughters. *J Am Soc Nephrol* **2005,** *16* (9), 2677-2689.
37. Song, H.; Hobbs, R. F.; Vajravelu, R.; Huso, D. L.; Esaias, C.*, et al.*, Radioimmunotherapy of Breast Cancer Metastases with Alpha-Particle Emitter 225Ac: Comparing Efficacy with 213Bi and 90Y. *Cancer Res* **2009,** *69* (23), 8941-8948.

38. Gao, Z. G.; Tian, L.; Hu, J.; Park, I. S.; Bae, Y. H., Prevention of Metastasis in a 4T1 Murine Breast Cancer Model by Doxorubicin Carried by Folate Conjugated Ph Sensitive Polymeric Micelles. *J Control Release* **2011,** *152* (1), 84-89.
39. Fischer, A. H.; Jacobson, K. A.; Rose, J.; Zeller, R., Hematoxylin and Eosin Staining of Tissue and Cell Sections. *Cold Spring Harb. Protoc.* **2008,** *2008* (5), pdb-prot4986.
40. Ballangrud, A. s. M.; Yang, W.-H.; Palm, S.; Enmon, R.; Borchardt, P. E.*, et al.*, Alpha-Particle Emitting Atomic Generator (Actinium-225)-Labeled Trastuzumab (Herceptin) Targeting of Breast Cancer Spheroids: Efficacy Versus Her2/Neu Expression. *Clin Cancer Res* **2004,** *10*, 4489-4497.
41. Bove, K.; Lincoln, D. W.; Tsan, M. F., Effect of Resveratrol on Growth of 4T1 Breast Cancer Cells in Vitro and in Vivo. *Biochem Biophys Res Commun* **2002,** *291* (4), 1001-1005.
42. Johnstone, C. N.; Smith, Y. E.; Cao, Y.; Burrows, A. D.; Cross, R. S.*, et al.*, Functional and Molecular Characterisation of EO771.Lmb Tumours, a New C57Bl/6-Mouse-Derived Model of Spontaneously Metastatic Mammary Cancer. *Dis Model Mech* **2015,** *8* (3), 237-251.
43. Huynh, M. M.; Jayanthan, A.; Pambid, M. R.; Los, G.; Dunn, S. E., Rsk2: A Promising Therapeutic Target for the Treatment of Triple-Negative Breast Cancer. *Expert Opin Ther Targets* **2020,** *24* (1), 1-5.
44. Schlom, J.; Siler, K.; Milenic, D. E.; Eggensperger, D.; Colcher, D.*, et al.*, Monoclonal Antibody-Based Therapy of a Human Tumor Xenograft with a 177lutetium-Labeled Immunoconjugate. *Cancer Res* **1991,** *51*, 2889-2896.
45. Liu, D.; Balkin, E. R.; Jia, F.; Ruthengael, V. C.; Smith, C. J.*, et al.*, Targeted Antisense Radiotherapy and Dose Fractionation Using a (177)Lu-Labeled Anti-Bcl-2 Peptide Nucleic Acid-Peptide Conjugate. *Nucl Med Biol* **2015,** *42* (9), 704-710.
46. Schott, M. E.; Schlom, J.; Siler, K.; Milenic, D. E.; Eggensperger, D.*, et al.*, Biodistribution and Preclinical Radioimmunotherapy Studies Using Radiolanthanide-Labeled Lmmunoconjugates. *Cancer Supplement* **1994,** *73* (3), 993-998.
47. Cai, Z.; Yook, S.; Lu, Y.; Bergstrom, D.; Winnik, M. A.*, et al.*, Local Radiation Treatment of Her2-Positive Breast Cancer Using Trastuzumab-Modified Gold Nanoparticles Labeled with (177)Lu. *Pharm Res* **2017,** *34* (3), 579-590.
48. González-Ruíz, A.; Ferro-Flores, G.; Jiménez-Mancilla, N.; Escudero-Castellanos, A.; Ocampo-García, B.*, et al.*, In Vitro and in Vivo Synergistic Effect of Radiotherapy and Plasmonic Photothermal Therapy on the Viability of Cancer Cells Using 177Lu–Au-Nls-RGD-Aptamer Nanoparticles under Laser Irradiation. *J Radioanal Nucl Chem* **2018,** *318* (3), 1913-1921.
49. Vilchis-Juarez, A.; Ferro-Flores, G.; Santos-Cuevas, C.; Morales-Avila, E.; Ocampo-Garcia, B.*, et al.*, Molecular Targeting Radiotherapy with Cyclo-Rgdfk(C) Peptides Conjugated to 177Lu-Labeled Gold Nanoparticles in Tumor-Bearing Mice. *J Biomed Nanotechnol* **2014,** *10* (3), 393-404.

50. You, J.; Zhao, J.; Wen, X.; Wu, C.; Huang, Q.*, et al.*, Chemoradiation Therapy Using Cyclopamine-Loaded Liquid-Lipid Nanoparticles and Lutetium-177-Labeled Core-Crosslinked Polymeric Micelles. *J Control Release* **2015,** *202*, 40-48.
51. Hamada, N.; Matsumoto, H.; Hara, T.; Kobayashi, Y., Intercellular and Intracellular Signaling Pathways Mediating Ionizing Radiation-Induced Bystander Effects. *J Radiat Res* **2007,** *48* (2), 87-95.
52. Marin, A.; Martin, M.; Linan, O.; Alvarenga, F.; Lopez, M.*, et al.*, Bystander Effects and Radiotherapy. *Rep Pract Oncol Radiother* **2015,** *20* (1), 12-21.
53. Bakker, R. C.; Lam, M.; van Nimwegen, S. A.; Rosenberg, A.; van Es, R. J. J.*, et al.*, Intratumoral Treatment with Radioactive Beta-Emitting Microparticles: A Systematic Review. *J Radiat Oncol* **2017,** *6* (4), 323-341.

Chapter 5 – Model Development for Testing Antibody Recruiting Small Molecule Therapies

With respect to this chapter, I was responsible for the chemical synthesis, design and execution of the studies and interpretation of the results. The biology work was done in collaboration with Nancy Janzen, Amber Faraday and Natalie Mercanti who were responsible for immunizing the mice and blood draws. The ELISAs were run by myself, Amber, Nancy and Natalie. Alyssa Vito was responsible for developing the mouse model and performing *in vivo* studies.

5.1 Overview

In Chapter 3 it was shown that an i.t. injection of radiolabelled TCO-BSA derivatives resulted in high tumoral retention over 5 days. Building on this information, an animal model to evaluate the efficacy of R-ARMs was developed. The model, which was derived from one studied in Chapter 4, required immunocompetent animals that produced a high anti-DNP antibody titre after DNP immunization. Once an appropriate antibody titre was established, the TCO-BSA platform was used to deliver a high concentration of DNP to a breast cancer tumour. The animals were monitored for survival advantage compared to the control with the goal of determining an optimal dosing regimen for ARM immune-stimulating therapy prior to combination therapy with radiation (i.e. R-ARM therapy).

5.2 Introduction

In the past decade, immunotherapies have proven to be highly effective at treating specific types of cancers that do not respond well to traditional forms of therapy.[1] One such example is the use of nivolumab, a checkpoint blockade

antibody targeting programmed cell death (PD-1), used to treat a variety of cancers such as melanoma, non-small-cell lung cancer, castration-resistant prostate cancer and colorectal cancer.[2, 3] Tumours release programmed cell death ligand 1 (PD-L1) which interacts with the PD-1 receptors expressed on T-cells. This interaction down regulates T-cell responses minimizing the efficacy of the immune system towards a tumour.[4] Through administration of an anti-PD-1 monoclonal antibody, PD-L1 can no longer interact with receptors leading to more active T-cells around the tumour. A phase III study compared the use of nivolumab to docetaxel for the treatment of patients with squamous-cell non-small-cell lung cancer (NSCLC). The median overall survival and one year survival rate in patients treated with nivolumab was 9.2 months and 42% compared to 6.0 months and 24% for docetaxel respectively.[5]

A second and increasingly popular strategy for immunotherapy involves modification of T-cells with chimeric antigen receptors (CARs), which redirect the T-cells to the surface of a tumour.[6, 7] This treatment has proven very successful in leukemia patients, with 90% showing a complete response in a 30 patient trial.[8] In a Phase I/II trial of 101 patients with refractory large B-cell lymphoma treated with anti-CD19 CAR T-cell therapy, 82% had an objective response and 54% had a complete response. This compares to existing therapies that have objective response and complete response rates of 26% and 7% respectively.[8, 9] Although CAR T-cell therapies have shown impressive results in the clinic, many of the patients suffer from disease relapse between 6 weeks and 8.5 months after treatment.

Both anti-PD-1 antibodies and CAR T-cell therapies have shown impressive results in the clinic, where the common factor between the treatments is an increased level of T-cells at the tumour site.[7, 10] Antibody recruiting small molecules (ARMs) offer an alternative means of developing immune-stimulatory therapies that can recruit immune cells to the tumour and potentially overcome immunosuppressive issues that promote tumour growth.[11-15]

It is apparent from the ARM literature that modifying a native targeting vector with a hapten can be deleterious to binding. For example Zhang *et al*. synthesized a library of PSMA targeted glutamate-urea-lysine derivatives that were functionalized with a DNP group through an oxyethylene (PEG) linker that ranged from 0 to 12 units in length (ARM-P0-ARM-P12).[16] The IC_{50} values of the compounds were measured, and showed an increase in binding affinity as the length of the linker increased from 0 to 4 PEG units (1.76 ± 0.41 and 0.46 ± 0.18 M respectively). Any subsequent increase in the linker length lead to a rapid decrease in affinity towards PSMA to the lowest recorded value of 37.3 ± 16.2 M for ARM P-12. The compounds were then evaluated for anti-DNP antibody recruitment and it was found that ARM-P4, the compound with the highest affinity towards PSMA, was not capable of binding the antibody and therefore could not be used for ARM therapy. ARM-P8 on the other hand had high affinity towards the antibody, but the binding affinity towards PSMA was 7 times lower than ARM-P4. These results highlight the weakness of the ARM platform; the binding affinity towards the target can be compromised while optimizing antibody recruitment.[16, 17]

The TCO-BSA platform developed in Chapter 3 offers a simple way to deliver ARMs into preclinical tumour models while alleviating issues of target binding affinity. Compound **7** can recruit anti-DNP antibodies and once reacted with TCO-BSA, can be retained in a tumour following i.t. injection. As was the case with the radiolabelled form, **15**, the amount of albumin derived ARM administered in the tumour can be readily varied by simply increasing the amount of **7** linked to TCO-BSA or by increasing the amount of protein conjugate administered. The BSA platform is advantageous over traditional methods of ARM therapy as the antigen is retained in the tumour after i.t. injection for prolonged periods of time. This is likely to maximize the immune response, limit the amount of injections required for efficacy, as well as reduce toxicity related events. Prior to evaluating the R-ARM approach *in vivo*, a suitable animal model was required in order to optimize the dosing regimen for ARM monotherapy.

5.2.1 Immunization for anti-DNP Antibody Production

It has been shown in the literature that humans natively produce detectable levels of anti-DNP antibodies. This is thought to be caused by exposure to pesticides and dyes containing nitroarenes or ingestion of food that develop nitroarenes during the cooking processes.[14] Since lab animals are not exposed to the same environmental toxins as humans, mice do not natively produce high levels of anti-DNP antibodies.[18] As a result, mice must be immunized to produce anti-DNP antibodies prior to performing ARM therapy studies.

Typically, the immunization process involves the repeated administration of the antigen in the presence of an adjuvant in order to produce a high titre in the

animal. One common adjuvant mechanism of action, the "depot" effect, uses a 1:1 oil-in-water emulsified antigen injected into the animal.[19] The emulsification process helps to encapsulate the antigen, which provides protection from degradation and conformational changes and allows for a slow, sustained release of the antigen over time. It has been shown that daily injections of an antigen for 50 days can result in a high antibody titre that is comparable to one injection of the antigen in an oil-in-water emulsion. However, it was also determined that after the 50 days, the antibody titre in the blood decreased rapidly for the group immunized daily but was sustained in the adjuvant group. This study is representative of a wealth of literature supporting the use of adjuvants in order to obtain a long-lasting immune response.[19-21]

The current gold standard adjuvant is Freund's Complete Adjuvant (FCA), due to the long lasting immunostimulatory properties.[19, 22] FCA takes advantage of the depot effect and has an added effect from dried mycobacterial cells.[19] These bacterial cells help to activate the innate immune response through the presence of toll-like receptors (TLR) on the cell surface, which are recognized by immune cells such as macrophages and dendritic cells. This leads to an inflammatory response which can potentially cause pain in the animal. Although TLRs are thought to be one of the main components in sustained production of an antibody, many organizations discourage the use of FCA due to animal welfare concerns. As a result, probing different approaches to induce an immune response that do not use TLRs were pursued.

5.3 Materials and Methods

5.3.1 Biology: Materials and Instrumentation

Antibodies and reagents were purchased from Sigma-Aldrich, Life Technologies, ThermoFisher, Bethyl Laboratories, Polysciences Inc, Acro Biosystems and Conjuprobe and used without further purification. ELISA absorbance measurements were performed with a Tecan infinite M1000 plate reader. Flow Cytometry was performed using a BD LSRII™ flow cytometer (BD Biosciences, USA).

5.3.2 ELISA Protocol to Determine anti-DNP Concentration in the Blood

Briefly, 1 mg/mL DNP-BSA (Life Technologies, A23018) in sterile PBS (ThermoFisher, 10010023) was diluted 1/1000 with coating buffer (Bethyl Laboratories, E107) and transferred (100 µL) to a 96 well plate. Following a 1 h incubation at room temperature, the wells were washed three times with 200 µL of ELISA wash buffer (Bethyl Laboratories, E106). ELISA blocking buffer (Bethyl Laboratories, E104) was then added to each well (200 µL) and left to incubate at room temperature for 0.5 h The plate was washed three times with ELISA wash buffer (200 µL/well) before the addition of 100 µL of serum dilutions (range 1:50 – 1:1 000 000 per well) or sample diluent alone and left to incubate at room temperature for 1 h. The plate was washed three times with ELISA wash buffer (200 µL/well) before the addition of 100 µL of anti-DNP-AP (Sigma-Aldrich, A2831; 64 ng/mL). Following a 1 h incubation at room temperature, the plate was washed three times with ELISA wash buffer (200 µL/well) before the addition of 100 µL of Goat anti-mouse IgG-AP 2°(1:5 000). Following a 1 h incubation at room temperature the plate was washed five times with ELISA wash buffer (200 µL/well)

before the addition of 100 μL of PNPP substrate and the plate incubated in the dark at room temperature for 0.5 h. To quench the reaction, 50 μL of 2 M NaOH was added to each well and the absorbance subsequently measured at 405 nm on a plate reader.

5.3.3 Intraperitoneal Immunization with DNP-KLH

Prior to starting immunization, blood was collected from a group (n=3) of Balb/c female mice (4-6 weeks) through a facial bleed. The mice were administered 400 μL DNP-KLH (0.5 mg/mL in PBS) i.p three times every two weeks and blood was drawn 3 days after each administration.

5.3.4 Intraperitoneal Immunization with FIA and FCA

Prior to starting immunization, blood was collected from two groups (n =5) of Balb/c female mice (4-6 weeks) through a facial bleed. For vaccination of group 1, 100 μL DNP-KLH (1 mg/mL in PBS) and 100 μL Freund's Incomplete Adjuvant (FIA) were administered to mice i.p. three times every two weeks. For vaccination of group 2, 100 μL DNP-KLH (1 mg/mL in PBS) and 100 μL FCA were administered to mice i.p. followed by 100 μL DNP-KLH (1 mg/mL in PBS) and 100 μL FIA i.p two times every two weeks. The mice were given access to drinking water containing Children's Tylenol (1.5 mg/mL) for 48 hours before and 48 hours after each administration. Blood was drawn through a facial bleed 3-5 days after each i.p. administration.

5.3.5 Subcutaneous Immunization with FIA

Prior to starting immunization, blood was collected from a group (n=5) of C57BL/6 female mice (4-6 weeks) through a facial bleed. For vaccination, 50 μL DNP-KLH

(1 mg/mL in PBS) and 50 μL FIA were administered to mice s.c. three times every two weeks. Blood was drawn through a facial bleed 3-5 days after each s.c. administration.

5.3.6 ARM Therapy Study

All animal studies were approved by the Animal Research Ethics Board at McMaster University. Mice were maintained under clean conditions in the Central Animal Facility with 12 hour light/dark cycles and given food and water ad libitum. Female, 13-15 week old, C57/BL6 mice ordered from Charles River Laboratory (Kingston, NY) were tumour inoculated with 5 x 10^6 E0771 cells in the left flank. Once palpable tumours arose (~100 mm^3) mice were treated three times per week with **17**. Mice were followed for survival and tumours measured every 2-3 days. Mice were sacrificed when they reached endpoint (tumour volume=1000 mm^3).

5.3.7 Calibration Curve of 7

Compound **7** was diluted in saline in decreasing concentration (0.38 – 24 nmol) and measured on the Tecan Plate Reader at 320 nm.

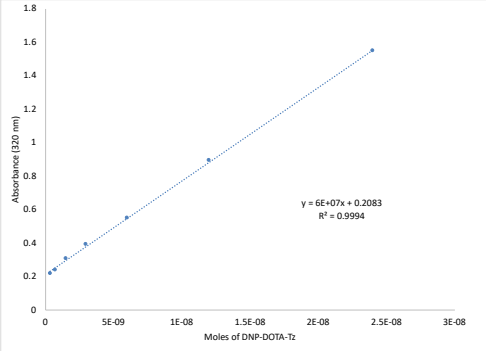

Figure 5-1. Calibration curve of **7** (dissolved in saline) at a concentration range of 0.38 – 24 nmol. Absorbance readings were taken at 320 nm.

5.3.8 ELISA Protocol to Determine anti-DNP Recruiting Capabilities of 17

Briefly, 1 mg/mL DNP-BSA (Life Technologies, A23018) or **17** in sterile PBS (ThermoFisher, 10010023) was diluted 1/1000 with coating buffer (Bethyl Laboratories, E107) and transferred (100 µL) to a 96 well plate. Following a 1 h incubation at room temperature, the wells were washed three times with 200 µL of ELISA wash buffer (Bethyl Laboratories, E106). ELISA blocking buffer (Bethyl Laboratories, E104) was then added to each well (200 µL) and left to incubate at room temperature for 0.5 h The plate was washed three times with ELISA wash buffer (200 µL/well) before the addition of 100 µL of anti-DNP-AP (Sigma-Aldrich, A2831; 64 ng/mL). Following a 1 h incubation at room temperature, the plate was washed three times with ELISA wash buffer (200 µL/well) before the addition of PNPP substrate and the plate incubated in the dark at room temperature for 0.5 h. To quench the reaction, 50 µL of 2 M NaOH was added to each well and the absorbance subsequently measured at 405 nm on a plate reader.

5.3.9 Pre-targeting Biodistribution Studies

Female 6-8 week old, Balb/c mice were injected i.t. with 100 µg of TCO-BSA (**11** or **12** in 0.9% saline) or 0.9 % saline. After 1 h approximately 0.37 MBq of **8** was administered. At 24 h post-injection (n=3 per time point), mice were anesthetized with 3% isoflurane and euthanized by cervical dislocation. Blood, adipose, adrenals, bone (arm bones including shoulder and leg bones including knee joint), brain, gall bladder, heart, kidneys, large intestine and caecum (with contents), liver, lungs, pancreas, skeletal muscle, small intestine (with contents), spleen, stomach (with contents), thyroid/trachea, urine + bladder and tail were collected, weighed and counted in a gamma counter. Decay correction was used to normalize organ

activity measurements to time of dose preparation for data calculations with respect to injected dose (i.e. %ID/g).

5.4 Results and Discussion

5.4.1 Immunization with DNP-KLH

In an attempt to immunize mice towards 2,4-dinitrophenyl, the antigen was administered without an adjuvant following the guidelines outlined by the animal facility at McMaster University. The mice were administered DNP-KLH, a 390 kDa protein that is functionalized with ≥ 400 DNP groups per protein. The mice were given three doses of DNP-KLH i.p. every two weeks, and their blood collected three days after each dose.[23] The animals were monitored for signs of distress, and after the three treatments, the mice appeared healthy with no significant loss in body weight. In order to evaluate the amount of antibody present, the mice were bled, and an ELISA was performed on the serum. Briefly, an ELISA plate was coated with DNP-BSA followed by the addition of serum samples (1:50 – 1:1 000 000 dilutions) and incubated for an hour. The plate was washed, and a secondary anti-mouse antibody added. After one hour at room temperature, the plate was washed, and the substrate added. The enzymatic reaction was stopped with the addition of sodium hydroxide and the absorbance signal of each of the wells was read on a Tecan plate reader at 405 nm. Following standard literature procedures, the obtained absorbance values were compared to published values.[12, 15, 24]

The results are shown in Figure 5-2, where each graph displays the serial dilutions of serum from one mouse and the absorbance reading at that dilution. As is depicted, there was a slight increase in the absorbance reading between the naïve (red) and the final (orange) bleed, with antibodies detected for two of animals at the

1:1 000 dilution, and at the 1:100 dilution for the third. Unfortunately, the reported titres were lower than that seen in the literature, where the antibodies can be detected anywhere between the 1:20 000 and 1:100 000 dilution, and therefore the mice were not suitable for therapy.[12, 24] Although there is evidence that the antibody titre could be increased through daily administration of the antigen, immunization with an adjuvant was pursued to ensure a long lasting titre.[20]

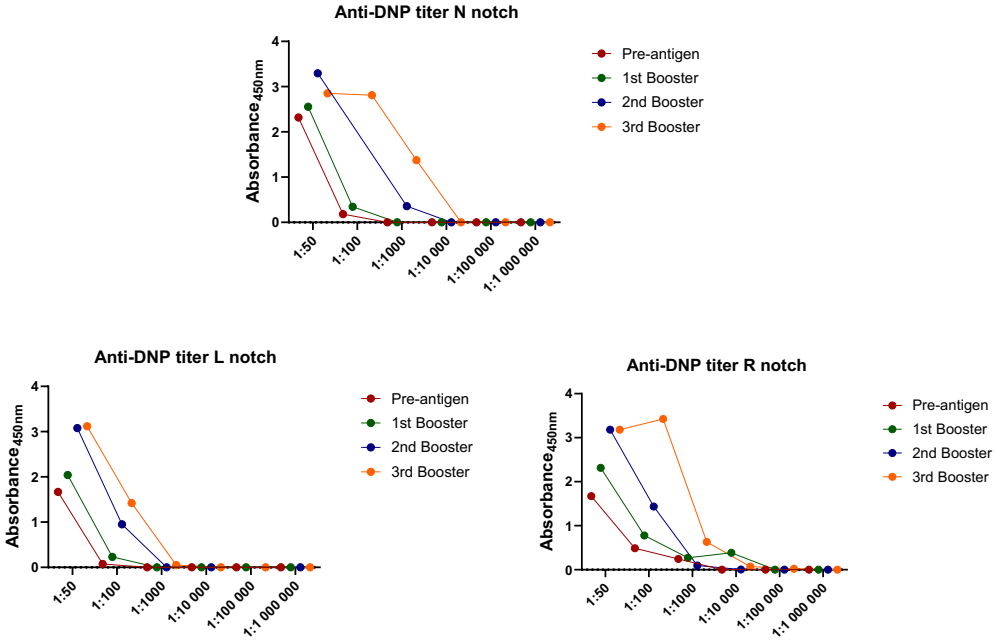

Figure 5-2. Anti-DNP antibody titre as determined by an ELISA. Each graph represents one mouse (N = no ear notch, L = left ear notch, R = right ear notch); the absorbance value can be related to the amount of antibody present in the serum at different dilutions (x-axis).

5.4.2 Immunization with DNP-KLH in PBS Emulsified with FCA or FIA Intraperitoneal Administration

As mentioned above, the current gold standard for adjuvants is FCA which leads to the production of a high, and sustained antibody titre.[19] In order to use FCA and Freund's incomplete adjuvant (FIA), the animal facility at McMaster required a pain management regimen to accompany the immunizations. It was initially

thought that the administration of pain medication, in particular anti-inflammatories, would be deleterious to antibody production. As previously mentioned, the mechanism of action of adjuvants is thought to be partially dependent on inflammation, therefore the use of the recommended pain medication could counteract this mechanism.[19] However, a publication from 2012 did a head to head comparison of mice immunized with FCA and FIA that were given one of four pain management regimens, none, acetaminophen, meloxicam or buprenorphine.[22] The results found no difference in average or maximum antibody production in the control group compared to the groups administered pain management. Based on these literature results, two groups of mice (n=5) were administered DNP-KLH in PBS emulsified with either FIA or FCA (1:1) i.p. for the primary injection, with all mice receiving two additional doses of DNP-KLH in PBS emulsified with FIA (1:1) every two weeks. The mice were given Children's Tylenol in their water 48 hours before and 48 hours after i.p. administration to help alleviate any pain, with additional buprenorphine if required.

Mice were bled three days after each dose, and the final antibody titre was compared to that of the naïve animals. The results of the study are shown in Figure 5-3, where all 10 of the serum samples show antibody titres above background at the 1:10 000 dilution. Figure 5-3 also shows the average serum antibody titres from the FCA and FIA groups where it was evident that the FCA was more effective in producing a high titre when compared to FIA, likely due to the TLR activation. The study concluded that FCA produced a higher titre, but both the FCA and FIA levels are suitable for therapy based on literature data for human anti-DNP antibody serum

levels, and previous work in mice.[12] Although the animals had sufficient antibody titres, they unfortunately suffered from severe dehydration making them unsuitable for tumour implantation. The dehydration was attributed to the decreased water intake of the mice due to the use of Tylenol in their drinking water.

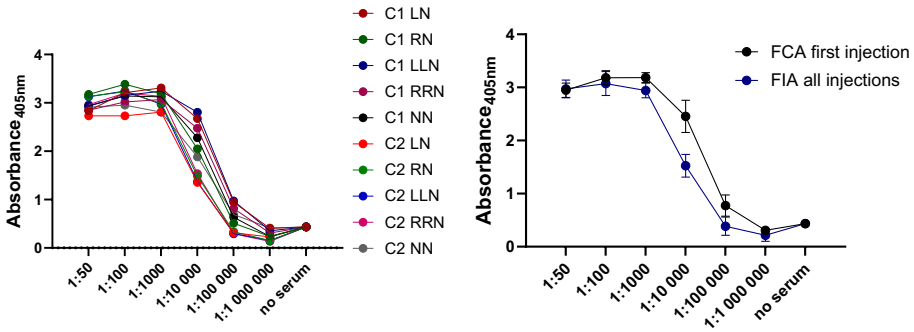

Figure 5-3. Left - Antibody titres from 10 mice vaccinated with DNP-KLH with either FCA (C1) or FIA (C2). Right – Average antibody titres from the 10 mice, black line represents FCA group, and blue line represents FIA group.

5.4.3 Immunization with DNP-KLH in PBS Emulsified with FCA or FIA Subcutaneous Administration

In an attempt to administer an adjuvant without pain medication, we opted to alter the method of administration. There is evidence in the literature that subcutaneous (s.c.) injections can be effective in producing a high antibody titre, while minimizing the pain associated with the injection.[19, 21] A group of mice (n=5) were administered DNP-KLH in PBS emulsified with FIA (1:1) s.c. three times every two weeks and bled after each dose. The antibody titre in the serum was determined through an ELISA and compared to that of naïve animals. As shown in Figure 5-4, 4/5 of the immunized animals showed a high titre at the 1:10 000 dilution with two of the animals showing a higher than background signal at 1:100 000. Although the antibody titre is lower than with FCA, the values were high

enough for use in therapy and the animals showed no signs of pain or distress post-immunization.

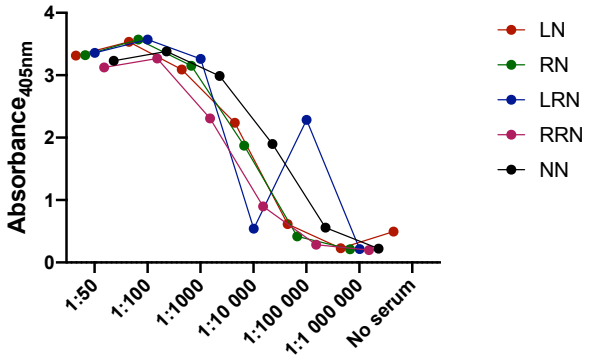

Figure 5-4. Absorbance readings representative of antibody titres from C57BL/6 (n=5) mice after 3 administrations of DNP-KLH with FIA. Each line is representative of an individual mouse (legend represents ear notch).

5.4.4 Pilot Antibody Recruiting Therapy Study

Due to the reasonable antibody titre and good health of the animals, a pilot ARM therapy study was performed. As a prelude to the future evaluation of the efficacy of the combination R-ARM therapy, the dosing regimen of the non-radiolabelled ARM monotherapy was first interrogated.

Up until this point, ARMs have been administered i.v. or i.p. making it difficult to determine the optimal i.t. dose.[12, 14, 24] Most ARMs are given at least three times per week at concentrations of 4-100 mg/kg, or approximately 0.5-1265 nmol of antigen per injection.[12, 15, 23, 25] Compounds that are administered i.v. seem to be given at lower doses (0.5-92.8 nmol) than when delivered i.p., however there is no information on the uptake or distribution of the reported ARMs. Since the tumour uptake has not been quantified in any of the mentioned therapy studies, a pilot study was performed to determine if i.t. administration of 1.5-1.9 nmol of DNP three times per week would show any efficacy in immunized mice compared to

non-immunized mice through measurement of tumour size and immune cell infiltration. This dose range was selected to be within the literature concentration range used in the published ARM studies and was compatible with reasonable i.t. injection volumes. Based on the autoradiography data presented in Chapter 4, the therapy study was performed with the non-aggregated material, **17**, due to the more extensive i.t. distribution compared to that for **16**.

Prior to performing the therapy study, an ELISA was used to ensure that compound **17** could recruit anti-DNP antibodies as the previously tested compound, **7**, had been modified with TCO-BSA. Commercially available DNP-BSA or **17** was coated on an ELISA plate followed by addition of anti-DNP-AP. The plate was then washed and PNPP substrate added. The wells were treated with sodium hydroxide after 30 min to stop the reaction and the absorbance read on a plate reader. The data (Figure 5-5) showed that the commercially available DNP-BSA, which is known to interact strongly with anti-DNP antibodies, had a similar level of antibody binding compared to **17**. In addition, **11** was used as a negative control and showed an absorbance signal comparable to background, suggesting that the antibody binding is sensitive to the presence of the DNP group. This supports moving forward with testing compound **17** *in vivo*.

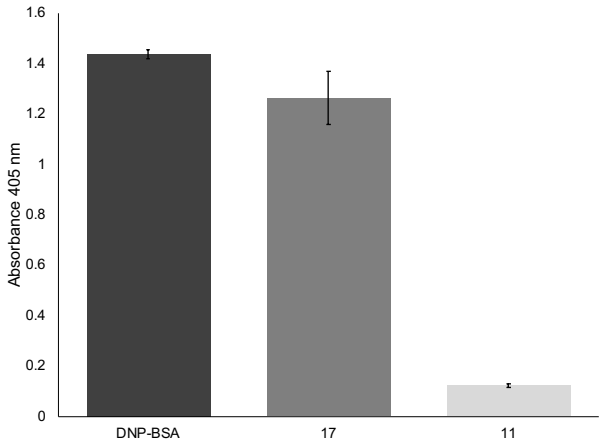

Figure 5-5. ELISA results demonstrating anti-DNP recruiting capabilities of the commercially available DNP-BSA, **17** and **11**.

Two groups of mice, one immunized with DNP-KLH, were inoculated with E0771 breast cancer tumours two weeks after the final DNP-KLH booster. Once the tumours reached a palpable size (~100 mm^3), the mice were administered **17** i.t. three times per week until they reached endpoint. Since **17** is produced through the reaction of **7** and **11**, it was necessary to quantify the amount of antigen, DNP, present on the BSA after the ligation reaction. After purification with a 50 kDa spin filter, an aliquot of the filtrate was removed and the absorbance read. The absorbance value was then used in conjunction with a calibration curve (Figure 5-1) derived from **7** to determine the amount of unreacted material in the filtrate. The mass of unreacted material was subtracted from the amount of **7** added to the reaction, where it was found that 62-78% of the tetrazine reacted **11** (n=3) giving an approximate dose of 1.5-1.9 nmol of DNP per 50 μL injection.

Both the control and immunized animals were treated until they reached endpoint, and the results shown in Figure 5-6. It can be seen that there was no statistically significant survival advantage between the control (non-immunized)

and immunized groups, which suggests limited therapeutic efficacy of **17** with the current dosing regimen.

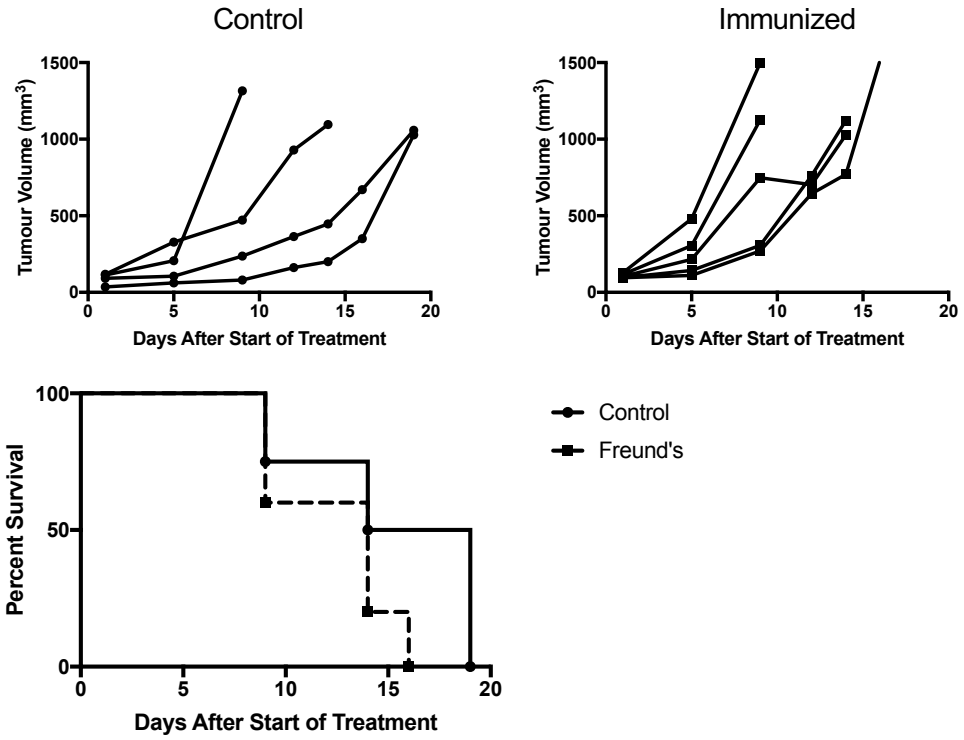

Figure 5-6. Pilot therapy study results. Top – Tumour growth charts representing the control (left) and the immunized (right) groups. Bottom – Kaplan Meier curve showing the survival time of the two groups.

5.4.5 Immunohistochemistry

To assess the impact of the treatment on the biology of the tumours, as opposed to simply looking at the change in volume and survival, tumours were harvested at endpoint for IHC analysis. The tumours were fixed and stained for cell morphology, as well as the presence of immune cells, specifically T-cells and macrophages. Since the main purpose of the study was to monitor tumour volume until endpoint, the tumours from the two groups were not all harvested on the same days. Traditionally, when comparing the overall health and immune cell presence in a tumour, the tissue samples should be a comparable age. Nevertheless, for this

study three tumours were harvested on both days 9 and 14 post-therapy for IHC analysis. IHC slides were quantified as shown in Figure 5-7 where the total number of cells on each slide were counted, and the positive signals relating to each type of immune cell compared to the total.

On day 9, one tumour was harvested from the non-immunized control group (grey), and two tumours from the immunized group (black and blue). The data shows that macrophages were the most common immune cell, followed by $CD8^+$ then $CD4^+$ T-cells. When comparing the number of immune cells in the control tumours to the immunized tumours, it is apparent that there are more of all four types of immune cells in the immunized animals. On day 14 one tumour was harvested from the non-immunized control group (grey), and two tumours from the immunized group (black and blue). Once again macrophages were the most common immune cell, however the control tumour had the highest percentage of macrophages, $CD3^+$ and $CD8^+$ T-cells. Based on the results of the immune cell quantification it appears that the immune cell infiltration is higher closer to the start of therapy, which then decreases by day 14. The increase in immune cells in the tumours of the immunized animals 9 days after treatment suggests that there is some therapeutic response to the treatment.

In addition to evaluating the presence of immune cells, the extent of necrosis in the tumours was analyzed (Figure 5-7). The tumour from the non-immunized animal (grey) had approximately 5% less necrosis compared to the two tumours from the immunized animals on day 9. On day 14 the non-immunized animal (grey) had less necrosis (by approximately 5% and 17%) compared to the tumours of the

two immunized animals. These results, which are in agreement with the immune cell data, suggest that there were morphological changes in the immunized group that was not seen to the same extent in the non-immunized group. Although these results were not reflected in the tumour volume measurements, they do suggest dose optimization is warranted. It is important to note that the IHC results are based off of individual tumours as all of the mice were not sacrificed on the same days. In order to get data that can be analyzed for statistical significance the experiment must be repeated and groups of control (non-immunized) and immunized animals sacrificed on the same days.

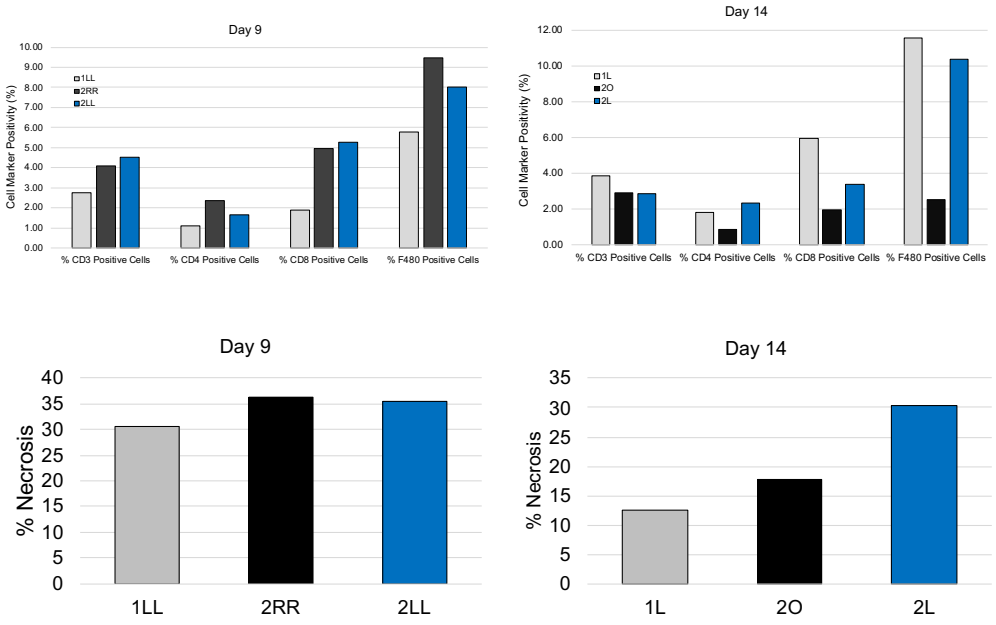

Figure 5-7. Graphs representing the quantification of IHC slides. Top left - Percentage of cells on the slide that were $CD3^+$ T-cells, $CD4^+$ T-cells, $CD8^+$ T-cells or macrophages (F480) from tumours harvested on day 9. The grey bar represents a tumour harvested from the non-immunized group, while the blue and black bars represent tumours harvested from the immunized group; Top right- Percentage of cells on the slide that were $CD3^+$ T-cells, $CD4^+$ T-cells, $CD8^+$ T-cells or macrophages from tumours harvested on day 14. The grey bar represents a tumour harvested from the non-immunized group, while the blue and black bars represent

tumours harvested from the immunized group; Bottom left- Percentage necrosis in the tumours harvested on day 9. The grey bar represents a tumour from the non-immunized control, while the black and blue bars represent tumours from the immunized group; Bottom right - Percentage necrosis in the tumours harvested on day 14. The grey bar represents a tumour from the non-immunized control, while the black and blue bars represent tumours from the immunized group. Legends represent the ear notch of each individual animal.

There is evidence in the literature that immunotherapies have a "peak" immune cell infiltration day, however there is limited literature documenting this data for ARMs. To our knowledge, the only example in the literature to analyze the immune cells in a tumour after ARM treatment was done through IHC in 2008.[26] In this article, M109 lung cancer tumours and 4T1 breast cancer tumours were treated with ARM, IL-2 and IFN-α. The tumours were harvested three days after the start of treatment and the immune cell infiltration ($CD4^+$ and $CD8^+$ T-cells, and macrophages) was analyzed. In this publication, an increase in immune cells relative to the control was apparent through visual analysis of the IHC slides, indicating a positive response to the therapy as early as three days post treatment. That being said, the earliest the tumours were harvested from our therapy study with compound **17** was 9 days after the start of therapy, therefore the IHC slides may not be representative of the peak T-cell infiltration.

5.4.6 Anti-DNP Antibody Titre Post-Therapy

In addition to harvesting the tumours at endpoint, blood was drawn from each animal to determine the longevity of the anti-DNP antibody titre. The titre from the FIA group was compared to that of the control to ensure there was a significant difference between the groups. Due to repeat administration of the therapeutic in both the naïve and FIA mice, there is a chance that the naïve group started producing anti-DNP antibodies. The level in the naïve animals however

should still be much lower than the FIA group as the antigen was administered without an adjuvant.[19]

The results of the ELISA, Figure 5-8, demonstrate that the antibody titre for the immunized mice decreased post tumour implantation with detectable amounts out to the 1:10 000 dilution. Although the values were lower than before tumour implantation, it is important to note that the titre was much higher than the non-immunized group in which only two mice showed an antibody titre higher than background at a 1:50 dilution. After vaccination towards an antigen, it is common for the antibody concentration in the blood to increase upon each subsequent exposure to the antigen.[27] The ELISA results show a reduction of the antibody concentration in the blood compared to that observed after the third DNP booster. Since the antibody titre was sufficient to elicit an immune response based on literature data, and compound **17** was shown to recruit anti-DNP antibodies *in vivo*, the poor therapy results suggest that the antigen on compound **17**, was not adequately recognized by the immune system.[12, 16, 23] This could be due to inadequate concentration of accessible ARM in the tumour.

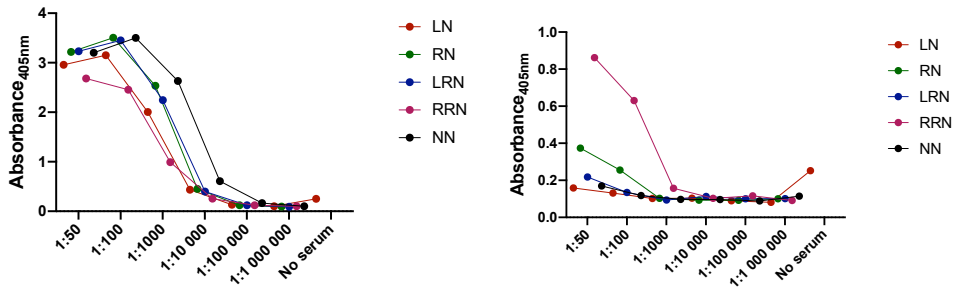

Figure 5-8. Left – ELISA results of anti-DNP antibody titre post-therapy of Freund's immunized mice; Right – ELISA results of anti-DNP antibody titre post therapy in non-immunized mice.

5.4.7 Antigen Accessibility by the Blood Stream After I.T. Administration

To evaluate whether TCO-BSA derivatives are accessible to molecules circulating in the blood stream when administered i.t., pre-targeting biodistribution studies were performed. Here, we took advantage of the bio-orthogonal capabilities of the platform by administering TCO-BSA, aggregated (**12**) and non-aggregated (**11**), i.t. followed by i.v. administration of **8**. A saline control group was implemented to ensure that there is no inherent accumulation of the radiolabelled ligand in the tumour. The results, Figure 5-9, show that the uptake in the tumour after i.t. injection of **11** or **12** was not statistically different compared to the saline control with the average tumour uptake less than 1 %ID/g in each group. This can be compared to pre-targeting studies in the literature where an antibody was administered i.v. followed by the radiolabelling coupling partner resulting in tumour uptake greater than 4 %ID/g.[28, 29] This was done with either coupling partner, TCO or tetrazine, in excess with molar ratios varying from 1:3.4 to1:7.7.[28-30] The ratio employed for our study had the TCO-albumin conjugate present in 8.5-fold excess compared to the tetrazine. While this value falls outside of the typical literature range, it is important to note that an i.t. injection strategy leads to the retention of the majority of the administered TCO groups in the tumour. When the TCO or tetrazine is administered i.v., a smaller portion of the injected molecule accumulates at the tumour site and the remainder is cleared from the body or taken up in other tissues. In order to quantify the amount of TCO-antibody that accumulated at the tumour site, one study directly labelled a TCO-derived antibody with iodine-125.[28] By quantifying the amount of iodine in the tumour, the

concentration of TCO was determined to be 0.9 nmol/g, which compares to our study which administered 5.6 nmol/g of TCO directly into the tumour.

Based on what has been published in the literature, the administered molar quantities of TCO-BSA and **8** should have been sufficient for the *in vivo* click reaction to occur. The low uptake can be explained for the aggregates, where the TCO groups may become less accessible in the globular structure of the protein or the heating process required to make the aggregates lead to isomerization of the *trans*-double bond. However, the low uptake seen with the non-aggregated version was surprising as there were no modifications to the compound prior to injection. The other tissues that were analyzed in the biodistribution study were similar between all three groups, indicating the i.t. administration of albumin derivatives did not significantly alter the distribution of **8**. The results ultimately suggest that when administered i.t., TCO-BSA is not readily accessible in sufficient concentrations to react with tetrazines administered i.v..

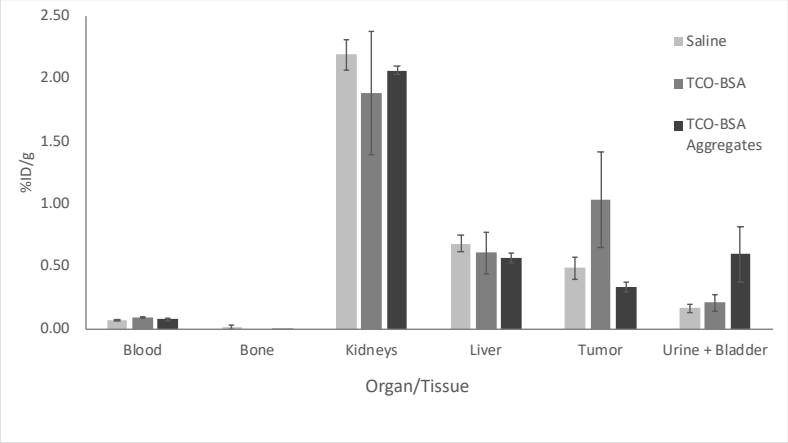

Figure 5-9. Pre-targeting biodistribution results of TCO-BSA injected i.t. in a 4T1 tumour model followed by i.v. administration of **8** after one hour. Mice, n=3, were sacrificed 24 hours after radioactive injection and their organs counted for radioactivity. The light grey bar is the data from the control where saline was given in place of TCO-BSA, the medium grey bar is for **11** and the dark grey **12**. Data at

the time points indicated are expressed as the mean percent injected dose per gram (%ID g^{-1}) ± SEM.

5.5 Conclusion

The ability of immunocompetent mice to produce anti-DNP antibodies was tested through administration of DNP-KLH with and without adjuvants. It was determined that immunization without an adjuvant resulted in a low antibody titre which was not useful for therapeutic studies. The use of FCA and FIA resulted in high antibody titres that could be used for antibody recruiting therapy, with the preferred method of immunization being a subcutaneous injection every 2 weeks, which reduced the site-pain associated with adjuvant administration. A pilot therapy study in immunized mice was performed in an E0771 breast cancer model with the mice receiving compound **17** i.t. three times per week. Unfortunately, no difference in tumour size was seen between the non-immunized control group and the immunized treatment group. That being said IHC results show an increase in the number of macrophages and T-cells at the tumour site for the immunized group on day 9 after the start of therapy. The immunized group also showed a higher percentage of necrotic tissue compared to the non-immunized control group, however a larger study is required to determine if the results are statistically significant. In an attempt to explain the lack of observed efficacy, a pre-targeting biodistribution study was performed which showed that TCO-BSA is not readily accessible for the *in vivo* click reaction in either aggregate or non-aggregate forms after i.t. injection. These results indicate that the i.t. administration of TCO-BSA in the manner described here is not suitable for ARM therapy as it is likely that the

anti-DNP antibodies are not able to reach the ARM, which is a key step in promoting immune cell recruitment and response.

5.6 References

1. Fellner, C., Ipilimumab (Yervoy) Prolongs Survival in Advanced Melanoma Serious Side Effects and a Hefty Price Tag May Limit Its Use. *P&T* **2012,** *37* (9), 503-530.
2. Hamid, O.; Robert, C.; Daud, A.; Hodi, F. S.; Hwu, W. J.*, et al.*, Safety and Tumor Responses with Lambrolizumab (Anti-PD-1) in Melanoma. *N Engl J Med* **2013,** *369* (2), 134-144.
3. Rizvi, N. A.; Mazières, J.; Planchard, D.; Stinchcombe, T. E.; Dy, G. K.*, et al.*, Activity and Safety of Nivolumab, an Anti-PD-1 Immune Checkpoint Inhibitor, for Patients with Advanced, Refractory Squamous Non-Small-Cell Lung Cancer (Checkmate 063): A Phase 2, Single-Arm Trial. *Lancet Oncol* **2015,** *16* (3), 257-265.
4. Schildberg, F. A.; Klein, S. R.; Freeman, G. J.; Sharpe, A. H., Coinhibitory Pathways in the B7-CD28 Ligand-Receptor Family. *Immunity* **2016,** *44* (5), 955-972.
5. Brahmer, J.; Reckamp, K. L.; Baas, P.; Crino, L.; Eberhardt, W. E.*, et al.*, Nivolumab Versus Docetaxel in Advanced Squamous-Cell Non-Small-Cell Lung Cancer. *N Engl J Med* **2015,** *373* (2), 123-135.
6. Adusumilli, P. S.; Cherkassky, L.; Villena-Vargas, J.; Colovos, C.; Servais, E.*, et al.*, Regional Delivery of Mesothelin-Targeted Car T Cell Therapy Generates Potent and Long-Lasting CD4-Dependent Tumor Immunity. *Sci Transl Med* **2014,** *6* (261), 261ra151.
7. Newick, K.; O'Brien, S.; Moon, E.; Albelda, S. M., Car T Cell Therapy for Solid Tumors. *Annu Rev Med* **2017,** *68*, 139-152.
8. Maude, S. L.; Frey, N.; Shaw, P. A.; Aplenc, R.; Barrett, D. M.*, et al.*, Chimeric Antigen Receptor T Cells for Sustained Remissions in Leukemia. *N Engl J Med* **2014,** *371* (16), 1507-1517.
9. Neelapu, S. S.; Locke, F. L.; Bartlett, N. L.; Lekakis, L. J.; Miklos, D. B.*, et al.*, Axicabtagene Ciloleucel Car T-Cell Therapy in Refractory Large B-Cell Lymphoma. *N Engl J Med* **2017,** *377* (26), 2531-2544.
10. Curran, M. A.; Montalvo, W.; Yagita, H.; Allison, J. P., PD-1 and CTLA-4 Combination Blockade Expands Infiltrating T Cells and Reduces Regulatory T and Myeloid Cells within B16 Melanoma Tumors. *Proc Natl Acad Sci U S A* **2010,** *107* (9), 4275-4280.
11. Chirkin, E.; Muthusamy, V.; Mann, P.; Roemer, T.; Nantermet, P. G.*, et al.*, Neutralization of Pathogenic Fungi with Small-Molecule Immunotherapeutics. *Angew. Chem. Int. Edit.* **2017,** *56* (42), 13216-13220.
12. Dubrovska, A.; Kim, C.; Elliott, J.; Shen, W.; Kuo, T. H.*, et al.*, A Chemically Induced Vaccine Strategy for Prostate Cancer. *ACS Chem Biol* **2011,** *6* (11), 1223-1231.

13. Genady, A. R.; Janzen, N.; Banevicius, L.; El-Gamal, M.; El-Zaria, M. E.*, et al.*, Preparation and Evaluation of Radiolabeled Antibody Recruiting Small Molecules That Target Prostate-Specific Membrane Antigen for Combined Radiotherapy and Immunotherapy. *J Med Chem* **2016,** *59* (6), 2660-2673.
14. McEnaney, P. J.; Parker, C. G.; Zhang, A. X.; Spiegel, D. A., Antibody-Recruiting Molecules: An Emerging Paradigm for Engaging Immune Function in Treating Human Disease. *ACS Chem Biol* **2012,** *7* (7), 1139-1151.
15. Rullo, A. F.; Fitzgerald, K. J.; Muthusamy, V.; Liu, M.; Yuan, C.*, et al.*, Re-Engineering the Immune Response to Metastatic Cancer: Antibody-Recruiting Small Molecules Targeting the Urokinase Receptor. *Angew. Chem. Int. Edit.* **2016,** *55* (11), 3706-3710.
16. Zhang, A. X.; Murelli, R. P.; Barinka, C.; Michel, J.; Cocleaza, A.*, et al.*, A Remote Arene-Binding Site on Prostate Specific Membrane Antigen Revealed by Antibody-Recruiting Small Molecules. *J Am Chem Soc* **2010,** *132*, 12711-12716.
17. Murelli, R. P.; Zhang, A. X.; Michel, J.; Jorgensen, W. L.; Spiegel, D. A., Chemical Control over Immune Recognition: A Class of Antibody-Recruiting Small Molecules That Target Prostate Cancer. *J Am Chem Soc* **2009,** *131* (47), 17090-17092.
18. Teague, P. O.; Friou, G. J., Antinuclear Antibodies in Mice. Ii. Transmission with Spleen Cells; Inhibition or Prevention with Thymus or Spleen Cells. *Immunology* **1969,** *17* (5), 665-675.
19. Stills, H. F., Adjuvants and Antibody Production: Dispelling the Myths Associated with Freund's Complete and Other Adjuvants. *ILAR* **2005,** *46* (3), 280-293.
20. Ahlstedt, S.; Björkstén, B., Specific Antibody Responses in Rats and Mice after Daily Immunization without Adjuvant. *Int Arch Allergy Imm* **1983,** *71* (4), 293-299.
21. Leenaars, P. P. A. M.; Koedam, M. A.; Wester, P. W.; Baumans, V.; Claassen, E.*, et al.*, Assessment of Side Effects Induced by Injection of Different Adjuvant/Antigen Combinations in Rabbits and Mice. *Lab Anim* **1998,** *32*, 387-406.
22. Kolstad, A. M.; Rodriguiz, R. M.; Kim, C. J.; Hale, L. P., Effect of Pain Management on Immunization Efficacy in Mice. *J Am Assoc Lab Anim* **2012,** *51* (4), 448-457.
23. Schrand, B.; Clark, E.; Levay, A.; Capote, A. R.; Martinez, O.*, et al.*, Hapten-Mediated Recruitment of Polyclonal Antibodies to Tumors Engenders Antitumor Immunity. *Nat Commun* **2018,** *9* (1), 1-10.
24. Nagano, M.; Carrillo, N.; Otsubo, N.; Hakamata, W.; Ban, H.*, et al.*, In Vivo Programming of Endogenous Antibodies Via Oral Administration of Adaptor Ligands. *Bioorg Med Chem* **2017,** *25* (21), 5952-5961.
25. Lu, Y.; Low, P. S., Folate Targeting of Haptens to Cancer Cell Surfaces Mediates Immunotherapy of Syngeneic Murine Tumors. *Cancer Immunol Immunother* **2002,** *51* (3), 153-162.

26. Sega, E. I.; Lu, Y.; Ringor, M.; Leamon, C. P.; Low, P. S., Low-Dose Radiation Potentiates the Therapeutic Efficacy of Folate Receptor-Targeted Hapten Therapy. *Int J Radiat Oncol Biol Phys* **2008,** *71* (2), 559-566.
27. Molnar, C.; Gair, J., *23.2. Adaptive Immune Response*. BCcampus: Victoria, B.C., 2015.
28. Rossin, R.; Verkerk, P. R.; van den Bosch, S. M.; Vulders, R. C.; Verel, I.*, et al.*, In Vivo Chemistry for Pretargeted Tumor Imaging in Live Mice. *Angew. Chem. Int. Edit.* **2010,** *49* (19), 3375-3378.
29. Zeglis, B. M.; Sevak, K. K.; Reiner, T.; Mohindra, P.; Carlin, S. D.*, et al.*, A Pretargeted Pet Imaging Strategy Based on Bioorthogonal Diels-Alder Click Chemistry. *J Nucl Med* **2013,** *54* (8), 1389-1396.
30. Billaud, E. M. F.; Belderbos, S.; Cleeren, F.; Maes, W.; Van de Wouwer, M.*, et al.*, Pretargeted Pet Imaging Using a Bioorthogonal (18)F-Labeled Trans-Cyclooctene in an Ovarian Carcinoma Model. *Bioconjug Chem* **2017,** *28* (12), 2915-2920.

Chapter 6 - Conclusions and Future Work

6.1 Summary of Findings

Due to the potential synergistic effects of combination radiotherapy and immunotherapy, the goal of this thesis was to develop a platform that would enable the evaluation of the efficacy of combined radionuclide and antibody recruitment therapies. The first step was to synthesize a molecule that contained a tetrazine, for rapid bio-orthogonal ligation to a targeting vector, a 2,4-dinitrophenyl group for antibody recruiting, and a DOTA macrocycle for chelation of radiometals (Chapter 2). The lead construct was radiolabelled with lutetium-177, and the clearance profile evaluated in a biodistribution study. Due to the ideal pharmacokinetics observed with the ligand, an additional biodistribution study was performed to determine the targeting potential of the platform. Prior to administration, the lutetium-labelled compound was incubated with TCO-BP, a bone targeting bisphosphonate, which revealed activity in the bone as early as one hour post-injection. In addition, there was high off-target uptake in the lungs rendering the platform impractical for therapy. Taking advantage of the versatility of the platform, a pre-targeting strategy was employed where TCO-BP was injected, followed by the radiolabelled tetrazine where after one hour, the lung uptake was significantly reduced while maintaining similar uptake in the bone.

Once the ability to target the ligand was confirmed through both active and pre-targeting strategies, the antibody recruiting capabilities were tested. Using both ELISA and flow cytometry, the ligand alone and clicked to a vector or surface showed dose dependent anti-DNP antibody recruitment. The *in vitro* and *in vivo*

data suggested that the ligand can be used to localize an antigen and a radionuclide to the site of interest for combination antibody recruiting and TRT.

Moving forward, a suitable target and targeting strategy were required to evaluate the therapeutic efficacy of the R-ARM platform. While the TCO-BP construct was successful in targeting regions of high calcium turnover, orthotopic bone tumour models were not optimal for testing R-ARM therapies. As a result, two other approaches were investigated: a TCO-derived vector targeting melanin was synthesized and tested for uptake in a melanoma tumour line, and two technetium-labelled bisphosphonates were evaluated in an osteosarcoma flank tumour model (Chapter 3). The melanin targeted vector showed uptake in the melanoma tumour, however the activity washed out over 24 hours. Although in the literature bisphosphonates have been known to accumulate in osteosarcoma flank tumours, neither of the radiolabelled bisphosphonates showed significant uptake in the tumour. As an alternative to developing biomolecule targeted TCO-derivatives, research into creating a construct that would allow for i.t. administration of the R-ARM was pursued. TCO-functionalized bovine serum albumin (BSA) derivatives were prepared and used as "protein anchors" to help retain the R-ARM in the tumour after i.t. injection. Both aggregated and non-aggregated BSA derivatives were highly retained in 4T1 breast cancer tumours for at least 120 hours. Based on these promising results, therapy studies were pursued using i.t. injections.

To interrogate the platform, both alpha and beta emitting radionuclides were evaluated through i.t. administration in a breast cancer tumour model (Chapter 4). Prior to performing a therapy study, a method for preparing the actinium-

labelled aggregates was developed and a tolerability study performed. After 7 days the mice showed no signs of radiotoxicity with the majority gaining or maintaining weight, however future studies were performed using lutetium-177 due to the facile detection of the isotope. Single and multi-dosing studies were performed with the lutetium-labelled aggregates, in which the latter showed a statistically significant survival advantage compared to the control, however the treatment was not curative.

To better understand the observed results, an autoradiography study was performed to evaluate the spatial distribution of the radiolabelled aggregated and non-aggregated material within tumours after i.t. administration. The aggregated material was concentrated in a few small areas of the tumour whereas the non-aggregated material was distributed throughout the tumour by 24 hours. Based on these findings, a multi-dosing therapy study was performed with the lutetium-labelled non-aggregated material which showed a statistically significant survival advantage compared to the control and the longest survival advantage to date. The results from the therapy studies were promising, and dose optimization for complete tumour regression will be pursued with the actinium and lutetium derivatives.

In addition to radiotherapy, the antibody recruiting efficacy of the platform was tested (Chapter 5) in an attempt to determine a dosing regimen which could then be applied to combination therapy. As shown in Chapters 3 and 4, the radiolabelled non-aggregated BSA was highly retained in the tumour and autoradiography data showed preferable spatial distribution versus the aggregates for ARM therapy. Prior to further *in vivo* experiments, an ELISA was performed

which showed the ligand clicked to TCO-BSA was still capable of recruiting antibodies. This was followed by extensive work to develop mice that had appropriate anti-DNP antibody titres. A protocol involving subcutaneous injections of DNP-KLH in Freund's incomplete adjuvant (FIA) every two weeks was found to create a titre that was sufficient for ARM therapy. To this end animals were administered the ARM linked to BSA (1.5-1.9 nmol of DNP) i.t. three times per week and tumour size was compared to treated but anti-DNP naïve animals. Unfortunately, there was no difference in survival advantage or change in tumour growth rate between the immunized group and the control. While analysis of the immune cells in the tumour provided preliminary evidence of an elevated immune response it is not yet possible to make the connection to ARM therapy. To probe the system further, both aggregated and non-aggregated TCO-BSA were given i.t. followed by the i.v. administration of the radiolabelled tetrazine. The study showed minimal uptake in the tumour for either agent with a clearance profile that was similar to that of the ligand alone. This data suggests that with i.t. administration the antigen was not readily accessible creating a barrier to anti-DNP recruitment and ultimately ARM therapy.

6.2 Future Work and Preliminary Data

6.2.1 Antibody Penetration

The concept of therapeutic antibodies being unable to reach the intended target is well known, which is often associated with limited tumour penetration of 20-130 μm from a blood vessel.[1] This is thought to be due to poor blood flow caused by distorted blood vessels and increased interstitial fluid pressure from the irregularly shaped, poorly connected endothelial cells lining the vessels.[2] It has

been documented that alpha radiation can be used to increase permeability in the tumour vasculature.[3, 4] Heyerdhal and colleagues used magnetic resonance imaging (MRI) to image ovarian cancer xenografts after RIT with [^{227}Th]Th-trastuzumab. The MRI scans were performed 1, 2 and 3 weeks post-treatment and it was found that over time the rate constant of diffusion from the extracellular extravascular space to plasma, k_{ep}, increased significantly. In addition, an increase was seen in A• $k_{ep,}$ the product anticipated to be released to vessel permeability, shown to be associated with increased vessel and tumour permeability.[3, 5, 6]

Based on these findings, it appears that first irradiating the tumour with an alpha emitter could help increase anti-DNP antibody penetration, leading to a more pronounced therapeutic effect. In addition, it has been noted that causing apoptosis in the tumour can lead to a decrease in tumour interstitial fluid pressure, leading to better antibody penetration.[2] Therefore, the R-ARM platform should be pursued in the future by first delivering cytotoxic radiation to the tumour followed by antibody recruiting therapy. Preliminary steps of this experiment have been completed through the labelling of **7** with actinium-225 (**18**), conjugation to TCO-BSA aggregates (**19**), followed by a tolerability study in a breast cancer tumour model.

6.2.2 Targeting The R-ARM Platform Using BSA

Preliminary work to evaluate the tumour uptake of **8** linked to TCO-BSA when administered i.v. was reported in Chapter 3. The resulting tumour uptake was thought to be caused by the enhanced permeability and retention (EPR) effect seen in many tumours.[7] With that being said there is evidence that BSA accumulation at a tumour site can be due to the interaction with secreted protein acidic and rich in

cysteine (SPARC); a glycosylated protein known to have a high binding affinity for albumin.[8-12] SPARC is overexpressed in many cancers, with the expression in healthy tissue limited to bone and tissues undergoing repair.[8] In a study of 119 patient samples, it was found that 61% of head and neck cancers were positive for SPARC, compared to 0% of healthy tissue biopsies.[8] It was also noted that patients with SPARC positive tumours treated with albumin-bound paclitaxel had an overall response rate of 83% compared to 25% in the SPARC negative group. A study by Hoang and colleagues found that in the presence of BSA, the uptake of docetaxel-functionalized nanoparticles increased two-fold in SPARC positive tumours.[9] Based on the promising clinical and preclinical data, the i.v. administration of **8** linked to TCO-BSA should be pursued further, specifically in SPARC positive tumours. This has the potential to increase therapeutic efficacy, as i.v. administration may help to increase the availability of the DNP-antigen to the anti-DNP antibody.

As noted in Chapter 3, it has been demonstrated that the number of conjugates linked to albumin can have a significant impact on its distribution. Stehle and colleagues compared the biodistribution of rat serum albumin conjugated with 1 to 20 methotrexate molecules.[13] It was found that as the number of methotrexate molecules increased, the circulation time of the compound in the blood decreased, tumour uptake decreased and liver uptake increased. At the highest conjugation ratio, the uptake in the liver and tumour were 60 and 2% compared to 6 and 25% respectively for the 1:1 ratio 24 hours post-injection. This study shows the impact that the level of functionalization can have on the

distribution of an albumin-drug conjugate. Using this information, the distribution of **8** linked to TCO-BSA should be re-evaluated with a conjugation ratio less than 3 in an attempt to increase tumour uptake and decrease liver uptake. Here there is also the opportunity to take advantage of the bio-orthogonal capabilities of the platform, as the molecular weight of the conjugate linked to albumin could play a role in the distribution. An active and pre-targeting study can be performed using TCO-BSA and the R-ARM (**8**), to evaluate the differences in distribution. After the biodistribution studies are performed, the model with the highest tumour to non-target ratios should be pursued for R-ARM therapy.

6.2.3 Evaluating the Distribution and Uptake of Anti-DNP Antibodies

Although ARMs have shown promising preclinical results, studies have not been done to determine the amount of antibody required at the site of interest in order to achieve a therapeutic response. The current method to demonstrate *in vivo* recruitment of anti-DNP antibodies is through therapeutic efficacy, which gives no insight into the amount of antibody at the tumour.[14-17] In 2018, Schrand and colleagues used IHC to analyze tumour slides for the presence of IgG/IgM antibodies in mice immunized towards DNP compared to naïve controls.[18] The IHC slides showed a distinct increase in the number of antibodies present in the tumour for the immunized group compared to the control. Although these results suggest that anti-DNP antibodies are being recruited to the tumour, it is difficult to differentiate antibodies reactive to DNP from other antigens as the IHC stain was for generic IgG/IgM antibodies. Additionally, IHC only takes into account a single

slice of the tumour at a specific time as it requires *ex vivo* analysis of the tumour, complicating its use to predict efficacy.

Instead of using a post-mortem form of analysis such as IHC, there is an opportunity to radiolabel anti-DNP antibodies in order to visualize their distribution and tumour uptake over time. Following administration of an ARM, the radiolabelled anti-DNP antibody can be administered and tracked through SPECT/positron emission tomography (PET) imaging. The amount of activity in the tumour can then be quantified *ex vivo* and used to determine the extent of ternary complex formation at the tumour site, which has traditionally been done through *in vitro* assays such as flow cytometry.[14, 17, 19, 20]

SPECT and PET have been used clinically to obtain images of antibody distribution.[21, 22] Of particular interest was zirconium-89, due to its multiday half-life of 78.4 hours, which accommodates the long circulation times of antibodies. In addition, its relatively low energy positron emission of 395.5 keV allows for high resolution PET images to be obtained.[21, 23-25] The most commonly used chelate for zirconium-89 is desferrioxamine (DFO), a hexadentate siderophore with three hydroxamate donor groups.[21] Some preliminary experiments were performed to this end.

Due to the high cost of anti-DNP monoclonal and polyclonal antibodies, initial conjugation and radiolabelling reactions were performed using the anti-DNP antiserum. The antiserum was incubated with the bifunctional chelator, *p*-isothiocyanatobenzyl (*p*-SCN)-DFO, in order to non-specifically functionalize free lysine residues on the protein.[26] The functionalized antiserum was purified using

size exclusion chromatography, and a MALDI mass spectrum confirmed functionalization of approximately 1.4 DFO groups per antibody. The DFO-antibody conjugate was radiolabelled with zirconium-89, purified by size exclusion chromatography and analyzed by iTLC with 20 mM citric acid as the eluent (Figure 6-1). The isolated radiochemical yield of the reaction was 57% with radiochemical purity of 95%, as determined by iTLC. Due to the reasonable yield and high radiochemical purity, the conjugation and labelling procedures were applied to anti-DNP polyclonal antibodies.

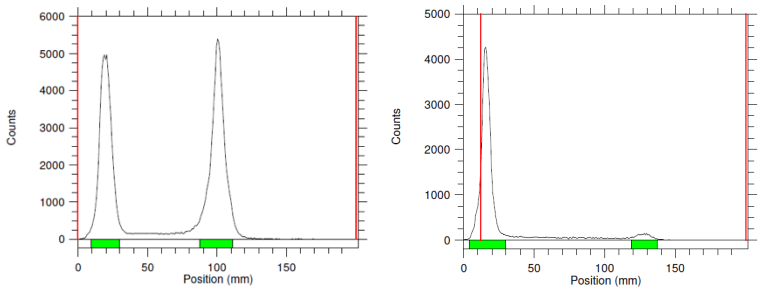

Figure 6-1. Radio-TLC spectra of the radiolabelling reaction (left) and the purified reaction (right) run in 20 mM citric acid pH 4.9-5.1. The peaks at the baseline are representative of the radiolabelled antibody, and the peaks at the solvent front represent the free zirconium-89.

Although anti-DNP antibodies are used frequently in the literature, it proved difficult to find a commercially available mouse anti-DNP antibody in quantities needed for radiolabelling and imaging studies. We were able to identify a rabbit polyclonal antibody reactive to DNP-KLH, however it was only available in 500 µg quantities at a concentration of 2 mg/mL. Due to commercial limitations, the previously employed procedure could not be used directly and was modified to accommodate the dilute, low mass antibody stock.[26] The procedure was scaled down, using 200 µg of antibody and when analyzed by MALDI, showed no conjugation. The reaction was repeated and purified by 100 kDa spin filter instead

of SEC but once again revealed no functionalization. The reaction was performed a third time with 1 mg of antibody and the MALDI spectrum once again revealed no conjugation. The dilute reaction conditions and solubility issues associated with the DFO chelate were likely responsible for the low yield, therefore conjugation with another radiometal chelate was pursued.

Although PET is often the preferred choice for diagnostic imaging, there are a wide variety of radionuclides suitable for SPECT imaging of antibody distribution, many of which use the macrocyclic chelate DOTA.[27] The antibody conjugation was attempted with 5 and 10 equivalents of DOTA-NHS, and purification was performed on a size exclusion column. Unfortunately, neither of the reactions showed successful conjugation to DOTA, suggesting that functionalization of the polyclonal anti-DNP antibody was not feasible. In order to circumvent this issue, direct radioiodination was pursed as no modifications to the antibody were required prior to radiolabelling.[28]

6.2.3.1 Radioiodination of Anti-DNP Antibodies

In order to maximize the data produced from these experiments, a mouse monoclonal antibody was iodinated in addition to the rabbit polyclonal antibody. The antibodies were radiolabelled through direct iodination with iodogen, as well as the Bolton-Hunter method which is thought to decrease *in vivo* deiodination.[29] Initial attempts at direct iodination methods suffered from low yield (2-11%), as well as low radiochemical purity (17-43%) after purification by size exclusion chromatography.

In an attempt to increase the radiochemical purity of the product, the polyclonal antibody was radiolabelled using the Bolton-Hunter method (Figure 6-2). The Bolton-Hunter reagent was iodinated using iodogen as the oxidant and purified through liquid-liquid extraction to give the product in 37% yield and >97% radiochemical purity. The polyclonal anti-DNP antibody (80 μg) was added to the radiolabelled ligand and agitated for 30 minutes followed by purification through a size exclusion cartridge. The radiolabelled antibody was isolated in 30% yield with RCP of 83%, which is an improvement from the direct iodination conditions. The radiolabelled antibody was then used in an ELISA to confirm the antibody was reactive towards the DNP target post-labelling. Unfortunately, the results of the ELISA showed only background binding of the antibody to the antigen, suggesting that the Bolton-Hunter method is not suitable as it renders the antibody unreactive to the antigen. That being said the direct iodination method was pursued further in an attempt to isolate a pure product that retains reactivity towards the antigen, DNP.

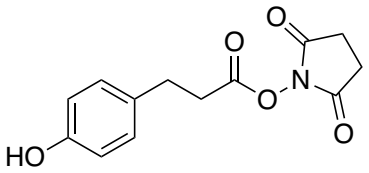

Figure 6-2. Structure of the Bolton-Hunter reagent

Due to the low mass of both the antibody and iodine used in the preliminary reactions, the amount of antibody was increased (30 – 200 μg). The reactions exhibited modest yields ranging between 65-74%, with radiochemical purity of 75-93%. In hopes of achieving a more consistent product with higher purity iodine-127, in addition to iodine-125, was added to the reaction mixture.[30, 31] To each of

the radiolabelling reactions was added NaI (0.01 μg) in addition to antibody, radioiodine and iodogen. The addition of non-radioactive iodine helped to increase the radiochemical purity of the polyclonal antibody to 95-97% (n=3) however the yield was reduced to 40-64%. The monoclonal antibody was labelled with a radiochemical yield of 13-64% and radiochemical purity of 88-93% (n=3). The radiochemical purity of the reaction was determined by iTLC and the concentration of antibody post-purification was determined by SEC HPLC.

6.2.3.2 Antibody Reactivity

As was reported earlier for the Bolton-Hunter labelled antibody, prior to evaluating the distribution in mice, the reactivity of the antibody towards the antigen must be tested. This was done through a sandwich ELISA using an alkaline phosphatase functionalized secondary antibody. The results, Figure 6-3, demonstrate that the radiolabelled antibodies have similar reactivity compared to the parent antibody and therefore are suitable for *in vivo* studies. It is apparent from the ELISA that the polyclonal antibody interacts more strongly with the antigen compared to the monoclonal antibody. This can be explained as the immunogen for the antibody was DNP-KLH, which is different than the antigen used in this assay, DNP-BSA.[32] Monoclonal antibodies are known to be highly specific towards a particular antigen as all of the antibodies are identical in structure, compared to polyclonal antibodies which can bind to different epitopes of the same antigen.[33, 34]

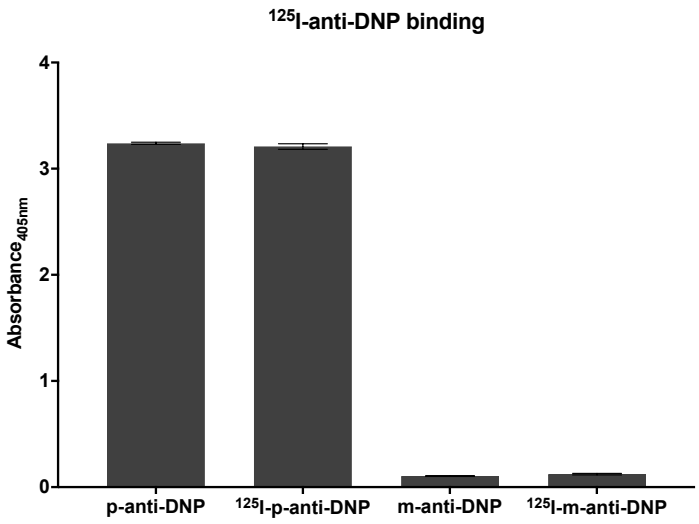

Figure 6-3. Sandwich ELISA results, where p-anti-DNP represents the unmodified polyclonal antibody and m-anti-DNP represents the unmodified monoclonal antibody.

6.2.3.3 Antibody Biodistribution

Once the reactivity of the antibody was confirmed, a biodistribution study was performed on both the radioiodinated monoclonal and polyclonal antibodies. The antibodies were administered to healthy, Balb/c mice and the distribution evaluated at 24, 48 and 96 h. It was apparent from the iTLC results that there would be some uptake of radioiodine in the thyroid as the radiochemical purity of the radiolabelled antibodies ranged from 93-98%, and iodide is known to accumulate in the thyroid.[35] After 96 hours, the thyroid uptake of the monoclonal and polyclonal antibodies were 198 ± 5 and 134 ± 21 %ID/g (Figure 6-4). Although this number seems high, when the absolute value is considered there is approximately 7% and 2% of the injected dose in the thyroid for the monoclonal and polyclonal respectively. This can be directly related to the starting iodide impurity and is comparable to the thyroid uptake seen in the literature for iodinated antibodies.[29] The monoclonal antibody seemed to clear the blood rapidly, with less than 1 %ID/g

left at 24 hours, with minimal uptake in other tissues. The polyclonal derivative showed a longer blood circulation time with 19.4 ± 0.8 %ID/g at 24 hours post-injection which decreased to 12.2 ± 1.0 %ID/g by 96 hours. Due to the high blood retention of the polyclonal antibody, it is difficult to determine if uptake in the other tissues such as the lung and liver are a result of residual blood in the organ, or actual uptake. Overall, the ability of the iodinated anti-DNP antibodies to bind the antigen and the promising biodistribution results suggest that this method could be used to visualize ARM recruitment of the anti-DNP antibodies *in vivo*.

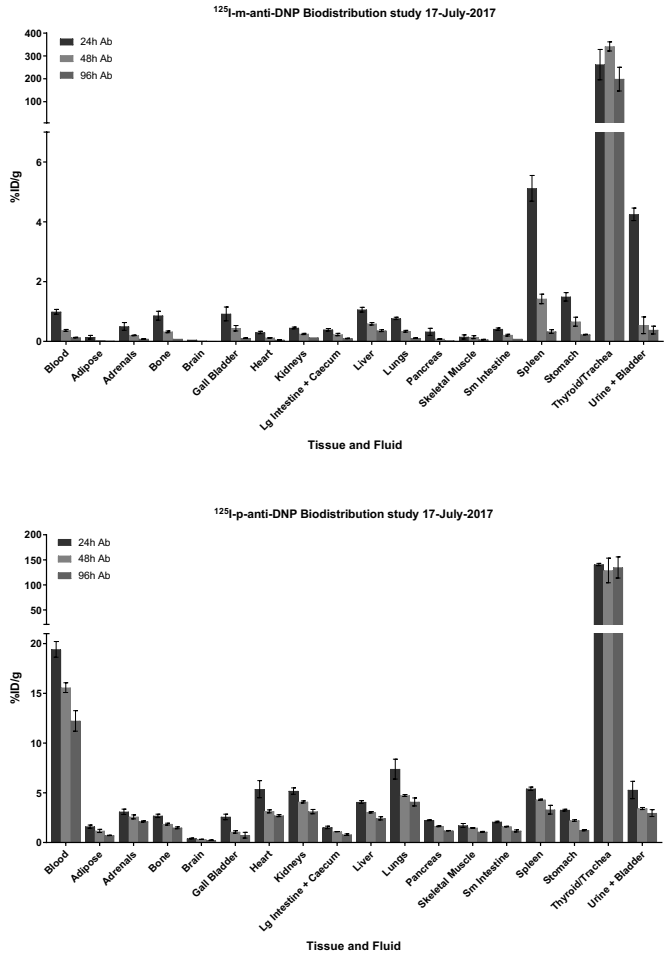

Figure 6-4. Biodistribution of [^{125}I]I-anti-DNP monoclonal antibody (top) and [^{125}I]I-anti-DNP polyclonal antibody (bottom) in Balb/c mice. Animals were administered 0.15-0.26 MBq i.v. and data at the time points indicated are expressed

as the mean percent injected dose per gram (%ID g^{-1}) ± SEM at 24, 48 or 96 hours post-injection (n=3).

6.2.4 Targeting Gram-Positive Bacterial Infection

In a world where bacterial resistance is increasing and antibiotics are becoming less efficacious, additional treatment options for infections are becoming increasingly important.[36] In order to combat this issue, TRT has been investigated in order to treat resistant infections.[37] In 2004, an antibody known to bind the surface of *Streptococcus pneumoniae*, a major cause of pneumonia, meningitis, sepsis, bacteremia, and otitis media, was linked to a CHXA'' chelate and radiolabelled with the alpha emitter, bismuth-213.[37, 38] *In vitro* assays demonstrated dose-dependent killing of the bacteria after a 30 minute incubation with the ^{213}Bi-D11 antibody (0-148 kBq).[37] This was compared to an untargeted antibody, ^{213}Bi-IgM, which showed no killing of the bacteria suggesting the antibody must be targeted for this approach to be efficacious. An *in vivo* study was then performed by administering infected mice with D11 antibody, ^{213}Bi-D11 antibody, ^{213}Bi-IgM or no treatment and the mice monitored over 14 days for survival. The study showed that the mice that received no treatment succumbed to the infection after 1-3 days and the mice treated with 2.96 MBq of ^{213}Bi-D11 antibody had an 87-100% survival rate over the treatment period. There was no survival advantage for the mice that received D11 antibody or ^{213}Bi-IgM compared to the control, with the ^{213}Bi-D11 treatment group showing no infection as early as 3 hours post-treatment. These results demonstrate the susceptibility of bacteria to TRT suggesting bacteria would be a good target for the R-ARM platform.

Infections caused by multi-drug resistant gram-positive bacteria are becoming more common in the USA, and pose a threat due to the minimal treatment options and the capability of the bacteria to evade the immune system.[36, 39-41] It is known that the antibiotic vancomycin can be used to target the cell walls of gram-positive bacteria through hydrogen bonds with the terminal D-alanyl-D-alanine peptide units.[39] Through facile functionalization of vancomycin, gram-positive bacteria have been imaged through both optical and nuclear techniques (Figure 6-5) using active and pre-targeting strategies.[39, 42-44] Building on this work, and as a proof of concept study, the previously validated TCO-vancomycin was used to target R-ARM **8** to a *Staphylococcus aureus* (*S. aureus*) infection. In 2011, Chung *et al.* demonstrated that pre-targeting TCO-vancomycin to *S. aureus* resulted in a 6-fold higher signal than active targeting of the same compound, therefore our *in vitro* experiments were tested using pre-targeting.[39]

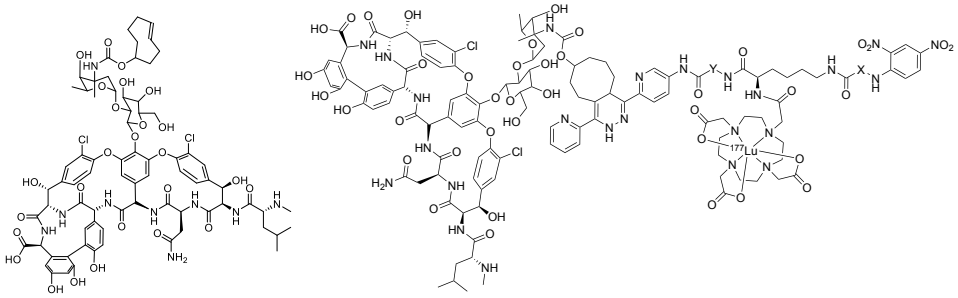

Figure 6-5. Structure of TCO-vancomycin (left)[42] and **20** (right)

TCO-vancomycin was synthesized as previously described[39] and used in a pre-targeting binding assay with **8** as previously described.[44] Briefly, *S. aureus* was incubated with TCO-vancomycin (20 μM) for 30 minutes followed by incubation

with **8** for 1, 4 and 24 hours. The bacterial binding was then determined by counting the radioactivity in the supernatant and the pellet, followed by normalization with the amount of protein in the pellet. The results are summarized in Figure 6-6, which shows 4% activity bound/µg of protein in the pellet after a 1 hour incubation, which decreases to 1% by 24 hours. To confirm that the radioactive uptake was dependent on the presence of TCO-vancomycin, a competitive inhibition study was performed by adding 200 µg of vancomycin to the 30 minute incubation step. The presence of vancomycin did reduce the amount of binding where at 1 and 24 hours a decrease in uptake of 1.6 and 0.65 %/µg of protein respectively was observed.

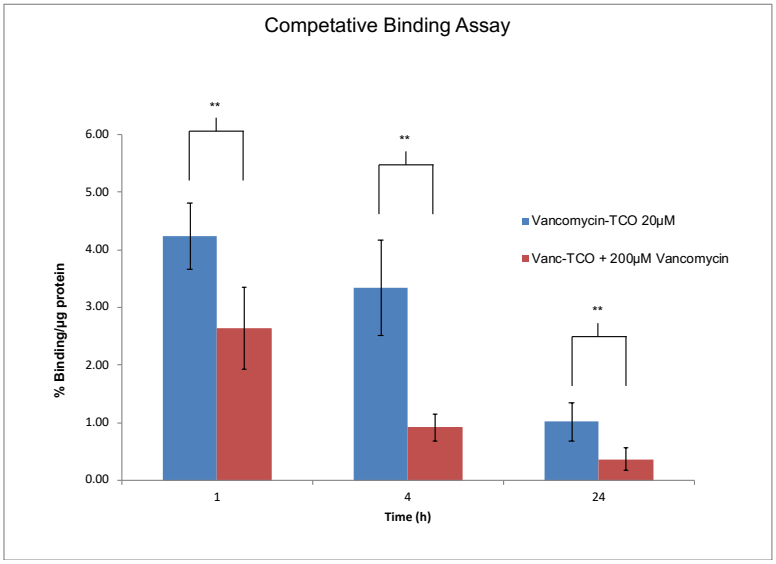

Figure 6-6. TCO-vancomycin binding assay with compound **8**. Blue bars represent incubation of the bacteria with TCO-vancomycin (20 µM), and the red bars represent incubation of the bacteria with TCO-vancomycin (20 µM) and vancomycin (200 µM) as a block.

To assess whether this strategy would allow for selective localization of the DNP group to infections *in vivo*, mice were incoluated with S. *aureus* in their right thigh and 24 hours later administered **20** i.v. (Figure 6-5). The animals were sacrificed 1 and 24 hours post-injection and their organs counted for radioactivity. The uptake in select tissues are shown in Figure 6-7, where the infected thigh (right)

showed 3.29 ± 1.00 and 0.38 ± 0.20 %ID/g relative the to the healthy thigh at 1.63 ± 0.84 and 0.09 ± 0.15 %ID/g at both 1 and 24 hours post-injection respectively. The results are not statistically different and the overall uptake in the infected tissue at 1 and 24 hours is low for use as a therapeutic. The blood concentration of 4.27 ± 1.16 %ID/g at one hour post-injection is higher than that observed in the infected and non-infected thighs, making it difficult to interpret whether the uptake is specific, or from residual blood in the tissue. The biodistribution should be repeated using a pre-targeting strategy in an attempt to increase uptake in the infection while decreasing blood retention.

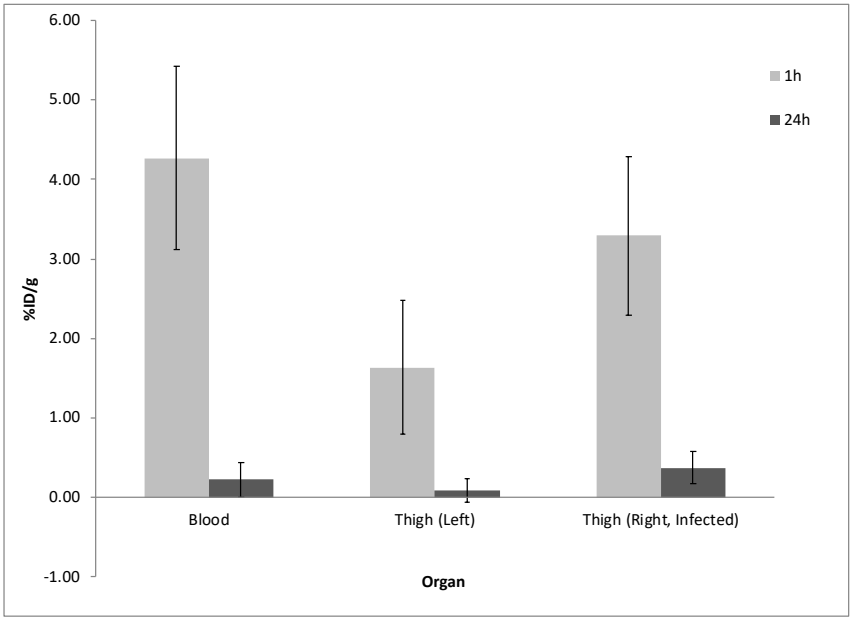

Figure 6-7. Biodistribution data for the active targeting study of **20** in Balb/c mice bearing a *S. aureus* infection in the right thigh (n=3) at 1 and 24 hours post-injection. Data at the time points indicated are expressed as the mean percent injected dose per gram (%ID g^{-1}) ± SEM.

In parallel with the *in vivo* studies, viability studies were performed to determine if TCO-vancomycin clicked with compound **8** had cytotoxic effects. Briefly, S. *aureus* were incubated with saline, TCO-vancomycin, **8** (3.6 MBq) or

TCO-vancomycin followed by **8** (3.6 MBq) and the viability monitored over time. After a 144 hour incubation, the number of viable bacteria in each treatment group were compared and it was determined that there was no cytoxic effect on the treatment group relative to the controls (Figure 6-8). Although the results were not ideal, this was the first attempt at a viability assay with lutetium-177 and there were many variables that would require optimization to generate the desired results. It has been reported in the literature that the half-life of the isotope should be similar to that of the doubling time of the bacteria in order to achieve the highest efficacy.[45] That being said the half-life of lutetium-177, 6.6 days, is significantly longer than the doubling time of *S. aureus*, 26 minutes.[45-47] Optimization of the assay with a shorter lived radionuclide such as bismuth-213 should be attempted to determine if *S. aureus* is succeptible to TRT.

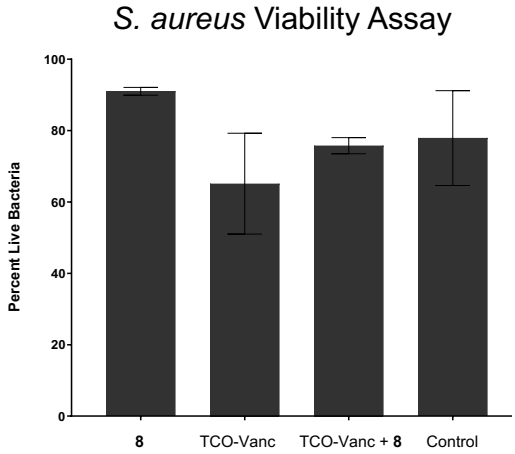

Figure 6-8. *S. aureus* was treated with **8**, TCO-vancomycin, TCO-vancomycin and **8** or saline and the viability monitored at 144 hours. The results show no statistically significant difference between the control and the treatment groups.

6.3 Future Work Summary

The priority for future work should focus on optimizing the dosing regimen for i.t. administration of both the lutetium-177 and actinium-225 labelled BSA, building on the results observed in Chapter 4. In addition, R-ARM therapy with the TCO-BSA platform should be pursued in immunized mice to determine if treatment with alpha or beta radiation can help to increase antibody penetration and therefore recognition of the antigen. Finally, the pharmacokinetics of the i.v. administered TCO-BSA should be optimized in order to increase uptake in the tumour by changing the number of conjugates and attempting a pre-targeting strategy. Once these experiments have been performed, the results can be used to shape the future direction of the R-ARM scaffold.

6.4 Materials and Methods

6.4.1 General Materials and Instruments

Chemicals and reagents for synthesis were purchased from Sigma-Aldrich, Invitrogen and Macrocyclics and used without further purification. Biological reagents from multiple sources were used and are listed in the text below. MALDI data were obtained using a Bruker Ultraflextreme spectrometer. High-performance liquid chromatography (analytical) were performed on a Waters 1525 Binary HPLC system connected to a Bioscan γ-detector and a 2998 photodiode array detector monitoring at 254 nm and 280 nm or a Waters 2545 binary gradient model, 2998 photodiode array equipped with a 2767 sample manager. For analytical runs a Phenomenix Yarra (3 μm, 7.8 × 300 mm, SEC-3000) was used, at a flow rate of 1.0 mL/min. The elution method for HPLC procedures were: Method A: Solvent A =

50 mM $NaPO_4$ pH 6.8 + 300 mM NaCl isocratic elution 0-20 min. [^{125}I]I was produced by the McMaster Nuclear Reactor (MNR, Hamilton, Ontario) and was provided as a solution of [^{125}I]NaI in 0.1 M NaOH. [^{89}Zr]Zr was produced by 3D Imaging (Little Rock, Arkansas) and was provided as a solution of [^{89}Zr]Zr-oxalate in 1M oxalic acid. Radio-TLC was performed using a Bioscan AR-2000 imaging scanner on iTLC-SG glass microfiber chromatography paper (SGI0001, Agilent Technologies) plates using 0.1 M EDTA as the eluent. For each TLC performed, plates were spotted with approximately 2 μL (~3.7 kBq) and run for 5 minutes.

6.4.2 DFO- Conjugation anti-DNP anti-serum

To a solution of 100 μL of anti-DNP antiserum (55.3 mg/mL) was added 0.9 mL of saline. The pH of the reaction mixture was adjusted to 8.9-9.1 using 30 μL of 0.1 M Na_2CO_3. To the mixture was added 2.1 μL *p*-SCN-Bn-DFO (1.1×10^{-8} mol) in DMSO, and the reaction was heated to 37°C for 30 minutes. The reaction was then loaded onto a preconditioned (20 mL of 5 mg/mL gentisic acid in 0.25 M sodium acetate pH 5.4-5.6) PD-10 column. The column was washed with 1.5 mL buffer, and the product eluted in 2 mL of buffer. The product was submitted for MALDI analysis and approximately 1.4 DFO moieties are present per antibody.

6.4.3 Condition 1- DFO-Conjugation to Polyclonal anti-DNP Antibody

To a solution of 100 μL of anti-DNP polyclonal antibody (2 mg/mL) was added 5 μL of 0.1 M Na_2CO_3 to adjust the pH of the reaction mixture to 8.9-9.1. To the mixture was added 1.6 μL *p*-SCN-Bn-DFO (4.0×10^{-9} mol) in DMSO, and the reaction was heated to 37°C for 30 minutes. The reaction was diluted to 1 mL with saline and loaded onto a preconditioned (20 mL of 5 mg/mL gentisic acid in 0.25

M sodium acetate pH 5.4-5.6) PD-10 column. The column was washed with 1.5 mL buffer, and the product eluted in 2 mL of buffer. The product was submitted for MALDI analysis and no difference was seen between product and parent antibody.

6.4.4 Condition 2- DFO-Conjugation to Polyclonal anti-DNP Antibody

To a solution of 100 μL of anti-DNP polyclonal antibody (2 mg/mL) was added 5 μL of 0.1 M Na_2CO_3 to adjust the pH of the reaction mixture to 8.9-9.1. To the mixture was added 1.8 μL *p*-SCN-Bn-DFO (3 equivs, 4×10^{-6} mol) and the reaction was heated to 37°C for 30 minutes. The reaction was purified using a high molecular weight (100 kDa) spin filter, centrifuging at 14000 × g for 10 minutes, followed by recovery through flipping the filter and running at 1000 × g for 2 minutes. The product was submitted for MALDI analysis and no difference was seen between product and parent antibody.

6.4.5 Condition 3- DFO-Conjugation to Polyclonal anti-DNP Antibody

To a solution of 500 μL of anti-DNP polyclonal antibody (2 mg/mL) was added 500 μL of saline and 80 μL of 0.1 M Na_2CO_3 to adjust the pH of the reaction mixture to 8.9-9.1. To the mixture was added 8.9 μL *p*-SCN-Bn-DFO (2×10^{-8} mol) in DMSO, and the reaction was heated to 37°C for 30 minutes. A portion, 200 μL, of the reaction mixture was purified using a high molecular weight (100 kDa) spin filter, centrifuging at 14000 × G for 10 minutes, followed by recovery through flipping the filter and running at 1000 × G for 2 minutes. The remaining 800 μL was diluted to 1 mL with saline and loaded onto a preconditioned (20 mL of 5 mg/mL gentisic acid in 0.25 M sodium acetate pH 5.4-5.6) PD-10 column. The column was washed with 1.5 mL buffer, and the product eluted in 2 mL of buffer.

The product was submitted for MALDI analysis and no difference was seen between product and parent antibody.

6.4.6 Condition 1- DOTA-Conjugation to Polyclonal anti-DNP Antibody

To a solution of 200 μL of anti-DNP polyclonal antibody (2 mg/mL) was added 5 equivalents of DOTA-NHS ester (6.67×10^{-9} mol in 5 μL of 5% $NaHCO_3$) and 100 μL of 0.1 M Na_2CO_3 to adjust the pH of the reaction mixture to 8.0-9.0. The reaction was gently agitated for an hour followed by purification using Sephadex resin pre swelled in saline 0.01% TWEEN 80. The reaction was loaded and the column was washed with 200 mL of saline 0.01% TWEEN 80, followed by product elution in 400 μL saline 0.01% TWEEN 80. The product was submitted for MALDI analysis and no difference was seen between product and parent antibody.

6.4.7 Condition 2- DOTA-Conjugation to Polyclonal anti-DNP Antibody

To a solution of 100 μg of anti-DNP polyclonal antibody (2 mg/mL) in 50 μL of PBS was added 50 μL of 0.5 M acetate buffer 0.01% TWEEN 80, followed by 2.5 μL of DOTA-NHS ester (10 equivalents, 6.67×10^{-6} mol, 0.0051 g). The pH of the reaction mixture was adjusted to 8.0-9.0 using 20 μL of 0.1 M $NaHCO_3$ at which point the reaction was gently agitated for an hour. The reaction mixture was purified using Sephadex resin pre swelled in 0.5 M acetate buffer 0.01% TWEEN 80. The reaction mixture was loaded and the column was washed with 275 μL of 0.5 M acetate buffer 0.01% TWEEN 80, followed by product elution in 400 μL 0.5 M acetate buffer 0.01% TWEEN 80. The product was submitted for MALDI analysis and no difference was seen between product and parent antibody.

6.4.8 Radioiodination of anti-DNP Monoclonal/Polyclonal Antibodies

To a precoated iodogen vial (25 μg) was added [^{125}I]NaI (36.1 - 39.2 MBq), 10 μL 0.1 M NaOAc, 10 μL 0.01 mg/mL NaI solution and anti-DNP antibody (100 μg and PBS to make the total reaction volume 130 μL). The reaction mixture was agitated for 30 minutes at room temperature at which point it was diluted to 1 mL with PBS and loaded on a preconditioned PD-10 column. The column was rinsed with 1.5 mL of PBS, and the antibody eluted in three 1 mL fractions. The fractions were analyzed by iTLC with isolated radiochemical yields between 13 – 64%, and radiochemical purity from 93 – 97%.

6.4.9 Sandwich ELISA Protocol

Briefly, 1 mg/mL DNP-BSA (Life Technologies, A23018) in sterile PBS (ThermoFisher, 10010023) was diluted 1/1000 with coating buffer (Bethyl Laboratories, E107) and transferred (100 μL) to a 96 well plate. Following a 1 h incubation at room temperature, the wells were washed three times with 200 μL of ELISA wash buffer (Bethyl Laboratories, E106). ELISA blocking buffer (Bethyl Laboratories, E104) was then added to each well (200 μL) and left to incubate at room temperature for 0.5 h. The plate was washed three times with ELISA wash buffer (200 μL/well) before the addition of 100 μL of either DNP (Sigma-Aldrich, D19850; 40 nmol per well), or sample diluent alone followed by 100 μL of monoclonal anti-DNP antibody (Sigma-Aldrich, D-8406; 1 μg/mL), polyclonal antibody (Life Technologies, A-6430; 1 μg/mL), [^{125}I]I-monoclonal anti-DNP antibody (1 μg/mL) or [^{125}I]I-polyclonal anti-DNP antibody (1 μg/mL). Following a 1 h incubation at room temperature, the plate was washed three times with ELISA

wash buffer (200 μL/well). To each well, 100 μL of 2° antibody was added Goat anti-rabbit IgG-AP 2° (Jackson ImmunoResearch, 111055045; 1:5000) or Goat anti-mouse IgG-AP 2° (Jackson ImmunoResearch, 115055062; 1:5000). Following a 1 h incubation at room temperature, the plate was washed three times with ELISA wash buffer (200 μL/well). PNPP substrate was added and the plate incubated in a dark at room temperature for 0.5 h. To quench the reaction, 50 μL of 2 M NaOH was added to each well and the absorbance subsequently measured at 405 nm on a plate reader.

6.4.10 Antibody Biodistribution Studies

Female 5-6 week old, Balb/c mice were injected intravenously with [^{125}I]I-labelled anti-DNP antibody (0.148 – 0.259 MBq, monoclonal or polyclonal). After 24, 48 and 96 hours post-injection (n = 3 per time point), mice were anesthetized with 3% isoflurane and euthanized by cervical dislocation. Blood, adipose, adrenals, bone (arm bones including shoulder and leg bones including knee joint), brain, gall bladder, heart, kidneys, large intestine and caecum (with contents), liver, lungs, pancreas, skeletal muscle, small intestine (with contents), spleen, stomach (with contents), thyroid/trachea, urine + bladder and tail were collected, weighed and counted in a gamma counter. Decay correction was used to normalize organ activity measurements to time of dose preparation for data calculations with respect to injected dose (i.e. %ID/g).

6.4.11 *Staphylococcus aureus* Biodistribution

Female, 6-7 week old Balb/c mice ordered from Charles Rive Laboratory (Kingston, NY) were inoculated with 1×10^8 *Staphylococcus aureus* CFU in the

right thigh. After 20 hours the mice were administered 0.370 MBq of **11** and at 1 and 24 hours post-injection (n = 3 per time point), mice were anesthetized with 3% isoflurane and euthanized by cervical dislocation. Blood, liver with gall bladder, spleen, kidneys and adrenals, small intestine (with contents), right thigh, left thigh, bladder (with urine), lymph nodes from leg and tail were collected weighed and counted in a gamma counter. Decay correction was used to normalize organ activity measurements to time of dose preparation for data calculations with respect to injected dose (i.e. %ID/g).

6.4.12 *Staphylococcus aureus* Viability Assay

For the viability: An aliquot of *Staphylococcus aureus* (*S. aureus*, ATCC 25923) culture was added to 7 mL (× 2) of TSB (ATCC, 25923) in a 15 mL snap cap tube. The culture was grown in a shaker incubator at 37˚C and 300 rpm for 16 to 24 h. The cells were pooled and 2 mL was removed for the standards, the remaining 12 mL was used for the viability. An aliquot of the bacteria was diluted (1:10) in PBS in a cuvette in duplicate. The OD_{600} and OD_{670} were measured using the plate reader. Cells were aliquoted in 1 mL portions to 12 × 1.5 mL Eppendorf tubes and centrifuged for 2 min at 10,000 × g at which point the supernatant was removed and the cells washed × 2 with 1 mL PBS-F. The cells were resuspended in PBS-F and incubated with TCO-vancomycin or vehicle for 30 minutes. The samples were then centrifuged for 2 min at 10,000 × g at which point the supernatant was removed and the cells washed × 2 with 1 mL PBS-F. The cells were resuspended in PBS-F and incubated with **8** or vehicle for 30 minutes. The cells were then washed with 1 mL of saline (× 2) and resuspended in saline at an OD_{670} ~ 0.3. The cells were then

incubated with rotation for 144 hours, removing samples at 1, 24 and 144 h to test for viability.

For the standards: The bacterial suspension aliquoted previously was centrifuged for 10-15 min at 10,000 × g. The supernatant was removed and the pellet was resuspended in 200 µL of saline. To create the live and dead standards 100 µL of the bacteria suspension was added to 2 mL of saline (live) and 100 µL was added to 2 mL of EtOH (dead). The samples were incubated with rotation for 1 h followed by centrifugation at 10,000 × g for 10-15 min. The supernatant was discarded and the cells washed with 0.5 mL of saline followed by resuspension in 1 mL of saline. The optical density at 670 nm was measured and the samples diluted to OD_{670} ~ 0.3. Mix the live and dead cells in the following ratios (Live:Dead): 0:100, 10:90 (40 µL:360 µL), 25:75 (100 µL:300 µL), 50:50 (200 µL:200 µL), 75:25 (300 µL:100 µL), 90:10 (360 µL:40 µL), 100:0. Mix 16.5 µL of Component A (Live/Dead BacLight Bacterial Viability Kit, Thermofisher, L7012) with 16.5 µL of Component B (Live/Dead BacLight Bacterial Viability Kit, Thermofisher, L7012) and dilute with 5.5 mL of DI water (2× staining solution). Load 100 µL of each control and experimental (TCO-vancomycin + **8**) cell suspension mixture, in triplicate, onto a 96-well black, clear bottom plate. Load 100 µL of the 2× staining solution to each well and mix well by pipetting up and down several times. Incubate the plate at room temperature in the dark for 15 minutes then read on the plate reader Ex: 485bnm, Em_1: 530 nm, Em_2: 630nnm.

6.5 References

1. Rudnick, S. I.; Lou, J.; Shaller, C. C.; Tang, Y.; Klein-Szanto, A. J.*, et al.*, Influence of Affinity and Antigen Internalization on the Uptake and

Penetration of Anti-HER2 Antibodies in Solid Tumors. *Cancer Res* **2011,** *71* (6), 2250-259.
2. Huang, C. Y.; Pourgholami, M. H.; Allen, B. J., Optimizing Radioimmunoconjugate Delivery in the Treatment of Solid Tumor. *Cancer Treat Rev* **2012,** *38* (7), 854-860.
3. Heyerdahl, H.; Roe, K.; Brevik, E. M.; Dahle, J., Modifications in Dynamic Contrast-Enhanced Magnetic Resonance Imaging Parameters after Alpha-Particle-Emitting (227)Th-Trastuzumab Therapy of HER2-Expressing Ovarian Cancer Xenografts. *Int J Radiat Oncol Biol Phys* **2013,** *87* (1), 153-159.
4. Repetto-Llamazares, A. H. V.; Malenge, M. M.; O'Shea, A.; Eiriksdottir, B.; Stokke, T.*, et al.*, Combination of (177) Lu-Lilotomab with Rituximab Significantly Improves the Therapeutic Outcome in Preclinical Models of Non-Hodgkin's Lymphoma. *Eur J Haematol* **2018,** *101* (4), 522-531.
5. Ma, H. T.; Griffith, J. F.; Yeung, D. K.; Leung, P. C., Modified Brix Model Analysis of Bone Perfusion in Subjects of Varying Bone Mineral Density. *J Magn Reson Imaging* **2010,** *31* (5), 1169-1175.
6. Stoyanova, R.; Huang, K.; Sandler, K.; Cho, H.; Carlin, S.*, et al.*, Mapping Tumor Hypoxia in Vivo Using Pattern Recognition of Dynamic Contrast-Enhanced MRI Data. *Transl Oncol* **2012,** *5* (6), 437-447.
7. Matsumura, Y.; Maeda, H., A New Concept for Macromolecular Therapeutics in Cancer Chemotherapy: Mechanism of Tumoritropic Accumulation of Proteins and the Antitumor Agent Smancs. *Cancer Res* **1986,** *46*, 6387-6392,.
8. Desai, N.; Trieu, V.; Damascelli, B.; Soon-Shiong, P., SPARC Expression Correlates with Tumor Response to Albumin-Bound Paclitaxel in Head and Neck Cancer Patients. *Transl Oncol* **2009,** *2* (2), 59-64.
9. Hoang, B.; Ernsting, M. J.; Roy, A.; Murakami, M.; Undzys, E.*, et al.*, Docetaxel-Carboxymethylcellulose Nanoparticles Target Cells Via a SPARC and Albumin Dependent Mechanism. *Biomaterials* **2015,** *59*, 66-76.
10. Miele, E.; Spinelli, G. P.; Miele, E.; Tomao, F.; Tomao1, S., Albumin-Bound Formulation of Paclitaxel (Abraxane® Abi-007) in the Treatment of Breast Cancer. *Int J Nanomed* **2009,** *4*, 99-105.
11. Sage, H.; Johnson, C.; Blornstein, P., Characterization of a Novel Serum Albumin-Bindingglycoprotein Secreted by Endothelial Cells in Culture*. *JBC* **1984,** *259* (6), 3993-4007.
12. Chlenski, A.; Dobratic, M.; Salwen, H. R.; Applebaum, M.; Guerrero, L. J.*, et al.*, Secreted Protein Acidic and Rich in Cysteine (SPARC) Induces Lipotoxicity in Neuroblastoma by Regulating Transport of Albumin Complexed with Fatty Acids. *Oncotarget* **2016,** *7* (47), 77696-77706.
13. Stehle, G.; Sinn, H.; Wunder, A.; Schrenk, H.; Schutt, S.*, et al.*, The Loading Rate Determines Tumor Targeting Properties of Methotrexate-Albumin Conjugates in Rats *Anti-Cancer Drugs* **1997,** *8*, 677-685.
14. Chirkin, E.; Muthusamy, V.; Mann, P.; Roemer, T.; Nantermet, P. G.*, et al.*, Neutralization of Pathogenic Fungi with Small-Molecule Immunotherapeutics. *Angew. Chem. Int. Edit.* **2017,** *56* (42), 13216-13220.

15. Dubrovska, A.; Kim, C.; Elliott, J.; Shen, W.; Kuo, T. H.*, et al.*, A Chemically Induced Vaccine Strategy for Prostate Cancer. *ACS Chem Biol* **2011,** *6* (11), 1223-1231.
16. Lu, Y.; Low, P. S., Folate Targeting of Haptens to Cancer Cell Surfaces Mediates Immunotherapy of Syngeneic Murine Tumors. *Cancer Immunol Immunother* **2002,** *51* (3), 153-162.
17. Rullo, A. F.; Fitzgerald, K. J.; Muthusamy, V.; Liu, M.; Yuan, C.*, et al.*, Re-Engineering the Immune Response to Metastatic Cancer: Antibody-Recruiting Small Molecules Targeting the Urokinase Receptor. *Angew. Chem. Int. Edit.* **2016,** *55* (11), 3706-3710.
18. Schrand, B.; Clark, E.; Levay, A.; Capote, A. R.; Martinez, O.*, et al.*, Hapten-Mediated Recruitment of Polyclonal Antibodies to Tumors Engenders Antitumor Immunity. *Nat Commun* **2018,** *9* (1), 1-10.
19. McEnaney, P. J.; Parker, C. G.; Zhang, A. X.; Spiegel, D. A., Antibody-Recruiting Molecules: An Emerging Paradigm for Engaging Immune Function in Treating Human Disease. *ACS Chem Biol* **2012,** *7* (7), 1139-1151.
20. Murelli, R. P.; Zhang, A. X.; Michel, J.; Jorgensen, W. L.; Spiegel, D. A., Chemical Control over Immune Recognition: A Class of Antibody-Recruiting Small Molecules That Target Prostate Cancer. *J Am Chem Soc* **2009,** *131* (47), 17090-17092.
21. Deri, M. A.; Zeglis, B. M.; Francesconi, L. C.; Lewis, J. S., PET Imaging with 89Zr: From Radiochemistry to the Clinic. *Nucl Med Biol* **2013,** *40* (1), 3-14.
22. Khalil, M. M.; Tremoleda, J. L.; Bayomy, T. B.; Gsell, W., Molecular SPECT Imaging: An Overview. *Int J Mol Imaging* **2011,** *2011*.
23. Verel, I.; Visser, G. W. M.; Boellaard, R.; Stigter-van-Walsum, M. S; Snow, G. B.*, et al.*, 89Zr Immuno-PET: Comprehensive Procedures for the Production of 89Zr-Labeled Monoclonal Antibodies. *J Nucl Med* **2003,** *44* (8), 1271-1281.
24. Jauw, Y. W.; Menke-van der Houven van Oordt, C. W.; Hoekstra, O. S.; Hendrikse, N. H.; Vugts, D. J.*, et al.*, Immuno-Positron Emission Tomography with Zirconium-89-Labeled Monoclonal Antibodies in Oncology: What Can We Learn from Initial Clinical Trials? *Front Pharmacol* **2016,** *7*, 131.
25. van de Watering, F. C.; Rijpkema, M.; Perk, L.; Brinkmann, U.; Oyen, W. J.*, et al.*, Zirconium-89 Labeled Antibodies: A New Tool for Molecular Imaging in Cancer Patients. *Biomed Res Int* **2014,** *2014*, 203601.
26. Vosjan, M. J.; Perk, L. R.; Visser, G. W.; Budde, M.; Jurek, P.*, et al.*, Conjugation and Radiolabeling of Monoclonal Antibodies with Zirconium-89 for PET Imaging Using the Bifunctional Chelate P-Isothiocyanatobenzyl-Desferrioxamine. *Nat Protoc* **2010,** *5* (4), 739-43.
27. Price, E. W.; Orvig, C., Matching Chelators to Radiometals for Radiopharmaceuticals. *Chem Soc Rev* **2014,** *43* (1), 260-290.
28. Behr, T. M.; Gotthardt, M.; Becker, W.; Behe, M., Radioiodination of Monoclonal Antibodies, Proteins and Peptides for Diagnosis and Therapy. *Nuklearmedizin* **2002,** *41* (02), 71-79.

29. Vaidyanathan, G.; Zalutsky, M. R., Protein Radiohalogenation: Observations on the Design of Jv-Succinimidyl Ester Acylation Agents. *Bioconjug Chem* **1990,** *1*, 269-273.
30. Chen, J.; Strand, S.-E.; Sjögren, H.-O., Optimization of Radioiodination and Biotinylation of Monoclonal Antibody Chimeric Br96: An Indirect Labeling Using N-Succinimidyl-3-(Tri-N- Butylstannyl)Benzoate Conjugate. *Cancer Biother Radiopharm* **1996,** *11* (3), 217-226.
31. McBride, W. J.; Zanzonico, P.; Sharkey, R. M.; Noren, C.; Karacay, H.*, et al.*, Bispecific Antibody Pretargeting PET (ImmunoPET) with an 124I-Labeled Hapten-Peptide. *J Nucl Med* **2006,** *47* (10), 1678-1688.
32. Sigma-Aldrich, Product Information Monoclonal Anti-Dinitrophenyl. 2020.
33. Stills, H. F., Polyclonal Antibody Production. In *The Laboratory Rabbit, Guinea Pig, Hamster, and Other Rodents*, Elsevier: 2012; pp 259-274.
34. Murphy, K.; Weaver, C., *Janeway's Immunobiology, 9th Edition*. Garland Science/Taylor & Francis Group: New York, NY, 2017.
35. Sternthal, E.; Lipworth, L.; Stanley, B.; Abreau, C.; Fang, S.-L.*, et al.*, Supression of Thyroid Radioiodine Uptake by Various Doses of Stable Iodide. *New Engl J Med* **1980,** *303* (19), 1083-1088.
36. Doernberg, S. B.; Lodise, T. P.; Thaden, J. T.; Munita, J. M.; Cosgrove, S. E.*, et al.*, Gram-Positive Bacterial Infections: Research Priorities, Accomplishments, and Future Directions of the Antibacterial Resistance Leadership Group. *Clin Infect Dis* **2017,** *64* (suppl_1), S24-S29.
37. Dadachova, E.; Burns, T.; Bryan, R. A.; Apostolidis, C.; Brechbiel, M. W.*, et al.*, Feasibility of Radioimmunotherapy of Experimental Pneumococcal Infection. *Antimicrob Agents Chemother* **2004,** *48* (5), 1624-1629.
38. Cherazard, R., Epstein, M., Doan, T., Salim, T., Bharti, S., Smith, M. A., Antimicrobial Resistant Streptococcus Pneumoniae: Prevalence, Mechanisms, and Clinical Implications. *Am J Ther* **2017,** *24*, e361-e369.
39. Chung, H. J., Reiner, T., Budin, G., Min, C., Liong, M., Issadore, D.,; Lee, H., Weissleder, R., Ubiquitous Detection of Gram-Positive Bacteria with Bioorthogonal Magnetofluorescent Nanoparticles. *ACS Nano* **2011,** *5* (11), 8834-8841.
40. Papadimitriou-Olivgeris, M.; Kolonitsiou, F.; Karamouzos, V.; Tsilipounidaki, K.; Nikolopoulou, A.*, et al.*, Molecular Characteristics and Predictors of Mortality among Gram-Positive Bacteria Isolated from Bloodstream Infections in Critically Ill Patients During a 5-Year Period (2012-2016). *Eur J Clin Microbiol Infect Dis* **2020**, 1-7.
41. McCarthy, A. J.; Lindsay, J. A., Staphylococcus Aureus Innate Immune Evasion Is Lineage-Specific: A Bioinfomatics Study. *Infection, Genetics and Evolution* **2013,** *19*, 7-14.
42. Beiraghi, O. Synthesis and Evaluation of Radiopharmaceuticals for Imaging Bacterial Infections. McMaster University, MacSphere, 2015.
43. van Oosten, M.; Schafer, T.; Gazendam, J. A.; Ohlsen, K.; Tsompanidou, E.*, et al.*, Real-Time in Vivo Imaging of Invasive- and

Biomaterial-Associated Bacterial Infections Using Fluorescently Labelled Vancomycin. *Nat Commun* **2013,** *4*, 2584.
44. Vito, A.; Alarabi, H.; Czorny, S.; Beiraghi, O.; Kent, J.*, et al.*, A 99mTc-Labelled Tetrazine for Bioorthogonal Chemistry. Synthesis and Biodistribution Studies with Small Molecule Trans-Cyclooctene Derivatives. *PLoS One* **2016,** *11* (12), e0167425.
45. Dadachova, E., Radioimmunotherapy of Infection with Bi-Labeled Antibodies. *Curr Radiopharm* **2008,** *1* (3), 234-239.
46. Al-Ghananeem, A. M.; Malkawi, A. H.; Muammer, Y. M.; Balko, J. M.; Black, E. P.*, et al.*, Intratumoral Delivery of Paclitaxel in Solid Tumor from Biodegradable Hyaluronan Nanoparticle Formulations. *AAPS PharmSciTech* **2009,** *10* (2), 410-417.
47. May, J. W.; Houghton, R. H.; Perret, C. J., The Effect of Growth at Elevated Temperatures on Some Heritable Properties of Staphylococcus Uureus. *J Gen Microbiol* **1964,** *37*, 157-169.

Appendix I

Supporting Information for Chapter 2

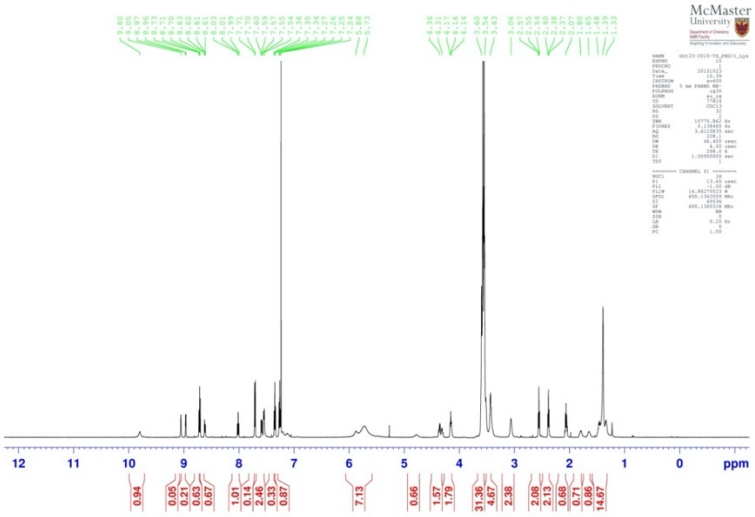

Figure S2-1. ^{1}H NMR spectrum of **2a** ($CDCl_3$, 600 MHz)

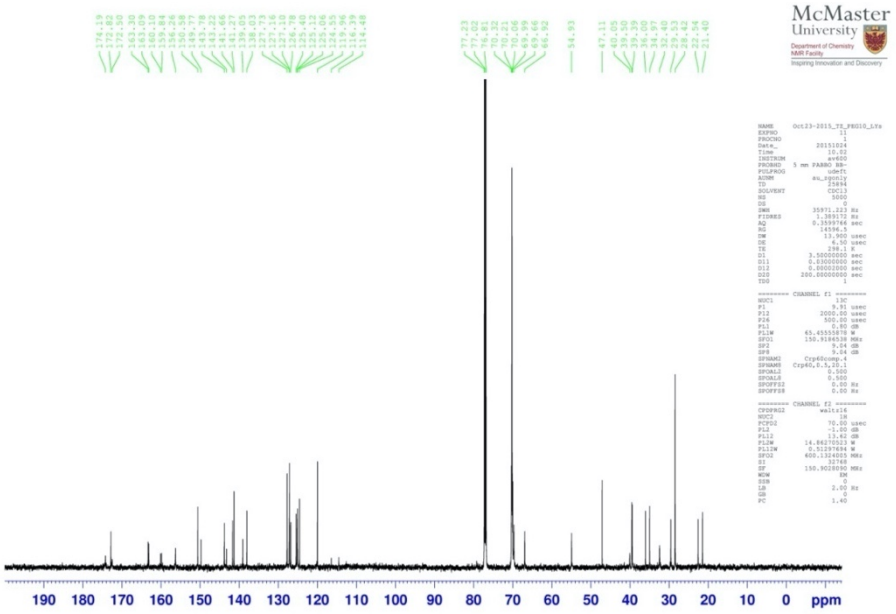

Figure S2-2. ^{13}C NMR spectrum of **2a** ($CDCl_3$, 150 MHz)

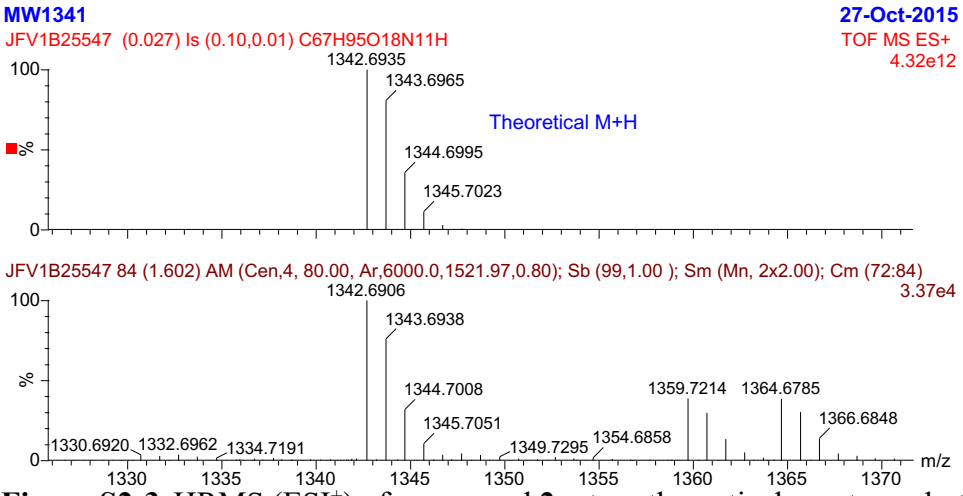

Figure S2-3. HRMS (ESI^+) of compound **2a**: top- theoretical spectrum; bottom- acquired spectrum

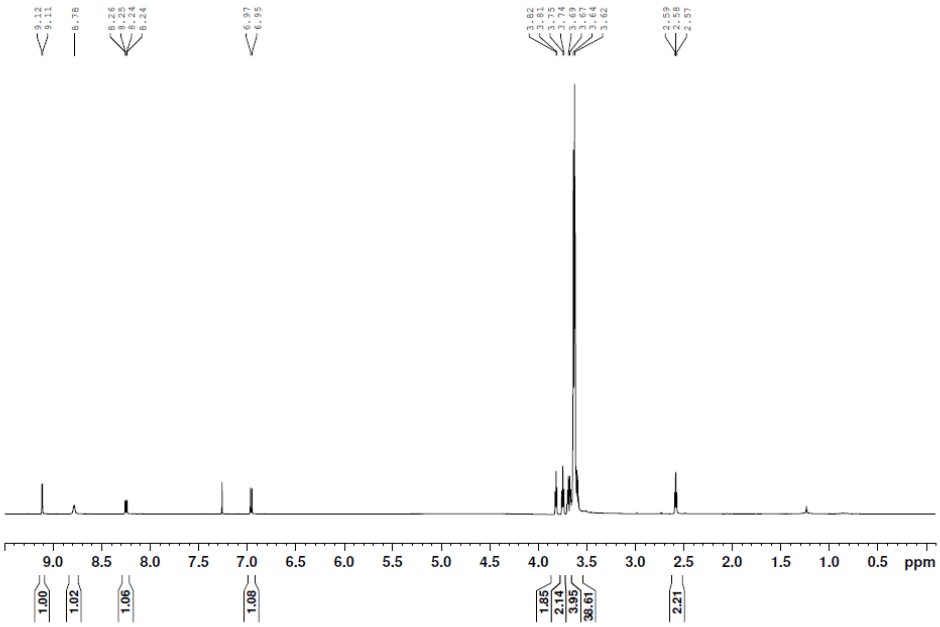

Figure S2-4. ^1H NMR spectrum of **3** ($CDCl_3$, 600 MHz)

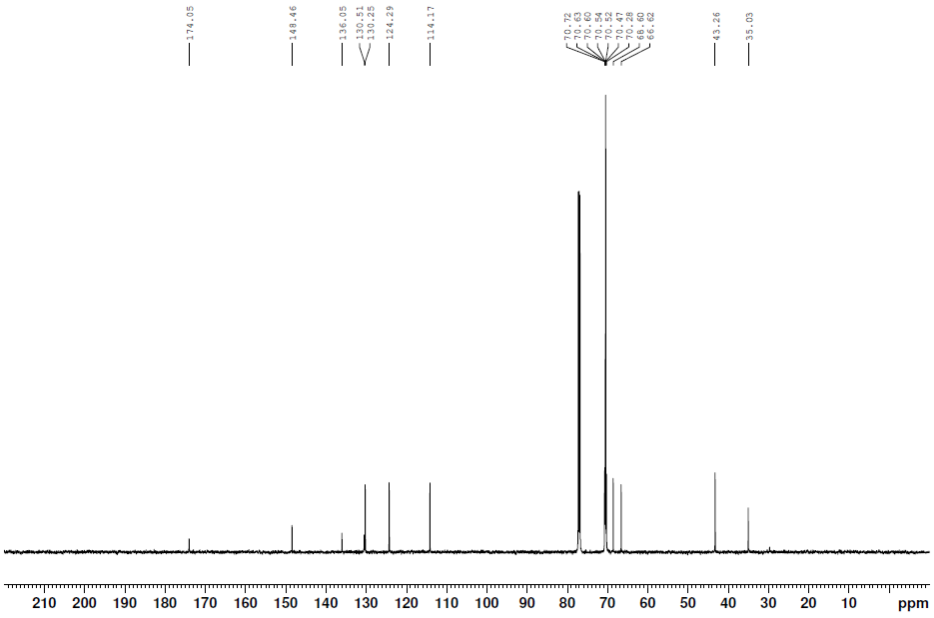

Figure S2-5. ^{13}C NMR spectrum of **3** ($CDCl_3$, 150 MHz)

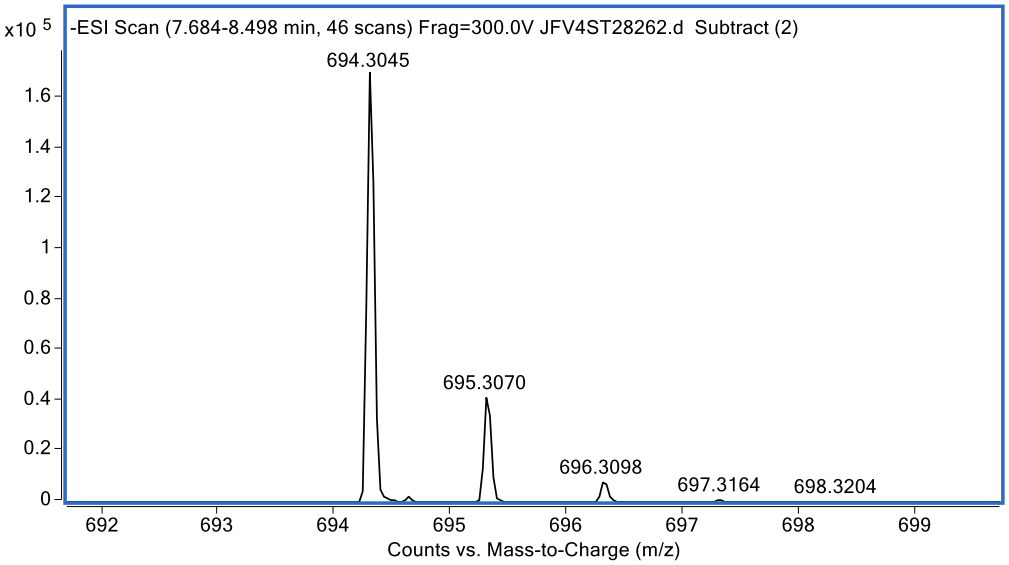

Figure S2-6. HRMS (ESI^-) of compound **3**

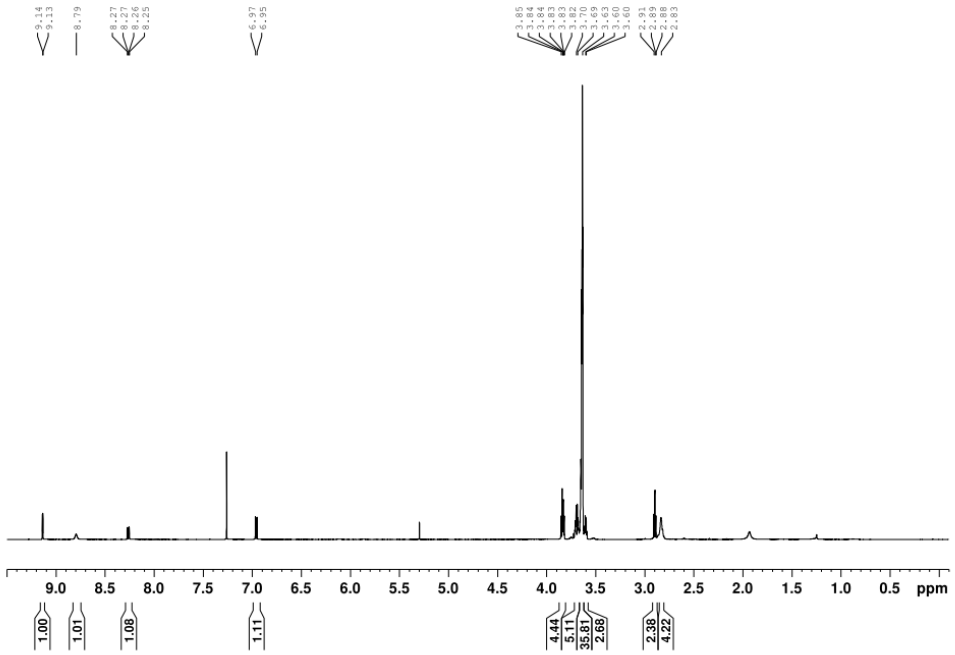

Figure S2-7. ^{1}H NMR of **4** ($CDCl_3$, 600 MHz)

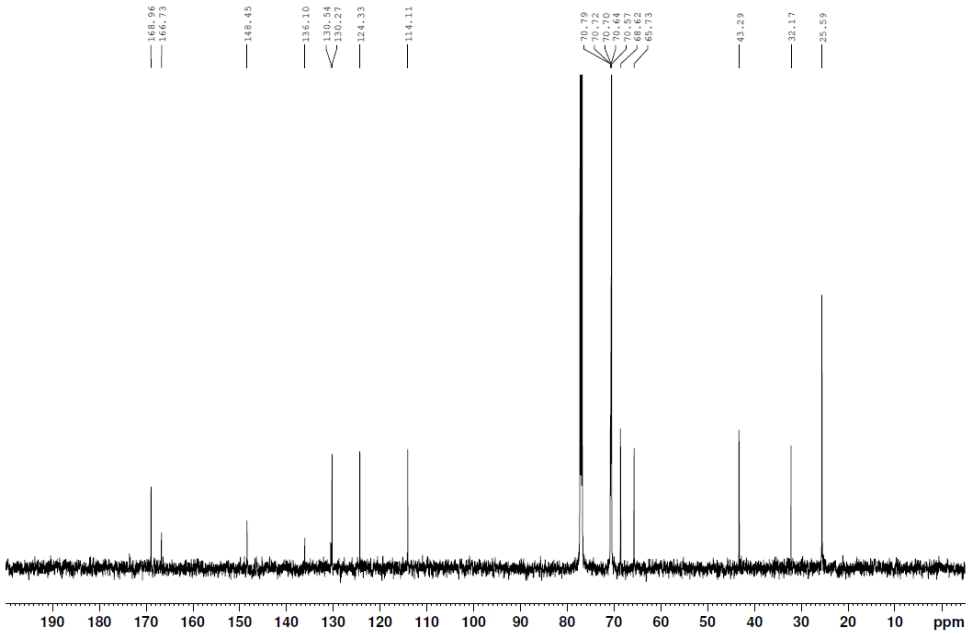

Figure S2-8. ^{13}C NMR of **4** ($CDCl_3$, 150 MHz)

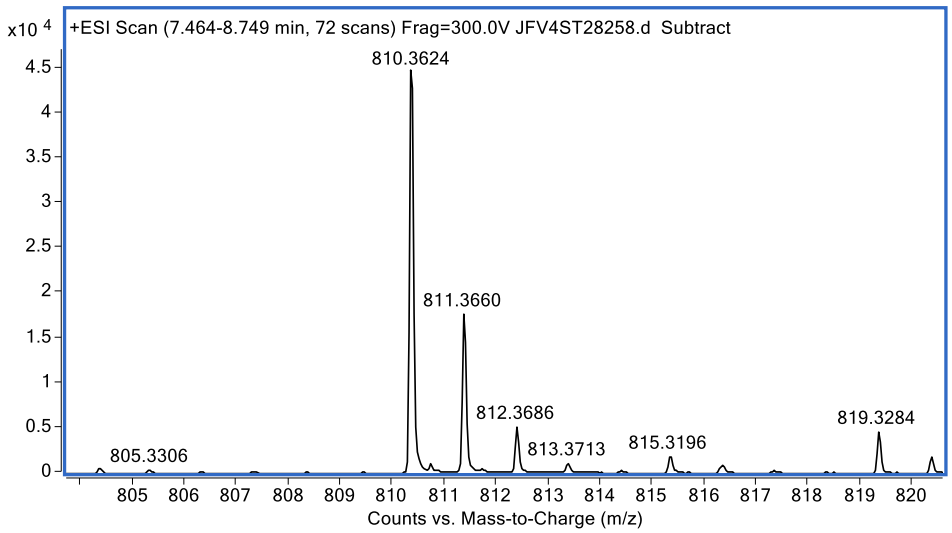

Figure S2-9. HRMS (ESI^+) of compound **4**

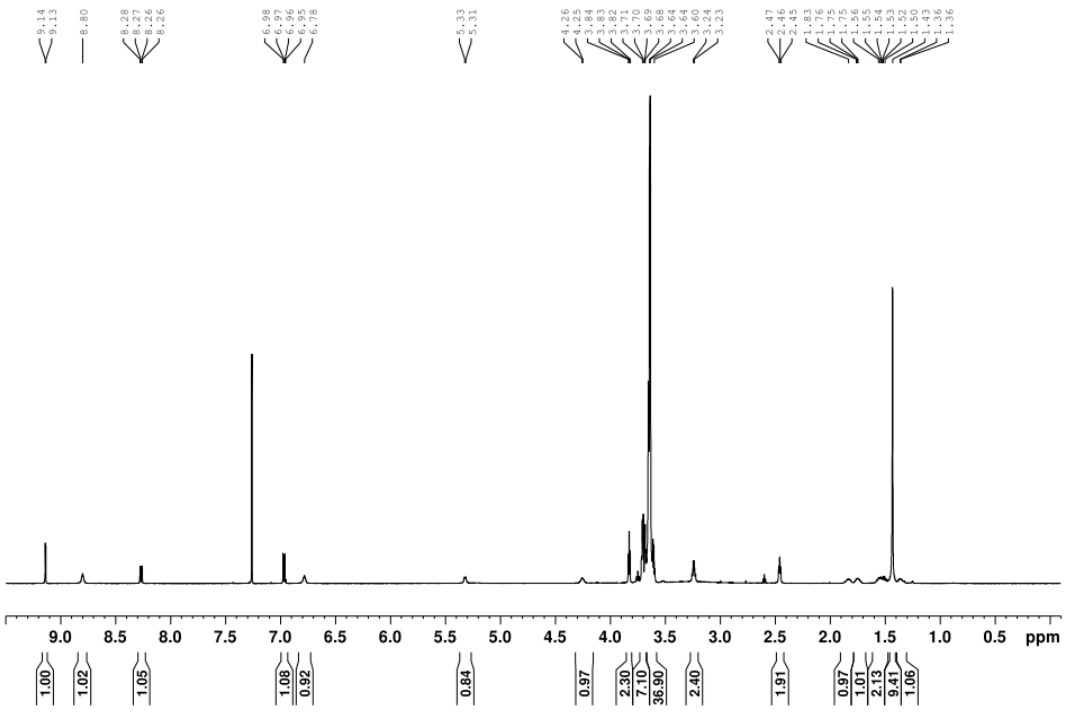

Figure S2-10. ^1H NMR spectrum of **5** ($CDCl_3$, 600 MHz)

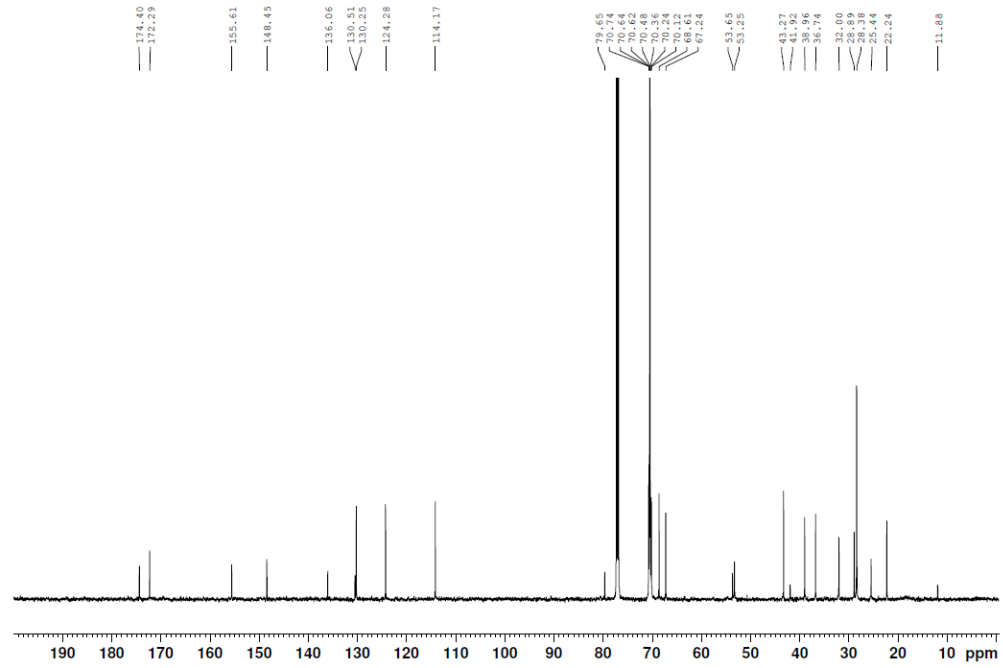

Figure S2-11. ^{13}C NMR spectrum of **5** ($CDCl_3$, 150 MHz)

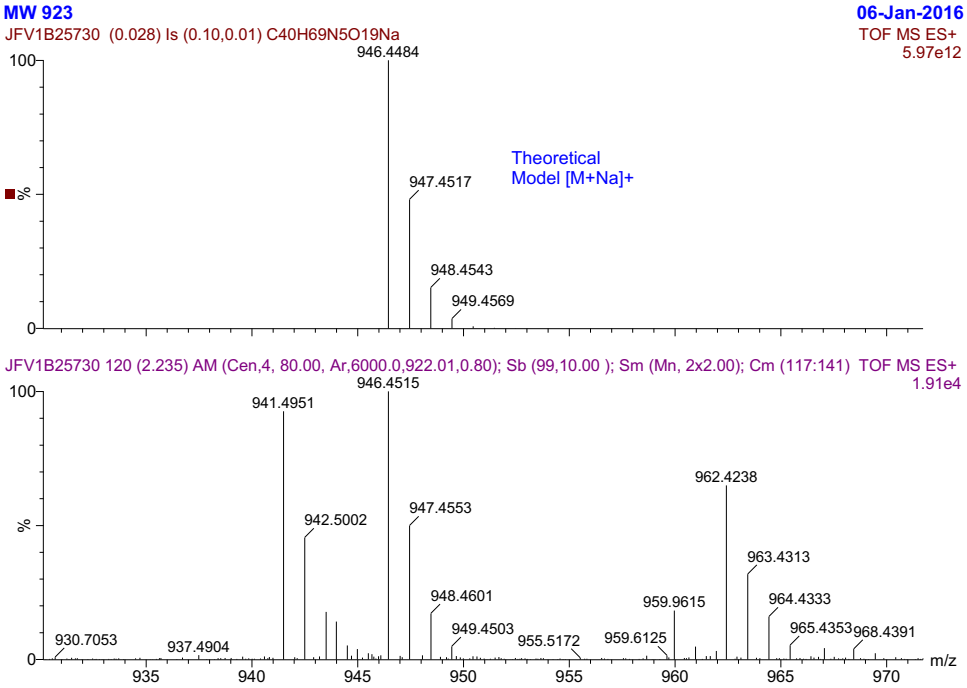

Figure S2-12. HRMS (ESI^+) of compound **5**

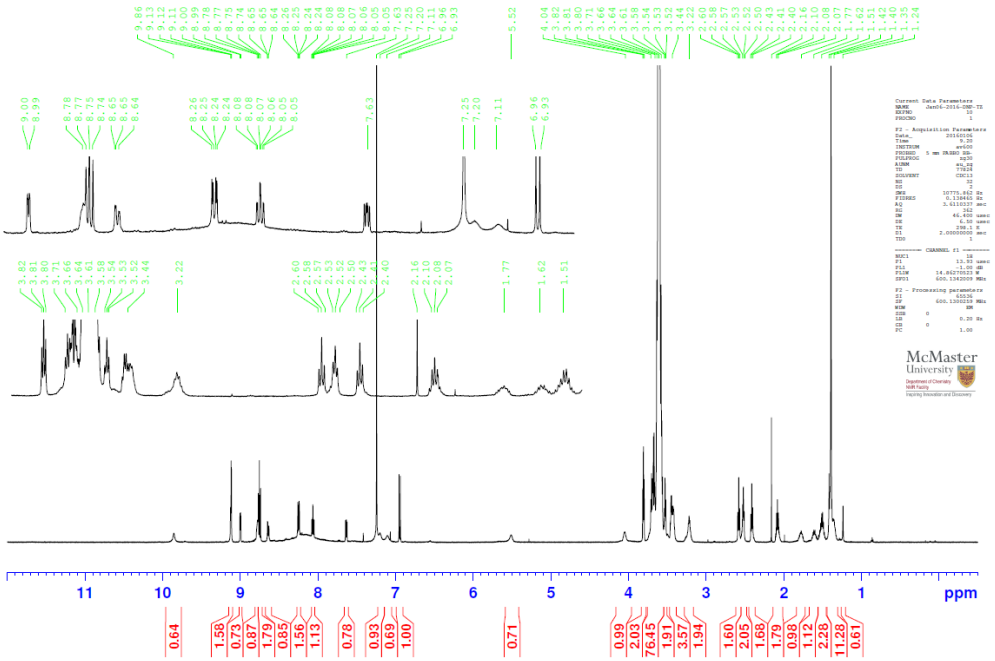

Figure S2-13. ^{1}H NMR spectrum of **6** ($CDCl_3$, 600 MHz)

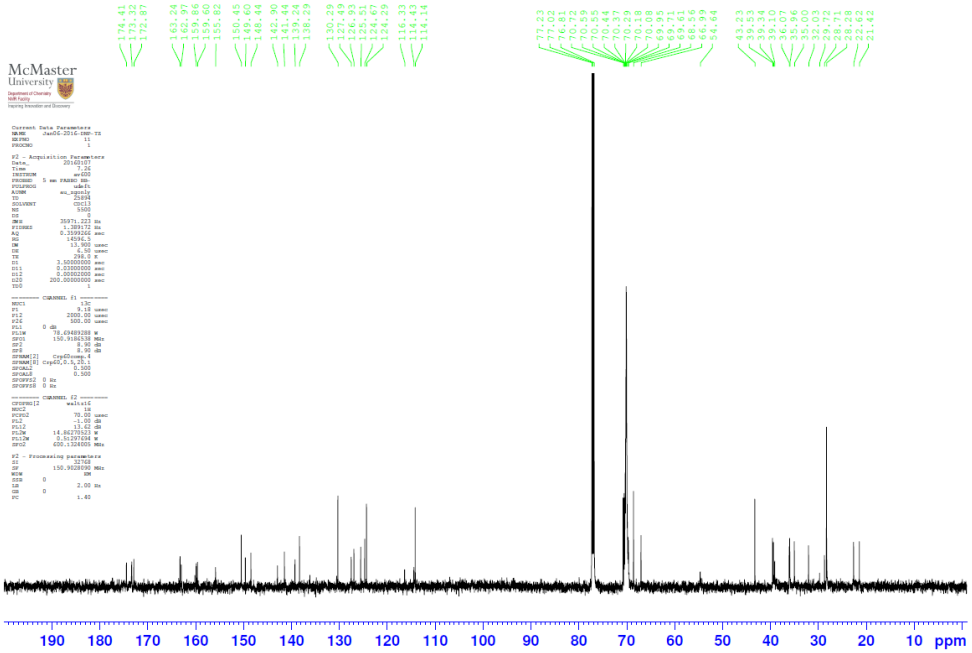

Figure S2-14. ^{13}C NMR spectrum of **6** ($CDCl_3$, 150 MHz)

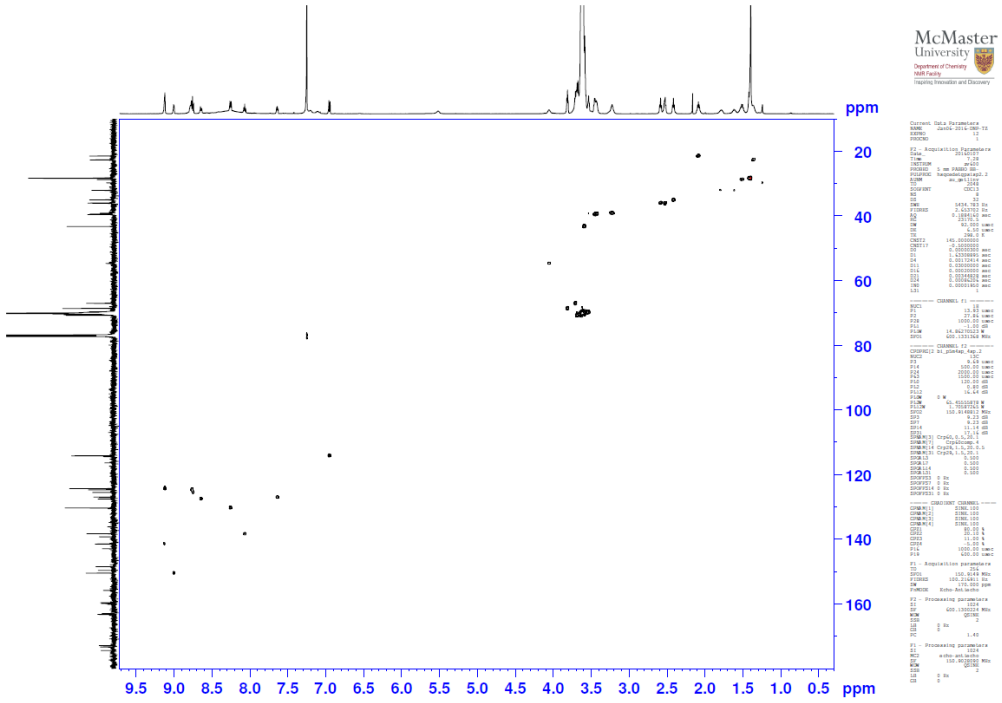

Figure S2-15. HSQC spectrum of **6** ($CDCl_3$, 600 MHz)

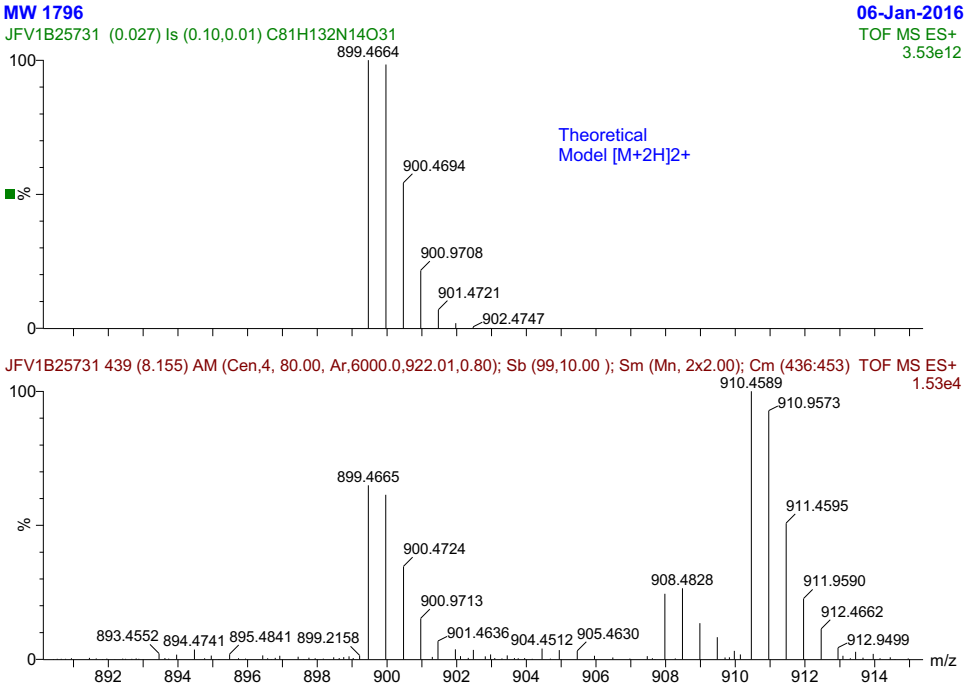

Figure S2-16. HRMS (ESI^+) of compound **6**

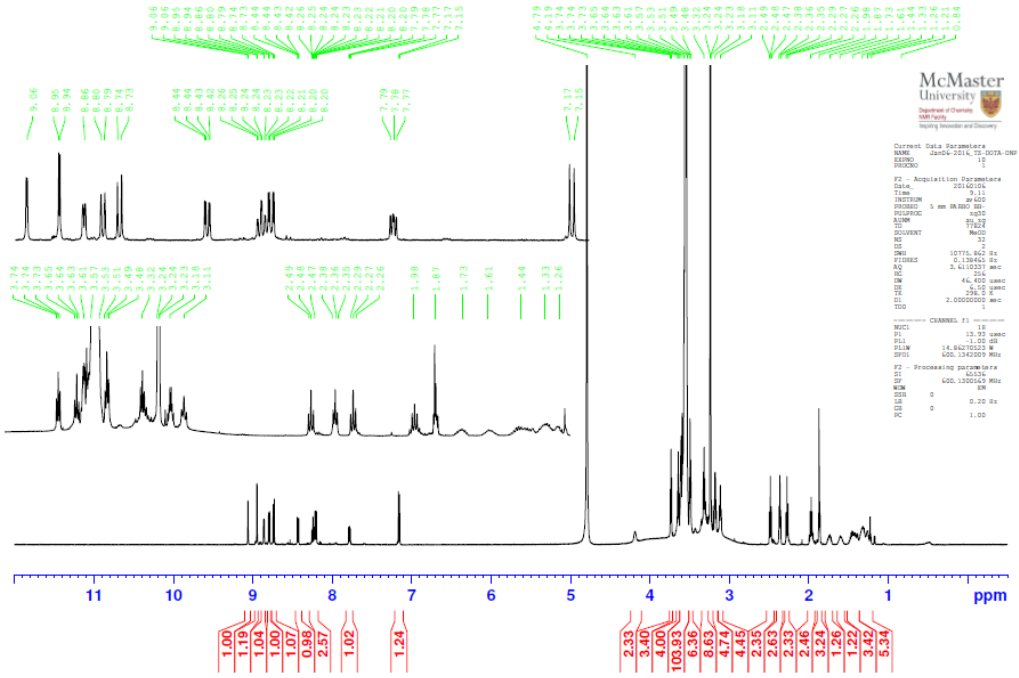

Figure S2-17. ^{1}H NMR spectrum of **7** (CD_3OD, 600 MHz)

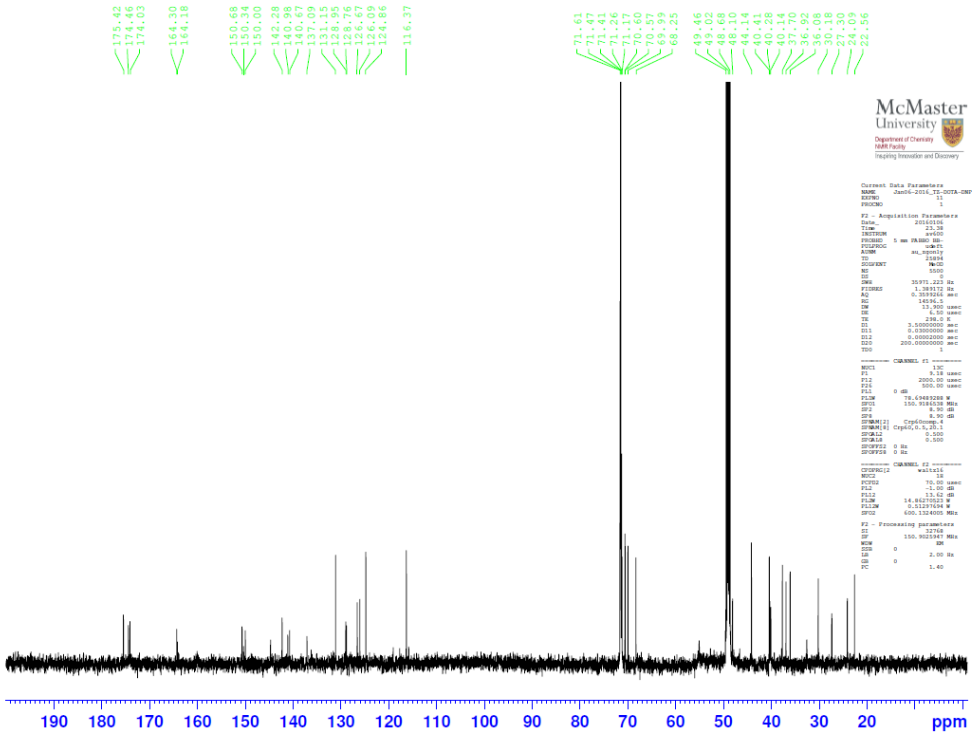

Figure S2-18. ^{13}C NMR spectrum of **7** (CD_3OD, 150 MHz)

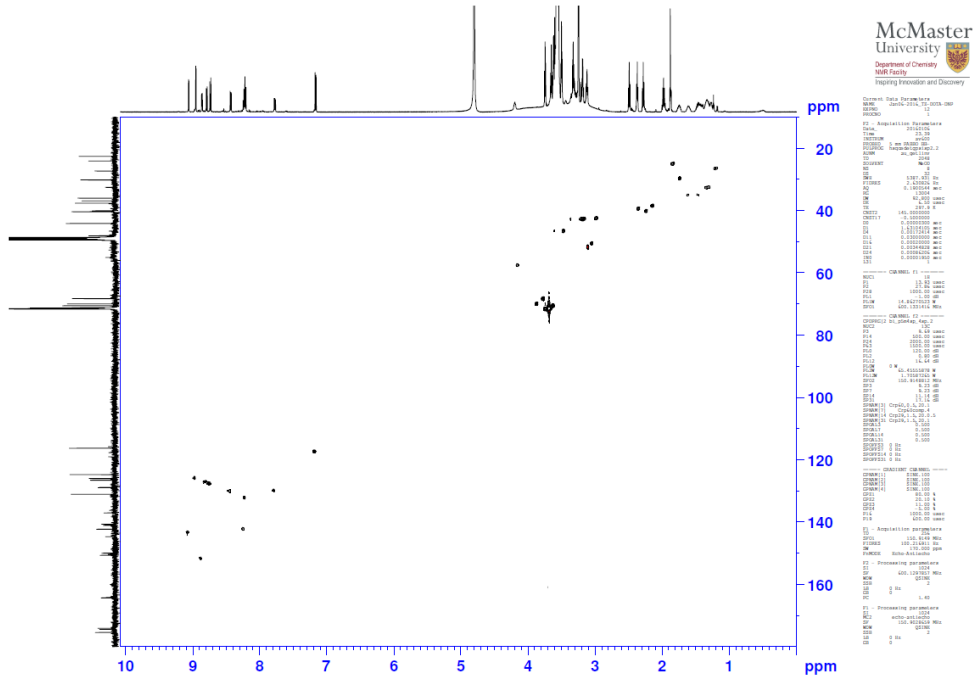

Figure S2-19. HSQC spectrum of **7** (CD_3OD, 600 MHz)

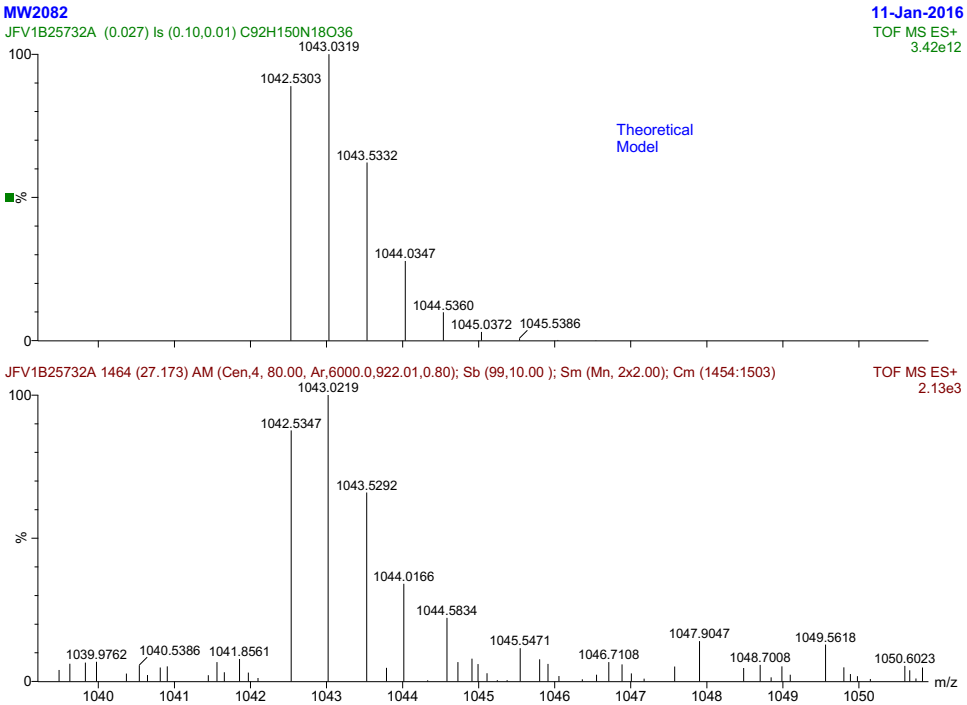

Figure S2-20. HRMS (ESI^+) of **7**

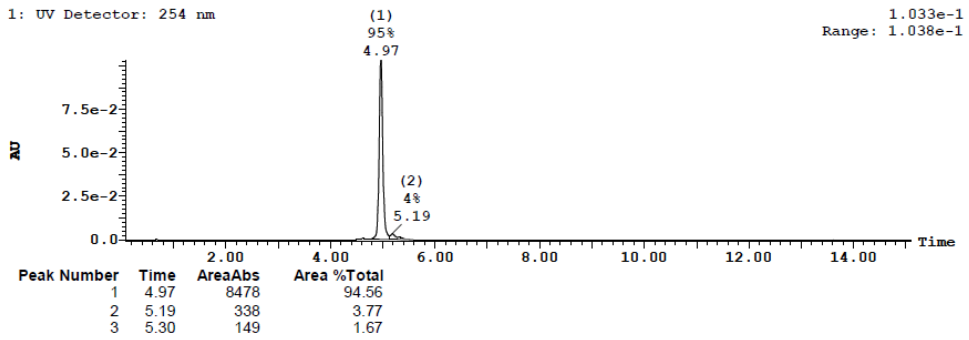

Figure S2-21. UV HPLC trace of **7** at 254 nm (Method B)

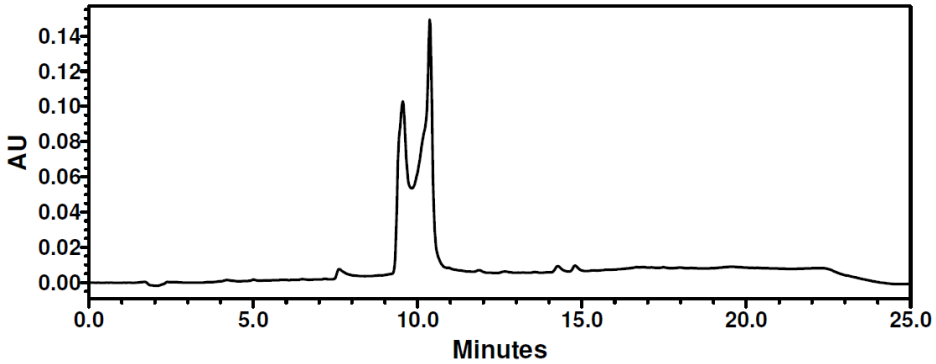

Figure S2-22. UV HPLC trace of **9** at 254 nm (Method A)

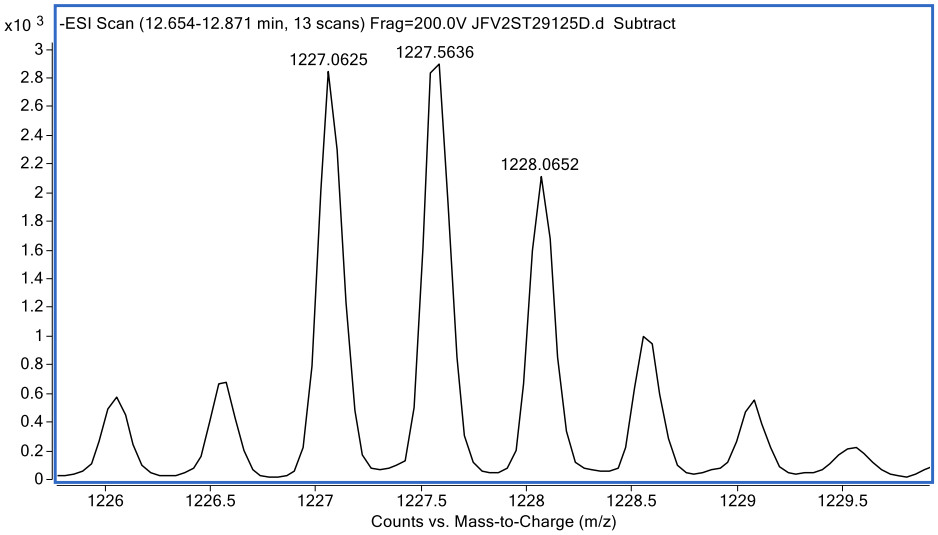

Figure S2-23. HRMS (ESI^{2-}) of **9** calculated 1277.0629, found 1277.0625

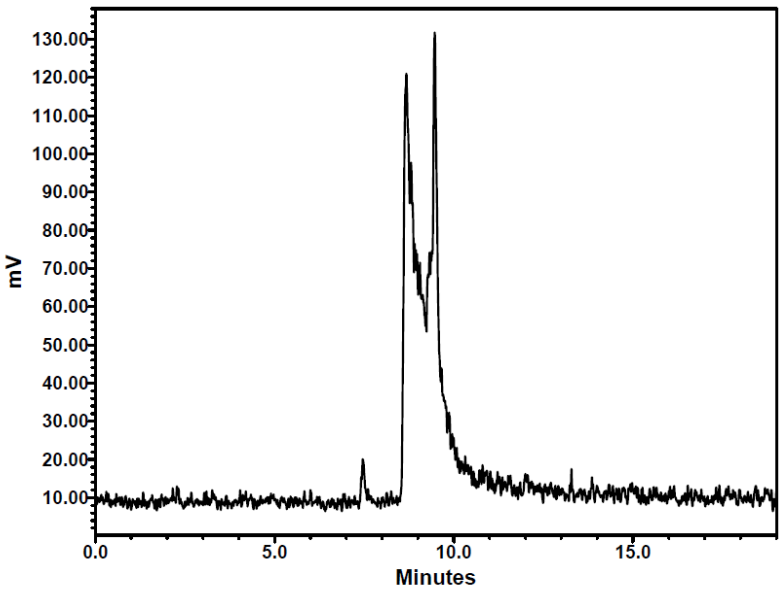

Figure S2-24. Gamma HPLC trace of **10**

Table S2-1. Biodistribution results for **8** reported as %ID/g ± SEM

	Time (h)								
Organs	1			4			24		
Blood	0.64	±	0.10	0.07	±	0.01	0.03	±	0.01
Adipose	1.17	±	0.38	0.39	±	0.37	0.00	±	0.00
Adrenals	1.30	±	0.75	0.10	±	0.09	0.00	±	0.00
Bone	2.91	±	0.94	1.47	±	1.47	0.00	±	0.00
Brain	0.21	±	0.09	0.06	±	0.06	0.00	±	0.00
Gall Bladder	2.59	±	1.71	0.00	±	0.00	0.00	±	0.00
Heart	0.30	±	0.07	0.03	±	0.01	0.00	±	0.00
Kidneys	3.14	±	0.05	2.54	±	0.85	1.38	±	0.16
Lg Intestine + Caecum	0.22	±	0.06	0.40	±	0.07	0.14	±	0.02
Liver	0.99	±	0.16	0.37	±	0.02	0.25	±	0.03
Lungs	0.51	±	0.07	0.19	±	0.06	0.06	±	0.01
Pancreas	0.21	±	0.02	0.04	±	0.01	0.01	±	0.00
Skeletal Muscle	0.89	±	0.26	0.41	±	0.41	0.00	±	0.00
Sm Intestine	0.83	±	0.60	0.07	±	0.04	0.04	±	0.00
Spleen	0.29	±	0.08	0.08	±	0.01	0.03	±	0.00
Stomach	13.26	±	12.52	0.13	±	0.03	0.08	±	0.02
Thyroid/Trachea	7.11	±	2.68	2.69	±	2.69	0.00	±	0.00
Urine + Bladder	1104.74	±	252.71	86.08	±	79.99	0.12	±	0.06

Table S2-2. Biodistribution results for **10** reported as %ID/g ± SEM

	Time (h)								
Organs	1			4			24		
Blood	1.43	±	0.09	0.29	±	0.04	0.01	±	0.01
Adipose	1.21	±	0.32	1.11	±	0.02	0.09	±	0.01
Adrenals	5.99	±	0.53	6.86	±	1.12	3.06	±	0.87
Bone (arm + shoulder)	9.30	±	0.41	8.24	±	2.65	9.08	±	0.50
Bone (leg + knee)	14.07	±	0.62	15.52	±	0.79	14.99	±	0.51
Brain	0.18	±	0.04	0.24	±	0.01	0.02	±	0.00
Gall Bladder	12.38	±	5.75	7.47	±	1.49	3.95	±	#DIV/0!
Heart	1.93	±	0.16	1.14	±	0.04	0.67	±	0.06
Kidneys	5.77	±	0.21	3.93	±	0.27	2.89	±	0.03
Lg Intestine + Caecum	0.38	±	0.10	0.56	±	0.10	0.25	±	0.10
Liver	6.48	±	0.47	6.71	±	0.21	6.81	±	0.23
Lungs	171.26	±	15.04	128.27	±	24.45	47.57	±	3.93
Pancreas	0.57	±	0.04	0.37	±	0.01	0.22	±	0.03
Skeletal Muscle	1.05	±	0.24	1.64	±	0.25	0.08	±	0.02
Sm Intestine	0.34	±	0.03	0.07	±	0.02	0.17	±	0.04
Spleen	7.40	±	0.39	13.24	±	1.52	14.91	±	0.85
Stomach	0.71	±	0.06	0.52	±	0.01	0.29	±	0.09
Thyroid/Trachea	6.35	±	2.02	16.23	±	3.67	1.34	±	0.24
Urine + Bladder	628.17	±	218.42	492.70	±	62.43	3.11	±	0.11

Table S2-3. Biodistribution results for pretargeting with TCO-BP followed by **8** reported as %ID/g ± SEM

	Time (h)								
Organs	1			4			24		
Blood	8.20	±	0.46	1.66	±	0.05	0.12	±	0.02
Adipose	0.53	±	0.08	0.35	±	0.10	0.11	±	0.03
Adrenals	4.02	±	0.45	1.55	±	0.10	1.09	±	0.39
Bone (arm + shoulder)	8.04	±	0.35	7.18	±	0.38	6.95	±	1.00
Bone (leg + knee)	11.23	±	0.43	11.61	±	0.53	9.99	±	1.24
Brain	0.15	±	0.03	0.04	±	0.00	0.01	±	0.01
Gall Bladder	1.87	±	0.17	0.94	±	0.08	0.11	±	0.06
Heart	1.51	±	0.10	0.42	±	0.01	0.16	±	0.03
Kidneys	6.34	±	1.24	3.40	±	0.10	2.25	±	0.22
Lg Intestine + Caecum	0.36	±	0.03	0.41	±	0.03	0.21	±	0.03
Liver	3.55	±	0.06	2.19	±	0.11	1.52	±	0.46
Lungs	5.28	±	0.27	3.57	±	0.21	1.65	±	0.38
Pancreas	0.52	±	0.02	0.17	±	0.01	0.09	±	0.03
Skeletal Muscle	0.43	±	0.03	0.15	±	0.03	0.05	±	0.00
Sm Intestine	0.60	±	0.02	0.27	±	0.01	0.12	±	0.01

Spleen	1.66	±	0.07	1.49	±	0.05	1.60	± 0.56
Stomach	0.51	±	0.04	0.35	±	0.04	0.13	± 0.02
Thyroid/Trachea	2.76	±	0.75	0.91	±	0.09	0.41	± 0.09
Urine + Bladder	179.67	±	68.75	51.85	±	5.47	2.13	± 0.77

Appendix II

Supporting Information for Chapter 3

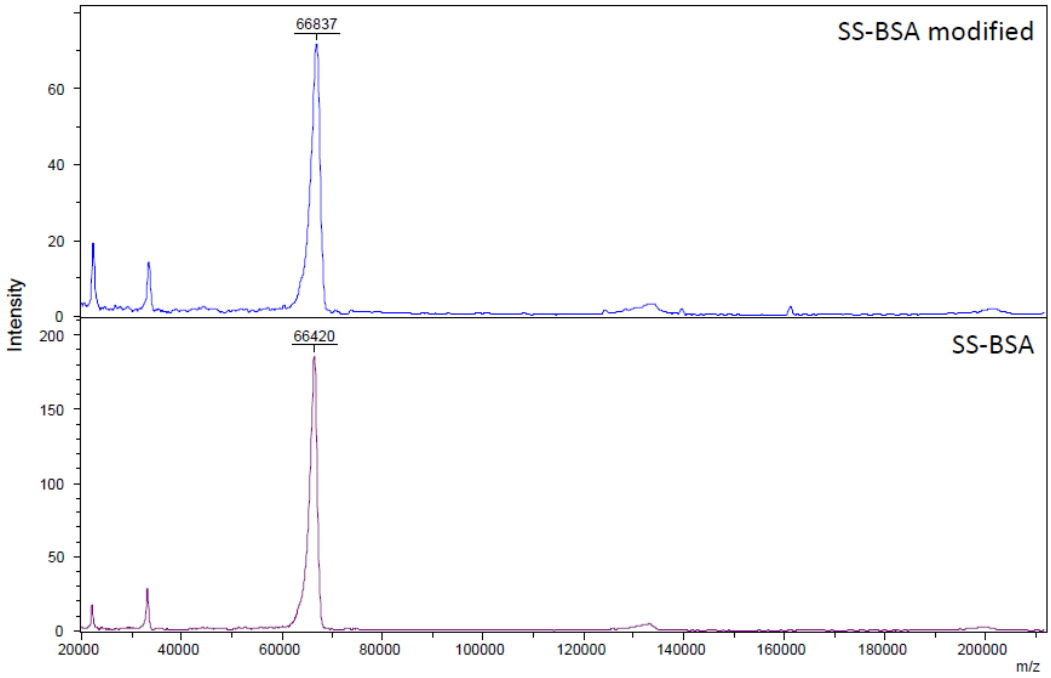

Figure S3-1. MALDI-TOF spectrum of unfunctionalized BSA (top) and TCO-BSA (**11**, bottom)

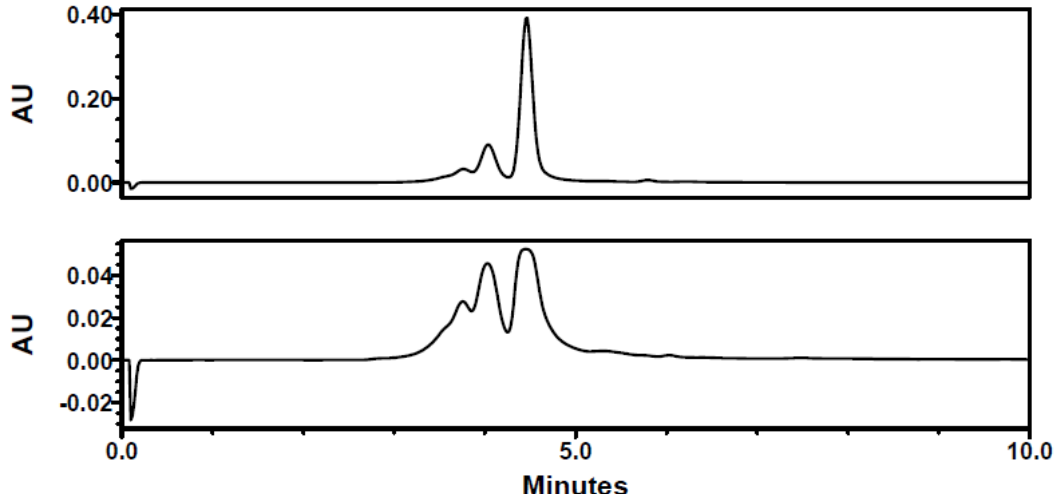

Figure S3-2. SEC HPLC of **11** at 214 nm (top) and 254 nm (bottom)

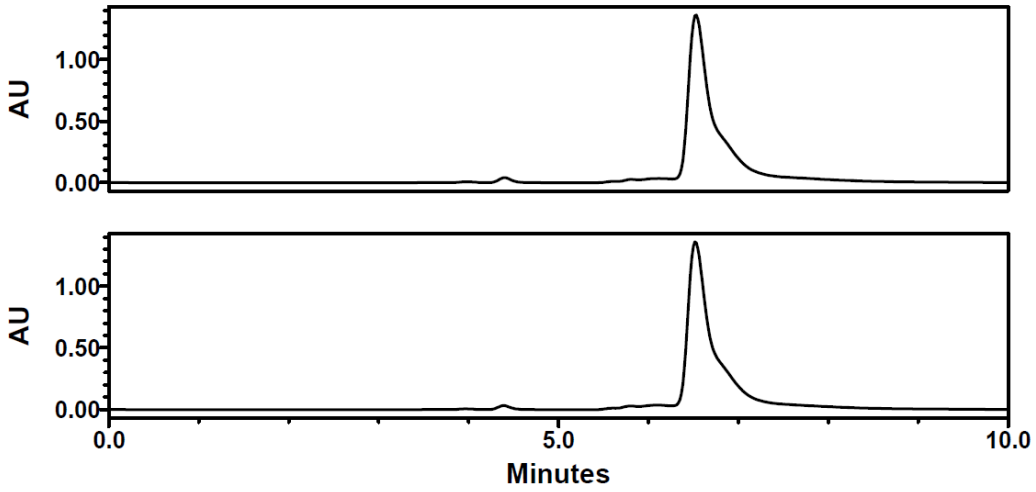

Figure S3-3. SEC HPLC of **7** at 214 nm (top) and 254 nm (bottom)

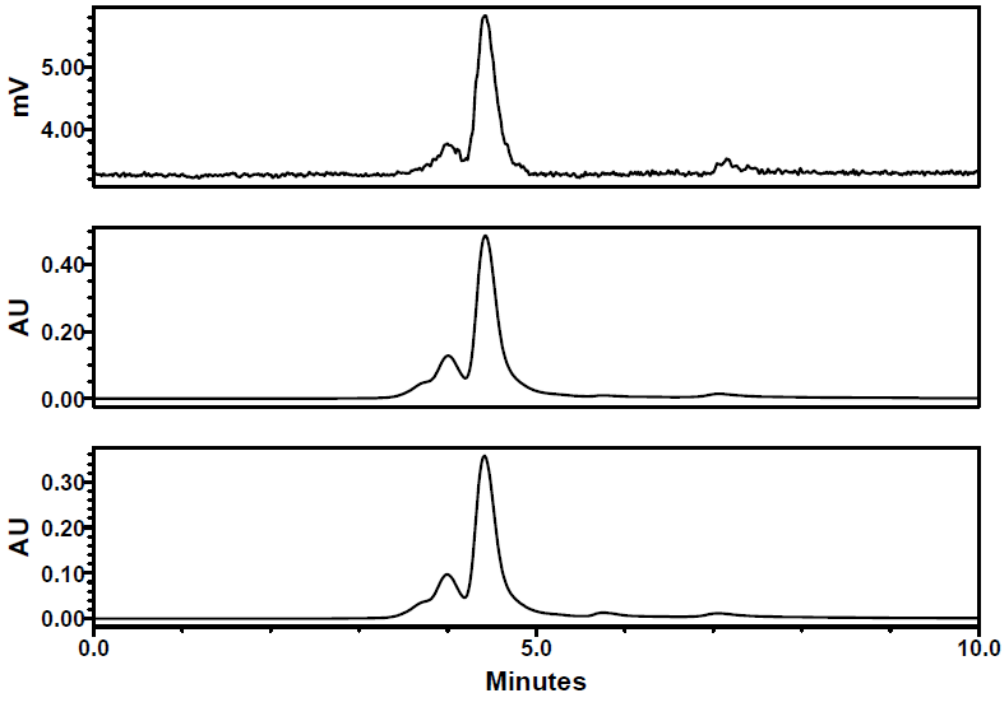

Figure S3-4. SEC HPLC of **15** gamma spectrum (top) 214 nm (middle) and 254 nm (bottom)

Table S3-1. Biodistribution results for pretargeting with TCO-BZA followed by **8** in a B16F1 melanoma tumour model. Results are reported as %ID/g ± SEM.

	n=2	n=3	n=2
	1h TCO	4h CTO	21h TCO

Organs	avg	SEM	avg	SEM	avg	SEM
Blood	3.06	0.15	2.13	0.17	1.83	0.46
Adipose	1.50	1.11	1.47	1.05	0.24	0.08
Adrenals	1.43	0.30	1.11	0.22	0.53	0.22
Bone	0.00	0.00	0.10	0.07	0.00	0.00
Brain	0.18	0.02	0.11	0.03	0.23	0.01
Eyes	0.30	0.02	0.16	0.02	0.11	0.03
Gall Bladder	2.65	1.60	1.20	0.54	1.02	0.39
Heart	0.73	0.03	0.54	0.07	0.47	0.08
Kidneys	9.52	0.46	5.94	0.33	5.57	0.93
Lg Intestine + Caecum	0.31	0.04	0.13	0.01	0.19	0.01
Liver	3.82	0.56	2.64	0.30	2.12	0.39
Lungs	1.64	0.10	1.16	0.12	1.16	0.25
Skeletal Muscle	1.83	0.58	1.04	0.55	1.53	0.17
Sm Intestine	0.70	0.03	0.45	0.02	0.42	0.07
Spleen	0.82	0.05	0.58	0.05	0.50	0.09
Stomach	0.48	0.20	0.52	0.13	0.41	0.15
Thyroid/Trachea	0.78	0.01	0.58	0.04	0.31	0.09
Tumour	2.22	0.23	1.30	0.17	0.99	0.09
Urine + Bladder	668.65	2.64	727.65	377.24	699.03	157.39

Table S3-2. Biodistribution results for [^{99m}Tc]Tc-MDP and [^{99m}Tc]Tc-TCO-BP in a 143B Osteosarcoma flank tumour model. Results are expressed as %ID/g ± SEM.

	n=3		n=3	
	^{99m}Tc-MDP		^{99m}Tc-TCO-BP	
Organs	avg	SEM	avg	SEM
Blood	0.67	0.03	0.97	0.20
Adipose	0.09	0.06	0.06	0.01
Adrenals	0.38	0.05	0.62	0.22
Bone	11.88	0.85	15.26	2.23
Brain	0.03	0.00	0.05	0.02
Gall Bladder	1.61	0.09	0.62	0.09
Heart	0.24	0.02	0.36	0.07
Kidneys	2.23	0.53	10.23	1.43
Lg Intestine + Caecum	0.47	0.03	0.16	0.03
Liver	0.52	0.02	0.53	0.10
Lungs	0.54	0.03	0.65	0.11
Pancreas	0.19	0.02	0.21	0.04
Skeletal Muscle	0.14	0.01	0.16	0.02
Sm Intestine	0.54	0.06	0.34	0.04
Spleen	0.32	0.04	0.43	0.08
Stomach	2.69	0.25	0.59	0.10
Tumour	1.00	0.07	1.03	0.14

Thyroid/Trachea	4.61	0.56	2.72	0.36
Urine + Bladder	198.81	112.63	619.27	319.64

Table S3-3. Biodistribution results for **14** administered intratumorally in a 4T1 flank tumour model. Results are expressed as %ID/g ± SEM.

	24h		72h		120h	
Organs	avg	SEM	avg	SEM	avg	SEM
Blood	0.16	0.05	0.07	0.03	0.07	0.03
Adipose	0.45	0.29	0.25	0.09	0.18	0.09
Adrenals	0.00	0.00	0.16	0.11	0.00	0.00
Bone	0.63	0.39	11.42	6.32	19.71	10.74
Brain	0.10	0.06	0.06	0.03	0.09	0.07
Gall Bladder	0.00	0.00	0.10	0.10	0.03	0.03
Heart	0.00	0.00	0.20	0.06	0.17	0.10
Kidneys	10.15	3.74	10.26	1.69	8.54	4.68
Lg Intestine + Caecum	0.31	0.13	0.47	0.06	0.31	0.08
Liver	0.33	0.17	4.08	0.56	1.83	0.76
Lungs	0.00	0.00	0.84	0.11	0.62	0.31
Pancreas	0.00	0.00	0.24	0.04	0.45	0.29
Skeletal Muscle	0.24	0.13	4.18	4.08	0.15	0.08
Sm Intestine	0.03	0.02	0.39	0.04	0.25	0.10
Spleen	0.10	0.10	2.25	0.43	0.28	0.17
Stomach	0.01	0.01	0.53	0.07	0.53	0.28
Thyroid/Trachea	1.79	0.95	4.16	0.71	3.74	1.81
Tumour	949.54	770.91	167.40	94.43	81.46	31.91
Urine + Bladder	7.29	2.73	2.45	0.35	1.90	0.83

Table S3-4. Biodistribution results for **15** administered intratumorally in a 4T1 flank tumour model. Results are expressed as %ID/g ± SEM.

	n=3 24h		n=3 72h		n=3 120h	
Organs	avg	SEM	avg	SEM	avg	SEM
Blood	2.12	0.61	0.13	0.02	0.02	0.00
Adipose	0.48	0.22	0.38	0.19	0.79	0.22
Adrenals	1.12	0.60	0.60	0.30	2.13	0.67
Bone	0.65	0.28	0.48	0.25	1.83	1.08
Brain	0.05	0.03	0.01	0.01	0.06	0.03
Gall Bladder	1.40	1.40	0.63	0.63	4.80	2.10
Heart	0.88	0.28	0.58	0.30	1.04	0.35
Kidneys	3.35	0.85	3.07	0.77	5.08	1.83
Lg Intestine + Caecum	0.58	0.18	0.44	0.10	0.52	0.12
Liver	3.09	0.71	4.67	1.98	6.72	1.81

Lungs	1.02	0.33	0.55	0.30	0.71	0.26
Pancreas	0.55	0.19	0.52	0.27	0.70	0.24
Skeletal Muscle	0.42	0.15	0.31	0.16	8.52	5.47
Sm Intestine	0.49	0.10	0.34	0.09	0.36	0.13
Spleen	1.67	0.52	1.91	1.02	2.32	0.87
Stomach	0.36	0.09	0.34	0.05	0.42	0.15
Thyroid/Trachea	1.37	0.63	0.61	0.34	1.00	0.16
Tumour	55.77	17.59	95.71	16.70	61.61	31.34
Urine + Bladder	3.22	2.10	3.97	2.44	6.12	2.56

Table S3-5. Biodistribution results for **15** administered intravenously in a 4T1 flank tumour model. Results are expressed as %ID/g ± SEM.

	24h		72h	
Organs	avg	SEM	avg	SEM
Blood	4.68	0.14	0.29	0.09
Adipose	1.39	0.12	1.04	0.11
Adrenals	4.64	0.60	2.95	0.44
Bone	1.57	0.08	0.97	0.13
Brain	0.09	0.00	0.02	0.00
Gall Bladder	5.88	2.10	2.56	1.39
Heart	2.63	0.19	1.50	0.22
Kidneys	5.01	0.09	3.33	0.43
Lg Intestine + Caecum	1.04	0.05	0.70	0.16
Liver	7.68	0.46	6.93	1.35
Lungs	2.31	0.22	0.96	0.18
Pancreas	1.82	0.47	0.99	0.14
Skeletal Muscle	1.05	0.11	0.57	0.09
Sm Intestine	1.00	0.10	0.46	0.09
Spleen	4.94	0.42	3.00	0.70
Stomach	0.68	0.02	0.52	0.12
Thyroid/Trachea	2.03	0.12	1.06	0.16
Tumour	7.76	0.54	5.12	0.89
Urine + Bladder	4.34	0.70	2.93	0.60

Appendix III

Supporting Information for Chapter 5

Table S5-1. Biodistribution results of a pre-targeting study (100 μg of **12** injected intratumorally to Balb/c mice with 4T1 tumours followed 1 or 24 hours later by **8** administered intravenously). Animals were sacrificed 24 hours post injection of **8**; results are reported as %ID/g.

	n=3		n=3	
	24h TCO-BSA		1h TCO-BSA	
Organs	avg	SEM	avg	SEM
Blood	0.08	0.01	0.08	0.01
Adipose	0.00	0.00	0.00	0.00
Adrenals	0.00	0.00	0.00	0.00
Bone	0.00	0.00	0.00	0.00
Brain	0.00	0.00	0.00	0.00
Gall Bladder	0.00	0.00	0.01	0.01
Heart	0.02	0.01	0.02	0.02
Kidneys	2.02	0.11	2.07	0.03
Lg Intestine + Caecum	0.14	0.02	0.14	0.03
Liver	0.54	0.02	0.57	0.04
Lungs	0.20	0.03	0.28	0.10
Pancreas	0.02	0.00	0.02	0.01
Skeletal Muscle	0.00	0.00	0.00	0.00
Sm Intestine	0.07	0.00	0.07	0.00
Spleen	0.21	0.02	0.45	0.06
Stomach	0.05	0.01	0.05	0.00
Thyroid/Trachea	0.00	0.00	0.00	0.00
Tumour	0.30	0.03	0.34	0.04
Urine + Bladder	0.71	0.24	0.60	0.22

Table S5-2. Biodistribution results of a pre-targeting study (100 μg of **11** or saline injected intratumorally to Balb/c mice with 4T1 tumours followed 1 hour later by **8** administered intravenously). Animals were sacrificed 24 hours post injection of **8**; results are reported as %ID/g.

	n=3		n=3	
	Vehicle		TCO-BSA	
Organs	avg	SEM	avg	SEM
Blood	0.07	0.01	0.09	0.01
Adipose	0.00	0.00	0.00	0.00
Adrenals	0.00	0.00	0.00	0.00
Bone	0.02	0.02	0.00	0.00

Brain	0.00	0.00	0.00	0.00
Gall bladder	0.21	0.16	0.22	0.13
Heart	0.01	0.01	0.02	0.02
Kidneys	2.19	0.12	1.88	0.49
Lg Int + Caecum (+cont)	0.13	0.01	0.27	0.06
Liver	0.68	0.07	0.61	0.16
Lungs	0.20	0.01	0.19	0.03
Pancreas	0.00	0.00	0.00	0.00
Skeletal Muscle	0.01	0.01	0.02	0.01
Sm Int (+ contents)	0.06	0.01	0.06	0.01
Spleen	0.15	0.02	0.11	0.04
Stomach (+ contents)	0.08	0.01	0.07	0.01
Thyroid/Trachea	0.00	0.00	0.00	0.00
Tumor	0.49	0.08	1.03	0.38
Urine + Bladder	0.17	0.03	0.21	0.07

Appendix IV

Supporting Information for Chapter 6

Table S6-1. Biodistribution results for [^{125}I]I-m-anti-DNP antibody administered intravenously. Results are expressed as %ID/g ± SEM.

	n=3 24h		n=3 48h		n=3 96h	
Organs	avg	SEM	avg	SEM	avg	SEM
Blood	0.99	0.08	0.37	0.03	0.13	0.01
Adipose	0.14	0.06	0.04	0.00	0.02	0.00
Adrenals	0.50	0.13	0.20	0.01	0.08	0.01
Bone	0.86	0.15	0.32	0.03	0.08	0.00
Brain	0.05	0.00	0.02	0.00	0.01	0.00
Gall Bladder	0.92	0.23	0.44	0.09	0.11	0.01
Heart	0.30	0.04	0.12	0.01	0.05	0.01
Kidneys	0.45	0.03	0.25	0.02	0.13	0.00
Lg Intestine + Caecum	0.39	0.04	0.23	0.04	0.10	0.01
Liver	1.06	0.08	0.59	0.04	0.36	0.03
Lungs	0.77	0.04	0.34	0.03	0.11	0.01
Pancreas	0.32	0.12	0.08	0.01	0.03	0.00
Skeletal Muscle	0.15	0.07	0.14	0.05	0.06	0.01
Sm Intestine	0.41	0.04	0.21	0.03	0.08	0.00
Spleen	5.12	0.43	1.42	0.16	0.33	0.06
Stomach	1.49	0.14	0.66	0.15	0.23	0.01
Thyroid/Trachea	261.98	66.29	341.46	19.95	198.57	51.75
Urine + Bladder	4.25	0.21	0.54	0.28	0.38	0.13

Table S6-2. Biodistribution results for [^{125}I]I-p-anti-DNP antibody administered intravenously. Results are expressed as %ID/g ± SEM.

	n=3 24h		n=3 48h		n=3 96h	
Organs	avg	SEM	avg	SEM	avg	SEM
Blood	19.42	0.79	15.57	0.49	12.23	1.03
Adipose	1.60	0.16	1.17	0.16	0.72	0.02
Adrenals	3.09	0.27	2.58	0.20	2.12	0.06
Bone	2.68	0.17	1.85	0.09	1.48	0.09
Brain	0.41	0.04	0.32	0.02	0.23	0.03
Gall Bladder	2.57	0.28	1.06	0.12	0.74	0.29
Heart	5.36	0.86	3.14	0.15	2.70	0.10

Kidneys	5.17	0.32	4.08	0.10	3.11	0.22
Lg Intestine + Caecum	1.52	0.12	1.10	0.01	0.79	0.08
Liver	4.06	0.14	3.05	0.07	2.43	0.16
Lungs	7.38	1.00	4.73	0.09	4.08	0.40
Pancreas	2.24	0.04	1.64	0.05	1.19	0.02
Skeletal Muscle	1.71	0.20	1.47	0.01	1.07	0.05
Sm Intestine	2.07	0.07	1.60	0.03	1.17	0.10
Spleen	5.40	0.17	4.30	0.06	3.30	0.44
Stomach	3.26	0.09	2.21	0.08	1.24	0.06
Thyroid/Trachea	140.67	2.28	128.85	24.61	134.76	21.15
Urine + Bladder	5.28	0.87	3.42	0.10	2.96	0.35

Table S6-3. Biodistribution results for **20** administered intravenously in a *S. aureus* infection model. Results are expressed as %ID/g ± SEM.

	n=3 24h		n=3 48h		n=3 96h	
Organs	avg	SEM	avg	SEM	avg	SEM
Blood	19.42	0.79	15.57	0.49	12.23	1.03
Adipose	1.60	0.16	1.17	0.16	0.72	0.02
Adrenals	3.09	0.27	2.58	0.20	2.12	0.06
Bone	2.68	0.17	1.85	0.09	1.48	0.09
Brain	0.41	0.04	0.32	0.02	0.23	0.03
Gall Bladder	2.57	0.28	1.06	0.12	0.74	0.29
Heart	5.36	0.86	3.14	0.15	2.70	0.10
Kidneys	5.17	0.32	4.08	0.10	3.11	0.22
Lg Intestine + Caecum	1.52	0.12	1.10	0.01	0.79	0.08
Liver	4.06	0.14	3.05	0.07	2.43	0.16
Lungs	7.38	1.00	4.73	0.09	4.08	0.40
Pancreas	2.24	0.04	1.64	0.05	1.19	0.02
Skeletal Muscle	1.71	0.20	1.47	0.01	1.07	0.05
Sm Intestine	2.07	0.07	1.60	0.03	1.17	0.10
Spleen	5.40	0.17	4.30	0.06	3.30	0.44
Stomach	3.26	0.09	2.21	0.08	1.24	0.06
Thyroid/Trachea	140.67	2.28	128.85	24.61	134.76	21.15
Urine + Bladder	5.28	0.87	3.42	0.10	2.96	0.35